Thesis for the Degree of Doctor of Philosophy

in

Thermo and Fluid Dynamics

HCCI combustion using Charge Stratification and Spark-assistance

by

Andreas W. Berntsson

Department of Applied Mechanics
Chalmers University of Technology
Göteborg, Sweden, 2009

HCCI combustion using Charge Stratification and Spark-assistance

ANDREAS W. BERNTSSON
ISBN 978-91-7385-342-2

Doktorsavhandlingar vid Chalmers tekniska högskola
Ny serie nr 3023
ISSN 0346-718X

Department of Applied Mechanics
Chalmers University of Technology
SE-412 96 Göteborg
Sweden
Telephone +46 (0)31-772 1000

This document was typeset using LaTeX

Printed at Chalmers Reproservice
Göteborg, Sweden 2009

"When you're racing, it's life. Anything that happens before or after is just waiting." Steve McQueen as Michael Delaney in 'Le Mans'

Abstract

SI engines have the ability to meet the strictest emission standards. However, data for current vehicles show there is a clear need for further reductions in CO_2 emissions. Future requirements for reductions in CO_2 emissions from ground vehicles might be met by using the HCCI combustion concept, in which a diluted, more or less homogenous air/fuel mixture is compressed to auto-ignition. This leads to less CO_2 emissions than normal SI combustion due to its ability to burn dilute mixtures, which is beneficial from a thermodynamic perspective, and low combustion temperatures have a positive impact on exhaust emissions. However, there are challenges associated with this concept, for instance its limited operating range and combustion control.

Residual gases can be trapped with the intention to achieve HCCI combustion in SI engines using gasoline. This leads to a significantly improved efficiency for the part-load region, which is essential since the standardized drive cycles involve a considerable amount of low-load operation. The operational range of HCCI engines using residual gas trapping is limited for a low load and speed range. In attempts to overcome this limitation and gain control over HCCI combustion in this region a concept combining initial flame front propagation using a stratified charge and subsequent HCCI combustion has been developed, and explored in studies underlying this thesis.

Both optical and conventional engine experiments have been conducted to develop this control concept. The optical experiments have shown that charge stratification is important in many respects, notably it induces air motions and generates regions in which HCCI combustion is likely to occur, in addition to enriching the region near the sparkplug (thus making flame propagation possible). These features have been used to reduce the minimum load achievable for HCCI, with little or no compromises in terms of efficiency or NO_X emissions. This extends the load range in which an engine can be efficiently operated, compared to SI combustion, and hence enables CO_2 emissions to be reduced.

List of Papers

This thesis is partly based on the following papers:

I Berntsson, A., Denbratt, I., "Spark Assisted HCCI Combustion Using a Stratified Hydrogen Charge", SAE Technical Paper Series, SAE Paper 2005-24-039.

II Berntsson, A., Denbratt, I., "HCCI Combustion Using a Spark Ignited Stratified Charge", Proceedings. JSAE Annual Congress, Volume 24-06, Pages 23-28 (2006), JSAE Paper 20065424.

III Berntsson, W., A., Denbratt, I., "HCCI Combustion Using Charge Stratification for Combustion Control", SAE Technical Paper Series, SAE Paper 2007-01-0210.

IV Berntsson, W., A., Denbratt, I., "Optical study of HCCI Combustion using NVO and an SI Stratified Charge", SAE Technical Paper Series, SAE Paper 2007-24-0012.

V Berntsson, W., A., Andersson, M., Dahl, D., Denbratt, I., "LIF imaging of OH during the Negative Valve Overlap of a HCCI Combustion Engine", Proceedings of The Spark Ignition Engine of the Future - Technologies to meet the CO_2 challenge conference, SIA Technical Paper.

VI Berntsson, W., A., Andersson, M., Dahl, D., Denbratt, I., "A LIF-study of OH in the Negative Valve Overlap of a Spark-assisted HCCI Combustion Engine", SAE Technical Paper Series, SAE Paper 2008-01-0037.

VII Dahl, D., Andersson, M., Berntsson, W., A., Denbratt, I., Koopmans, L., "Reducing Pressure Fluctuations at High Loads by Means of Charge Stratification in HCCI Combustion with Negative Valve Overlap", SAE Technical Paper Series, SAE Paper 2009-01-1785.

VIII Berntsson, W., A., Andersson, M., Denbratt, I., "Characterization of a HCCI Engine Using Charge Stratification and Spark-Assist with Simultaneous PIV, Multi-Species LIF and High Speed Video", Submitted for publication.

Acknowledgments

First of all I would like to express my gratitude to my supervisor Professor Ingemar Denbratt for giving me the opportunity to explore phenomena in combustion engines from a scientific perspective, and for providing a bottom-less well of knowledge concerning combustion engines.

In addition, I would like to thank:

Associate Professor Sven Andersson for allowing my institutional duties to provide very important lessons in project management. Being the project leader of Chalmers Formula Student has not only been very enjoyable, but also given me invaluable knowledge and a large number of friends.

The Swedish Energy Agency, STEM, for funding this work.

The Department of Applied Mechanics at Chalmers for giving me the opportunity to be head of the Ph.D. student board, which has been a great experience for me and taught me a great deal about management and organization.

My additional co-authors of some of the papers. Collaborating with Dr. Mats Andersson has been very easy and fruitful. I have enjoyed the numerous, challenging hours we spent setting up and discussing optical experiments. Mr. Daniel Dahl, who shares my desire for perfection, also thoroughly deserves a mention.

Dr. Lucien Koopmans and Mr. Göran Josefsson at Volvo Cars Corporation for providing access to experimental equipment and support.

My roommate during the whole project, Mr. Henrik Salsing, who was my colleague at the beginning of the project and is now my friend. It has been a pleasure to share the office with you.

All my colleagues at the department for their contributions to making the depart-

ment a joyful place. Special thanks go out to my friends Andreas Mark, Alfhugo Magnusson, Daniel Dahl, Henrik Salsing, Jonas Edman, Johan Hjärne, Mats Andersson, Martin Eriksson and Tobias Husberg, who I was blessed to work with: you have enriched the department. Lars Jernqvist for support with electronics. Ulla Lindberg-Thieme, who is always helpful and constantly has a smile on her lips, should also not be forgotten.

A man needs a hobby that enriches his spare time and can help to clear his head. My friends at the dirt and road racing tracks are gratefully acknowledged in this respect, with special thanks to Alfred Björback, Jonas Engelbrektsson and Ingemar Johansson, it has been important for me to have this joyful, educational and challenging activity which you have helped me with.

Last but not least my girlfriend, family and friends, are gratefully acknowledged for their support during all my studies.

Nomenclature

p	Pressure	Pa
V	Volume	m^3
n	Polytropic coefficient	-
γ	Polytropic coefficient	-
κ	Adiabatic polytropic coefficient	-
c_p	Specific heat at constant pressure	$J/(kg \cdot K)$
c_v	Specific heat at constant volume	$J/(kg \cdot K)$
c_n	Polytropic specific heat	$J/(kg \cdot K)$
m	Mass	kg
R	Gas constant	$J/(kg \cdot K)$ or $J/(kg \cdot mole)$
T	Temperature	K or $^\circ C$
Q	Added heat	J
W	Thermodynamic work	J
r_C	Compression ratio	-
M	Molecular weight	$kg/kmole$
λ	Air equivalence ratio	-
St_V	Stokes number	-
τ_F	Characteristic time of the flow	s
τ_F	Momentum response time	2
μ_C	Dynamic viscosity	$Pa\ s$
D	Diameter	m
ρ	Density	kg/m^3
U	Flow field velocity	m/s
v	Particle velocity	m/s
u	Instant flow field velocity	m/s
$\bar{U}$	Averaged flow field velocity	m/s
Re	Reynolds number	-
C_D	Drag coefficient	-
t	Time	s
U_{RMS}	Root mean square fluctuation of flow velocity	m/s
Θ	Crank angle degree	CAD

Abbrevation

BMEP	Brake Mean Effective Pressure
BSFC	Brake Specific Fuel Consumption
CA10	Crank Angle when 10% of the chemical energy have been converted
CA50	Crank Angle when 50% of the chemical energy have been converted
CA90	Crank Angle when 90% of the chemical energy have been converted
CAD	Crank Angle Degree
CAI	Controlled Auto Ignition
CO_2	Carbon dioxide
CO	Carbon monoxide
DI	Direct Injection
DISI	Direct Injection Spark Ignition
EGR	Exhaust Gas Recirculation
EOI	End Of Injection
EVC	Exhaust Valve Closing
FSN	Filter Smoke Number
FTM	Fast Thermal Management
FTP75	Federal Test Procedure - test cycle
FWHM	Full Width at Half Maximum
HC	Hydrocarbon
HCCI	Homogenous Charge Compression Ignition
HCHO	Formaldehyde
HR	Heat Release
IMEP	Indicated Mean Effective Pressure
ISFC	Indicated Specific Fuel Consumption
IVC	Intake Valve Closure
IVO	Intake Valve Opening
LEV	Low Emission Vehicle
LIF	Laser Induced Fluorescence
N_2	Nitrogen
NEDC	New European Driving Cycle
NMOG	Non-Methane Organic Gases
NO_X	Nitrogen Oxides
NVH	Noise Vibration Harshness
NVO	Negative Valve Overlap
O_2	Oxygen
OH	Hydroxyl
PIV	Particle Image Velocimetry
PLIF	Planar Laser Induced Fluorescence
PM	Particulate Matter

PMEP	Pumping Mean Effective Pressure
PRF	Primary Reference Fuel
PZEV	Partially Zero Emission Vehicle
RoHR	Rate of Heat Release
SCCI	Stratified Charge Compression Ignition
SGDI	Spray Guided Direct Injection
SI	Spark Ignition
TDC	Top Dead Center

Contents

Preface

In Homogenous Charge Compression Ignition (HCCI) fuel is combusted in a different manner from modes used in current passenger cars. Instead of being combusted by conventional flame propagation it is ignited at multiple regions simultaneously since the combustion is controlled by chemical kinetics. Thus, limiting factors for conventional SI combustion, such as the lean limit for flame propagation, can be overcome since the combustion is not governed by flame propagation. Hence, dilution with EGR and/or excess air can be used to greater degrees in HCCI combustion than in SI combustion. For these reasons efficiencies similar to those of Diesel engines can be achieved using HCCI combustion, but unlike classic Diesel combustion the dilute and homogenous mixture leads to low NO_X and low soot levels. Thus, it combines the strengths of Diesel and SI combustion, but with the downside that no direct means of controlling HCCI combustion are currently available.

In the introductory chapter of this thesis the motivation for and objective of the project it is based upon are briefly described. The following chapter gives the reader background information regarding legislative limits of hazardous emissions and CO_2 emissions for passenger cars. To demonstrate that there is a need to make more efficient engines, data from present vehicles are also shown, and the drive cycles used for evaluating emissions are described. Furthermore, the piston engine is analyzed from a simplified thermodynamic perspective, to give some background information regarding concepts that are thermodynamically sound.

The third chapter describes HCCI combustion and reviews work carried out by other authors regarding HCCI in general and other control methods. Since HCCI combustion using trapped residuals by negative valve overlap aims to achieve HCCI combustion in SI combustion engines, in accordance with the project's objective, this method of HCCI combustion is separately described.

The fourth chapter provides information that was not documented in the appended papers regarding the methods and equipment used to acquire the results.

Some further analysis is also included showing that the core data have sufficient reliability to provide valid representations and thus there is at least the potential to obtain valid interpretations from the observations.

The fifth chapter highlights and summarizes the key results presented in the papers, and further investigations probing the reliability and accuracy of the conclusions drawn in the papers. Background results are also included showing that there really is a need for increased control in the low load region for an HCCI engine using NVO. In addition, background information is supplied regarding results of investigations of other approaches in which dilution is used, to allow the reader to set HCCI into perspective.

Finally, the project and the overall results obtained are briefly outlined, and each paper is summarized in the eighth chapter. References can be found in the bibliography and Papers I-VIII are attached at the end.

Andreas William Berntsson
Chalmers University of Technology, Göteborg
2009

Chapter 1

Introduction

1.1 Motivation

Homogenous Charge Compression Ignition (HCCI) combustion has been shown to reduce the fuel consumption of SI engines [1; 2]. Thus, the need to reduce the fuel consumption of SI engines to meet future legal CO_2 limits provides ample motivation to explore the possibility of achieving HCCI combustion in SI engines. There are, however, several challenges associated with this concept, the main two being the lack of control and its limited (to part loads) operational range.

1.2 Objective

The primary objective of the project this thesis is based upon was to develop a control method that combines initial flame front propagation through a stratified charge and subsequent HCCI combustion, in order to achieve control of HCCI combustion in the lower load regions for HCCI in a passenger car SI engine. The increased control should allow the minimum load possible for HCCI combustion to be decreased, and the extension of the operational range should allow fuel consumption to be reduced, since HCCI combustion is more efficient. The low NO_X emissions and high efficiency of HCCI combustion should only be marginally compromised when applying this control method. Further objectives of the project were to acquire general knowledge about HCCI combustion and (if possible) identify, explore and develop other methods to control it.

1.3 Delimitation

The proposed concept was only studied with the intention of gaining control of steady state combustion. It might be useful to apply this concept during transient operation too, but this possibility was beyond the scope of the project.

Chapter 2

Background

Ever since Karl Benz built his first automobile with a piston engine for propulsion, the *Motorwagen*, similar concepts have been further developed and produced in diverse shapes and sizes all over the globe. The use of automobiles has become deeply rooted in the core of most modern cultures and is now a key element of personal transportation. However, this mode of transportation also has some downsides; the internal combustion engine generates emissions that can be either hazardous or harmful to the environment. This fact only begun to be addressed, or at least received attention, long after the introduction of the technology. California has been a pioneer in emission legislation and has set restrictions on vehicles for several decades, but other authorities have increasingly followed suit, and some examples of emission levels can be seen in tables 2.1, 2.2 and 2.3.

2.1 Emission standards

Table 2.1: Californian emission standards for passenger cars after 100000 miles (LEV_1) and 120000 miles (LEV_2) [3], all values in g per mile measured in FTP75.

Category	NMOG	CO	NO_X	PM(for Diesel)	HCHO
$TLEV_1$	0.156	4.2	0.6	0.08	0.018
LEV_1	0.09	4.2	0.3	0.08	0.018
$ULEV_1$	0.055	2.1	0.3	0.04	0.011
LEV_2	0.09	4.2	0.07	0.01	0.018
$ULEV_2$	0.055	2.1	0.07	0.01	0.011
$SULEV_2$	0.010	1.0	0.02	0.01	0.004

Table 2.2: European emission standards for passenger cars with petrol engines [3], all values in g per km.

Category	CO	HC	HC+NO_X	NO_X	PM
EURO1	2.72	-	0.97	-	-
EURO2	2.2	-	0.5	-	-
EURO3	2.3	0.2	-	0.15	-
EURO4	1.0	0.1	-	0.08	-
EURO5	1	0.1	-	0.06	0.005 (DI)
EURO6	1	0.1	-	0.06	0.0045 (DI)

Table 2.3: European emission standards for passenger cars with Diesel engines [3], all values in g per km.

Category	CO	HC	HC+NO_X	NO_X	PM
EURO1	2.72	-	0.97	-	0.14
EURO2	1.0	-	0.7	-	0.1 (DI) 0.08 (IDI)
EURO3	0.64	-	0.56	0.5	0.05
EURO4	0.5	-	0.3	0.25	0.025
EURO5	0.5	-	0.23	0.18	0.005
EURO6	0.5	-	0.17	0.08	0.0045

From tables 2.1, 2.2 and 2.3 it can be seen that the strict modern emission limits are dramatically lower than the older ones. It is also worth noting that European emission limits for Diesel and petrol engines differ, but Californian limits are the same for both kinds of engines (except that limits are placed on particulate matter, PM, emissions from Diesel engines). It is important to bear in mind that when new combustion processes for passenger cars are developed it is essential to meet the relevant emission limits, since they are legally enforced, and it will not be possible to use new concepts that cannot meet them in passenger cars (in the respective markets). Thus, since the aim of the work underlying this thesis was to investigate a new concept for combustion that is intended for passenger car use, a brief introduction to these legal emission limits is required.

2.2 CO_2 emission legislation

In addition to the legal limits presented in tables 2.1, 2.2 and 2.3 other undesirable species are emitted from combustion engines and have been receiving increasing attention, especially carbon dioxide, which is directly connected to fuel consumption. The amount of carbon dioxide that an engine emits has become increasingly

important, especially since the legally restricted hazardous emissions have reached sufficiently low levels, in absolute terms, to make the environmental effects of carbon dioxide relatively important.

To reduce carbon dioxide levels a proposal to limit average CO_2 emissions from all newly registered cars in the EU to 130 g/km CO_2 has been made by the Commission of the European Communities [4]. The manufacturers will all have to meet individual targets, depending on the mass of the vehicles they produce, and the formula for the limit value is:

$$CO_2 = 130 + a \cdot (M - M_0) \tag{2.1}$$

where M is the average weight of the vehicles produced by the manufacturer, while M_0 and a are constants (1289 kg and 0.0457, respectively).

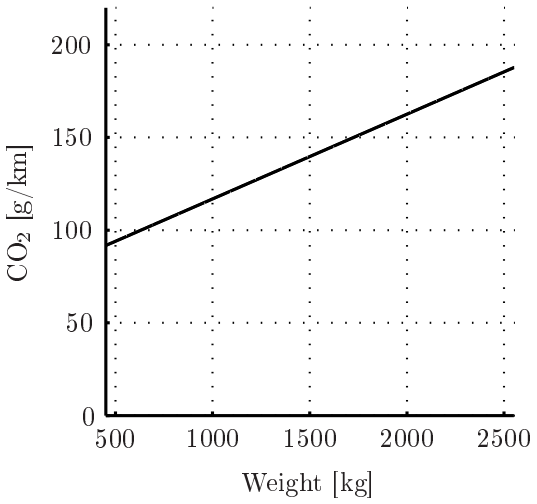

Figure 2.1: CO_2 emission limits for cars of manufacturers selling cars in the EU (from 2012) during NEDC operation versus vehicular weight.

If the value for the average car of a manufacturer is above this limit line (see figure 2.1) then an excess emissions premium will be imposed. If the value exceed the limit by more than 3 g/km then the premium is 95 € per g/km and smaller charges between 5 € and 25 € per g/km if the value exceed the target by 1 to 3 g/km. The values show that it will be costly for the manufacturers to produce and sell vehicles that generate high CO_2 emissions, and the additional costs will ultimately paid by the customer, so it will be of great importance for the manufacturers to address this issue. However, manufacturers selling less than

10 000 vehicles per year can apply for individual targets, and there is also the possibility to form a "pool" with other manufacturers to jointly meet their target. Nevertheless, there will still be a great need to reduce CO_2 emissions overall.

2.3 Engines

The vast majority of passenger cars on the market at the time of writing (2009) are powered by piston engines based on the principles defined by either Nikolaus August Otto [5] or Rudolf Diesel [6], *i.e.* petrol or Diesel engines, respectively. For petrol engines the introduction of catalysts has played a key role in enabling tailpipe emissions to be reduced to the values shown in tables 2.1 and 2.2. The combination of a three way catalyst and a lambda sensor allows the emission levels to be reduced to partial zero-emission vehicle (PZEV) levels. For example, in 2002 Volvo Cars Corporation presented a Volvo S60 capable of achieving PZEV levels [7]. The possibility of achieving such levels (and at a reasonable price) is the main strength of current Otto engines. On the other hand, Diesel engines have displayed greater efficiencies, which are seen as their main strength.

2.4 Car fleets

The work this thesis is based upon focused on techniques designed to increase the control of HCCI combustion in engines for passenger cars with the main goal of achieving lower CO_2 emissions. This section provides some background information on the passenger cars in production at the time of writing, to ascertain if there really is a need to further improve present technology. All data in this section are based on vehicles approved in Germany (in 2008) by the German motor vehicle inspection agency, TÜV [8], since the data were readily available and the models approved in Germany are representative of the models approved in Europe generally. In table 2.4 The numbers of models with various kinds of propulsion units that the analysis in this section is based on are listed in table 2.5. As can be seen, the numbers are large - with over 8000 versions in total and over 4500 models with specified weights. The models are divided into four groups: cars with Diesel engines, petrol engines with port fuel injection, petrol engines with direct injection and hybrid vehicles.

Table 2.4: Car models approved in Germany [8].

Cars	Models with weight	Models without weight
All versions	4576	8299
Diesel	1929	3334
Petrol SI	2174	4393
Petrol using DI - DISI	473	572
Hybrid	7	-

2.4.1 Vehicle weight

Emissions from the different types of passenger cars during NEDC operation and highway operation are shown in figure 2.2. The vehicular weights (for vehicles with specified weights) ranged from around 800 to 2300 kg. In the figure trend lines are plotted

$$y = ax^b + c \tag{2.2}$$

where a, b and c are fitted in the least squares sense (see equation 2.3) to the data (*xdata* and *ydata*), hence this is a representative trend line.

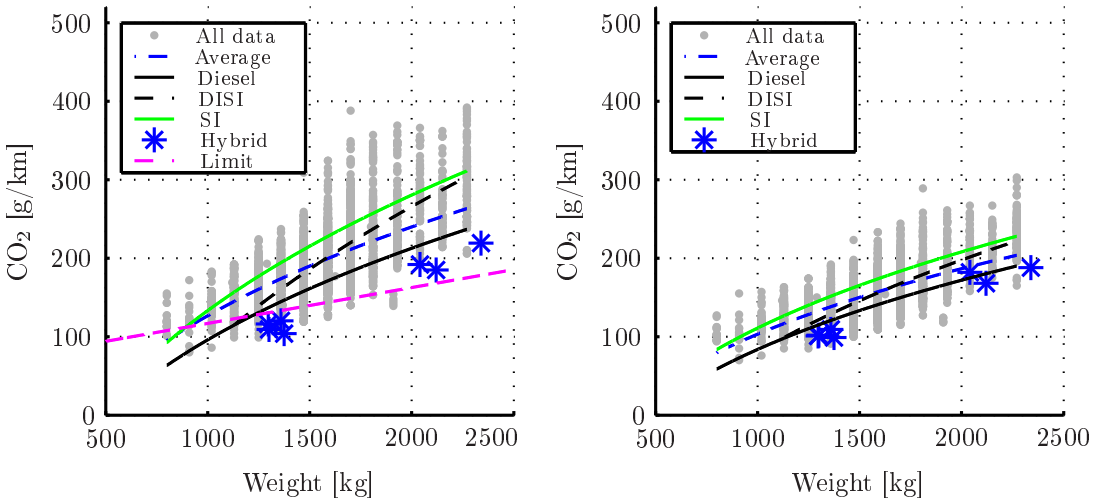

(a) (b)

Figure 2.2: CO_2 emissions during NEDC (a) and highway (b) operation of vehicles approved in Germany in 2008 versus their weight.

$$\min_{a,b,c} \frac{1}{2}|F(a,b,c,xdata) - ydata|_2^2 = \frac{1}{2}\sum_i (F(a,b,c,xdata_i) - ydata_i)^2 \qquad (2.3)$$

In both NEDC and highway operation increases in the vehicular weight have adverse effects on emissions, as can be seen in the figure since all the trend lines show an increase in CO_2 emissions with increases in vehicular weight. The average car weighing 1000 kg emits around 140 g CO_2 per km in NEDC operation, which is almost half that of the average car weighing 2000 kg. For highway operation the difference between a 1000 kg vehicle and a 2000 kg vehicle in this respect is smaller; the average larger car emits around 70 % more CO_2 in this case. In terms of engine type, it can be seen that the traditional SI engines generate the highest CO_2 emissions for a certain vehicular weight, while Diesel engines and hybrid cars generate the lowest levels. The hybrid models for which data are included in figures 2.2 (marked by stars) are listed in table 2.5. Lexus and Honda produce cars with hybrid technology in models for which traditional types of engine are also available, and data for the closest petrol models are also shown in the table.

Table 2.5: Hybrid car models and comparison.

Model	Weight [kg]	Power [kW]
Honda Civic HYBRID	1300	70
Honda Civic (Petrol)	1190	66
Honda CIVIC IMA	1297	61
Lexus GS 450 H	2120	218
Lexus RX 400 H	2040	155
Lexus LS 600 H	2340	290
Lexus LS 460 (Petrol)	1958	280
Toyota PRIUS I	1360	53
Toyota PRIUS II	1375	57

The hybrids perform well in comparison to versions of other types with similar weight. However, it should be noted that including hybrid technology increases the weight of cars, thus a direct comparison is not necessarily valid. When models for which both hybrid and conventional petrol engines are available in the same car body are compared (see table 2.5) then the mass addition associated with the hybrid technology can be estimated. The Honda Civic hybrid is around 10 % (110 kg) heavier than the traditionally powered version, and the Lexus LS is proportionally even heavier with hybrid technology. The increase in weight inevitably reduces the performance of the hybrids, but their performance is still competitive compared to the average.

When petrol engines using direct injection (DISI) are considered, it can be seen that their CO_2 emissions are consistently lower than those from average port fuel injection engines. Furthermore, it can be seen that the light DISI cars display CO_2 emissions that are similar to those of diesel engines in both NEDC and highway operation.

When the data are compared to the proposed limit values, as defined by equation 2.1, it can be seen that generally there is a need for further improvements for all types of propulsion units (see figure 2.2, where the dashed magenta line indicates the limit line).

2.4.2 Engine displacement

The first impression from the data presented in the previous section regarding vehicles on the current market is that (unsurprisingly) small, light vehicles generate less CO_2 emissions than larger, heavier vehicles. However, the weight of the vehicle cannot be the only parameter responsible for the differences in this respect between vehicles, since different sizes of vehicles may also be associated with other characteristics, such as demands for performance and engine displa-

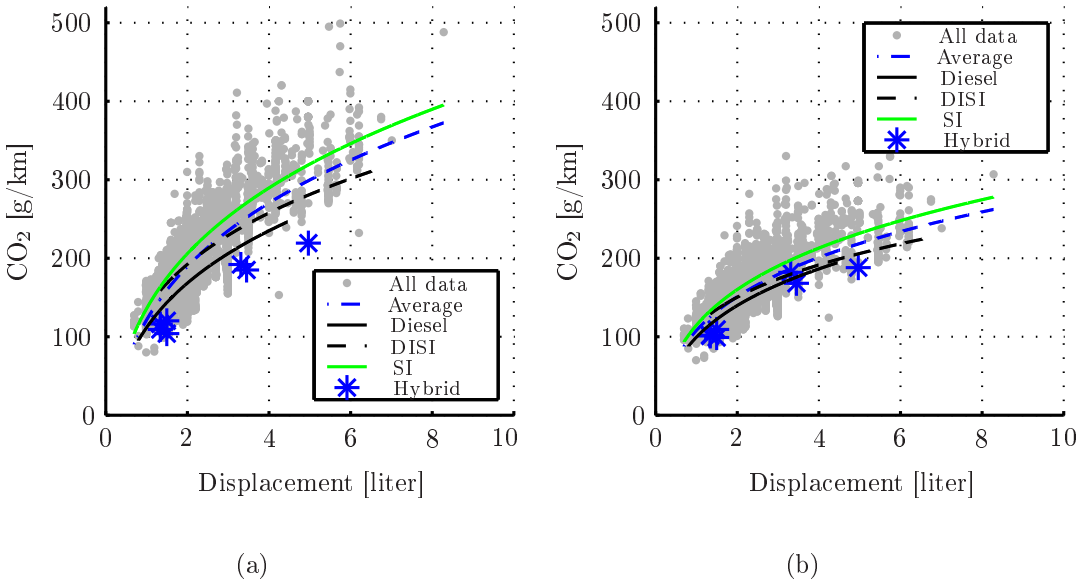

Figure 2.3: CO_2 emissions during NEDC (a) and highway (b) operation of vehicles approved in Germany in 2008 versus their engine displacement.

cement. Indeed, many parameters change with differences in vehicle sizes. In figure 2.3 CO_2 emissions in NEDC and highway operation are plotted against vehicles' engine displacements. The apparent trend is for fuel consumption to increase as displacement increases, for vehicles with all types of engine. However, there are differences in the range of displacement of the different types, and the port fuel injection petrol engines show the greatest range (from 0.7 to 8.3 liter displacements). For a given displacement the port fuel injection SI engines show the greatest CO_2 emissions in NEDC operation and the Diesel and hybrid vehicles the lowest values. This trend is also apparent in highway operation, but with smaller differences (and for vehicles with larger engines there is almost no difference in this parameter between the Diesel, DISI and hybrids).

2.4.3 Engine power

In figure 2.4 the CO_2 emissions of vehicles with different kinds of propulsion plant are plotted against their power. The range of power is greatest for the SI engines, some models with petrol engines have almost twice the power of all Diesel engines, and an obvious trend is that the greater the power the greater the CO_2 emissions. Between 150 and 300 kW the CO_2 emissions from hybrid

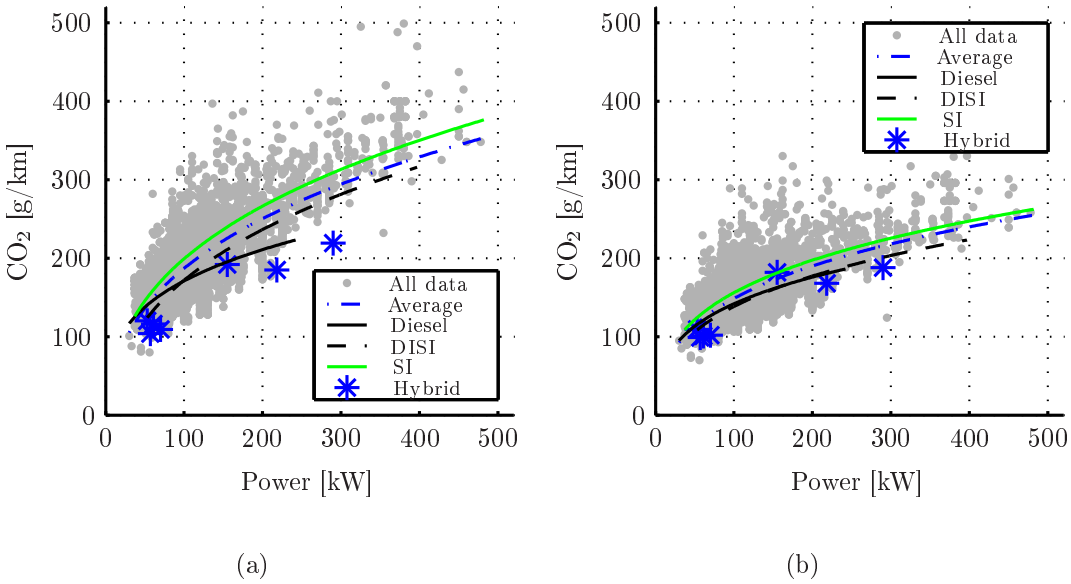

Figure 2.4: CO_2 emissions in NEDC (a) and highway (b) operation of vehicles approved in Germany in 2008 versus their power.

and diesel engines are the lowest in NEDC operation, but under 100 kW DISI and hybrid engines show the lowest values. For highway operation the DISI and diesel engines show very similar trends and for low power vehicles there are only modest differences in emissions between all the different engine types. As for the vehicle weight, the effect of power on emissions cannot be completely separated from other factors since it too is related to other parameters, for instance a larger vehicle will probably have a larger engine with more power.

2.4.4 Performance

The weight to power ratio can be associated with the acceleration performance of a vehicle. A rule of thumb (found by the author's father) is that a vehicle can accelerate from standstill to 100 km/h by slightly over the ratio in seconds between its weight to power in kg per unit horsepower, thus a low weight to power ratio leads to greater performance. The CO_2 emissions of vehicles with different weight to power ratios can be seen in figure 2.5. For low performance vehicles ($>$ 17 kg/kW, corresponding to acceleration from 0 to 100 km/h in $>$ 13 seconds) the hybrids show the lowest CO_2 emissions and the diesel and DISI engines show similar emission levels in both NEDC and highway operation. For medium per-

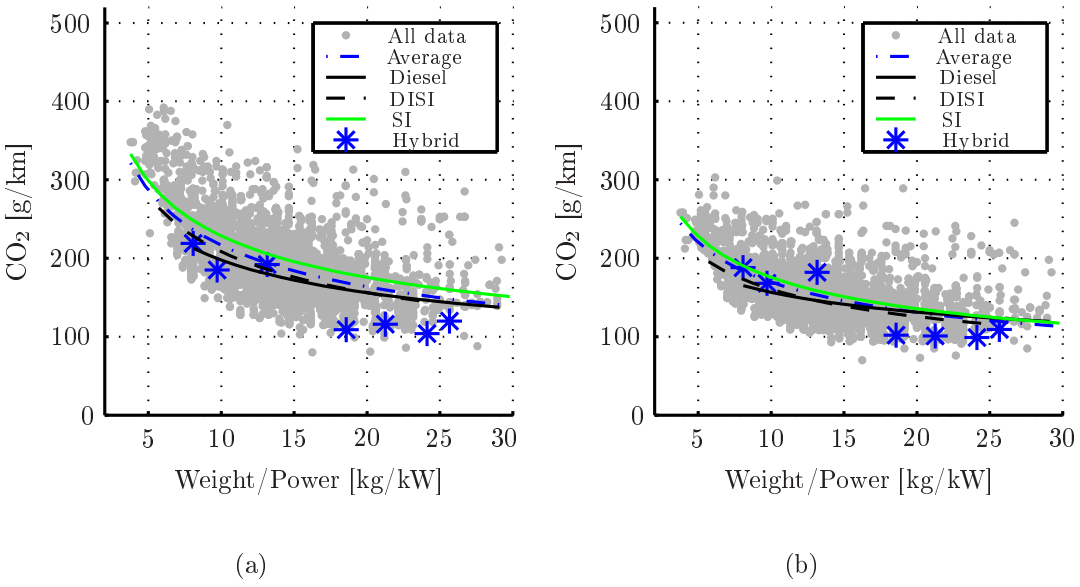

Figure 2.5: CO_2 emissions for NEDC (a) and highway (b) operation of vehicles approved in Germany in 2008 versus their weight to power ratios.

formance vehicles (8-17 kg/kW), the DISI and diesel vehicles show more or less identical values for highway operation and the values are lower than those of the hybrids. For high-performance vehicles only petrol engines are available and for those the DISI versions generate the lowest CO_2 emissions.

2.4.5 Weight and displacement

As mentioned above, it is difficult to separate the parameters that influence CO_2 emissions. Large, heavy vehicles are likely to have larger, more powerful engines than small, light cars, all of which contribute to increases in CO_2 emissions. To shed more light on parameters of current vehicles that lead to high CO_2 emissions, the vehicles' emissions are plotted against their weight to displacement ratios in figure 2.6. A low ratio will correspond to a vehicle that has a large engine relative to its weight and vice versa for high ratios. In NEDC operation this ratio appears to be significant, but the difference between the different kinds of engine in this respect are relatively small, although the Diesel and low-performance hybrids seem to be somewhat better than the alternatives for a specific ratio. In highway operation the differences between the different types of engine are even smaller,

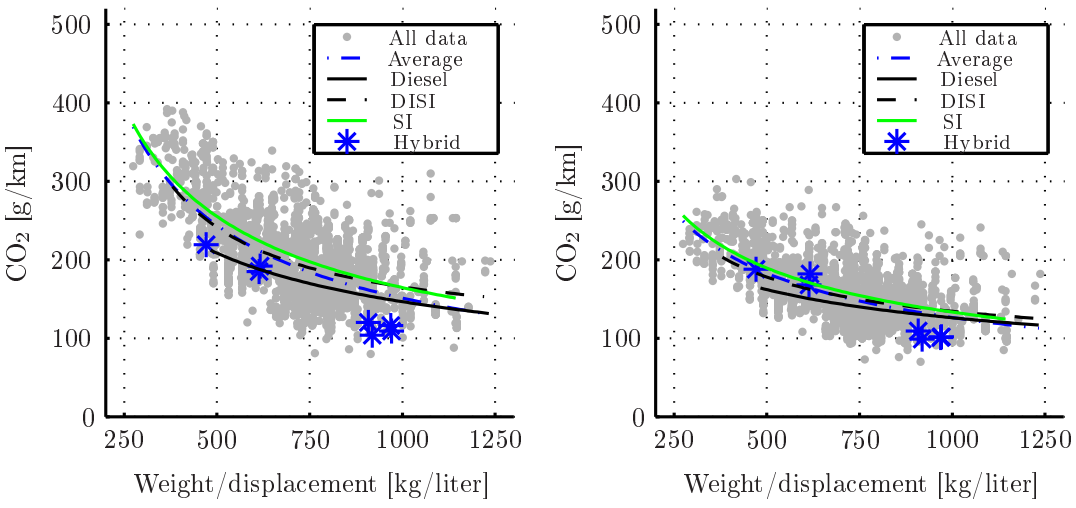

Figure 2.6: CO_2 emissions from vehicles in NEDC (a) and highway (b) operation of vehicles approved in Germany in 2008 versus their power versus their weight to displacement ratios.

and little can be said about which type is most favorable, but the main trend is that a low weight to displacement ratio results in higher CO_2 emissions.

2.4.6 Discussion - Car fleet

When currently produced passenger car models were studied, as in this section, no parameter could be completely separated and evaluated since they are connected to each other in a complex manner. The lighter vehicles are more competitive in terms of CO_2, but exactly how much of the emissions are connected solely to the vehicular weight is challenging to determine accurately. How much of the reduction was due to lower power or smaller engine displacement has not been precisely determined. However, from the trends the following generalized conclusion can be drawn; a light vehicle will generate less CO_2 emissions than a large car, especially if it has a small, low-powered engine, so the customer's choice will make a substantial difference.

In the attempt to separate the different kinds of propulsion unit it is difficult to draw any conclusions with statistical significance. At first glance the Diesel engines and hybrids appear to be most suitable. For a certain weight and displacement they display lower levels of CO_2 emissions during NEDC operation. So, if this is the main criterion for selection, then assuming that a customer wants to buy a vehicle of a certain size and displacement (variables that are related to the vehicle's weight) then a vehicle with a Diesel or hybrid engine would be the right choice. However, if the additional weight and price of hybrids are taken into account then the conclusion might be different. If the criterion for selection is to meet certain performance specifications in terms of acceleration, which is associated with the weight to power ratio, then the different propulsion units are more equal, especially for vehicles that are operated mainly on highways. However, obviously there are models with high-performance, large, powerful SI engines and if a customer chooses any of these versions the average CO_2 emissions for the fleet will be increased. Furthermore, SI engines have consistently shown higher CO_2 emissions and thus (despite the spread in the data) they probably need to be improved more than the other types of engines. So, there is a need for research aiming for further improvement of SI engines.

One factor that should be kept in mind when comparing the results from hybrids to other kinds of vehicles is the influence of start/stop technology. During standstill, unlike many other kinds of vehicles, the hybrids can leave the combustion engine off. However, this difference will disappear in the near future, since many car suppliers have announced that technology allowing the engine to be turned off

during standstill will soon be available for most cars. This will lead to reductions in differences between different types of engines in the future (similarly to the less competitive results achieved by the hybrids during highway operation, in which this start/stop technology plays no role).

2.5 Drive cycles

Vehicle owners' drive patterns naturally vary greatly, depending on numerous variables. However, in evaluations of passenger cars' fuel consumption and emissions two standard drive cycles are often used.

2.5.1 NEDC

For the European market the New European Driving Cycle, NEDC, is used in assessments of the fuel consumption and emissions of light duty vehicles on a chassis dynamometer [9]. A brief summary of the NEDC can be found in table 2.6.

Table 2.6: NEDC data.

Characteristics	Value
Distance [km]	11
Duration [s]	1180
Average speed [km/h]	33.5
Vehicle start temperature [°C]	20

The cycle consists of four repeated urban sections (ECE15) followed by an urban section (EUDC). The torque needed (for a certain gear ratio) to perform this cycle (and FTP75) can be seen in figure 2.7, based on geometry and weight corresponding to a large passenger vehicle using an engine with 3 liter displacement. The dashed green lines corresponds to constant power, where 5, 10 and 15 kW lines is shown. Generally, the power needed is relatively low and with the gearing in this example the load is mainly below 4 bar BMEP. The average power for the cycle is below 5 kW, thus for most (if not all) vehicles the powertrain is operated at low loads during this cycle, making their part load efficiency important.

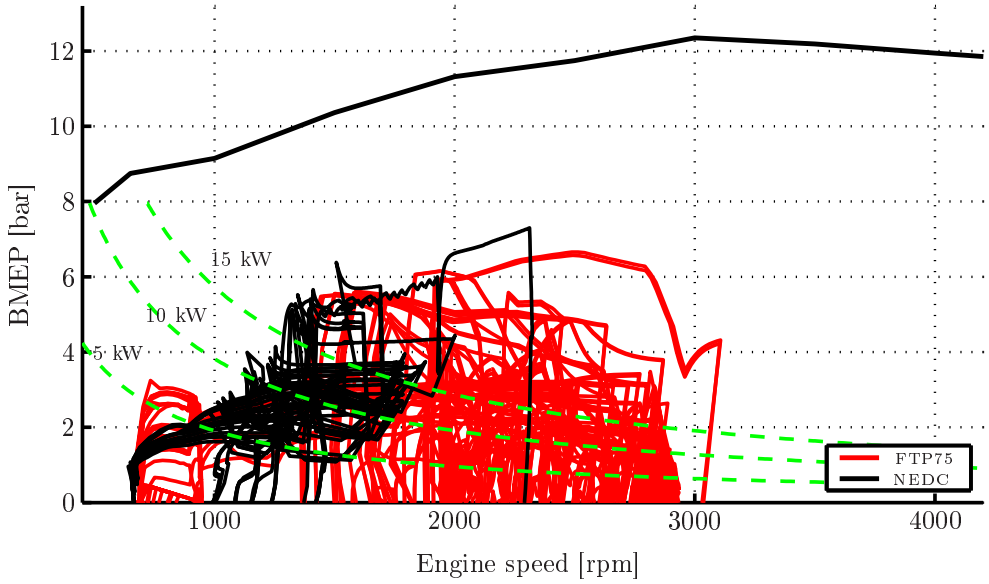

Figure 2.7: Examples of BMEP and engine speed for NEDC (black line) and FTP75 (blue line) operation, for a vehicle with a manual gearbox and 3 liter engine displacement. The 3 dashed lines corresponds to 5, 10 and 15 kW of power.

2.5.2 FTP75

For the American market a different test cycle is used: the Federal Test Procedure 75 (FTP75). The vehicle speeds during FTP75 are similar to those in the NEDC, but with a significant difference in gradients. The average speed for the complete cycle is around 34 km/h. Due to the greater gradients in velocity the power required is higher, and the average power needed for the complete cycle is slightly more than 6 kW for a vehicle that would require 5 kW during NEDC operation. However, the power needed for FTP75 operation is still low in absolute terms, making low load performance highly important, this can be seen in figure 2.7.

In both the FTP75 and NEDC cycles the vehicle spends considerable amounts of time at standstill, thus there is potential for reducing fuel consumption if the engine is stopped when the vehicle is at standstill. Technology allowing this was introduced in 1998 by Volkswagen in their Lupo 3l [10], and many manufacturers have announced intentions to use similar technologies in the near future.

2.6 Thermodynamics

A simplified thermodynamic model of a reciprocating engine was constructed with the intention to mathematically evaluate the effects of various parameters (since the effects of many parameters cannot be separated in a real engine and, hence, it can be difficult to ascertain if certain parameters have any effects or not). It should be noted that the model was constructed by the simplest of methods and does not accurately describe reality, but the intention was merely to facilitate identification of possible reasons for any differences that may appear in measurements.

2.6.1 Polytropic Behavior

In a four-stroke cycle engine one revolution is used for compression and expansion and one for gas exchange. During the compression and expansion strokes the volume inside the cylinder is enclosed and during the gas exchange strokes valves allow the fluid to exit or enter the cylinder. During the period when the volume inside the cylinder is enclosed, the changes in volume lead to pressure changes, and a polytropic function is commonly used to describe the relationship between the pressure and volume [11; 12; 13; 14].

$$pV^n = constant \tag{2.4}$$

where p is the in-cylinder pressure, V is the volume and n is the polytropic coefficient. If the process is completely adiabatic then the polytropic coefficient will be κ [15].

$$\kappa = \frac{c_p}{c_v} \tag{2.5}$$

where c_v is the specific heat at constant volume and c_p is the specific heat at constant pressure for the fluid inside the cylinder under the specific conditions. However, the polytropic coefficient is usually lower than κ since the process is not completely adiabatic. When this polytropic relationship is combined with the assumption that the enclosed gases will behave in accordance with the ideal gas law [16]

$$pV = mRT \tag{2.6}$$

where m is the in-cylinder mass of the fluid, R its gas constant and T the temperature, then the temperature can be described as a function of the in-cylinder pressure, as:

$$\frac{T}{p^{\frac{n-1}{n}}} = constant \tag{2.7}$$

Using this expression a pressure and temperature trace can be calculated from the volume. In order to deliver mechanical work, an internal combustion engine must combust some fuel inside the cylinder or combustion chamber. During the combustion chemically bound energy in the fuel is converted to heat in the fluid in the combustion chamber. This heat influences the pressure inside the enclosed combustion chamber and the thermodynamic work achieved can be converted to mechanical work by using the piston motion. The addition of heat to the fluid will be a direct consequence of the combustion if adiabatic conditions are assumed. Here the combustion is simulated as pure addition of heat to an ideal gas as

$$Q = mc_n\Delta T \tag{2.8}$$

is the amount of heat added, m is the mass of the fluid, ΔT the resulting temperature increase and c_n the polytropic specific heat [15] which is defined as

$$c_n = -c_v\frac{\kappa - n}{n - 1} \tag{2.9}$$

To replicate the behavior of combustion this added heat will be added over a defined period of time and with varying intensity, as indicated by the example in

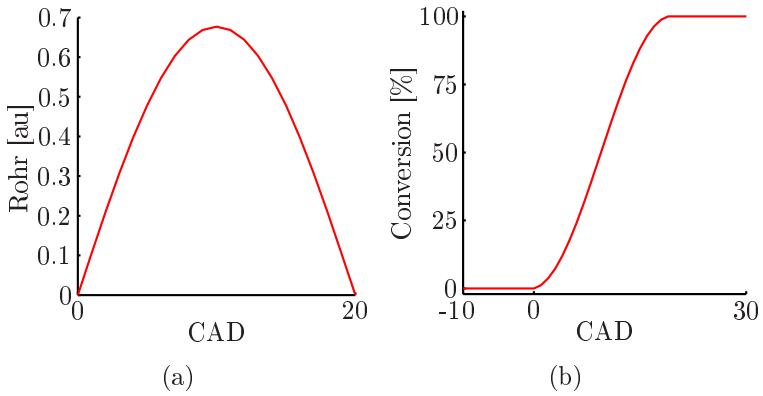

Figure 2.8: The chosen rate of heat release as a function of CAD (a) and the equivalent conversion of the chemical energy to heat (b).

figure 2.8, in which heat is added at the rate illustrated in figure 2.8(a), starting from TDC for a duration of 20 CAD.

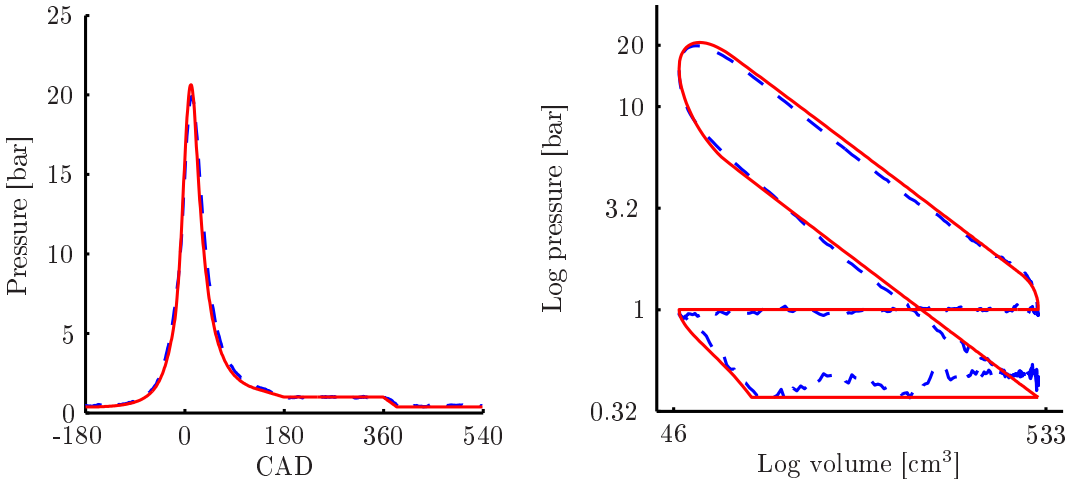

Figure 2.9: Averaged in-cylinder pressure (dashed blue line) in a six-cylinder SI engine during combustion throttled to 0.46 bar and the calculated polytropic pressure (solid red line) for the same intake pressure as a function of CAD (a) and logarithmic pressure as a function of logarithmic volume (b).

In figure 2.9 and table 2.7 results obtained from real measurements and the simplified polytropic model can be seen. Even with this basic polytropic approach, the combustion of a real cycle in an engine can be replicated with reasonable accuracy. Even the gas exchange phase is represented reasonably well, despite the crudity of the approach, and realistic valve events can be used. However, the effect of the oscillating pressure during the intake stroke is lost to some extent in this simple model and the pump losses are thus slightly over-predicted, as indicated in table 2.7. This model has been used to estimate the effects of various changes in parameters (compared to the measured cases) on the thermodynamic work, W, which is the enclosed integral of the pressure, p, and volume, V,

$$W = \oint pdV \tag{2.10}$$

i.e. the area enclosed by the pressure in figure 2.9(b).

Table 2.7: Parameters for the measured and calculated pressure trace.

Parameter	Measured	Polytropic
Torque [Nm]	50	-
Engine speed [rpm]	1500	-
IMEP [bar]	2.52	2.52
PMEP [bar]	0.52	0.62
Intake pressure [bar]	0.46	0.46
Exhaust pressure [bar]	1.01	1.01
Start of combustion [CAD]	-	-20
Combustion duration [CAD]	-	40
n during compression	-	1.28
n during expansion	-	1.25
Exhaust valve opening [CAD]	130	130
Exhaust valve closing [CAD]	380	380
Intake valve opening [CAD]	350	360
Intake valve closing [CAD]	620	620

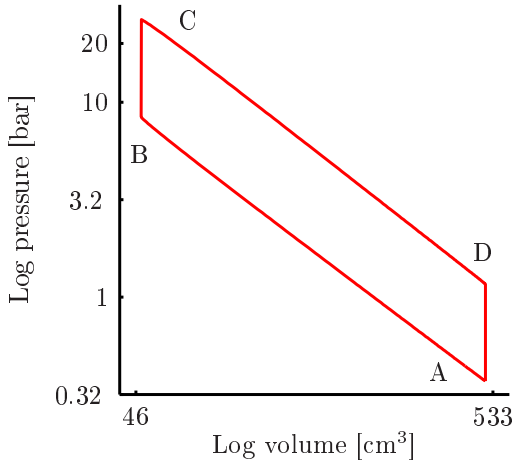

Figure 2.10: Schematic diagram of logarithmic pressure as a function of logarithmic volume.

2.6.2 Polytropic isochoric behavior

Here the scenario is simplified even further merely to highlight the main parameters that influence the thermodynamic work. If the compression and expansion are assumed to be polytropic and reversible, for an ideal gas with a constant polytropic coefficient, and the addition of heat occurs under isochoric conditions, then an artificial cycle as illustrated in figure 2.10 can provide an adequate re-

presentation. Here, A, B, C and D represent the conditions prior to compression, after compression, after addition of heat and after expansion, respectively. Since the addition and subtraction of heat occur under isochoric conditions (at constant volume) the volume V can be described at each point as

$$V_A = V_D \quad , \quad V_B = V_C \quad and \quad \frac{V_A}{V_B} = r_C \tag{2.11}$$

so all volumes can be described by the displacement of the "engine" and its compression ratio, r_C. The thermodynamic work, W, as defined in equation 2.10, can be simplified as

$$W = \frac{p_A V_A - p_B V_B + p_C V_C - p_D V_D}{n-1} \tag{2.12}$$

for this isochoric situation. The conditions at point B will be inherited from the conditions at point A since the process is polytropic. From equation 2.4 and 2.11 the conditions at point B can be determined as

$$p_B = p_A r_C^n \quad and \quad T_B = T_A r_C^{n-1} \tag{2.13}$$

Equation 2.8 describes heat addition under polytropic conditions, and for isochoric heat addition the specific heat will be the specific heat under constant volume instead, c_V. So the conditions at point C can be described by the conditions from the previous point as

$$T_C = T_B + \frac{Q}{mc_V} \quad and \quad p_C = \frac{T_C}{T_B} p_B \tag{2.14}$$

The conditions at point D can be described by polytropic expansion of the conditions at point C to

$$p_D = \frac{p_C}{r_C^n} \tag{2.15}$$

With this expression, all points are described by the conditions from the previous point, so if the information from equation 2.13 is used in 2.14 and then in 2.15 all points can be described, based on the conditions at point A. If this is then used in equation 2.12 and simplified the thermodynamic work, W, can be expressed as

$$W = \frac{p_A Q V_A (1 - r_C^{1-n})}{mc_V T_A (n-1)} \tag{2.16}$$

The mass will vary, depending on how the engine is ventilated, but if the simplest approach is used, which assumes a volumetric efficiency of unity and ideal gas, then the mass can be defined as in equation 2.17

$$m = \frac{p_A V}{R T_A} \tag{2.17}$$

then equation 2.16 can be reduced to:

$$W = \frac{RQ(1 - r_C^{1-n})}{c_V(n-1)} \tag{2.18}$$

From equation 2.18 it can be noted, in addition to the obvious feature that the added heat is proportional to the work, that the effect of the compression ratio will depend on the polytropic coefficient. Since the combustion occurs under isochoric conditions the thermodynamic work will be inversely proportional to the specific heat for constant volume, hence reducing c_V will lead to increased work. Furthermore, the properties of the medium pumped also influence the work achieved since it is proportional to the gas constant for the medium, which depends on the molecular weight of the medium (for instance the gas constant of a stoichiometric fuel/air mixture with iso-octane is about 5 % lower than that of air, and the gas constant of the exhaust gas is around 1 % higher than that of air). See the properties of the gases in table 2.8.

Table 2.8: Properties of some gases [12].

Gas	Specific heat at constant pressure c_p [J/kgK]	Molecular weight M [kg/kmole]	Gas constant R [J/kgK]
C_8H_{18}	1590	114	73
N_2	1047	28	297
O_2	913	32	260
CO_2	909	48	189
H_2O	1000	18	462

Equations 2.19 to 2.21 express combustion of: a stoichiometric mixture of iso-octane and air, a mixture of iso-octane and air with 50 % excess air (lean combustion), and a stoichiometric mixture of iso-octane and air with 30% dilution by exhaust gases (combustion with EGR), respectively.

$$C_8H_{18} + 12.5(3.77N_2 + O_2) \longrightarrow 9H_2O + 8CO_2 + 47N_2 \tag{2.19}$$

$$C_8H_{18} + 18.75(3.77N_2 + O_2) \longrightarrow 9H_2O + 8CO_2 + 71N_2 + 12.5O_2 \tag{2.20}$$

$$C_8H_{18}+12.5(3.77N_2+O_2)+2.4CO_2+2.7H_2O+14N_2 \longrightarrow 11.7H_2O+10.4CO_2+61N_2 \quad (2.21)$$

Table 2.9: Properties of the gases before (indexed A) and after combustion (indexed B) for the cases in equations 2.19 to 2.21.

Case	R_A [J/kgK]	$c_{p,A}$ [J/kgK]	$c_{v,A}$ [J/kgK]	R_B [J/kgK]	$c_{p,B}$ [J/kgK]	$c_{v,B}$ [J/kgK]
Stoichiometric (eq. 2.19)	275	1052	777	291	1092	801
Lean (eq. 2.20)	279	1040	761	289	1065	776
EGR (eq. 2.21)	280	1061	781	291	1092	801

In table 2.9 the properties before and after combustion can be seen for the three cases described in equations 2.19 to 2.21. After combustion the gas constants for the mixtures are more or less identical for the three cases. However, prior to combustion the gas constant in the stoichiometric case is lower than in both the lean and EGR cases. In addition, the specific heat at constant volume and the specific heat at constant pressure is lower for the lean case.

2.6.3 Discussion - Thermodynamics

From equation 2.18 it was noted that the thermodynamic work is proportional to the gas constant. For instance, iso-octane fuel vapor has a significantly higher molecular weight than air, so if an over-stoichiometric medium (with excess air) was pumped then the average molecular weight would be lower than that of a stoichiometric medium. This would lead to an increased gas constant for the medium, thus contributing to an increase in the thermodynamic work. Hence, techniques that allow the engine to be operated lean appear to be beneficial in this respect. Dilution with air leads to lean operation, but dilution with exhaust gases is another scenario that does not lead to lean operation. The gas constant for the exhaust gases from a stoichiometric iso-octane and air mixture is also significantly lower than that of the gases in an unburned stoichiometric iso-octane and air mixture. By adding exhaust gases to the mixture of air and iso-octane vapor the average molecular weight will be reduced, leading to increased thermodynamic work, similar to dilution with air. Hence, a combustion concept that involves dilute operation, using either air or exhaust gases, will have inherent features that could increase the thermodynamic work. The differences in gas constant resulting from dilution by air and exhaust gases can be seen in table 2.9. In equation 2.18 it can also be noted that the thermodynamic work is inversely

proportional to the specific heat at constant volume, so in addition to a high value for the gas constant a low value of c_v is beneficial. The stoichiometric cases with and without EGR display similar values for c_v, and identical values after combustion since the constituent components and relative ratios are the same. However, the value for c_v both prior and after combustion is significantly lower for the case with excess air. This indicates that there is additional potential for increasing the thermodynamic work if excess air is introduced. However, it should be noted that the values in table 2.9 are calculated from values under ambient conditions. More realistically, these would change with time due to changes in pressure and temperature, but the intention here is merely to identify ways that could increase thermodynamic work rather than determine any absolute value.

2.7 Conclusions

For the main passenger car markets there are strict emission standards dictating maximum levels of hazardous species that can be emitted, and there are also limit values for CO_2 emissions. The levels set for CO_2 emissions for the European market are strict, and manufacturers of vehicles emitting more than the limit values will be penalized with emission premiums. Data from the present car fleet indicate that some models emit CO_2 levels that exceed the limits, various factors influence the CO_2 emissions and the customer's choice influence them to a great extent. Further, only a very limited proportion of models currently meet emission limits that will be introduced in the near future, so generally a significant improvement is required. SI engines appear to need the most improvement and their continued production is motivated by their ability to meet the stringiest emission levels, so research aiming to increase the efficiency of SI engines is required, and this is the main objective of the project this thesis is based upon.

The emission levels and fuel consumption are measured during operation in standardized drive cycles, with low average vehicle speeds, and even for relatively large vehicles only small amounts of power are needed to perform the cycle, especially the European cycle. Hence, part-load efficiency important for meeting CO_2 emission requirements. So, even if HCCI is limited to part load it may play an important role, since the drive cycles mainly involve part load operation.

A thermodynamic mathematical model was created to allow mathematical evaluation of different parameters for an artificial engine, and it was shown that the model could be used to replicate empirically determined pressure traces with only minor discrepancies. An analytical expression was also derived for the thermo-

dynamic work obtained from combustion under isochoric conditions. From this analytical expression it was shown that it makes sense thermodynamically to use dilution. Dilution with either EGR or air was identified as measures that could potentially lead to increased thermodynamic work. So, from this perspective one way to reduce the CO_2 emissions from passenger cars could be to apply concepts using dilution, such as HCCI, since increasing the thermodynamic efficiency will increase the overall efficiency of the engine.

Chapter 3

HCCI engines

3.1 Principle

In an HCCI engine a homogenous air/fuel mixture is compressed to auto-ignition. If the conditions within the combustion chamber are homogenous in terms of pressure, temperature and equivalence ratio (which is not the case in a real engine), all the mixture within the combustion chamber will ignite at the same time, and the combustion will be controlled by chemical kinetics [1; 17]. The temperature and pressure of the mixture will increase during the compression stroke, giving rise to a certain ignition delay and if this ignition delay is sufficiently short to prevent the mixture expanding and cooling during the expansion stroke the mixture will ignite, see figure 3.1.

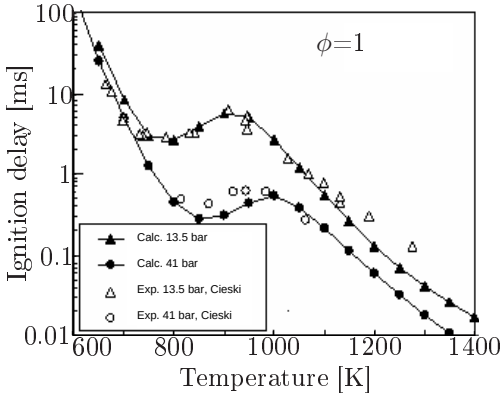

Figure 3.1: Calculated and measured ignition delays for stoichiometric n-heptane/air mixtures.

The temperature and mixture will not be completely homogenous within the combustion chamber, so the combustion will start at certain spatial locations where the conditions are most favorable for auto-ignition, for instance hot spots near the exhaust valves or in rich regions. If the combustion occurred within the whole combustion chamber and all the fuel combusted simultaneously the pressure rise would be excessively steep and the peak pressure would be too high. Fortunately, this will not occur in practice and the fuel will be combusted during a short period of time rather than instantaneously, see figure 3.2. However, the high rates of heat release associated with HCCI combustion can lead to problems with higher than optimal pressures and noise.

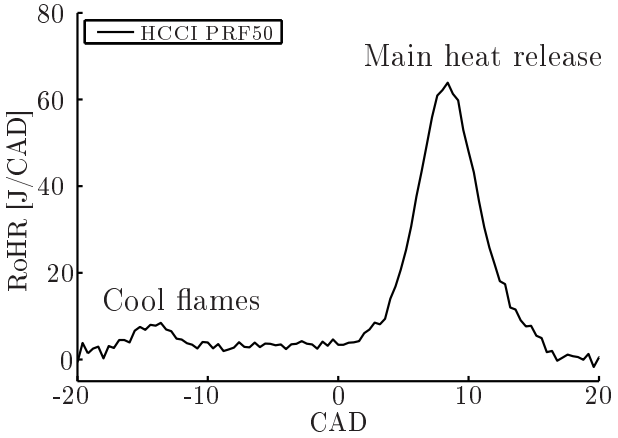

Figure 3.2: Illustrative rate of heat release (RoHR) trace of an HCCI combustion of PRF50.

3.2 Emissions

The production of nitrogen oxides, NO_X, is strongly dependent on temperature [11]. If the temperature can be kept low only small amounts of NO_X will be produced. The HCCI engine normally operates with a diluted mixture, leading to more mass being introduced to the combustion chamber than in throttled SI operation with stoichiometric mixtures, and thus temperature increases are lower since more molecules are exposed to equal amounts of energy. In diesel engines, which also operate under globally lean conditions, diffusion combustion occurs around the spray *i.e.* the flames develop in regions with rich conditions and consequently flame temperatures are high. In HCCI engines the reaction zone is spatially larger than in a comparable diesel engine. These differences give the HCCI combustion a real advantage over "traditional" combustion modes. A disadvantage of the SI engine is that the combustion is initiated prior to TDC

by a flame propagating during compression, leading to high temperatures that are major contributors to NO_X emissions. This tendency is not present in a HCCI engine, since the combustion duration is short, providing scope to phase the combustion in such a way that the main heat release occurs after TDC.

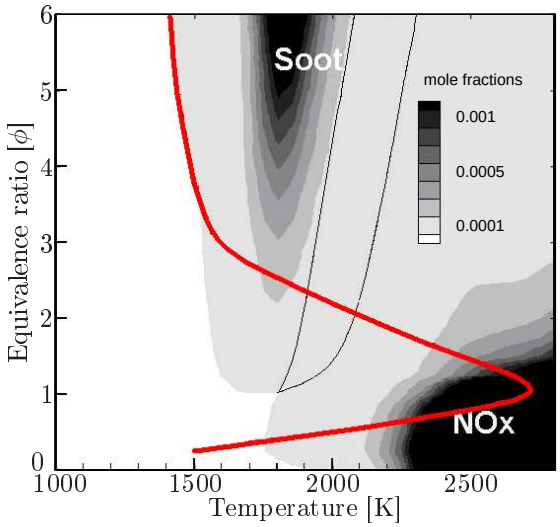

Figure 3.3: Mole fractions of NO_X and soot as functions of temperature and equivalence ratio for a mixture of Diesel fuel ($C_{14}H_{28}$) and air. Courtesy of Valeri Golovitchev [18].

Soot or particulate matter, PM, is produced in rich regions, notably in diesel engines with diffusion combustion, see figure 3.3, however soot production can also occur in direct injected SI engines due to inadequate mixing. If the mixture is more or less homogenous and lean there will be virtually no soot production, thus HCCI combustion is in many cases considered soot-free.

Unburned hydrocarbon (HC) emissions occur when some of the fuel is not combusted [11]. There are various causes of this, such as rich mixtures with insufficient oxygen for the hydrocarbon fuel to create carbon dioxide, quenching near cool cylinder walls or crevices, oil films, liquid fuel on walls, partial burns or misfiring. In HCCI combustion the mixture within the combustion chamber is more or less homogenous, so the mixture reaches the cool cylinder walls as well as the crevices between the piston top and the top of the piston rings. This, in combination with the lean mixture, which requires more heat to combust compared to a stoichiometric mixture, can result in decreased combustion efficiency and some of the fuel leaving the combustion chamber unburned. In addition, the cylinder wall cools the mixture in a boundary layer beside it to such an extent that it fails to ignite during the combustion cycle and thus quenches combustion. The depth of this layer and the proportion of the mixture that is quenched both increase as the leanness of the mixture increases.

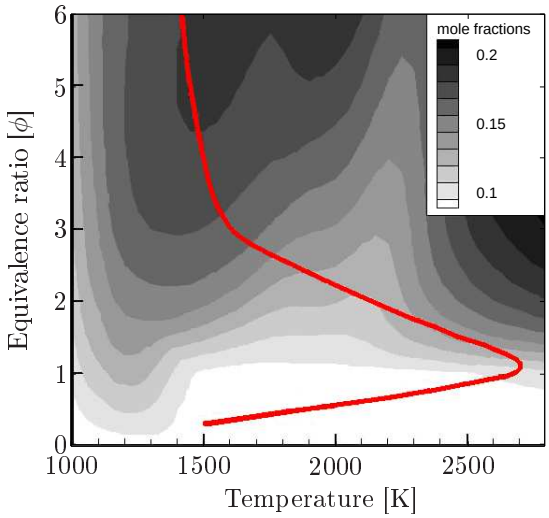

Figure 3.4: Mole fractions of CO as a function of temperature and equivalence ratio for a mixture of Diesel fuel ($C_{14}H_{28}$) and air. Courtesy of Valeri Golovitchev [18].

Carbon monoxide (CO) formation is normally strongly dependent on the mixture's equivalence ratio, see figure 3.4. Operation during rich conditions, for instance during full load in SI engines, leads to large amounts of CO being generated. A standard diesel engine operates with globally lean conditions and the CO emissions are generally low [11]. However, in cases with lean mixture and low temperature, such as in diesel engines operated with high amounts of exhaust gas recirculation (EGR) or in HCCI combustion, significant amounts of CO formation are formed. This is because low temperature, below 1500 K [19], leads to the generation of too few OH radicals to oxidize all the CO to CO_2.

3.3 Challenging areas

The HCCI engine differs from traditional SI and diesel engines in terms of combustion control, because after the inlet valve is closed there is no direct means to control the combustion; when the pressure and temperature reach a certain level the combustion starts. In SI engines the spark timing provides a direct means for controlling the combustion and in diesel engines the fuel is injected into an environment in which the temperature and pressure exceed requirements for combustion to start. The lack of control over HCCI combustion is recognized as one of its three main challenges, the others being its limited operating range and NVH (Noise Vibration and Harshness) issues.

The timing of the HCCI combustion is a crucial parameter that the engine manufacturer needs to develop means to control before HCCI engines can be commercially produced. The CA50 timing can be considered an indicator of the combustion phasing [11].

HCCI combustion has a limited operating range [2; 20]. The upper load limit is restricted by noise emissions due to rapid increases of pressure during short periods of time, in comparison to the time needed for pressure relaxation, leading to ringing or knock, and by excessive rates of heat release and high peak cylinder pressures. The lower load limit is limited by cycle-to-cycle variations, the lateness of combustion phasing and combustion efficiency both declining as the load decreases, with consequent increases in HC and CO emissions since the thermal environment is inadequate for HCCI combustion.

HCCI combustion is controlled by chemical kinetics [1; 17], so slight changes in temperature, pressure or mixture will all affect the combustion process. When an engine is operated in HCCI mode and the load is varied it will need significant time to stabilize since the cylinder wall, valves and piston must thermally equilibrate and the gas exchange must stabilize at the changed load in order to stabilize the HCCI combustion. There is a need to control the ignition timing for HCCI [21]. Since the HCCI process is more sensitive to the conditions within the cylinder than either SI or traditional CI combustion. Thus, there is a clear need for a control system that can influence the HCCI combustion over short time scales to make HCCI combustion engines commercially viable.

3.4 Control methods

Key aims of the project this thesis is based upon were to explore and develop means to control HCCI combustion, and in this section some potential control methods found in the scientific literature are briefly discussed.

3.4.1 Temperature

The ignition delay is highly dependent on the mixture temperature [22], so a straightforward way of phasing the combustion is to adjust the inlet air temperature. A further advantage of this approach is that the surrounding air is used to cool the internal combustion engine in a road vehicle, so large amounts of thermal energy are wasted that could be used for this purpose. However, exploiting this

energy in practice is not straightforward since heaters with high thermal inertia will not be able to make adjustments sufficiently quickly to compensate for rapid changes in load. Several authors [23; 24; 25; 26; 27] have heated the incoming air to influence the combustion, and a so-called "fast thermal management", FTM, system has also been applied [28]. Alternatives to inlet heaters designed to increase charge temperatures (and thus phase the combustion) by controlling the coolant temperature have also been proposed [29]. This approach has the advantage that it only requires minor modifications to a production engine and could be used in combination with a control method that provides more rapid responses. The thermal energy in the exhaust gases can also be recycled to influence the mixture temperature, as discussed in a separate paragraph.

3.4.2 Compression

The temperature needed for autoignition decreases as the pressure increases [22], and even though an internal combustion engine is not adiabatic the compression stroke will of course give rise to increases in both pressure and temperature, so varying geometric compression ratio provides a powerful way of controlling the combustion, since both temperature and pressure are affected. The transient responses of this control method are only limited by the mechanical response time of the system. Other positive features of this control method include its scope for combining HCCI combustion with SI combustion. The major drawback is production-oriented; an ordinary engine cannot be used, since additional physical parts must be added, which is costly. Furthermore, when the compression ratio is increased the surface to volume ratio increases, leading to higher heat losses. Several authors have successfully implemented geometrically variable compression ratio systems to control HCCI combustion [30; 31; 32; 33; 34], but no such systems have been mass produced for commercialization.

3.4.3 Fuels

Fuel properties also play important roles in the timing of autoignition, *i.e.* the ignition delay at a certain pressure and temperature varies dramatically between different fuels. Thus, another approach for controlling HCCI combustion is to vary the fuel parameters. In several studies [34; 35; 36] this has been done by using two fuels with distinctively differing octane numbers (either iso-octane and n-heptane or ethanol and n-heptane) and varying their proportions. This allows mixtures to be introduced with appropriate ignition temperatures to adjust the

phasing of the combustion and appropriate amounts of fuel to adjust the load as desired. The approach provides a wide range of control and the engine can be operated over a wide load range. The transient response is only restricted by the injection systems, which have shown good transient responses in practice, the drawback of course is the requirement for two fuel systems with variations in consumption of the two fuels depending on the driving cycle.

3.4.4 Homogeneity/Stratification

The homogeneity of the mixtures has been found to have modest effects on the combustion process [37], although the cited study only examined the effects of small changes in heterogeneity. However, if the charge is stratified (in terms of mixture), which can be regarded as inhomogeneity on a large scale, the variation between different regions will give rise to variations in ignition delays depending on the equivalence ratio, pressure and temperature. At the lower load limit the HCCI combustion could be stabilized by using charge stratification [38] and at the higher load limit the stratification was limited by the high-pressure rise rate. Varying the heterogeneity have also been shown to affect the combustion duration [39]. [40] used stratification to stage the combustion in such way that the rate of heat release was smoothed, thereby allowing the load to be increased. It was found that single-stage ignition fuels showed less sensitivity to local variations in equivalence ratios.

3.4.5 Fuel Additives/Reaction Suppressors

Fuel additives provide additional scope to influence the ignition delay of primary reference fuels [41]. For instance, adding 2-ethyl-hexyl-nitrate or di-tertiary-butyl-peroxide can increase the first stage combustion heat release, and hence reduce the ignition delay. The same tendency is observed if the molar ratio of n-heptane is increased, but the effects are larger for the additives due to their lower activation energy. Additives can also be added for various purpose, e.g. to increase mass, decrease temperature or increase ignition delay. For example, injecting water in HCCI combustion retards ignition timing [42]. However, in the cited study this also increased the amount of HC and CO emissions, which even in normal HCCI operation can be problematic, so the scope for phasing the combustion by adding water is limited in practice.

3.4.6 Valve Timing

The valve timing can influence the charge temperature and mixture composition by changing the effective compression or trapping residuals. By varying the intake valve closure (IVC) the effective compression can be controlled and by closing the exhaust valve before the intake valve opens a negative valve overlap (NVO) is introduced that can influence the amount of trapped residuals. NVO have been used to capture sufficient residual mass from the preceding cycle to reach auto-ignition [43].

3.4.7 Spark assistance

If the HCCI engine is equipped with a spark plug then it can be used to influence the combustion by combining initial flame propagation caused by spark discharge and subsequent HCCI combustion within the same cycle. In this manner the thermal environment at the end of compression can be influenced by the initial flame propagation, providing increased control of the HCCI combustion since it is influenced by the thermal environment. A drawback is that conventional SI combustion has shown lower thermodynamic efficiencies than HCCI combustion, but if the intention is to increase control of the HCCI combustion then this idea could still be useful. This concept has been used to promote the transition between HCCI and SI combustion [28; 44]. It has also been used to expand the HCCI operational range [45; 46].

3.4.8 Spark assistance with charge stratification

The proposed concept explored in the work underlying this thesis involves the use of spark assistance in combination with charge stratification. The thermodynamic and chemical state within the cylinder will depend on the way HCCI combustion is achieved, but generally all HCCI concepts involve dilution (with air, EGR or both), which makes flame propagation challenging. Hence the role of the stratification is to supply a region in which the situation for flame propagation is less challenging, thereby enhancing the effect of the initial flame propagation and increasing the degree of control that can be achieved.

In this project this concept has been investigated during steady state operation. As previously mentioned, conventional SI combustion has shown lower thermodynamic efficiencies than HCCI combustion. However, extending the HCCI ope-

rational range by combining conventional SI combustion and subsequent HCCI combustion within the same cycle may at least deliver significantly higher efficiency than pure SI combustion due to the higher efficiency of HCCI. Thus, it may be effective, in efficiency and emission terms, to use SI combustion in combination with HCCI combustion during steady state operation within the boundaries of the HCCI mode. Furthermore if a greater operational range is achieved less mode changes would be needed during normal operation, which is desirable.

3.5 HCCI using NVO

HCCI combustion can be achieved in many ways. For instance, laboratory fuels can be used to achieve HCCI combustion at certain loads with more or less any engine configurations. However, that will not necessarily provide a solution that leads to fuel consumption reductions for any vehicle fleet in the near future. To take HCCI technology closer to mass production it is important to develop a solution that offers similar power output to current powertrains, but with reduced fuel consumption. Furthermore, few changes should need to be made to current hardware, because if substantial additional equipment is needed to adopt a solution then the probability of its introduction will be greatly reduced.

3.5.1 Principle

A method to trap residual gases in order to achieve HCCI combustion was described in [47], involving closing the exhaust valve before TDC and thus trapping residuals. This method has been shown experimentally [48] to allow HCCI combustion in SI engine geometry using commercially available fuels in conjunction with simulations [49]. Using this approach HCCI combustion could be achieved for part load and for higher loads the engine could be operated as a conventional SI engine, thus similar power output to that of a conventional powertrain could potentially be achieved, while the SI engine's poor part-load efficiency could be increased by HCCI operation in those regions.

3.5.2 NVO

Various car manufacturers use dual valv lift or, like BMW, variable valve lift systems [50]. If such technologies are used on both intake and exhaust camshafts

then a so-called negative valve overlap, NVO, can be implemented. Schematic examples of in-cylinder pressure traces obtained in motored conditions with low lift, short duration camshafts and high lift, long duration camshafts can be seen in figure 3.5. The short duration camshafts allow the exhaust valve to be closed before TDC and the intake valve to open after TDC, leading to a negative valve overlap, in contrast to conventional valve timing, where the intake valve opens before the exhaust valve closes, and hence there is a positive valve overlap (solid line versus the dashed line in figure 3.5).

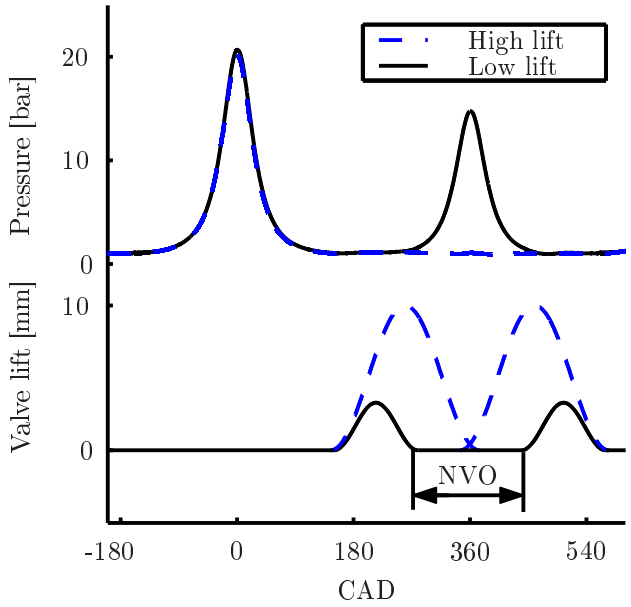

Figure 3.5: In-cylinder pressure traces during motored conditions with two different valve timings (top), and the lift profiles for the two valve timings (bottom). Reprinted with permission from SAE Paper No. 2007-24-0012 © 2007 SAE International.

3.5.3 Control

During combustion the reduced camshaft duration leads to a reduced mass flow and since the exhaust valve closes prior to TDC residuals will be trapped, in accordance with the basic concept, allowing the temperature within the combustion chamber to be increased to such an extent that gasoline can be auto ignited, but only within a modest load region for a given setting. To increase this region,

control of the combustion must be achieved, and to do this means to influence the thermal and/or chemical environment within the combustion chamber.

Valve timing

If the engine is equipped with a valve train that allows the phasing of the camshafts to be adjusted then a direct means of controlling the combustion is available since the amount of residuals can be influenced [48] (in addition to changing the mass flow). Unfortunately, however, a single camshaft usually sets the intake timing for the valves of all cylinders (or half the cylinders in v-engines) and another sets the exhaust timing of all of the cylinders. Thus, it will probably not be possible to control the amount of trapped residuals individually for each cylinder (which would be highly desirable since both the thermal and geometric states will differ between individual cylinders, so cylinder individual control systems would be ideal). Furthermore, it can be assumed that the valve timing mechanism will not display sufficiently fast responses to handle real drive cycle transients, at least for hydraulic camshaft phasing systems.

Injection strategy

During the period when the exhaust and intake valves are closed prior to TDC, there is a pressure increase during the traditional gas exchange phase (see figure 3.5). A method of influencing the combustion by using this pressure increase was pioneered and described in [51; 43], in which direct injection of fuel during this period was used to influence the combustion. In these studies the increased amount of control over combustion was experimentally verified. The reason for this increased control is discussed in both the cited studies, [51] highlights the effect of the fuel reformation induced by injecting the fuel during this pressure rise in the NVO. In [43] simulations were carried out using detailed chemistry in two sequences, one in which only fuel components, N_2, O_2, H_2O, CO_2, CO and H_2 formed during the NVO were used as input for the calculation during the main combustion and one in which all components with concentrations exceeding 10^{-8} in mole fraction formed during the NVO were used as input for the calculation during the main combustion. In this way, using detailed chemistry calculations, the effects of the radicals formed during the NVO could be estimated. With this approach it was found that radical formation played a significant role in the effects observed when fuel was injected during the NVO. The simulations also showed that exothermic reactions occurred during the NVO due to this fuel injection during the NVO, which also influenced the main combustion, however this was

not experimentally validated in the cited studies. It was also concluded that exothermic reactions occurred [51], and the conclusion was experimentally validated to some extent by optical analyses, in which signs of light were observed during the NVO using high speed video. However, very little background information regarding the optical setup is documented, for instance the spectrum studied is not mentioned so little is known about the light seen. The role of chain branching on ignition and the ignition sequence in HCCI engines was found to be dominated by the decomposition of H_2O_2 through kinetic analysis [52]. Ignition occurs when the decomposition temperature for H_2O_2 is reached, at approximately 1000 K. The relative importance of the exothermic reactions and the reformation of the fuel or radical formation in [51; 43] can be debated. Did the effect caused by the injection in the NVO mainly result from the decomposition temperature being reached at an earlier point due to the exothermic reactions? Or was it mainly due to greater amounts of radicals, for instance H_2O_2 at the point of ignition? Further indications of exothermic reactions were found experimentally by the author in [53], manifested by chemiluminescence of the OH radical and by both LIF of OH and pressure trace analysis [54]. In the studies described in Paper VI [55] pressure trace analyses showed that observed changes in combustion phasing caused by varying amounts of fuel injected during the NVO were mainly due to the exothermic reactions during the NVO dictating the temperature during the compression stroke, and thus controlling the combustion phasing.

Hence, fuel injection during the NVO, pilot injection, provides a means to increase control over the combustion. More importantly the combustion can be influenced in shorter time scales and in individual cylinders. By combined use of a pilot injection and variable valve timing control of combustion can be achieved over a significant load and speed range, by crude adjustments via settings of the valve timing and fine tuning via appropriate pilot injections.

3.5.4 Hardware requirements

The hardware requirements of a system that can effectively reduce emissions to meet legal standards will dictate if it will be commercially applied or not; solutions that use cheap, known technology and only require a small additional volume will have a higher probability of commercialization. The space taken up by any proposed technological system should also be considered, since packaging of all components is becoming increasingly challenging (no empirical evidence to support this statement will be presented, but skeptics can open the bonnet of a ten year old car and compare what they see to the innards of a new car then guess how tight the packing will be ten years from now).

To implement the use of NVO to achieve HCCI combustion, systems allowing dual valve lift profiles (or variable lift) are needed, which are already available (often currently applied to just one camshaft, but it is assumed that only small modifications would be needed to allow both intake and exhaust profiles to be adjustable). The same applies to the requirement for variable valve timing, many manufacturers already use variable valve timing (in phasing) on either intake or exhaust camshafts (or both). Hence, only a small step, mechanically, is needed to introduce this technology. In order to control the combustion via the pilot injection, a slightly greater step is required. The fuel needs to be directly injected, however it is assumed that direct injection systems will not be unusual features of engines in the near future. Indeed, direct injection systems have been available for many years, ever since Jonas Hesselman demonstrated the Hesselman engine using direct injection and spark ignition in 1925 [56]. Direct injection was only introduced in mass produced engines, by Mitsubishi, in 1996 [57]. However, compared to other solutions to achieve HCCI combustion this method is seen as the one needing the least modification (if commercially available fuels are to be used) and thus the most promising, especially since it can be combined with conventional SI engine functionality, thereby providing an acceptable power to weight ratio for the powertrain. Various cars or engine manufacturers have studied HCCI using this concept. GM have studied HCCI or controlled auto ignition (CAI) using short duration camshafts to achieve a NVO and injecting fuel during the NVO [58] and have presented demonstration vehicles using this technology. Bosch have also studied similar concepts involving use of direct injection and short duration valve events to achieve the NVO [59; 60] with estimated reductions in fuel consumption of 15 % for NEDC operation of a middle-class vehicle with a 2.0 l engine [59]. Mahle powertrain have presented a solution, also with negative valve overlap, that is claimed to be focused on production feasibility and cost effectiveness [61]. VW have also used NVO to achieve HCCI combustion, however only using shorter duration on one camshaft rather than both of the measures described above, and have successfully applied the approach in a demonstration vehicle [62; 63; 64].

3.5.5 Operational window

To achieve HCCI by trapping residuals, low lift and short duration camshafts are used, which leads to less air being pumped than when high lift and long duration camshafts are used. So, if the air pumped by the engine is the only oxidizer then less fuel can be combusted when these valve events are used due to the reduced volumetric efficiency. Thus, HCCI with NVO can only be achieved over smaller speed and load ranges than SI combustion without NVO. This can be seen as the

concept's strength and weakness, since full load SI operation shows high efficiency and there is not necessarily a need to improve this value, rather the need is to achieve similar absolute values in efficiency over a greater speed and load range. This is where this limited range of HCCI operation is suitable, due to the reduced mass flow imposed by the NVO, HCCI operation with NVO will only be possible over low load/low speed regions, but fortunately this is where the SI engine needs the greatest improvement.

3.5.6 Spark assistance with charge stratification for HCCI with NVO

Since this concept of achieving HCCI with NVO is intended for use in SI engines, in which a spark plug is present, spark-assistance can be used to increase control. Furthermore, if pilot injections are used then the engine must also use DI technology, therefore the additional hardware demands for applying spark-assistance with charge stratification will be minimal; the only additional requirement for the injector being that it should be capable of creating a stratified charge. From figure 5.18 it can be seen that HCCI combustion near the higher load limit only displays marginally better efficiency than SI combustion, but for the lower loads HCCI combustion shows significantly higher efficiency, so for this region a combination of SI and HCCI combustion would probably lead to greater efficiency than SI combustion. In other words, the minor additional requirements for the hardware can be justified if they extend the operational window of HCCI, especially for lower loads since the low load limit is normally above idle load for HCCI using NVO [20].

The thermodynamic and chemical states for low HCCI loads with NVO are not ideal for flame propagation, as shown by the global stoichiometric ratios in figure 5.20, which indicate that conditions are significantly lean in these cases. There is also dilution with trapped residuals beside excess air, see figure 5.19. So, achieving flame propagation under these conditions can be challenging. Furthermore it has been shown in experiments conducted by the author with several colleagues (Paper VIII [65]) and in [66] that the charge motion is very weak (during the compression) when NVO is used, which also increases the challenge of achieving flame propagation. So, the degree of influence of spark-assistance alone depends on the setup; in [67; 68; 69] no effect on combustion was seen when spark-assistance was used and in [20; 70] some effect was observed on HCCI with NVO. So, for HCCI with NVO it can be crucial to make it less challenging for the flame to propagate and here the combination of spark-assistance and charge stratification is promising. In initial tests documented in Papers I [71] and II [72]

conventional valve timings were used and charge heating was used to achieve HCCI combustion. In the studies described in Paper IV, the method was implemented in an engine using NVO to achieve HCCI combustion and it was found that the lowest possible load without misfire could be reduced significantly by using spark-assistance in combination with charge stratification.

Chapter 4

Experimental methods

The experimental apparatus and methods used for each published study are described in detail in each paper, but this chapter summarizes and adds some additional information regarding the methods used.

4.1 Single cylinder engine

The main published experiments were carried out using a single-cylinder AVL research engine. Its displaced volume corresponds to that of a contemporary passenger car engine. In all experiments prototype cylinder heads were used with geometry similar to that of SI engines. The engine parameters can be seen in table 4.1.

Table 4.1: Engine parameters.

Bore	83 mm
Stroke	90 mm
Swept Volume	487 cm ^{3}
Compression ratio	8-12.3:1
Conrod length	139.5 mm

This engine can be arranged as an optical engine with an extended piston housing a mirror that provides, in conjunction with a quartz window in the piston crown, optical access to most of the combustion chamber from below (see figure 4.1). The pent roof side walls consist of quartz windows, which provide optical access to the clearance volume in the combustion chamber. Since some metallic material

has been replaced by quartz glass there are naturally some consequences. The optical engine is restricted to low engine speeds since the elongated piston leads to great friction, especially at higher engine speeds. Furthermore, quartz glass is much less durable than, for instance, aluminum and even small temperature gradients or rough handling can cause it to fail. This limits the peak pressure that such engines can tolerate, compared to engines built purely of conventional material. Furthermore, cylinder heads were used that did not have cooling and thus intermittent operation was needed. This leads to variations in the thermal state, which can make precise measurements challenging. For this reason, in Studies IV-VIII [53; 54; 55; 73; 65] a reference combustion specific for each study was used until a certain cylinder head temperature was reached, then the settings selected for the respective study were applied, to standardize the initial thermal conditions for all measurements in the measurement campaign. For this project, which mainly focused on enhancing control of HCCI near the lower limits of HCCI operation, the shortcomings of the optical engines were not major constraints due to the low loads (at which the rate of temperature increase is small) and relatively low peak pressures associated with low-load HCCI.

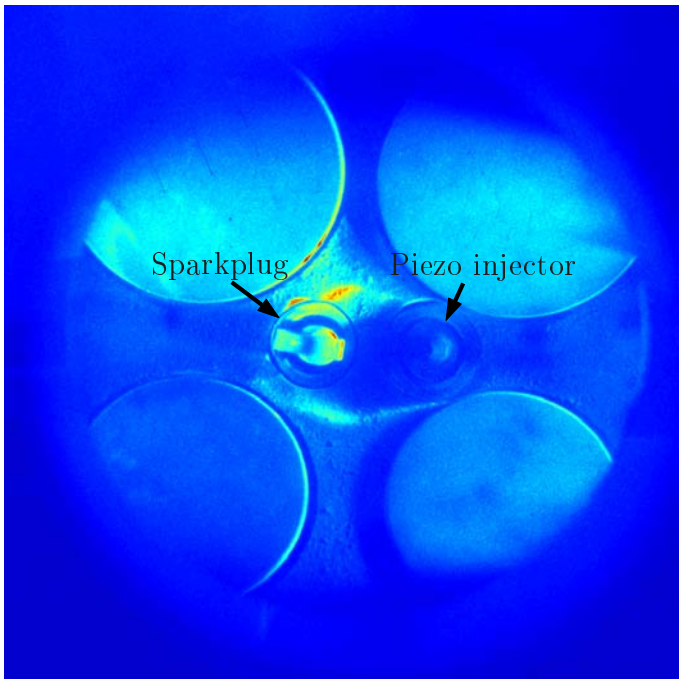

Figure 4.1: The optically accessible combustion chamber. The diameter of the optically covered zone was 76 mm. Reprinted with permission from SAE Paper No. 2007-24-0012 © 2007 SAE International.

4.2 Optical setup

4.2.1 Chemiluminescence measurements

Optical measurements have been key elements of the experiments for this project and all studies, except Study II [72], involved optical measurements in some form. It was essential to initially validate the proposed idea of combining initial flame propagation and HCCI combustion within the same cycle (*i.e.* that it worked as intended). A pressure transducer can naturally measure the pressure within the combustion chamber, but it will only provide a mass-averaged representation of the reactions occurring within the combustion chamber. The threshold for reaction detection can make it difficult to detect such small and slow additions of heat caused by the initial flame propagation. However, with optical access the threshold for detecting reactions can be reduced significantly, especially for flame propagation. Since the propagating flame leaves a region with higher temperature and thus lower density behind it, the geometrical area covered by the flame will be great even when small portions of the fuel are combusted by flame propagation due to the difference in density between the unburned and burnt regions (compare the mass fraction burnt and the area covered by the reaction zone in figure 4.3). In order to study the flame front a filter was used to isolate the emitted light from the OH radicals, since they are associated with the reaction zone. A schematic diagram of the setup is presented in figure 4.2.

$$\mathrm{H} + \mathrm{OH} = \mathrm{H_2O} + h\nu \tag{4.1}$$

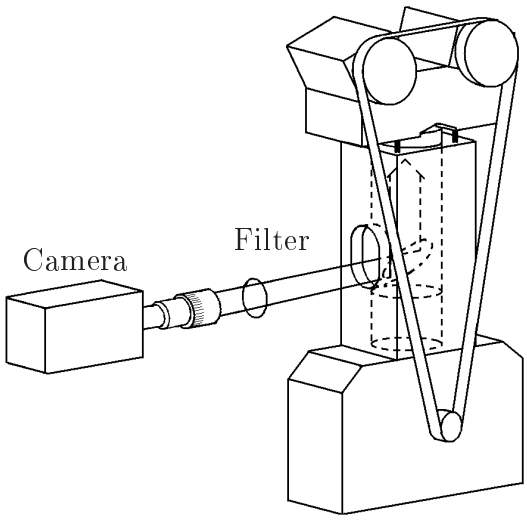

Figure 4.2: Schematic setup for chemiluminescence measurements.

The reaction gives intensity peaks for the emitted light at wavelengths between 306 and 309 nm [74]. The chemiluminescence from the OH radicals was isolated by using a Melles Griot 03FIV119 narrowband filter with a center wavelength of 310 nm and a full width at half maximum (FWHM) of 14 nm. This procedure was used for the chemiluminescence measurements of OH presented in Papers I and IV [71; 53]

For the study of the effect of charge stratification without spark-assistance described in Paper III [75], the focus was slightly different compared to when initial flame propagation was investigated. In this case light from all chemiluminescent reactions covered by a high speed camera and its traditional lens wavelength span was measured, to allow the camera to acquire as much light as possible, thereby permitting use of a high frame rate and the capture of many images of the combustion process in single cycles.

The optical setup for chemiluminescence measurements requires only minimal equipment and less optical access compared to, for instance, laser-induced fluorescence (LIF), where optical access is needed for both excitation and emission rather than just for the emission, as in chemiluminescence measurements. Some weaknesses are lower signal intensity, which often requires compensation by increasing exposure times. In addition, reactions other than the reaction of interest may generate chemiluminescence with similar wavelengths, making the separation problematic. It can be difficult to precisely determine what is measured and if no filters are used then disturbances from, for instance, IR thermal radiation from water vapor may be captured during the later part of the combustion. Another disadvantage is naturally the obvious one, that not all reactions generate chemiluminescent light. Despite these disadvantages good representations of the flame front can be obtained using chemiluminescence imaging, as shown in figure 4.3 where LIF of OH is compared to chemiluminescence of CO_2 and the resemblance between the two (within the measured laser plane) can be clearly seen.

4.2.2 LIF measurements

LIF measurements were acquired in Studies IV-VIII [53; 54; 55; 73; 65]. LIF measurements require more complex setups than chemiluminescence measurements, as illustrated by the schematic setup in figure 4.4. For LIF optical access is needed for both emission and excitation light, provided by the laser plane in this case. LIF affords the possibility of measuring various parameters that cannot be assessed by chemiluminescence measurements and can detect flame radicals at

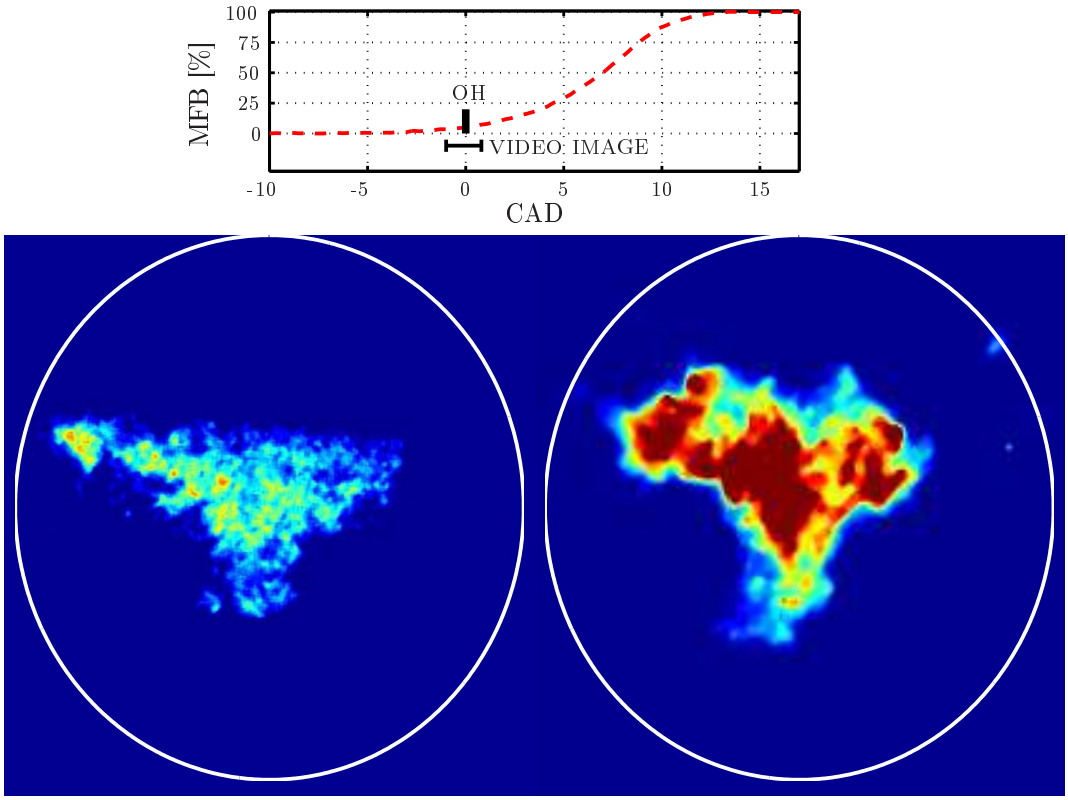

Figure 4.3: Mass fraction burned and timing of measurements for OH and the chemiluminescence of CO_2 (top). LIF image of OH (left) and a video image of the chemiluminescence of CO_2 (right) obtained simultaneously in the same cycle.

very small levels [76]. Another advantageous feature (for PLIF, for instance) is that information is acquired about events in a single plane, unlike chemiluminescence measurements which provide line of sight representations of the ongoing reactions. Furthermore, exposure times can be reduced to mere fractions of those required for chemiluminescence measurements since the emission decays rapidly after the end of the inducing laser pulse and there is thus no need to prolong the exposure time any further after the emission has decayed. This can in many practical cases make the influence of chemiluminescence negligible.

The proposed concept explored in the project involved, as mentioned above, the use of charge stratification through which an initial flame should propagate. To validate that a stratified charge was created and that the flame propagated through it, the initial use of LIF involved the fuel tracer 3-pentanone, together with measurements of HCHO (which represents the low temperature reactions [77]), as described in Paper IV [53]. The reason for using fuel tracer and PRF fuel instead of conventional gasoline, which can give strong LIF signals

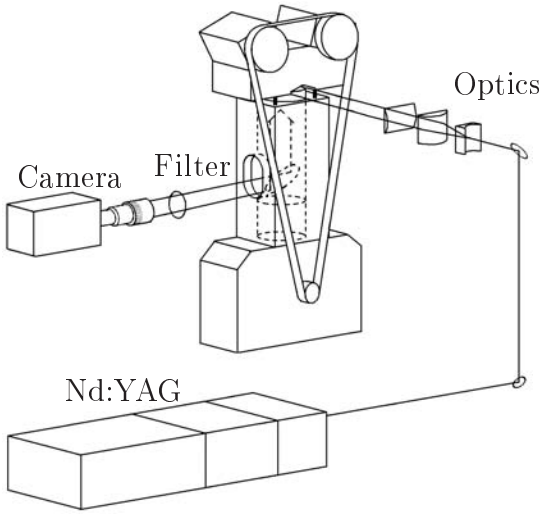

Figure 4.4: Schematic setup for LIF measurements. Reprinted with permission from SAE Paper No. 2007-24-0012 © 2007 SAE International.

with excitation in the UV band was that the species that leads to the fluorescent signal is not known [78]. Both of these species can be conveniently measured using a Nd:YAG laser since the fuel tracer can be excited using the fourth harmonic light and HCHO by the third harmonic (see the excitation spectrum to the left in figure 4.5), since they have a wide excitation spectrum. For the studies described in Papers V-VIII [54; 55; 73; 65], LIF of OH was measured. The requirements for excitation of such a small molecule differ from those of, HCHO for instance, for LIF of OH a specific excitation wavelength is required (compare the excitation spectra in figure 4.5). For this reason a tune-able excitation source is needed, which significantly increases the complexity of the required setup. For all LIF measurements of OH a Dye laser pumped by a Nd:YAG laser was used and the Q1(6) transition in the A(ν=1) - X(ν=0) band at a wavelength of 283 nm was used for excitation (the reason for this choice and the adopted procedure is described further in the papers). Since a precise wavelength is required thorough calibration of the wavelength is needed; this was done by using a reference burner and a photomultiplier.

The only quantitative LIF measurements that were published were measurements of local air equivalence ratio in Paper IV [53], and more attention is here directed towards these measurements for evaluation of the effect of local temperature. The temperature distribution within the combustion chamber is unknown, which can lead to the local air equivalence ratio being slightly incorrectly calculated since the local temperature can differ between the measured cases and the reference cases. The effect of temperature on the LIF of 3-pentanone was investigated in [80]

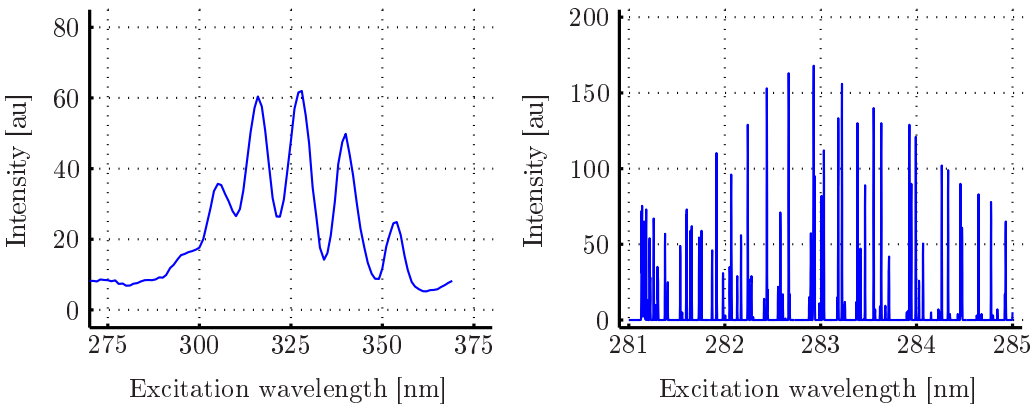

Figure 4.5: Excitation spectrum of formaldehyde (left) from a cuvette at atmospheric pressure and 90°C and simulated absorption spectrum of OH (right) using LIFBASE [79] (Reprinted with permission from SAE Paper No. 2008-01-0037 © 2008 SAE International.).

and it was found that the absorption spectrum is red-shifted as temperature increases. For the excitation wavelength used here this will mean that the actual air equivalence ratio will be lower for regions with lower temperatures. So, if there are greater amounts of evaporation in the richer regions in figure 5.4, then these regions may have lower temperatures than the same geometrical regions in the reference images with homogenous mixtures. Hence the air equivalence ratio may be over-estimated. Four LIF images of combustion events observed with different air equivalence ratios are shown, and it can be seen that there is a strong connection between the fuel concentration and signal. This can be seen both directly from the images and by analyzing the signal strength along a line through the images. In figure 4.6(c) it can be seen that the signal is related to the amount of excess air. This strong correlation suggests that the discrepancy between the calculated air equivalence ratio and actual air equivalence ratio will be low, but it will still depend on the absolute level of the temperature difference. It was found in [80] that a temperature increase of 150 K (from 383 to 533 K) led to a relative fluorescence intensity difference of around 17 % at 20 bar. Estimating the degree to which the evaporation caused by the stratification injection decreases the temperature of the stratified region is problematic, but if 100 K is used as an example and similar trends are valid, as found in [80], then the air equivalence ratio would be over-estimated by around 0.02 for these measurements. This measurement accuracy was acceptable, since the main aim was to validate that a stratified charge was created and to obtain a rough estimate of the local air equivalence ratio.

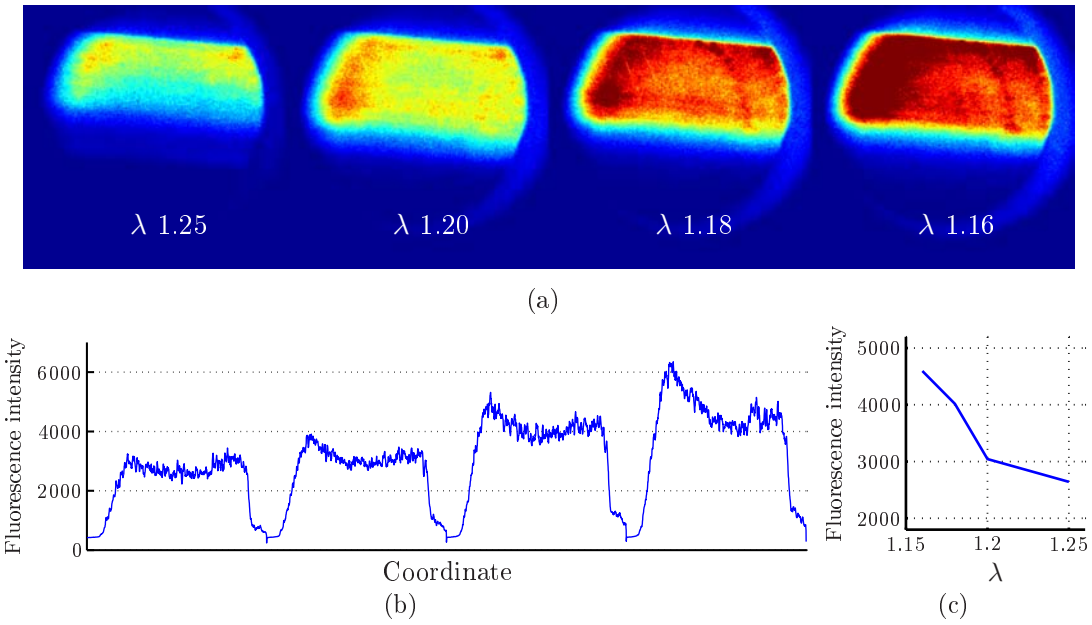

Figure 4.6: Average LIF images of 3-pentanone for four different air equivalence ratios at -40 CAD (a), its signal strength along a line (b) and average signal strength for the different air equivalence ratios.

4.2.3 Simultaneous multi-species LIF, PIV and Video measurements

For the last measurement campaign in this project several different measurement techniques were used simultaneously, as described in detail in Paper VIII [65]. A schematic diagram of the setup can be seen in figure 4.7 and the laser beams' paths to the engine can be seen in figure 4.8. This procedure was chosen since there are disadvantages of performing each measurement separately and then comparing averaged values obtained using the different techniques. If it is possible to measure many parameters simultaneously then the drawbacks of averaging can be reduced and the confounding effects of variations in combustion can be reduced since all simultaneously measured parameters correspond to the same cycle. Basically, if it was possible it would be highly advantageous. With the setup used LIF of OH, LIF of HCHO, PIV, high speed video and pressure measurements could be acquired simultaneously, and they were complemented by separate simultaneous measurements of LIF of OH, LIF of 3-pentanone and pressure. All of these techniques were used since all of the measured parameters were thought to influence events when initial flame propagation through a stratified charge was combined with subsequent HCCI combustion, as more fully reported and discussed in Paper VIII [65].

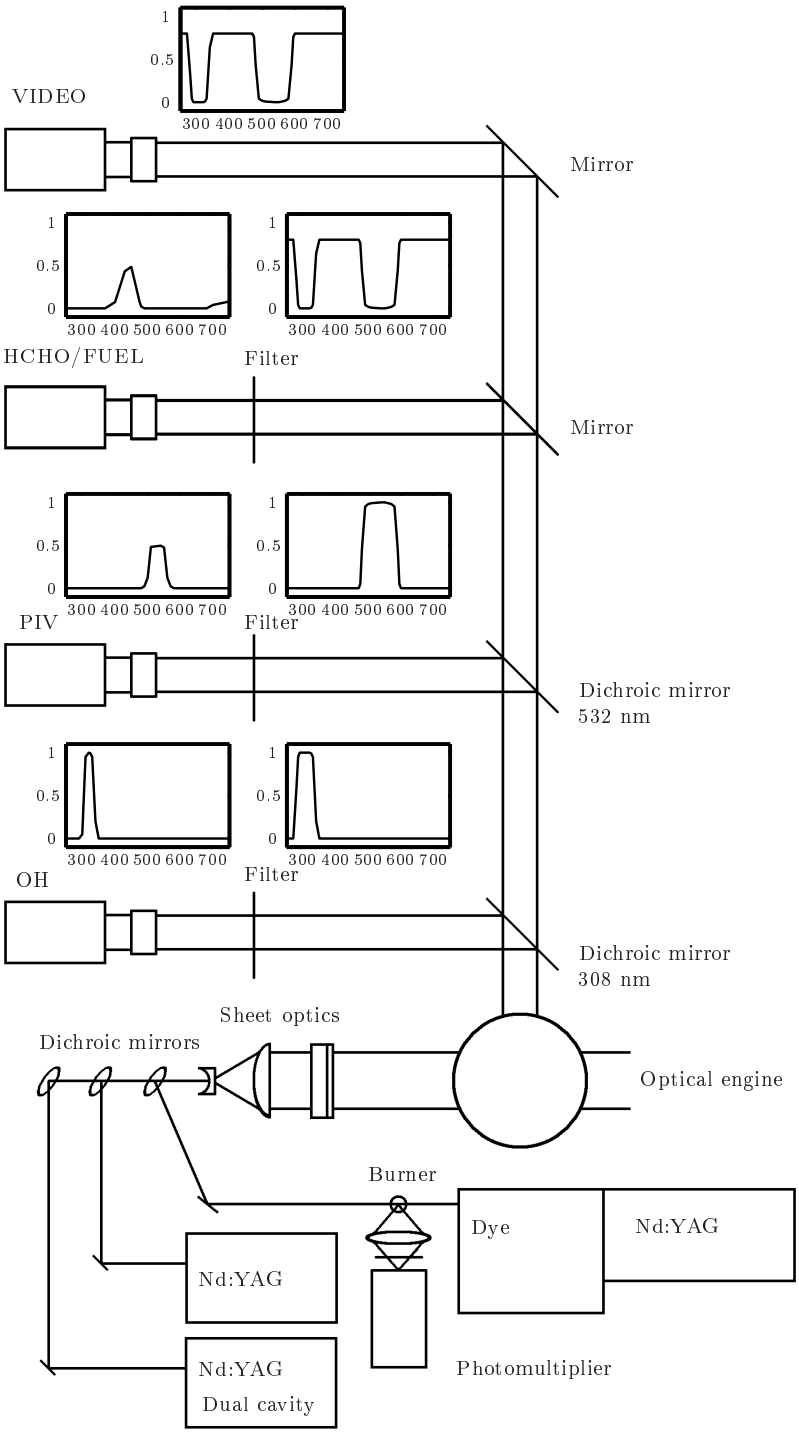

Figure 4.7: Schematic setup for simultaneous multi-species LIF, PIV and Video measurements.

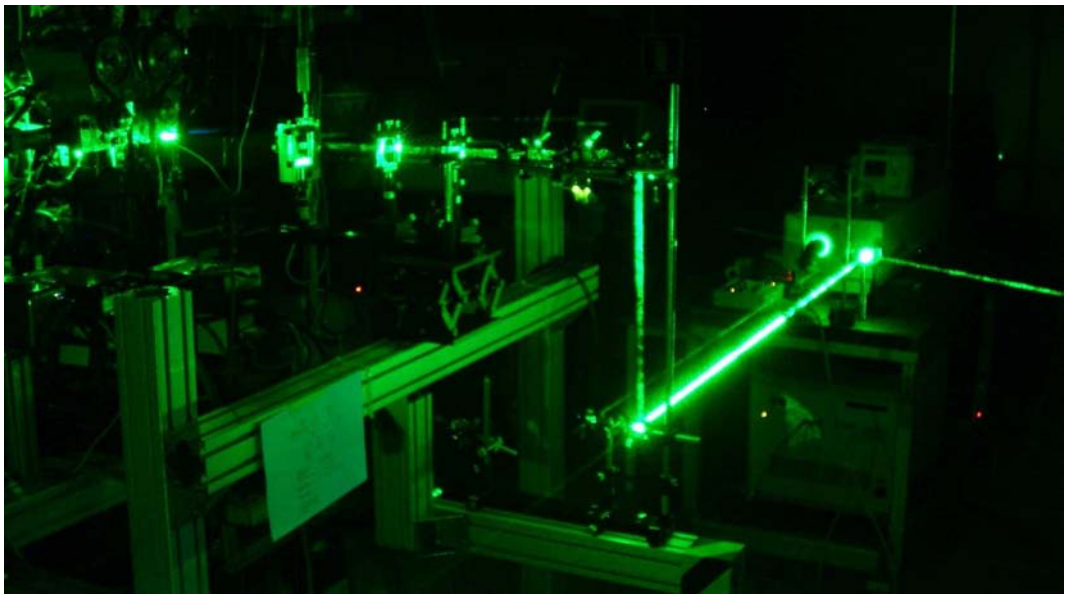

Figure 4.8: The paths for the laser beams to the engine.

4.2.4 PIV measurements

Particle Image Velocimetry (PIV) can be used to calculate velocity fields over a measured plane and the basic principle of PIV measurements is simple; the displacement of a particle over a known period of time correlates to its velocity. As many optical methods PIV is non-perturbing [76] and no probe disturbs the flow. For these measurements two laser pulses, with a known period of time between them, provided by a dual cavity Nd:YAG laser, were used to illuminate seeded particles. The displacement of the particles was measured using a camera capable of taking two images with small time separation between them, which allows two images (one for each laser pulse) of the illuminated particles to be taken. In figure 4.9 illustrative images of illuminated particles obtained with different seeding densities can be seen.

To calculate the displacement of the particles the information from the image is divided into smaller regions, so-called interrogation areas [81]. The size needed for each interrogation area depends on the seeding density, examples of seeding density can be seen in figure 4.9, since it is essential to have information from particles inside this area, preferably from large numbers of particles. To illustrate how this displacement is calculated by the PIV system a case with very low seeding density is chosen due to the simplicity of illustrating similarities in intensity between the two images, as shown in figure 4.10.

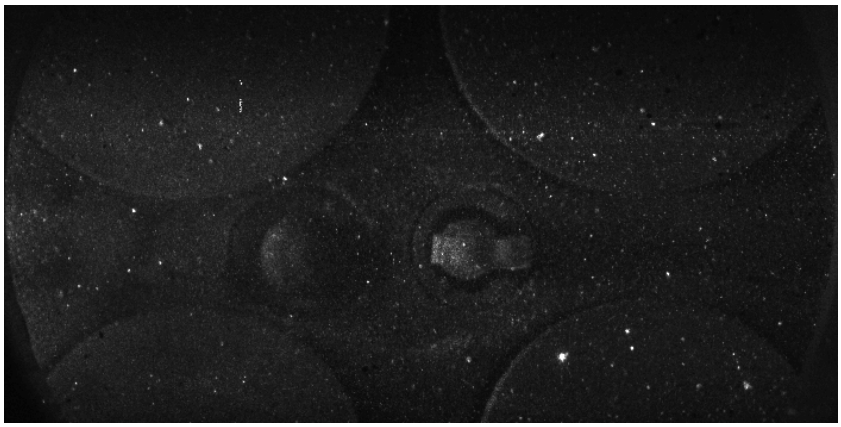

(a)

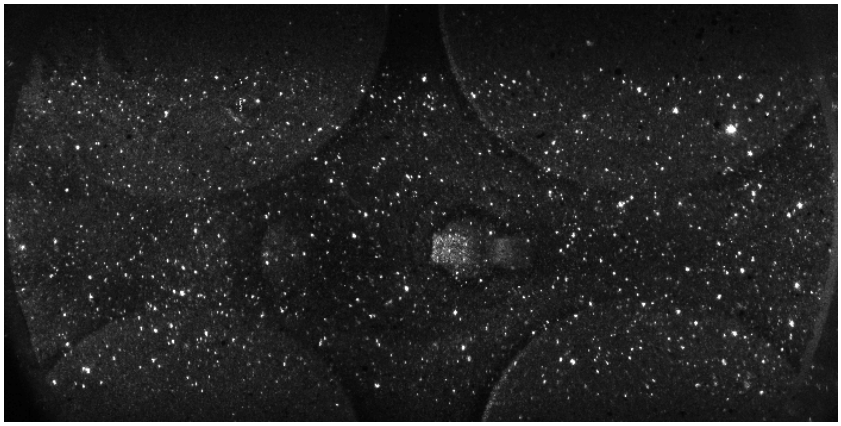

(b)

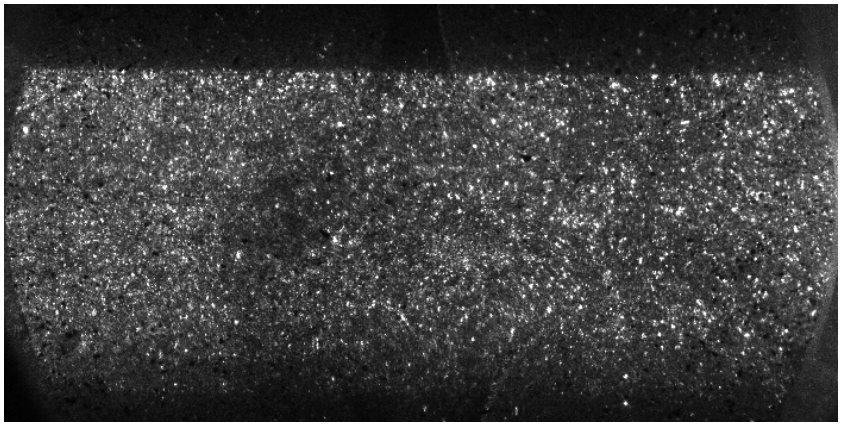

(c)

Figure 4.9: Images of illuminated particles with seeding densities ranging from very low (a), moderate (b) to high (c).

For this example (figure 4.9) two distinguished intensity peaks (*i.e.* particles, marked A and B) with similar shapes rise above the surrounding noise. The displacement in this interrogation area can be calculated from the difference in position of these peaks between the two images [81]. When this displacement in pixels is calculated an average velocity for this interrogation area can be found by relating the displacement in pixels to a geometrical distance, which is then divided by the time between the two images, giving the velocity.

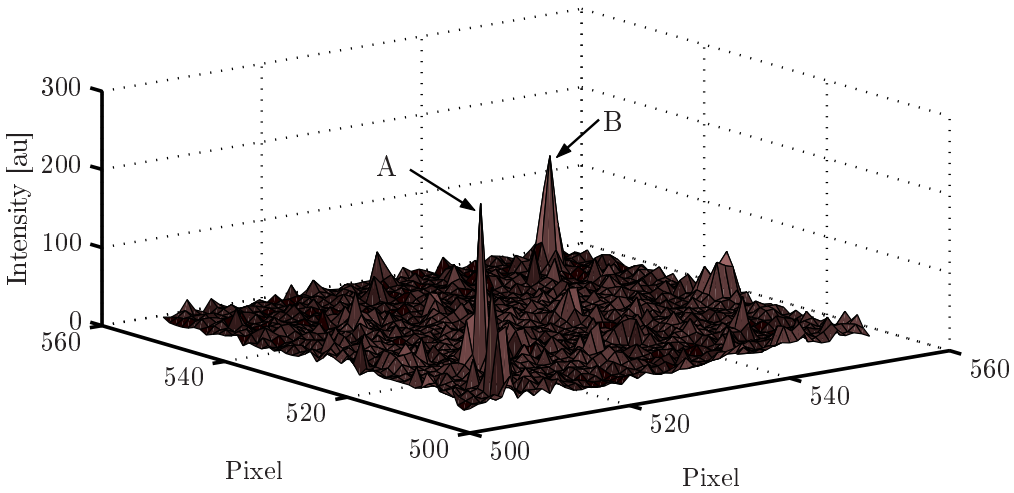

(a)

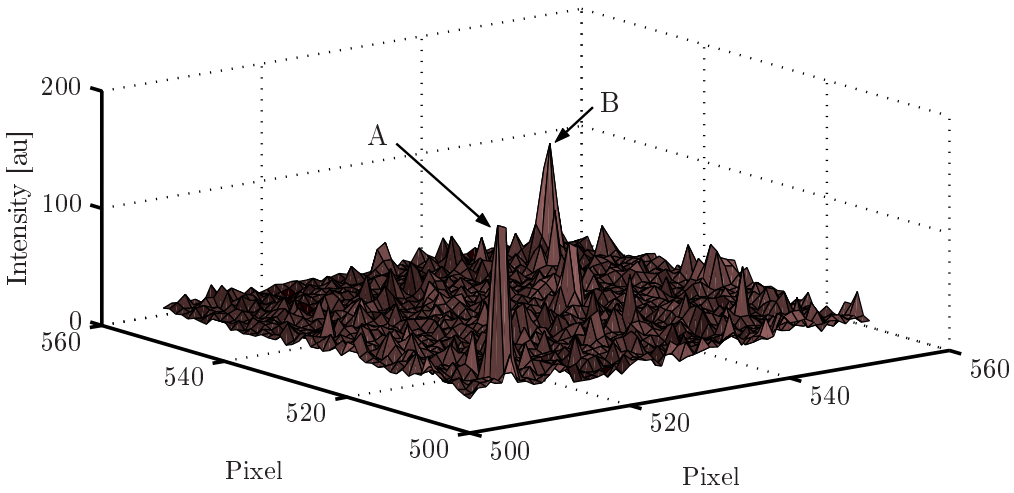

(b)

Figure 4.10: Image intensity over an example interrogation area with low seeding density for illustrative purposes, for two images separated in time.

In figure 4.11 an additional example is shown of the intensity over an interrogation area, but with the difference compared to the examples in figure 4.10 that a realistic seeding density is shown. Multiple particles within the interrogation area allow more robust measurements, since the average displacement for the interrogation area provides a more accurate assessment if it is based on the displacement of several particles. There will also be particles that only appear in one of the images because of their speed perpendicular to the measured plane.

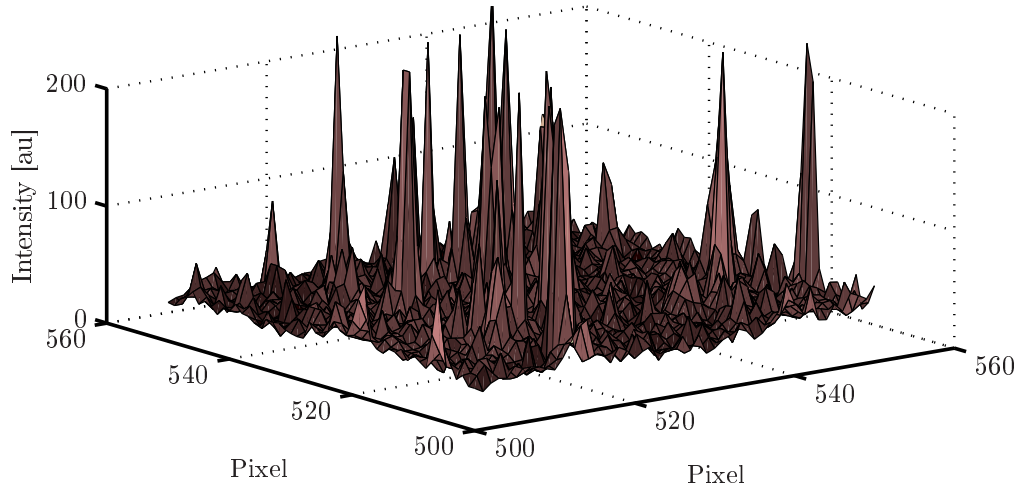

Figure 4.11: Image intensity over an example interrogation area with realistic seeding density.

Seeded particles

In Study VIII [65] PIV measurements of seeded particles were performed in order to calculate the flow field. Since the PIV measurements calculate the velocity of the seeded particles they must have fluid dynamic properties that allow them to follow the flow and hence represent the velocity of the flow. In Paper VIII the Stokes number is used to evaluate whether the particles follow the flow or not. This will be slightly more thoroughly described here since the measurement accuracy is strongly connected to the extent to which the particles follow the flow, hence it is essential to estimate how well they reflect it. The Stokes value is defined as [82]:

$$St_V = \frac{\tau_V}{\tau_F} \tag{4.2}$$

where

$$\tau_F = \frac{T}{U} \tag{4.3}$$

and

$$\tau_V = \frac{\rho_p D^2}{18\mu_C} \tag{4.4}$$

T is the distance between the piston and the cylinder head and U is the velocity of the flow. D is the seeded particle's diameter, ρ_p its density, μ_C the dynamic viscosity of the gas and ρ_C is the density of the gas. So, if the response of the particles to the flow near TDC is of interest then T will be the height of the clearance volume and the structural integrity of the seeded particles is sufficient to maintain its diameter. Thus, if the parameters listed in the table 4.2 are valid then the Stokes number will be far less than unity for velocities (U) occurring near TDC, as noted in the paper.

Table 4.2: Properties of seeded particles at -30 CAD and near TDC.

T	21 mm	15 mm
D	18-28 μm	18-28 μm
ρ_p	60±5 kg/m^3	60±5 kg/m^3
μ_C	3.7×10^{-5} Pa s	4.15×10^{-5} Pa s
ρ_C	5.7 kg/m^3	9 kg/m^3

To more precisely estimate how well the seeded particles follow the flow the equation of motion for a spherical particle in a gas [82] is applied:

$$m\frac{dv}{dt} = \frac{1}{2}C_D\frac{\pi D^2}{4}\rho_C(U-v)|U-v| \tag{4.5}$$

where m is the mass of the particle, v is its velocity and C_D is the drag coefficient. The relative Reynolds, Re_r, number can be defined as:

$$Re_r = \frac{\rho_C D|U-v|}{\mu_C} \tag{4.6}$$

The mass of the particle can be defined as:

$$m = \frac{\pi D^3}{6}\rho_p \tag{4.7}$$

Equation 4.5 can then be simplified to:

$$\frac{dv}{dt} = \frac{6}{8}\frac{C_D Re_r \mu_C}{D^2 \rho_p}(U - v) \tag{4.8}$$

and even further with the momentum response time to:

$$\frac{dv}{dt} = \frac{1}{24}\frac{C_D Re_r}{\tau_V}(U - v) \tag{4.9}$$

For low relative Reynolds numbers the factor $\frac{C_D Re_r}{24}$ is close to unity, for moderate relative Reynolds numbers this representation will under-predict the drag coefficient. In this context, this means that such a representation will indicate that the particles have slower responses to the flow than they really would in high relative Reynolds number cases. But in such cases equation 4.9 can be analytically solved to:

$$v = u(1 - e^{-\frac{t}{\tau_V}}) \tag{4.10}$$

This means that if the particles are suddenly exposed to a change in the surrounding air flow they will adopt 90 % of that speed within 0.5 CAD at conditions near TDC. This is promising, but only valid for low relative Reynolds numbers whereas if Lapple's expression for C_D [83]

$$C_D = \frac{24}{Re_r}(1 + 0.125 Re_r^{0.72}) \tag{4.11}$$

which is valid for Reynolds numbers below 1000, is used in equation 4.5 and then numerically solved some additional results can be achieved, as shown in figure 4.12 where the reaction time for the particles to adapt to the flow can be seen. In this example data for two gas velocities are shown, with conditions at both the point of injection and at TDC. The particles can be stated to be correctly chosen since they rapidly adapt to any changes (at least changes under the measured operational conditions) in the gas flow. This is of great importance since the flow field calculations are based on the movement of the seeded particles, and if they had not followed the flow properly none of the calculated data would have correctly represented the gas flow. Thus, the assumption underlying the PIV measurements, that the particles follow the flow, appears to be valid in this case.

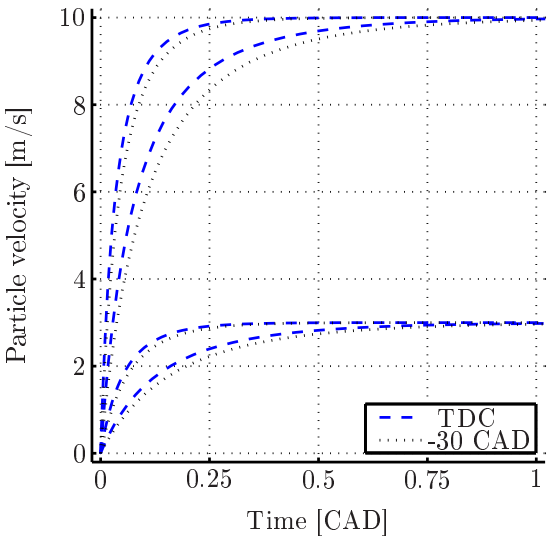

Figure 4.12: Particle velocity as a function of time (CAD) for conditions at -30 CAD and TDC with two sudden changes in velocity of the flow fields (3 and 10 m/s). The two lines for each flow field velocity and set of conditions correspond to changes in velocity described by the lightest, smallest(ρ_p=55 kg/m^3 and D=18 μm) and the heaviest, largest particles (ρ_p=65 kg/m^3 and D=28 μm).

4.3 Post-processing

4.3.1 Pressure trace analysis

Rate of heat release and combustion phasing

The cylinder pressure trace measurements were post-processed, in all cases, using MatLab. Pressure traces were recorded by a Kistler 6061B or 6053C piezo electric pressure transducer, with a sampling rate between 1 and 10 samples per CAD using an AVL Indimaster. The data were converted to ASCII-format and imported to MatLab.

The rate of heat release was calculated by assuming that the combustion process is close to an adiabatic isentropic process.

$$pV^{\gamma} = const \tag{4.12}$$

and

$$\gamma = \frac{c_p}{c_v} \tag{4.13}$$

Then the heat release can be written [11]

$$\frac{dQ}{d\theta} = \frac{\gamma}{\gamma - 1} p \frac{dV}{d\theta} + \frac{1}{\gamma - 1} V \frac{dp}{d\theta} \tag{4.14}$$

if the convective heat transfer and the crevice volume are small. CA50, the rate of heat release and the amount of heat released were all based on this equation with the assumption that γ remained constant. However, as described in earlier chapter, in many cases the behavior could not be assumed to be close to adiabatic and isentropic, hence a more representative representation was to assume that the process was polytropic. In such cases γ was replaced with the polytropic coefficient, n in equation 4.14.

Filtering

In any experiments noise and other disturbances are always present in addition to measurement errors. These noises can sometimes significantly affect the measurements, so to limit their effects all measured pressure traces were filtered. For this purpose the remezord function in MatLab was used, which applies the algorithm suggested in [84]. This function can be used for highpass, lowpass or bandpass filters and setting the input parameters provides the possibility to control the passband frequency (the frequency at which the filter starts to interact), the stopband frequency and the tolerable ripple for the passband and stopband. Figure 4.13 illustrates the effects of applying filters with various parameters. In all examples the same stopband filter frequency (3000 Hz) has been applied, the two black lines originate from application of the same passband frequency, but with different stopband ripple. The difference between the solid black and grey line is in the passband frequencies and the dashed grey line arises from a higher passband ripple compared to the other cases. From these examples it can be seen that these parameters provide sufficient control of the filters, however use of filters with small differences between passband and stopband frequencies combined with minor ripple, which were consistently used, demands significant post-processing time, but for the presented studies this time was not limiting.

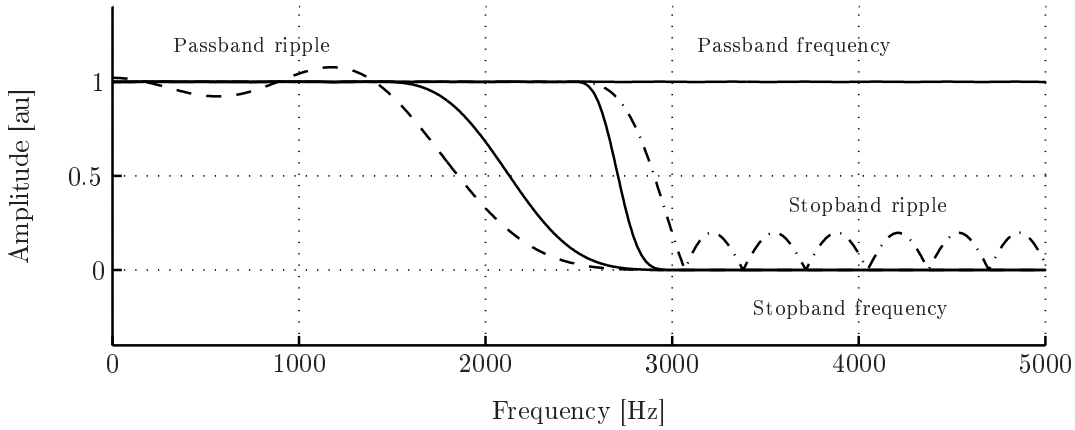

Figure 4.13: Examples of effects of filter parameters for the filters used.

An example of a pressure trace and its associated information can be seen in figure 4.14. For this example the engine was run at 1200 rpm and the pressure was sampled every 0.1 CAD, thus the sampling rate was 72 kHz. In figure 4.14(a) 20 sampled pressure traces are plotted (however, the individual traces strongly coincide with each other, making it impossible to see each trace). The pressure trace will contain information below 36 kHz, since information can only be acquired at half the sampling rate, this is called the Nyquist frequency [85], or less. Preferably a low pass hardware filter should be applied for the analog signal below this Nyquist frequency before sampling, this can often be done using the charge amplifier for the pressure transducer. In figure 4.14(b) the discrete Fourier transform of the pressure traces can be seen as the intensity of the signal at different frequencies and, as expected, the main information is obtained at low frequencies compared to the Nyquist frequency (the engine was rotating at 20 Hz).

In figure 4.14(c) the effect of low pass filtering with four filtering frequencies (1, 3, 8 and 15 kHz) can be seen, the top line corresponds to the signal obtained with the lowest filtering frequency and the one at the bottom to the highest. For representation, the pressure traces with the different filtering frequencies were separated in an absolute scale (filtering with a low frequency will naturally not elevate the pressure). In this example it can be seen that the disturbances caused by the EVC (at around 270 CAD) was effectively removed when the low pass filter with a filtering frequency of 1 kHz was used. However, it is clearly important to only eliminate noise and not the signal of interest. In figure 4.14(d) the same filter frequencies were used but in a highpass sense. It can be seen that with the lowest filter frequency (at the top) most of the disturbance at EVC is captured by the highpass filter, but some of the information regarding the combustion is also captured (*e.g.* the signal that arises at TDC). Hence, care must be taken to filter the signals correctly so the correct information is retained. One way of doing this

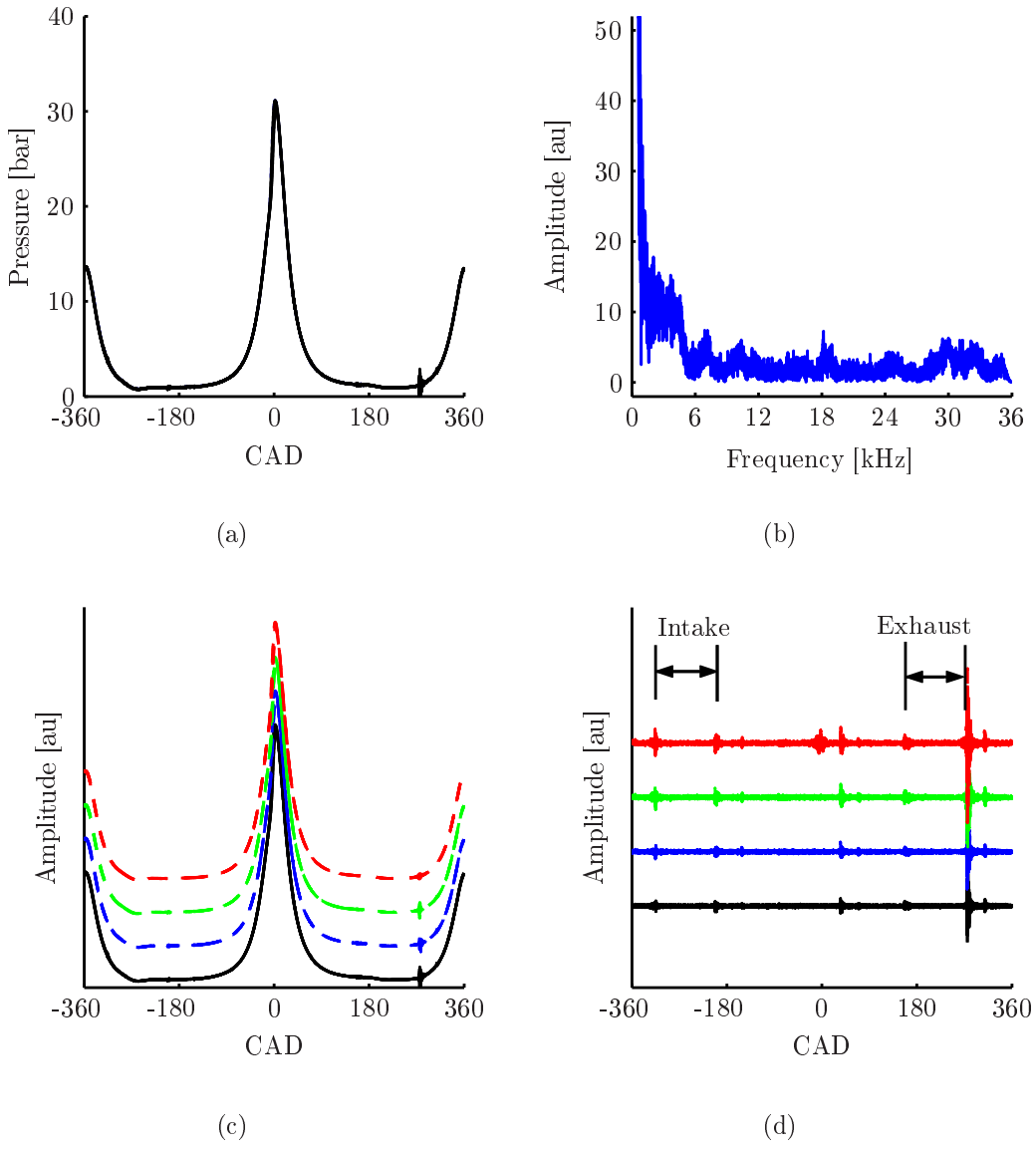

Figure 4.14: Twenty pressure traces sampled at each 0.1 CAD for an example with HCCI combustion using NVO (a), the amplitude of different frequencies for the pressure traces (b), effects of lowpass (c) and highpass (d) filtering of the pressure traces using 1, 3, 8 15 kHz filters.

is to use different filter frequencies for different regions in the pressure trace, in this example the region around EVC could be filtered using a low pass filter at a lower frequency compared to the region with combustion. This approach was mainly applied to data acquired from the prototype 6-cylinder Volvo engine. The disturbances caused by the valves can also be used to estimate the valve timing, since the valves induce high frequency noise in the cylinder head, which can be separated using a highpass filter as shown in figure 4.14(d) where the timing of the intake and exhaust opening and closing is marked. All frequency analysis and filtering was done using MatLab.

4.3.2 Image analysis

During the optical measurements several different cameras were used to gather the information. All post-processing of the images was performed in MatLab beside the PIV measurements in [65] where FlowManager (Dantec) was used to calculate the flow fields from the images. All LIF images were captured using image-intensified LaVision Dynamight cameras (see the blue cameras in figure 4.15), providing 1024x1024 resolution, equipped with LaVision DaVis 6.2 software. These images were then imported into MatLab for post-processing. Image intensification leads to different amounts of noise due to the high intensification of the weak signals, and thus post-processing of the images was essential.

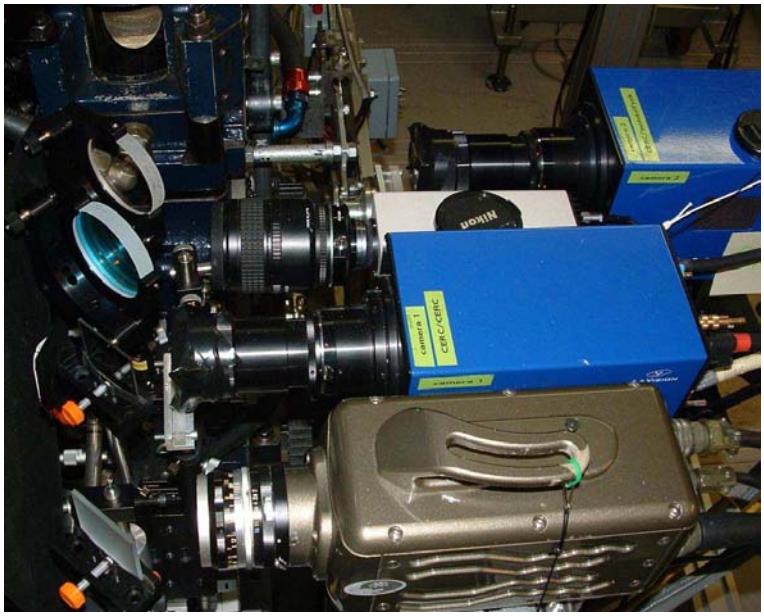

Figure 4.15: Cameras used for optical measurements.

This filtering process was thoroughly studied in order to verify that the filter worked properly and thus reduced the extremely high gradients in the images while maintaining the proper signals. The noise or sharp gradients in intensity caused by the image intensification was studied in images on- and off-resonance as well as in regions in the combustion chamber and regions outside the optically accessible region to obtain knowledge about these disturbances. In figure 4.16 two unfiltered, intensified LIF images of HCHO and OH can be seen (with typically grainy appearance). The intensity along a line in the image can be seen and along this line the noise can be estimated, outside the laser plane (*i.e.* outside the measured region) between 0 and 100 and above 400 pixel numbers (locations) the noise outside can be estimated. From these regions the background noise can be estimated.

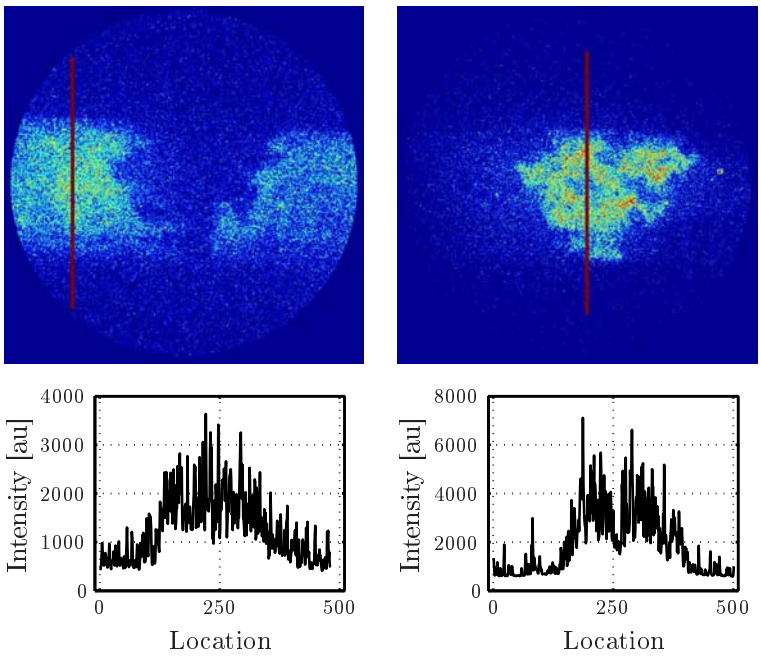

Figure 4.16: Examples of unfiltered LIF images of HCHO (left) and OH (right) and corresponding signals along a line in the image (bottom).

In figure 4.17 identical information to that shown in figure 4.16 is presented, following filtration in MatLab using a 2-dimensional median filter (medfilt2 [86]) to limit the noise that arose from the intensification. Naturally, great care must be taken since proper signals can be influenced by filtering (more information about the procedure can be found in the Appendix to Paper VI [55]). Since noise is completely stochastic, averaging leads to reductions in background noise, but if time-resolved information is required this method can be practically unfeasible.

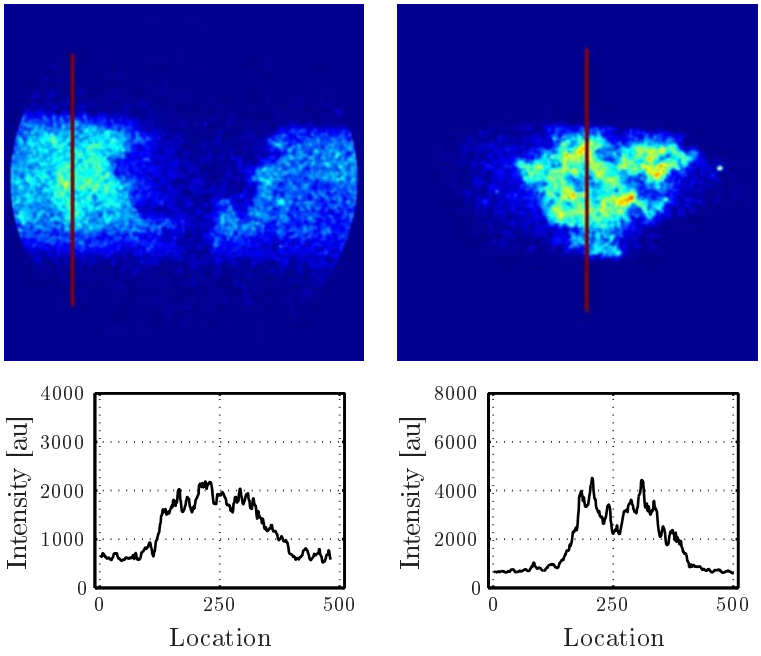

Figure 4.17: Examples of filtered LIF images of HCHO (left) and OH (right) and corresponding signals along a line in the image (bottom).

Direct imaging was also performed in the studies, and for this a monochrome Vision Research Phantom V 7.1 high speed video camera (see the green/gray camera in figure 4.15) was used to capture the propagation of the reaction zones with multiple images within the same cycle. When background light was required a Dedacool 250 W floodlight was used to illuminate the combustion chambers. The post-processing of the direct images was limited to filtering and flame propagation speed calculations. An AVL Visioscope was also used to capture direct images of the combustion in color, but no images captured by this camera have been published.

Chapter 5

Results

In this chapter some of the results documented in the papers and some additional results are presented and interpreted in the context of the project objectives. Results that highlight the challenges for the different regions in the operational range of HCCI are also presented to provide background information (as are results related to other, rival concepts besides HCCI in which dilution of the combustion mixture is applied).

5.1 Initial control studies

The initial published study was an essential first step in validating the feasibility of the concept of combining initial flame propagation through a stratified charge and subsequent HCCI combustion. From the presented results, the main conclusion relevant to the objective was that it is possible to combine flame propagation and HCCI combustion in one cycle, *i.e.* the concept appears to be feasible [71]. The results acquired by chemiluminescence imaging indicated that there is initially a propagation region and pressure trace analysis showed that the rapid heat release typical of HCCI combustion occurs in the later part of the combustion. For the following study it was essential to evaluate the levels of emissions generated when the concept was applied, especially the NO_X levels [72]. A hypothesis examined in the project was that NO_X levels similar to those generated in HCCI combustion could only be achieved using this combined combustion concept if hydrogen was used as the stratification fuel (since the wide flammability limits of the hydrogen would allow the flame to propagate through a very dilute mixture, thereby reducing the flame temperature and thus restricting the NO_X levels). The

results showed that there is potential to add this control method to a HCCI system without any major increases in NO_X if the parameters are chosen wisely. More importantly, they showed that the initial hypothesis was incorrect; NO_X levels similar to those of HCCI combustion could be achieved when using the proposed concept even without hydrogen. In terms of making this control method usable in a real vehicle, this is beneficial since the hardware requirement is reduced if only one fuel is to be used. Furthermore, the amount of hydrogen needed for the stratified charge would have been high, which would have made it challenging to achieve such levels with, for instance, onboard reforming. Only one fuel was used in all subsequent studies for this reason.

5.1.1 The role of charge stratification

In the third published study the concept of using initial flame propagation was set aside, since interesting effects caused by the charge stratification alone were found for some operational settings during some experiments, which were further investigated and documented in Paper III [75]. Since the concept involves the use of charge stratification, it was essential to evaluate the effect of the charge stratification alone. To allow a lower HCCI load, in accordance with the key objective, the control method should allow the combustion to be phased earlier since a reduction in load will retard the phasing. However, by using charge stratification alone the rate of heat release and pressure rise rates could be reduced (hence the maximum load for HCCI combustion could be increased). So by this point in the project, control methods potentially allowing both an increase of the maximum and reduction of the minimum HCCI load had been identified. Extending the HCCI operational range would allow use of the more thermodynamically sound HCCI combustion (relative to SI combustion) in a vehicle to a greater extent and thus enable reductions in fuel consumption, which was the main goal of the project.

In the studies I to III, [71; 72; 75], conventional SI valve lift profiles, intake air heaters and PRF and hydrogen fuels were also used to induce HCCI combustion. These are not the most likely methods of achieving HCCI combustion in passenger cars; a more likely concept for commercialization is to use NVO. So, even if methods for both high and low loads had been identified at this point, they were not necessarily directly compatible with the more production-feasible solution of achieving HCCI with NVO. Therefore, further studies were all conducted in engines using NVO.

5.2 Control of HCCI using NVO

5.2.1 HCCI using NVO and an SI Stratified Charge

In HCCI using conventional SI valve lift profiles and intake air heating (as described in Papers I to III) substantially lower levels of trapped residuals are applied than in HCCI using NVO (as described in Papers IV-VIII), thus, the conditions in which flame propagation must occur are completely different.

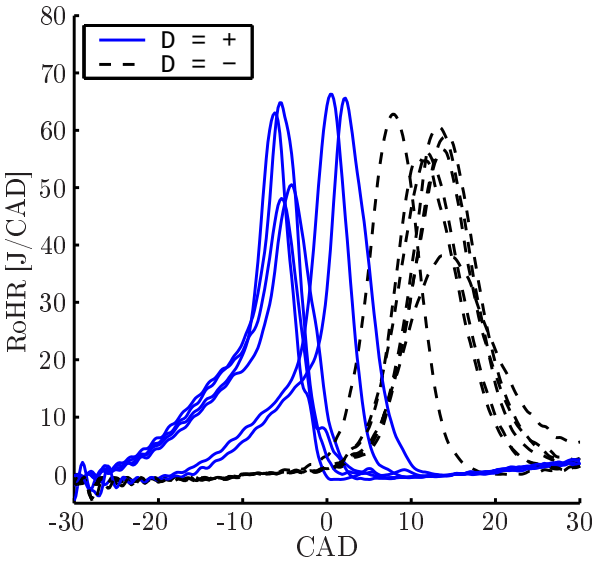

Figure 5.1: Averaged rates of heat release when spark ignition was (solid line) and was not (dashed line) used. Reprinted with permission from SAE Paper No. 2007-24-0012 © 2007 SAE International.

The results presented in Paper IV [53] are important in many senses. The use of NVO allows HCCI combustion to be achieved in real SI engine geometry with commercially available gasoline (see the previous chapter for further information). So, the concept is compatible with a production-feasible solution to achieve HCCI, and although PRF was used to allow optical measurements to be performed it is likely that the control concept can be used with HCCI achieved by applying NVO since realistic (for NVO concepts) valve profiles and compression ratios were used. In Study IV [53] a 2^{IV} factorial design scheme was used to evaluate four variables in two different states, and averaged rates of heat release for the different cases are shown in figure 5.1. The solid traces correspond to cases in which sparks were used and the dashed traces to cases in which no spark was used. There is a clear initial gentle rate of heat release, indicating the presence of a propagating

flame, in cases in which a spark is used (solid traces) and the subsequent more rapid heat release corresponds to HCCI combustion. This concept was then used to reduce the minimum load and three cases were thoroughly studied, see figure 5.2. The full implications of this reduction in load for the operation of a real engine will depend on many parameters, but the key finding is that for a certain configuration the indicated load could be decreased by almost half and the results obtained from (for instance) tests with the 6-cylinder engine indicate that there is a clear need for additional control at lower load, and this possibility of reducing the minimum load will be very welcome. Other important findings relevant to achieving the main objective were the possibility of achieving NO_X and indicated fuel consumption levels similar to those of HCCI combustion, even when the concept was used to significantly reduce the minimum HCCI load.

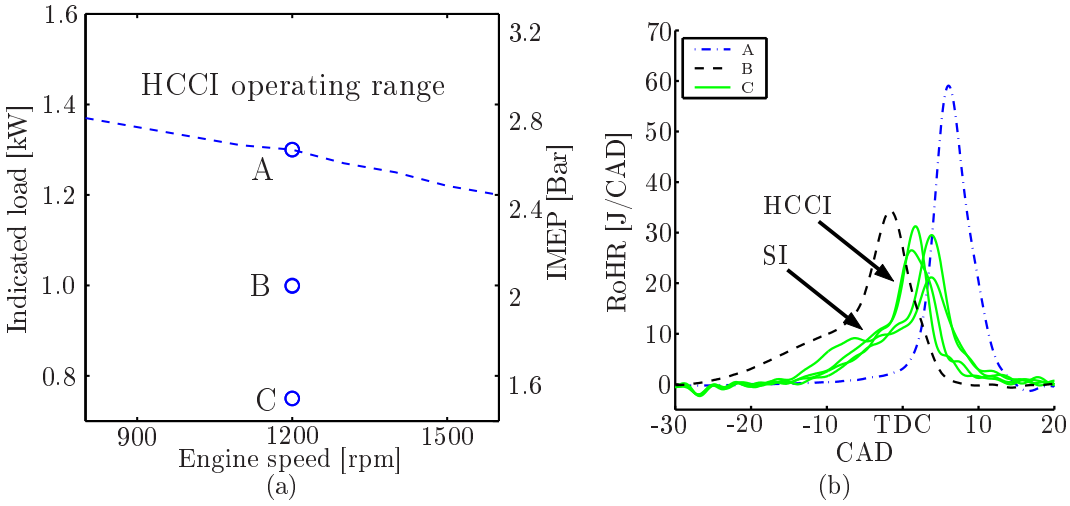

Figure 5.2: Loads and rates of heat release for the three operating conditions used in the optical studies described in Paper IV. Reprinted with permission from SAE Paper No. 2007-24-0012 © 2007 SAE International.

Furthermore, the fundamental aspects of the concept were validated in this study, *i.e.* that a stratified charge was created, see figure 5.3 and 5.4, and that the flame propagated through it. The local air equivalence ratio was also measured and found to be slightly lean. So these results fully validated the basic idea of the control method.

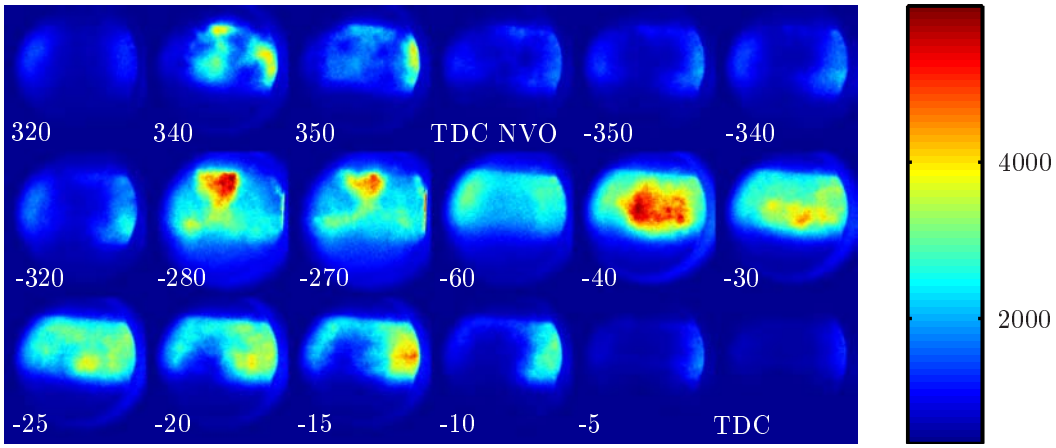

Figure 5.3: Averaged images (from 10 separate cycles) (and corresponding timings) for case B (Paper IV) of LIF from the fuel tracer 3-pentanone. Reprinted with permission from SAE Paper No. 2007-24-0012 © 2007 SAE International.

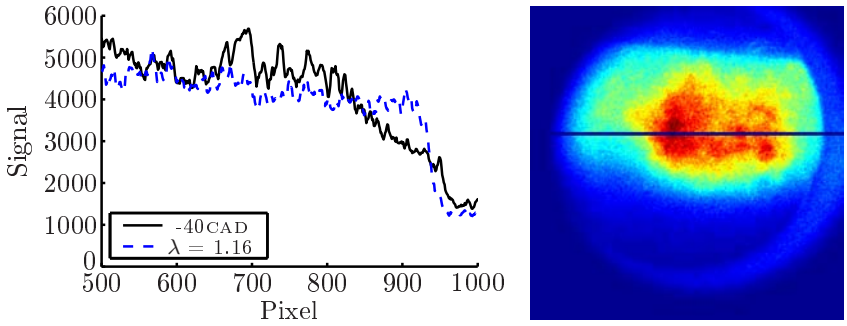

Figure 5.4: Average LIF image of the fuel tracer 3-pentanone at -40 CAD and its signal strength. Reprinted with permission from SAE Paper No. 2007-24-0012 © 2007 SAE International.

There were also other findings that were not directly related to the main objective but shed light on fundamental aspects of existing control methods. Chemiluminescence images were captured in order to locate the propagating flame during the compression, but they also indicated that high temperature reactions occurred during the NVO, these reactions were further investigated to experimentally examine the underlying reason for the control that can be achieved by using pilot injections in combination with NVO. The signs of chemiluminescence during the NVO can be seen in figure 5.5, with weak signals at 350 CAD, and slightly stronger signals at TDC during the NVO.

In addition to the high temperature reactions associated with chemiluminescence of OH, low temperature reactions manifested by signals of formaldehyde were also noted (see figure 5.6 where LIF from formaldehyde is shown). Formaldehyde

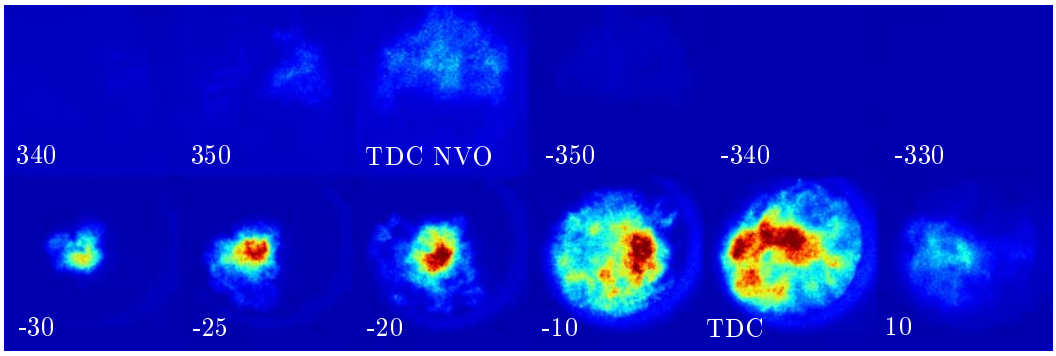

Figure 5.5: Average images (from 10 separate cycles), and corresponding timings, for case B (Paper IV) of the chemiluminescence of OH. Reprinted with permission from SAE Paper No. 2007-24-0012 © 2007 SAE International.

signals were observed during both the NVO and the main combustion, as expected since LIF of formaldehyde during the NVO was detected in [87], and the generation of formaldehyde during the main combustion process has been well documented by various authors, for instance [88] for SI combustion and in [89; 90] for HCCI combustion. The initial propagating flame is manifested by an expanding region of OH chemiluminescence signals in the later part of the compression (see figure 5.5). This flame can also be seen in the formaldehyde signals (figure 5.6), since the flame leaves a region with low intensity, in which the reactions have passed beyond the low temperature stage. So, at this point the fundamental idea of the proposed concept had been validated; initial flame propagation through a stratified charge can be combined with subsequent HCCI, and the concept can reduce the minimum achievable HCCI load.

5.2.2 Reactions during the NVO

In the following experiments, reported in Papers V and VI [54; 55], fundamental aspects of the control that can be obtained by using pilot injections were thoroughly studied. These studies were not directly connected to the main proposed concept, but the discoveries made concerning combustion during the NVO reported in Paper IV [53] could not be ignored since fundamental understanding is essential for further progress. For this reason alone these detailed studies would have been warranted, but in addition the use of pilot injections is a key element of obtaining (and controlling) HCCI using NVO. The reactions during the NVO were analyzed both by conventional pressure trace analysis and optical measurements. In figure 5.7 the reactions detected by analysis of pressure traces obtained from both the optical and multicylinder engines can be seen. Heat-generating reactions

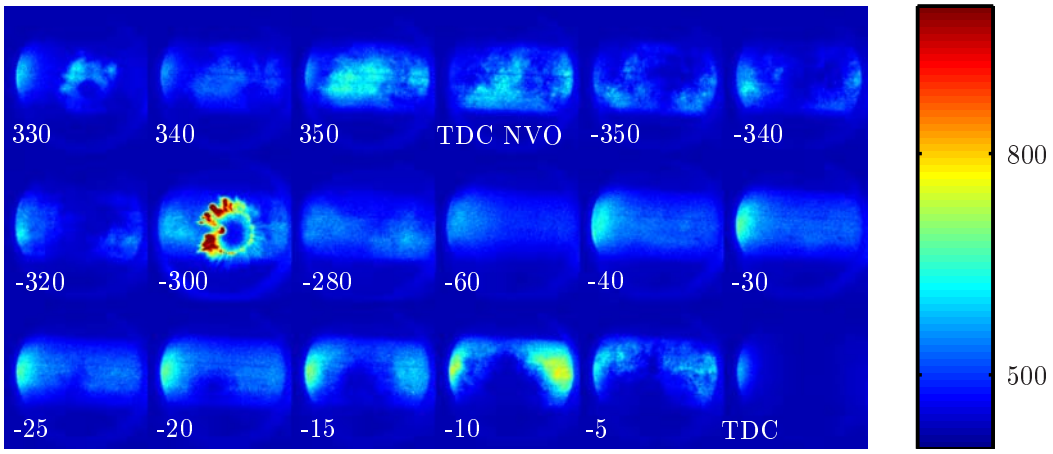

Figure 5.6: Average images (from 10 separate cycles), and corresponding timings, for case B (Paper IV) of LIF from formaldehyde. Reprinted with permission from SAE Paper No. 2007-24-0012 © 2007 SAE International.

were detected using the pressure transducers for both engines, and the quantity of heat generated using each tested pilot to main injection ratio was analyzed to evaluate how much this variable influenced the temperature prior to the main combustion. Other findings that are important in terms of the credibility of all results obtained from the optical engine, are the small discrepancies between the results from the multi-cylinder HCCI engine using gasoline and the optical engine using elevated intake air temperatures and PRF. Hence (provided the settings are carefully chosen) the results obtained from the optical engine can replicate the results in a multi-cylinder engine using gasoline even for a delicate combustion mode, such as HCCI, and for reactions during the NVO (as illustrated by the rates of heat release during the NVO in the two engines shown in figures 5.7(c) and 5.7(d)).

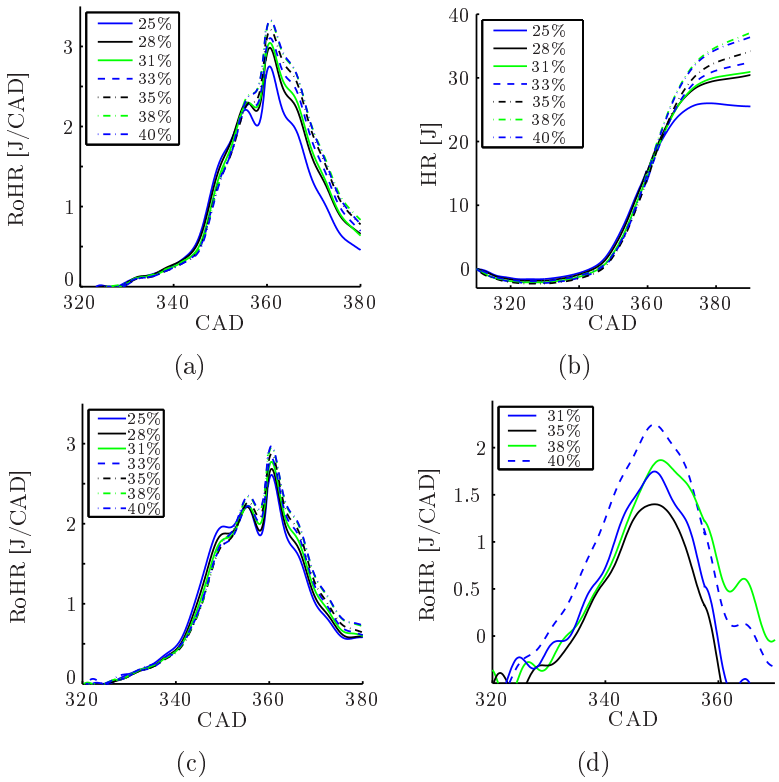

Figure 5.7: Rate of heat release and accumulated heat release during the NVO obtained with various pilot to main injection ratios in tests with the 6-cylinder HCCI engine with 160 CAD NVO (a) and (b), with 180 CAD NVO in the 6-cylinder HCCI engine (c) and the optical engine (d). Reprinted with permission from SAE Paper No. 2007-01-0037 © 2008 SAE International.

As previously mentioned, pilot injections can be used to control the combustion. In these experiments the relative proportion of the pilot injection was incrementally increased from 25 % to 40 %, which advanced combustion phasing by around 5 CAD, see figure 5.8(a). The influence of the heat-generating reactions measured during the NVO on charge temperature can be seen in figure 5.8(b).The difference in temperature at 10 CAD before TDC is 45 K, based on polytropic calculations from the pressure traces. Gas-phase temperature was studied during HCCI combustion by using Coherent Anti-Stokes Raman Spectroscopy (CARS) [91], to analyze HCCI combustion with similar amounts of EGR, but at slightly higher loads. It was found in the cited study that a difference in temperature at TDC of 7 K would change the combustion phasing (CA50) by around 1 CAD. Similar ratios of changes in the CA50 timing to changes in temperature were found in this study and the temperature at the start of combustion (SOC) was similar for the two cases. Thus, it was concluded that the difference in heat generated by the two different pilot to main injection ratios was the major contributor to the

difference in combustion phasing between the two cases.

These results validate the conclusion drawn in [51; 43] that exothermic reactions do occur and provide indications of their impact on combustion phasing. However, the role of the radicals formed during the NVO should not be neglected. The results indicate that the observed changes in phasing were largely due to the increased rates of exothermic reactions during the NVO associated with higher relative amounts of pilot injections, but increases in levels of radicals may play a major role in promoting HCCI combustion.

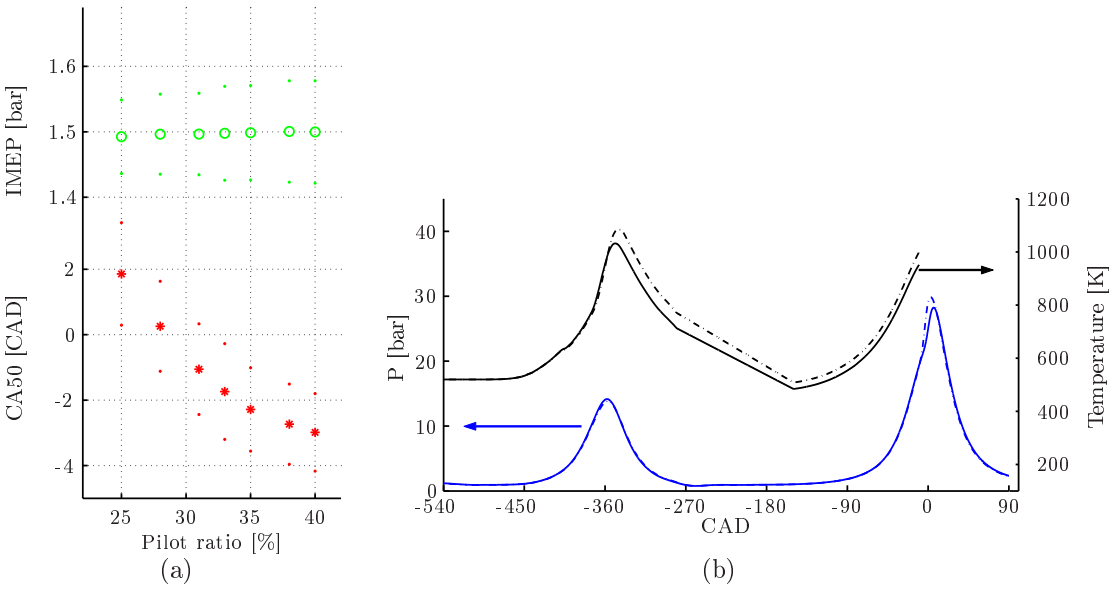

Figure 5.8: IMEP, air equivalence ratio and combustion phasing observed in tests with 160 CAD NVO and different pilot to main injection ratios (a). Standard deviations are indicated by dots. Pressure traces and calculated mass-averaged temperatures in tests with 25% and 40% pilot injections, with 160 CAD NVO (b). Dashed lines correspond to 40% pilot and solid lines to 25%. Reprinted with permission from SAE Paper No. 2008-01-0037 © 2008 SAE International.

Evidence of low temperature reactions during the NVO was found and signs of high temperature reactions were also seen in the studies described in Paper IV [53]. However the high temperature reactions were detected by observing the chemiluminescence of OH, which can be misleading since emissions from species generated in reactions other than the target species may influence the measurements, see earlier chapter. For this reason LIF of OH was measured since it can isolate OH signals from those of species generated in other reactions that emit chemiluminescent light in the measured wavelength band. LIF signals of

OH were observed during the NVO, see figure 5.9. Further, the signal arose at identical timing to the heat-generating reactions detected by pressure trace analysis (compare the LIF signals in figure 5.9 and the rate of heat release in figure 5.7(d)). However, OH was present within the combustion chamber for a short period after the peak of rate of heat release. These results validated the previous indication of high temperature reactions reported in Paper IV [53] and provided further fundamental understanding of the control that can be obtained using pilot injections.

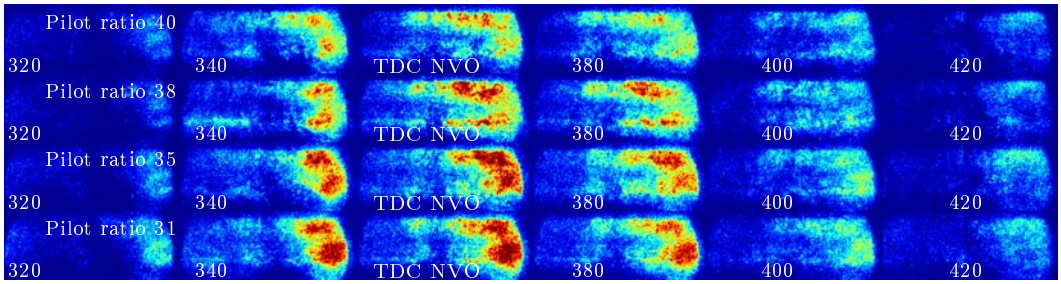

Figure 5.9: Averaged LIF images from OH in tests with different pilot to main injection ratios and different timings. Reprinted with permission from SAE Paper No. 2008-01-0037 © 2008 SAE International.

5.2.3 Simultaneous measurements

The last measurement campaign was intended to investigate all the main parameters that are influenced by combining initial flame front propagation through a stratified charge with subsequent HCCI combustion (mostly simultaneously to limit any misinterpretation that could arise, for instance, from averaging). The results, reported in Paper VIII [65], are important since they summarize many aspects of the concept.

The main results yet again showed (as in Paper IV [53]) that the minimum load for HCCI could be reduced with modest, or no, compromises in terms of HC, CO or NO_X emissions or indicated fuel consumption, which was the main objective for the proposed concept (see table 5.1, where data obtained at three different settings are presented). In figure 5.10 the average pressure traces and corresponding mass fractions burned (MFB) derived for the three studied cases can be seen.

The three cases were investigated using both averaged and simultaneously obtained data. In figure 5.11 the averaged LIF of the fuel tracer 3-pentanone observed in the three studied cases can be seen, where cases B and C include use of the

Table 5.1: Operational settings and results for tested cases in paper VIII [65].

	Case A	Case B	Case C
Indicated load	1.3 kW	1.0 kW	0.8 kW
IMEP	2 bar	1.65 bar	1.3 bar
ISFC	282 g/kWh	270 g/kWh	268 g/kWh
λ	1.21	1.27	1.30
HC (C3)	1725±50 ppm	2525±250 ppm	2275±170 ppm
NO_X	16±2 ppm	10±2 ppm	22±2 ppm
CO	0.5-0.6%$_{volume}$	0.5-0.6%$_{volume}$	0.5-0.6%$_{volume}$
Pilot injection duration	1.6 CAD	1.1 CAD	1.2 CAD
Main injection duration	1.0 CAD	1.1 CAD	0.6 CAD
Stratification injection duration	No stratification	0.8 CAD	1.0 CAD
Spark timing	No spark	-26 CAD	-26 CAD
EOI main	-310 CAD	-310 CAD	-310 CAD
EOI pilot	310 CAD	310 CAD	310 CAD
EOI stratification	No stratification	-30 CAD	-30 CAD

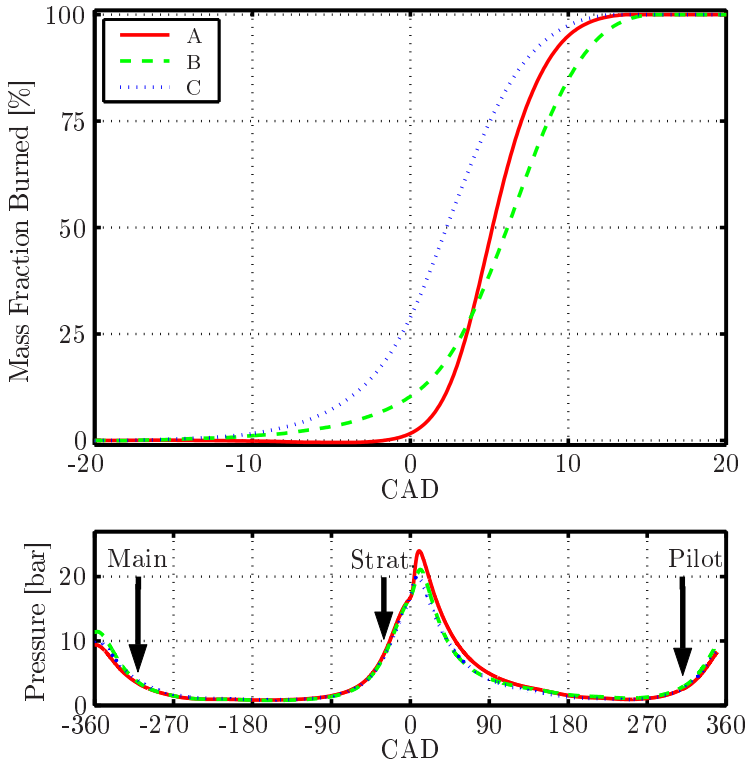

Figure 5.10: Averaged pressure traces, with injection timings (bottom) and averaged mass fractions burned for the three cases reported in Paper VIII.

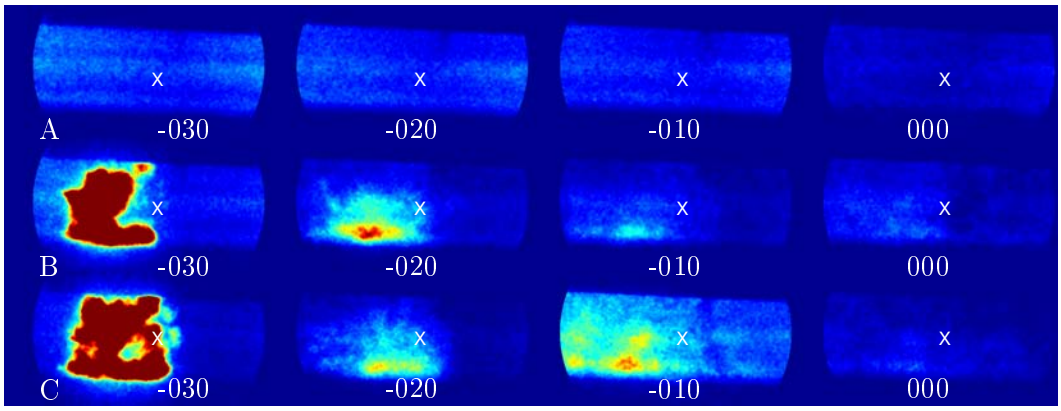

Figure 5.11: Averaged LIF images of the fuel tracer 3-pentanone for the three studied cases (A, upper row; B, middle row; and C, lower row). The columns, from left to right, show images recorded at 30, 20, 10 and 0 CAD before TDC, respectively. X corresponds to the sparkplug position.

proposed concept with charge stratification and spark-assistance, neither of which was used in case A. The stratified regions can be seen as local regions with strong signals from the fuel tracer, and the initial flame propagation can be seen as small regions with LIF signals from OH in the vicinity of the spark plug at around -10 CAD, see figure 5.12. At around 10 CAD after TDC OH signals can be seen in most of the measured region (although in case B the OH signals have not peaked at 10 CAD, due to the late combustion phasing), and the intensity for case A reaches such levels that a significant amount of absorption can be seen in reduced signal strengths as the laser sheet passes through the engine.

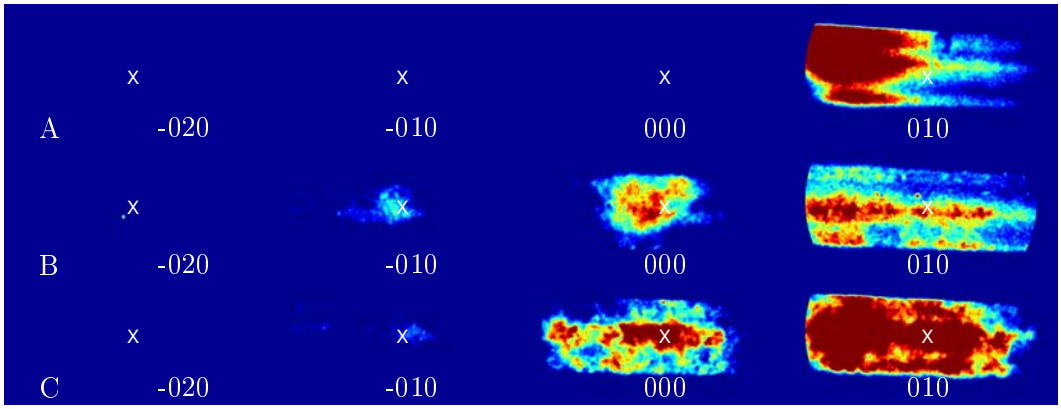

Figure 5.12: Averaged LIF of OH images for the three studied cases (A, upper row; B, middle row; and C, lower row). The columns, from left to right, show images recorded at 20, 10 and 0 CAD before TDC and at 10 CAD after TDC. X corresponds to the sparkplug position.

Averaged images from formaldehyde LIF can be seen in figure 5.13. The intensity of the formaldehyde signal is initially weak, at -20 CAD, and increases thereafter. For the cases with charge stratification, strong intensity was seen for an extended period, especially in the rich regions just prior to TDC. Clearly, therefore, the spark-initiated flame induced a temperature increase that contributed to fuel decomposition and HCHO formation in the richer regions. At -10 CAD, and especially at TDC, evidence of the flame was manifested in a reduced HCHO signal in regions where OH was present, although the complete separation cannot be seen in averaged images.

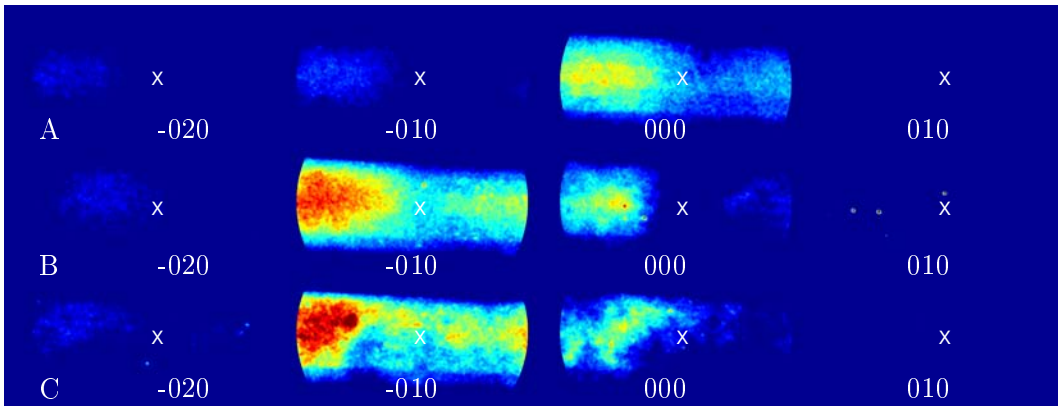

Figure 5.13: Averaged LIF of formaldehyde for the three studied cases (A, upper row; B, middle row; and C, lower row). The columns, from left to right, show images recorded at 20, 10 and 0 CAD before TDC and at 10 CAD after TDC. X corresponds to the sparkplug position.

In the averaged LIF images the propagating flame can be seen as regions with low signals for formaldehyde or the fuel tracer and with strong regions for OH, but the images are diffuse since there are cycle to cycle variations in the flame. Hence, the averaged images have less sharp edges than the separate images. Furthermore, the transition from initial flame propagation to HCCI combustion occurs at different timings due to the variations, which can lead to unrepresentative results if averaging is used. In figure 5.14 a single shot of formaldehyde LIF is combined with iso-lines representing the chemiluminescence of CO_2 obtained using a high speed video camera just prior to, during and after the single shot was taken. From this it can be seen that the delicate transition and propagation of the HCCI combustion occur in regions that display high levels of formaldehyde just prior to the transition or propagation. These regions were found to be due to the charge stratification. So the stratified charge not only resulted in flame propagation but also supplied regions that were more prone to HCCI combustion.

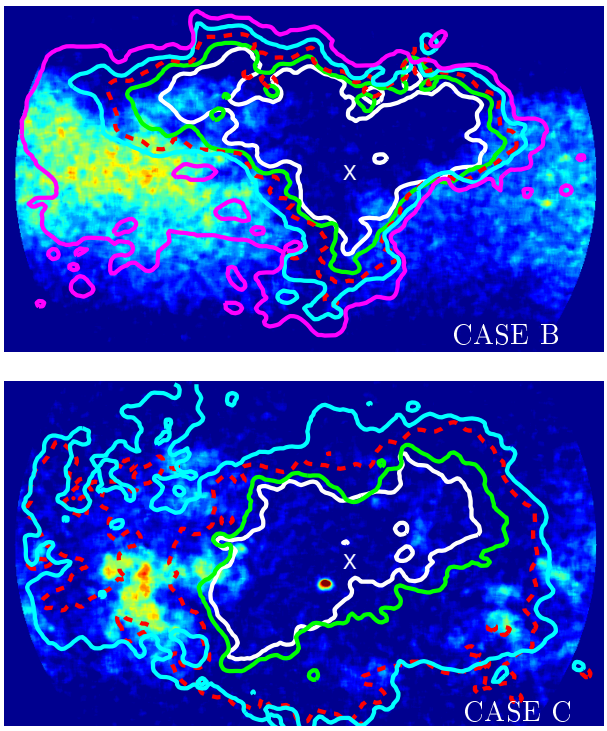

Figure 5.14: LIF of formaldehyde images at TDC and iso luminosity lines (from high speed video images acquired prior to, during and after TDC) obtained in the same cycle for cases B and C at TDC. X corresponds to the sparkplug position.

Turbulence

The influence of turbulence was not addressed in the studies described in Paper VIII [65], but will be discussed here. In the paper it is shown that the proposed concept influences many parameters, unsurprisingly since the intention is to use charge stratification to promote flame propagation through a globally lean charge, and this was the fundamental reason for using charge stratification throughout the project. However, the charge stratification also has other effects, notably it induces air motions in the otherwise quiescent environment and when initial flame propagation is achieved the flame also contributes to air motions.

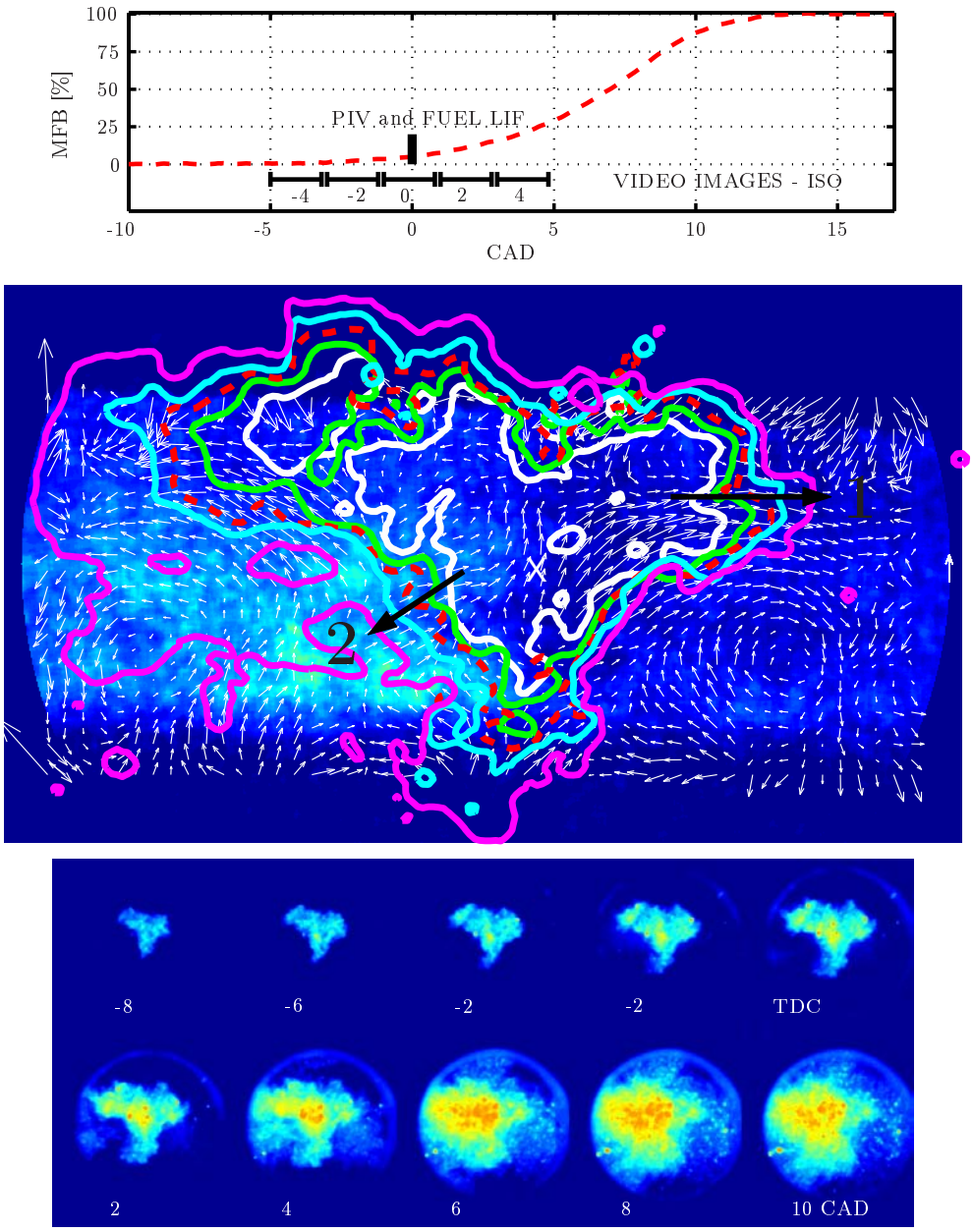

Figure 5.15: Mass fraction burned and timing of measurements (top) in case B (Paper VIII). The timings of the video images correspond to those of the iso lines acquired from video images. Averaged LIF of the fuel tracer, cycle-resolved flow field and iso lines from the high speed video images obtained in the same cycle for case B near TDC (middle). X corresponds to the sparkplug position. A vertical reference arrow corresponding to 3 m/s is shown to the right of the flow field. The iso lines (white, green, dashed red, cyan and magenta) represent threshold values from the video images prior to, during and after TDC (-4 to 4 CAD). Video images from -8 to 10 CAD (bottom).

Turbulence within the combustion chamber promotes flame propagation [11] and, since greater air motions are associated with greater turbulence increasing the air motion can be an effective way of promoting flame propagation. In Study VIII it was found that the flame propagated with great speed, relative to the air motion, towards the rich regions during the initial stages of flame propagation, and this was explained as being due to the stratified region increasing the flame speed.Let us compare the flame propagation in regions 1 and 2 in figure 5.15. In region 1 the flame propagation speed is high relative to some fixed geometrical point and it propagates towards the leaner regions in the same direction as the flow. In contrast, in region 2 the flame propagation speed is lower relative to some geometrical point and it propagates towards the richer region in the opposite direction to the flow. However, if the flame propagation speed is calculated relative to the air flow, then for this case (which represents the early stage of flame propagation), the flame propagation speed is considerably higher for the propagation towards the richer region.

The role of turbulence in the cases examined in the paper has not been determined and to accurately measure the turbulence in a single cycle is at least challenging. With the results from the measurements the only possible way to estimate the impact of turbulence is to evaluate how the different cycles behave compared to the average. In [11] the root mean square fluctuation is defined as:

$$U_{RMS} = \sqrt{\frac{1}{N_c}\sum_{i=1}^{N_c}(u - \bar{U})^2} \tag{5.1}$$

where N_c is the number of measured cycles, u is the velocity for an individual cycle and $\bar{U}$ is the average velocity for all measured cycles. However, this will not represent the true turbulence for a specific cycle of interest since it will include the natural variance of the flow field within the combustion chamber, and will be an average value for several cycles, while the video image, pressure trace and flow field shown in figure 5.15 were all measured in the same cycle.

As concluded in the paper, the proposed concept leads to greater air motions within the combustion chamber, induced by both the stratification injection and the expanding gas behind the flame, as can be seen in figure 5.16(a), in which air motions are significantly weaker for the case of HCCI combustion without any stratification or spark assistance (top) than for the cases in which the proposed concept is applied (middle and bottom). As mentioned earlier, stronger air motions are generally associated with higher turbulence. This can be seen in figure 5.16(b), where the U_{RMS} value is shown for the same geometrical regions as in figure 5.16(a). It should be noted that the highest values are observed at the boundaries of the measured plane, but this is mainly due to higher measure-

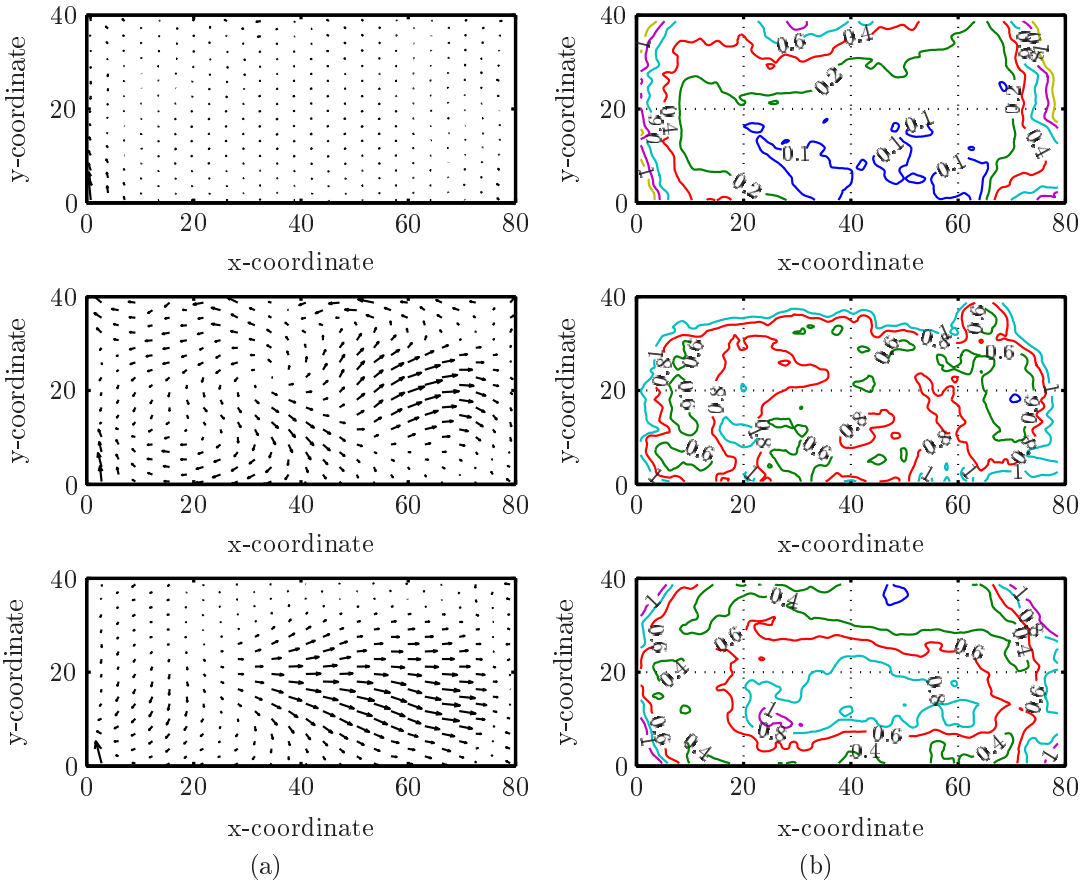

Figure 5.16: Averaged flow fields (from data acquired during 30 individual cycles) (left) and iso lines for U_{RMS} (right) for the cases addressed in Paper VIII: HCCI without spark assistance or charge stratification (top), HCCI with spark assistance and a minor stratification injection (middle) and with a greater stratification injection (bottom).

ment errors near the boundaries. It was found in Study VIII [65] that the flame propagated with great speed relative to the flow towards the richer regions during the initial stage of the flame propagation. However, this may be a fundamental misinterpretation, since the richer regions may merely be more turbulent and it may be the greater turbulence that increases the flame speed. This possibility will be further investigated here by using the U_{RMS} value as a representation of the turbulence.

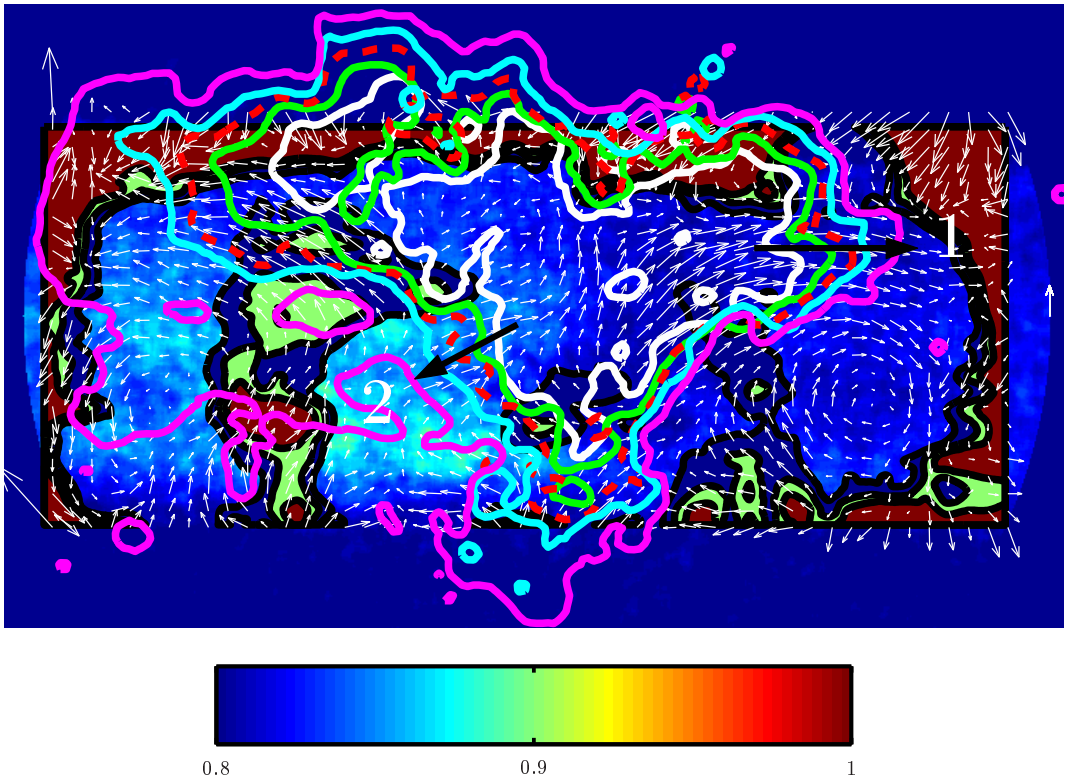

Figure 5.17: Averaged LIF of the fuel tracer, cycle-resolved flow field and iso lines from the high speed video images obtained in the same cycle for case B near TDC. A vertical reference arrow corresponding to 3 m/s is shown to the right of the flow field. The iso lines (white, green, dashed red, cyan and magenta) represent threshold values from the video images prior to, during and after TDC (-4 to 4 CAD). Turbulence intensity is represented by iso lines of U_{RMS} for values > 0.8 m/s.

In figure 5.17 the intensity of U_{RMS}, as shown in figure 5.16, is added to the information presented in figure 5.15 to determine if it is the turbulence that increases the flame speed towards the richer region. As previously mentioned, the greater cyclic variation or turbulence near the boundaries is likely due to measurement errors. It should also be noted that the seeded particles do not

respond immediately, as seen in figure 4.12, hence they do not provide complete information about the turbulence spectra. There are regions that display slightly higher levels of U_{RMS}, in figure 5.17, indicated by filled iso lines that highlight regions with U_{RMS} values > 0.8 m/s. However, those regions are not geometrically located in the same region that showed high flame propagation speeds, so the conclusion in Paper VIII [65] that the flame speed is increased due to the fuel equivalence ratio in the studied region is likely valid. However, the turbulence will clearly play a general role in increasing the flame speed, and the turbulence was significantly higher in cases in which the proposed concept was applied than in the case where it was not used (figure 5.16). Nevertheless, the levels are in the same order of magnitude for the regions where the flame propagates, thus turbulence does not dictate the direction of propagation for the flame, but merely makes the conditions more fluid dynamically more suitable for flame propagation in any direction.

5.3 Operational window for HCCI with NVO

The results presented in this section provide background information for HCCI using NVO, to give the reader the necessary information to put the published results into context. A similar engine to that used in Studies V and VI [54; 55] (but with different valve lift profiles) was used to acquire the results presented in this section, and basic parameters for the engine are listed in table 5.2.

Table 5.2: Engine parameters for the prototype 6 cylinder Volvo engine used for the operational window evaluation.

Parameter	Value	Unit/Parameter	Name/Value
Bore [mm]	84	Injectors	Bosch HDEV 1.2
Stroke [mm]	96	Displacement [cm^3]	3192
Compression ratio [au]	11.5	Fuel	RF-02-03
Water and oil temperature [C°]	90		

5.3.1 Fuel consumption for HCCI with NVO

Naturally a new concept for future vehicles is only promising if it offers a significant improvement in efficiency compared to its costs. For this reason the same engine was operated in both HCCI and conventional SI modes to investigate the improvement in fuel consumption the former could offer. For this study high lift

profiles were used for both intake and exhaust in SI mode and low lift for both intake and exhaust in HCCI mode. This approach could give slightly misleading indications at very low loads since an SI engine would not need to switch cam profiles in this comparison, in which only high lift was used, thus the results for the SI could have been slightly better if the engine did not have the capacity to switch profiles, which is associated with minor additional friction. Hence, the improvement at very low loads offered by HCCI will be slightly over-estimated here.

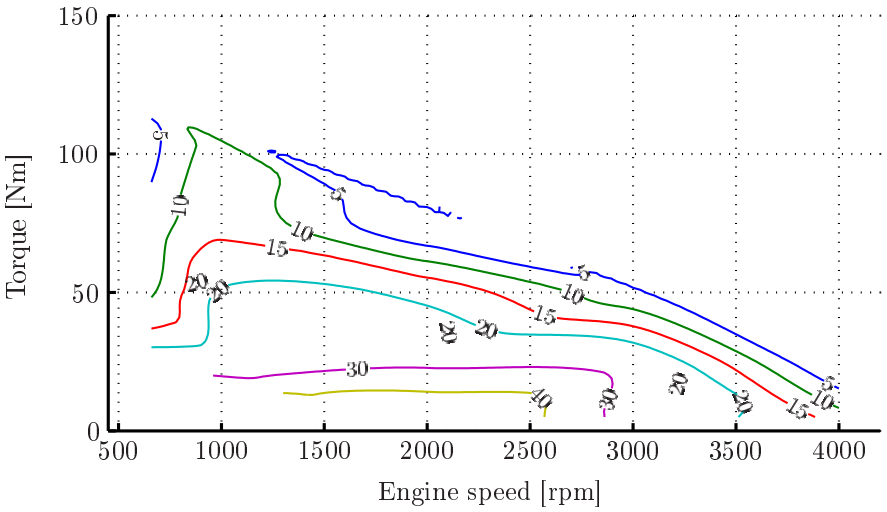

Figure 5.18: Reductions in fuel consumption by the prototype 6-cylinder Volvo engine offered by HCCI operation, compared to SI operation, at various loads and speeds, in percent BSFC.

In figure 5.18 the observed improvements in BSFC can be seen, and generally it can be stated that HCCI reduces consumption across its complete operational range. The degree of its impact varies from marginal to significant improvement, and the levels presented are similar to or slightly better than those presented in [61; 20]. So from this perspective, achieving HCCI by using NVO appears promising.

5.3.2 Dilution for HCCI with NVO

Measuring the exact amount of trapped residuals is challenging, but the timing of exhaust valve closure, the in-cylinder and exhaust back pressure and the exhaust gas temperature can be used to estimate the in-cylinder trapped mass, which in turn can be related to the mass flow of incoming air and fuel.

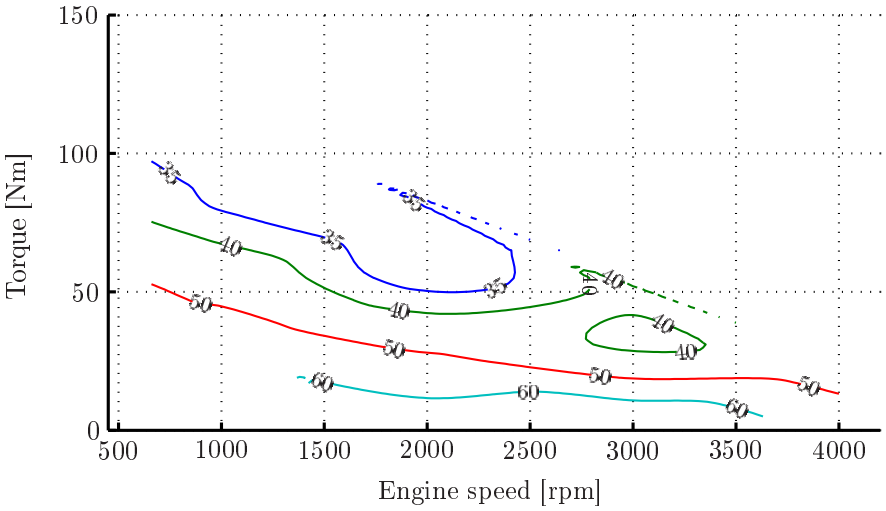

Figure 5.19: Estimated amounts of residuals (in $\%_{\text{mass}}$) trapped in-cylinder during operation of the prototype 6 cylinder Volvo engine at various loads and speeds.

The estimated amounts of trapped residuals can be seen in figure 5.19. Generally it can be stated that the absolute values are high, but for the higher loads lower amounts of residuals are needed to establish HCCI combustion. The higher loads lead to higher cylinder wall temperatures, higher exhaust and residual temperatures and the richer mixtures lead to shorter ignition delays and hence the observed trend. For the lower loads greater amounts are needed since the lower loads have opposite effects to those of the higher loads. However, with the possibility of changing the valve timing, and thus the residual amounts, a major step has been taken towards increasing the operational range for HCCI. In earlier chapter it was shown that it also makes sense thermodynamically to use dilution with air, and this also applies to HCCI with NVO, as can be seen in figure 5.20. For this engine the air equivalence ratio varies between unity and 1.6.

5.3.3 High load region

Beside the reduced mass flow, which clearly reduces the maximum HCCI load with NVO compared to the SI load without NVO, several other factors limit the maximum HCCI load. The rapid heat release, leading to short combustion duration, which is beneficial in terms of thermodynamic work, will also lead to too rapid combustion at a certain load point. This, in combination with the intensity of the combustion becoming more intense at higher loads, leads to various problems. If the peak pressure becomes too high in comparison to the

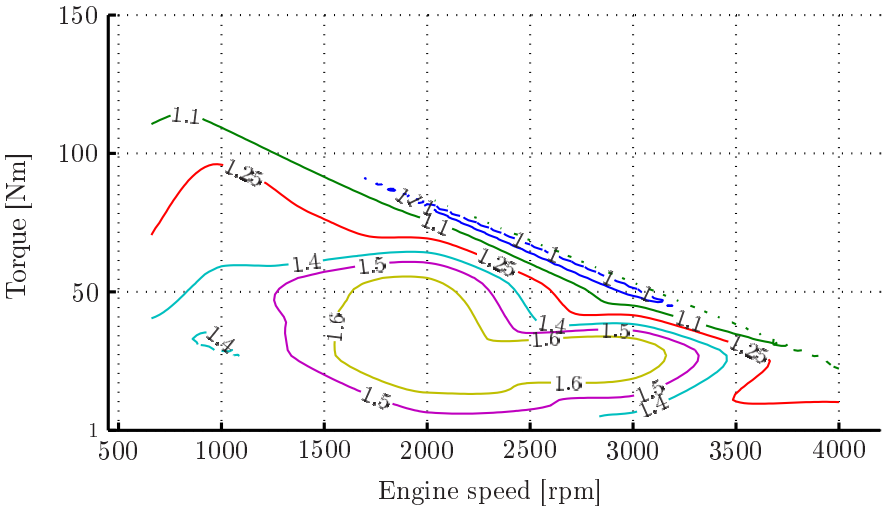

Figure 5.20: Stoichiometric ratio [λ] during operation of the prototype 6 cylinder Volvo engine at various loads and speeds.

structural integrity of the engine then it could cause mechanical failure. However, this is not the main issue (for naturally aspirated engines) since the amount of oxygen available for combustion with NVO valve events limits this maximum peak pressure somewhat, hence the peak pressure achieved during HCCI combustion will often be lower than the pressure achieved at full load for SI operation. A factor of greater importance is the rate of increase of pressure with time (or increase of pressure per crank angle); at higher HCCI loads the rate of the pressure rise due to the rapid combustion will cause noise, and it is assumed that this will be limiting before excessive pressures are reached in absolute terms (especially since the SI engine's slow combustion and reduced intake pressure at low loads leads to very low pressure rise rates, i.e. there will be a great difference in mechanical noise between HCCI at its highest load and SI combustion at similar load, which is an important issue for customers).

The pressure gradients obtained at different speeds and loads can be seen in figure 5.21 (averaged values for all six cylinders in terms of increases in the absolute pressure over one CAD). The absolute value of the pressure gradient depends strongly on how it is calculated, the values here are average values of the maximum pressure gradient observed in each of 100 recorded cycles, which are then averaged for all cylinders. Inevitably, in some individual cycles the values in some specific cylinders will be much higher than the engine average, but the average provides good indications of general trends in pressure rise rates. The maximum limit for HCCI is represented as a grey area (it is not a clear, absolute limit since it will be heavily dependent on NVH requirements for the specific vehicle). It can

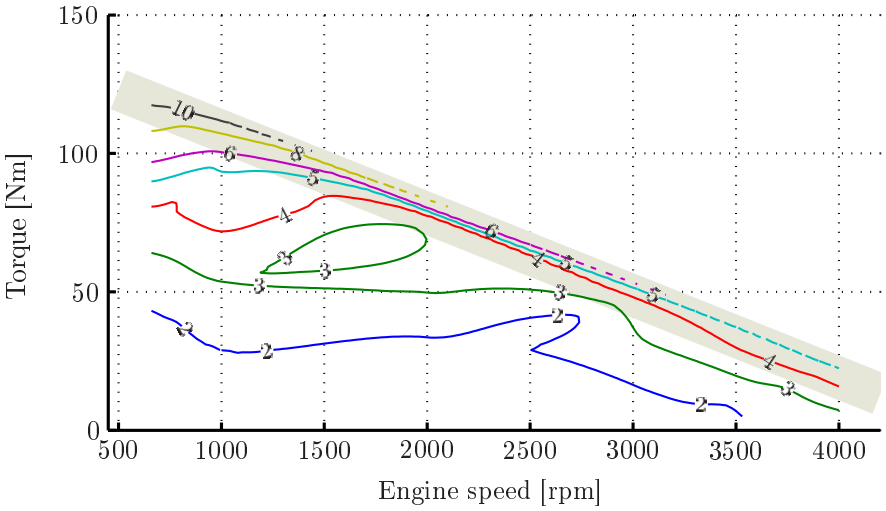

Figure 5.21: Averaged pressure gradient, $\frac{dp}{d\Theta}$ [bar/CAD] during operation of the prototype 6 cylinder Volvo engine at various loads and speeds.

be seen that the pressure rise rate depends on both speed and load. Further, it is especially sensitive when the maximum limit is reached. Near the limit a small load reduction leads to a greatly reduced pressure rise gradient. This sloping gradient has been noted by various authors, and is assumed to be due to limitations in aspiration at high engine speeds [20].

As described in previous chapter, HCCI operation leads to low levels of NO_X emissions and the levels for the prototype 6-cylinder Volvo engine can be seen in figure 5.22, where the molar ratio of NO_X is presented. There are regions with ultra-low engine-out NO_X emissions, but there are also regions with NO_X levels that cannot be tolerated for extended periods of time if stringent emission limits are to be met. Alternatively, the maximum limit for HCCI could be set for a specific NO_X level. In figure 5.23 identical information to that shown in figure 5.22 is displayed, but in brake specific values. It is obvious that the NO_X levels may influence the maximum load for HCCI since the levels rise rapidly when approaching the grey area. Naturally, the engine-out levels that can be tolerated will also depend on the exhaust after-treatments that are applied, *i.e.* whether a lean NO_X after-treatment system is used or not.

To summarize information acquired regarding the high load region it can be stated that the high load limit will be governed by various parameters, the absolute maximum being limited by aspiration (λ approaching unity). More likely, in practice the limit will be set by NVH or emission levels. There are various ways of influencing conditions near the high load limit. In Study III [75] the effect of

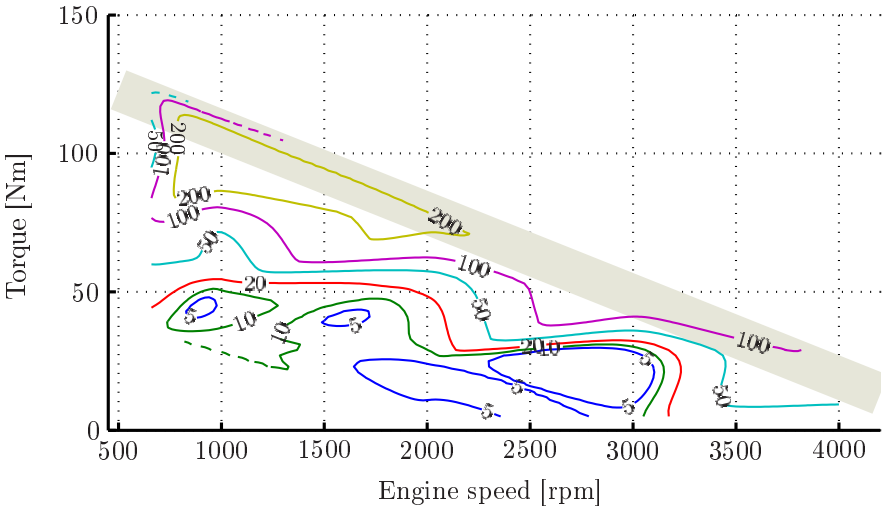

Figure 5.22: Engine-out NO_X [ppm] emissions from the prototype 6-cylinder Volvo engine at various loads and speeds.

charge stratification on high load conditions was investigated (although not on HCCI achieved with NVO) and the trends observed could facilitate attempts to extend the high load limit by, for instance, reducing the maximum rates of heat release. This concept with charge stratification was further investigated on HCCI using NVO in Study VII [73].

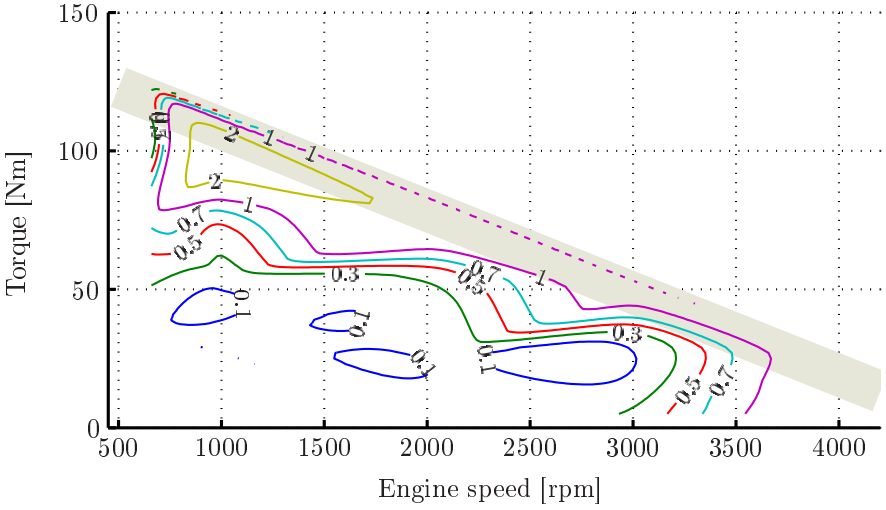

Figure 5.23: Engine-out Brake Specific NO_X [g/kWh]emissions from the prototype 6-cylinder Volvo engine at various loads and speeds.

5.3.4 Low load region

The valve lift and duration of the low lift camshafts dictates the maximum air flow through the engine during HCCI operation and this maximum air flow will influence the maximum limit for HCCI to a certain degree. It will also influence conditions in the low load (or low mass flow) region. As shown in figure 5.19 there is a need to increase the residual amount for the lower loads, and depending on the configuration for the low lift camshafts (lift, duration and phasing capability) there will be a maximum amount of trapped residuals and thermal heat, hence a certain load below which HCCI combustion cannot be achieved solely by using pilot injections and NVO. At this point marked changes in behavior will be seen, misfires marking the absolute lowest point achievable (which is assumed to be unacceptable for vehicle application). Before misfires occur, effects on unburned hydrocarbons will be seen and the reduced load will also reduce the exhaust gas temperature to a point which does not allow the catalyst to function. So, the low load limit will also not be a definitive point; the catalyst function is essential for meeting the legislated emission limits, and thus both the exhaust gas temperature and levels of unburned hydrocarbons will be important factors. These trends, which make it challenging to achieve HCCI combustion down to idle and still achieve a sufficient maximum load have also been reported in [20; 92] for instance.

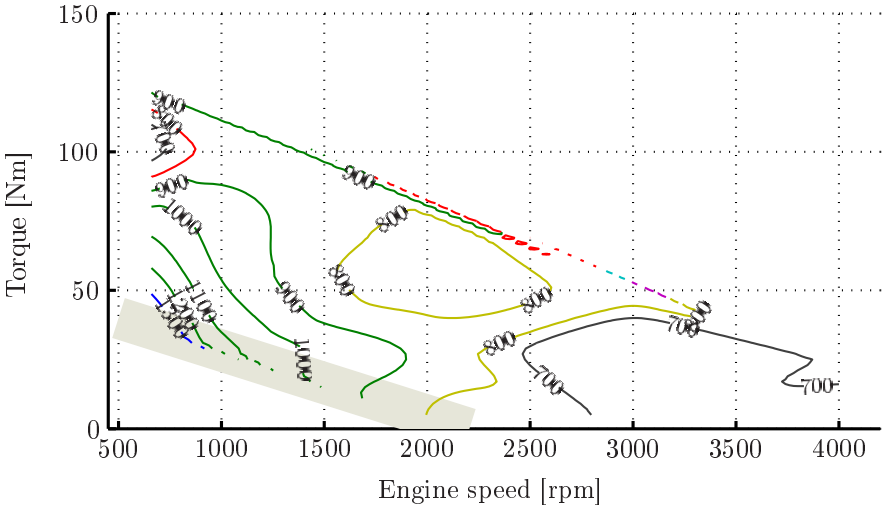

Figure 5.24: Hydrocarbon emissions in ppm (C3 calibrated) from the prototype 6-cylinder Volvo engine at various loads and speeds.

Generally, it can be stated that low levels of unburned hydrocarbon can be achieved when using HCCI with NVO, as seen in figure 5.24. Where the hot residuals caused by the NVO ensure a high combustion efficiency [77]. As mentioned earlier, however, the amount of hydrocarbon emissions can be problematic, especially near the lower load limits (the grey area). The absolute levels of hydrocarbon emissions are acceptable, or even low, compared to those generated by SI combustion, but the efficiency of the catalyst will determine if they are sufficiently low. Figure 5.25 shows the exhaust gas temperature, which is correlated with the mass flow, *i.e.* higher mass flows lead to higher temperatures and the mass flows are lower at lower loads since more trapped residuals are required to achieve combustion (see figure 5.19). So, for the lower loads the exhaust gas temperature reaches levels which could reduce catalyst function and thus even if the hydrocarbon emissions are low from an absolute perspective they may still be sufficiently high to set the minimum limit for HCCI.

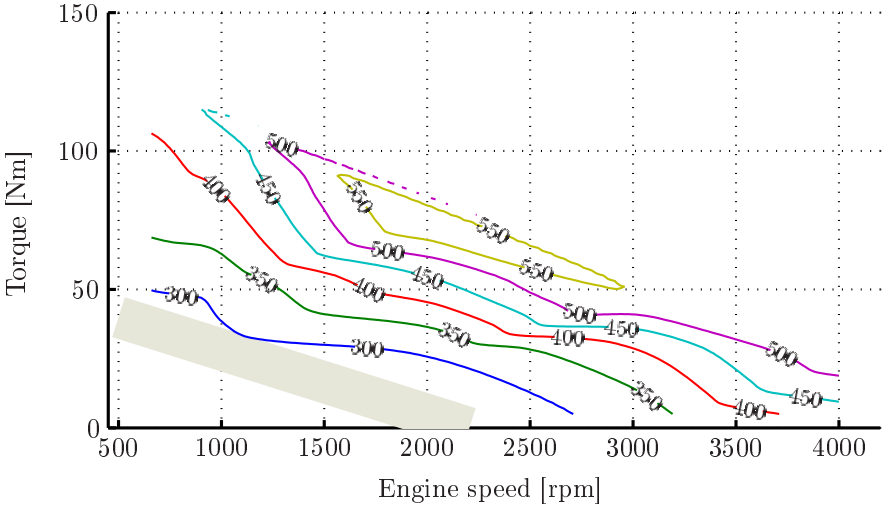

Figure 5.25: Exhaust gas temperature in °C during operation of the prototype 6-cylinder Volvo engine at various loads and speeds.

Carbon monoxide emissions may also potentially lead to problems near the lower limit for HCCI. However, when using NVO to achieve HCCI the levels of carbon monoxide may be low (see figure 5.26) compared to the levels during SI operation.

As mentioned earlier, the exhaust gas temperature is important for catalyst function and in figure 5.27 the conversion efficiency for hydrocarbon emissions of a conventional three-way catalyst originally intended for SI operation during HCCI operation can be seen. The conversion efficiency is defined as

$$\text{Conversion efficiency } [\%] = (1 - \frac{\text{HC}_{\text{before catalyst}}[\text{ppm}]}{\text{HC}_{\text{after catalyst}}[\text{ppm}]}) \cdot 100 \qquad (5.2)$$

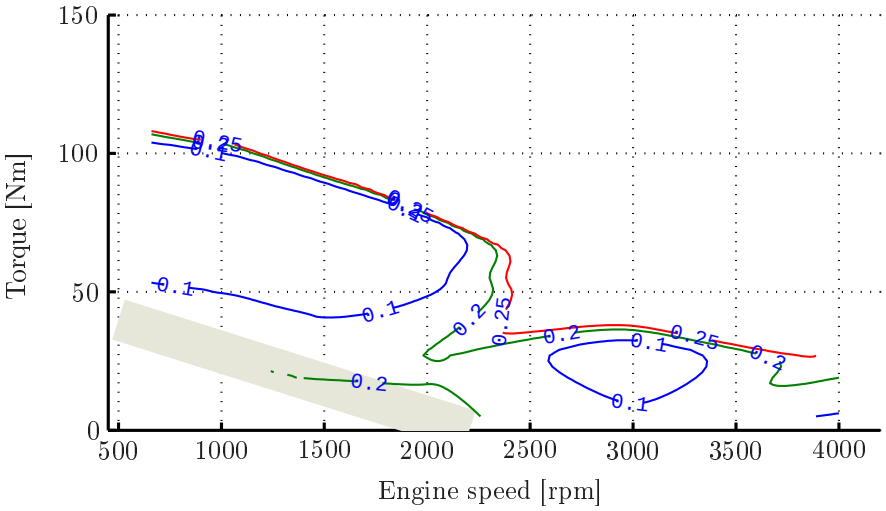

Figure 5.26: Carbon monoxide emissions, in $\%_{\text{volume}}$, from the prototype 6-cylinder Volvo engine at various loads and speeds.

A trend line, y, fitted by least squares regression to the data,

$$y = 1 - e^{-kT} \tag{5.3}$$

shows that the exhaust gas temperature is important for the conversion efficiency. Below 300°C the efficiency is significantly lower than unity (and thus the values achieved for temperatures above 400°C for instance). It should be noted that the absolute levels achieved after the catalyst are marginally higher than, or in some cases identical to, the accuracy of the measurement equipment. So, the conversion efficiency values near unity (98-100 %) could be viewed as more or less identical, but for this analysis the goal was to determine the effective temperature range of the catalyst, rather than to precisely determine the conversion efficiency for the best cases. With this in mind it is believed that the observed trend is representative.

5.4 Other dilute concepts

This chapter briefly discusses various dilute concepts, to give background information on other techniques, beside HCCI, in which dilution is applied.

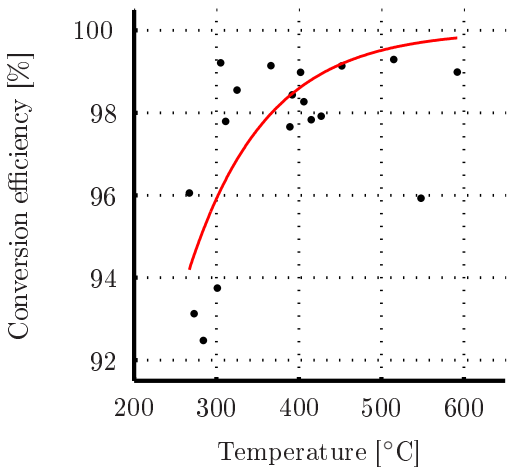

Figure 5.27: Conversion efficiency of a three-way catalyst for hydrocarbon emissions from the prototype 6-cylinder Volvo engine at various loads and speeds.

5.4.1 Stoichiometric SI with EGR

Dilution with exhaust gases has been investigated by various authors and applied in commercially available vehicles for many years. The effects of EGR was studied on both stoichiometric and lean SI operation and it was found that it was potentially capable of reducing fuel consumption in addition to reducing NO_X emissions [93]. In the investigation of the fundamentals of the piston engine presented in Chapter 2, the potential ability of EGR to increase thermodynamic work was identified. The gas constant was found to be influenced by EGR in a way that is beneficial for the thermodynamic work. However, an assumption underlying these conclusions was that the combustion *per se* was unaffected. To more realistically assess the effects of EGR on SI combustion, results from two different operational settings are presented in figures 5.29 and 5.30. In the presented results the EGR level is defined as

$$\text{EGR } [\%] = \frac{CO_{2_{\text{intake}}}}{CO_{2_{\text{exhaust}}}} \cdot 100 \tag{5.4}$$

where the $CO_{2_{\text{intake}}}$ was measured close to the intake valve as shown in the schematic figure of the setup 5.28. The recycled exhausts gases were directed to the intake plenum to allow ample mixing, and both the EGR-valve and EGR-cooler were originally intended for use in multi-cylinder diesel engines. The parameters for the engine parameters are listed in table 5.3.

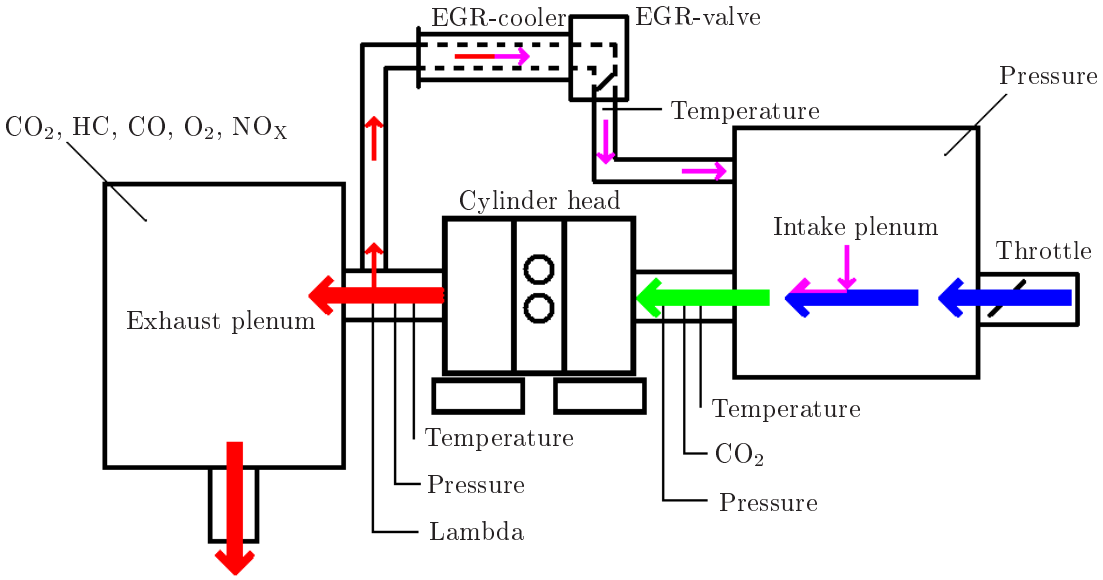

Figure 5.28: Schematic layout of the experimental setup used to evaluate the effects of EGR on SI combustion.

Table 5.3: Parameters of the single-cylinder engine used to evaluate the effects of EGR on stoichiometric SI combustion.

Parameter	Value	Unit	Name
Bore [mm]	84	Injector	Bosch HDEV 5.1
Stroke [mm]	90	Ignition coil	max70mJ@15.6V
Compression ratio [au]	10.5	EGR cooler	D5
Water and oil temperature [°C]	90	Spark plug	SIP
Fuel pressure [bar]	105	Fuel	RF-02-03
IVO 0mm [CAD BTDC]	25	Pressure sensor	Kistler 6061B
EVC 0mm [CAD ATDC]	23		

As seen in [93], and described in chapter 2, the fuel consumption can be improved by dilution with EGR, as indicated by the reduction in BSFC when the EGR is increased (see figure 5.29(a)). The effect on the pumping losses associated with the increase in plenum pressure can also be seen. The thermodynamic work, or IMEP, is positively influenced by EGR, and the improvement exceeds the reduction in pumping work. Thus, the results indicate that parameters in addition to pumping losses are influenced by dilution; the positive effect of dilution (as discussed in chapter 2) and the increased mass reduce the peak temperature, which in turn also reduce heat losses.

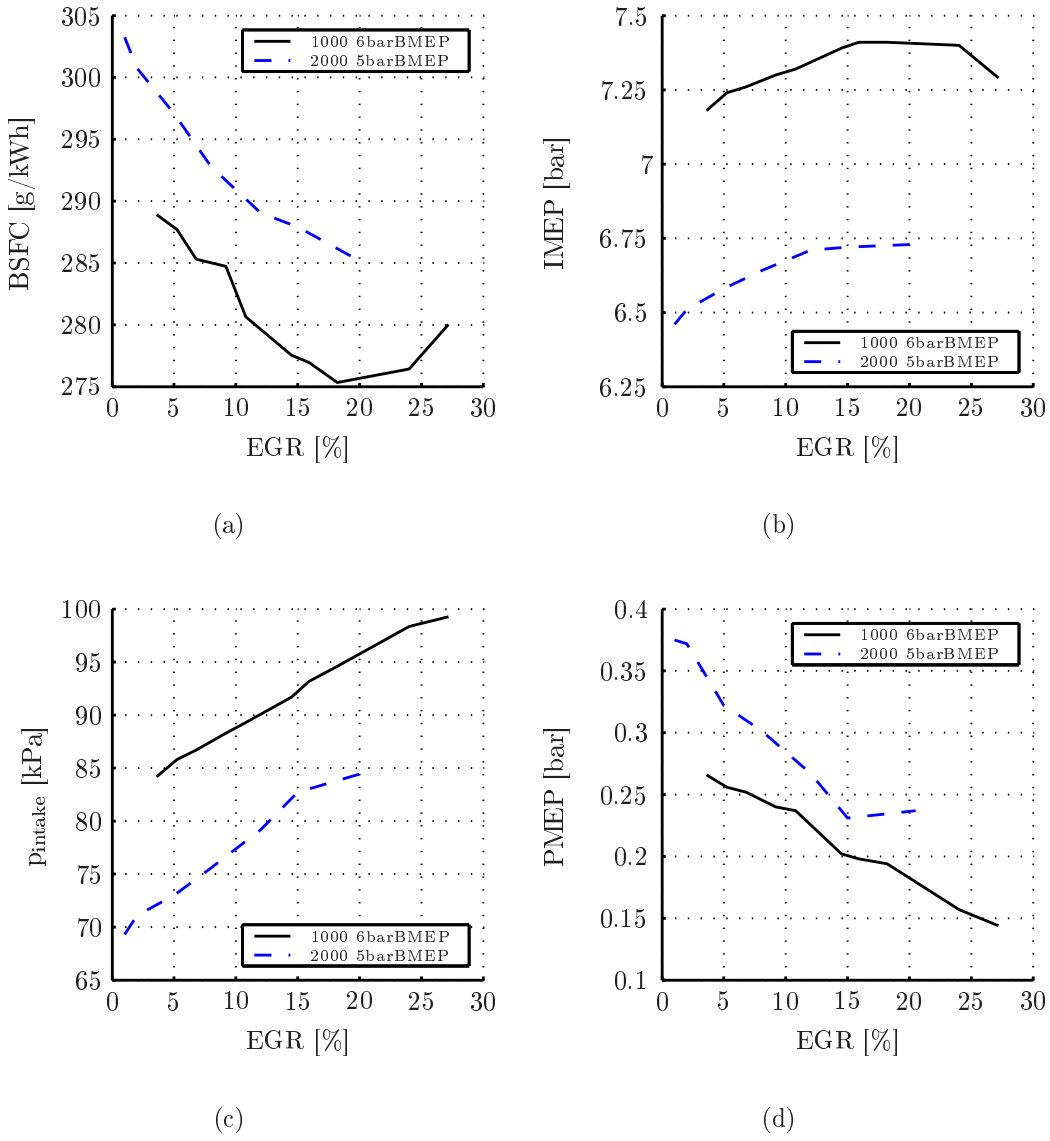

Figure 5.29: Effects of external EGR on stoichiometric SI combustion in terms of Brake Specific Fuel Consumption (a), Indicated Mean Effective Pressure (b), intake plenum pressure (c) and Pumping Mean Effective Pressure (d).

The laminar flame speed of premixed air and fuel mixtures depends on the flame temperature [22; 94] which in turn will be affected when the EGR level is changed [95; 94]. So EGR will reduce the laminar flame speed negatively [96], and thus reduce the rate of combustion. This will be a negative consequence of EGR since prolongation of heat addition results in reduced thermodynamic work [11]. The prolonged combustion duration (defined, for convenience as the period between

the points, in CAD, where 10 % and 90 % of the mass of the fuel has been converted) can be seen in figure 5.30(a). The operational case with the initially rapid combustion (1000 rpm, 6 bar BMEP) was influenced to a greater extent in terms of prolonged combustion duration than other cases. This led to the combustion duration becoming sufficiently long to reverse the positive trends of the reduction

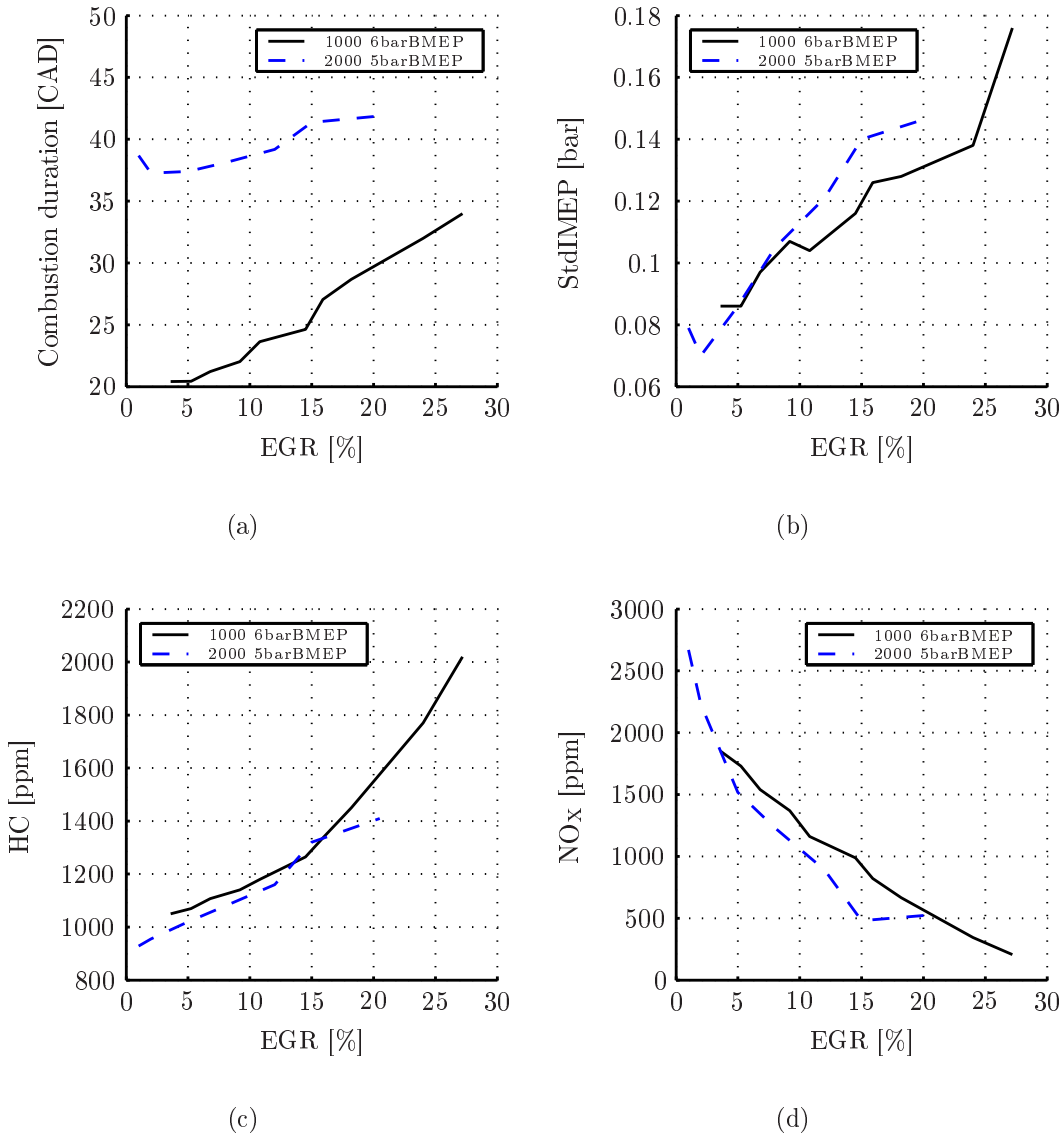

Figure 5.30: The effect of external EGR on stoichiometric SI combustion for combustion duration (CA10-CA90) (a), standard deviation of Indicated Mean Effective Pressure (b), hydrocarbon emission (c) and nitrogen oxides emissions (d).

in BSFC and increase in IMEP. For the other operational settings, EGR levels > 20 % led to misfires. EGR also leads to combustion instability, as can be seen in the standard deviations of the thermodynamic work parameter IMEP, which can be associated with drivability issues when it is related to absolute values of IMEP [11]. Other aspects of concern include reduced combustion efficiencies, as indicated by increases in hydrocarbon emissions, and a drastic effect on nitrogen oxide emissions can also be seen in figure 5.30(d). To summarize the effects of EGR on stoichiometric SI combustion, it can be stated that the amount of EGR that can be applied is limited due to its negative effect on the combustion quality and the strength of the technique is associated with its ability to maintain proper three-way catalyst function.

5.4.2 Lean SI

As discussed in earlier chapter, dilution can also be achieved using excess air, *i.e.* by operating the engine in globally lean conditions. The studies in [97] investigated the effect of homogenous globally lean SI combustion in comparison to conventional SI combustion at several low load points, and for some points found benefits in fuel consumption. The same engine as described in table 5.2 was used by the author to investigate the potential benefits of homogenous lean SI combustion in comparison to conventional stoichiometric SI combustion.

Interpolated contours of BSFC for the prototype six-cylinder engine can be seen in figure 5.31, where the black solid line corresponds to the maximum ISO-calibrated load [98]. The contours show the traditional behavior of an SI engine, displaying greatest efficiency slightly below the maximum line and at medium engine speeds. However, it should be noted that the engine is a prototype engine with functionality to operate in several combustion modes (and hence slightly higher friction, and perhaps slightly lower BSFC than would be observed for a series-production engine). However, since the focus is on evaluating different combustion modes in the same engine the comparison is assumed to provide useful indications of relative performance.

BSFC contours for lean SI operation can be seen in figure 5.32. The engine was mainly operated at an air equivalence ratio (λ) of 1.3, and for higher loads (which did not allow operation at λ 1.3) a ratio of 1.1 was used. The two dashed lines correspond to the maximum load with λ of 1.3 and 1.1, *i.e.* for contours below the lowest dashed line the engine was operated at λ 1.3 and for contours between the dashed lines at λ 1.1. It can be seen that the absolute levels are reduced by lean operation throughout the operating domain beneath the dashed lines. To

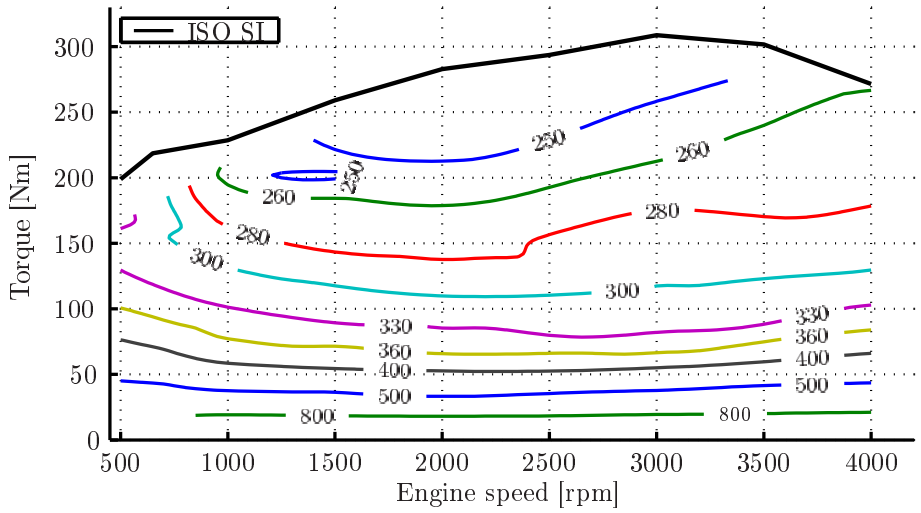

Figure 5.31: Brake Specific Fuel Consumption contours for a six-cylinder SI (reference) engine operated at various loads and speeds.

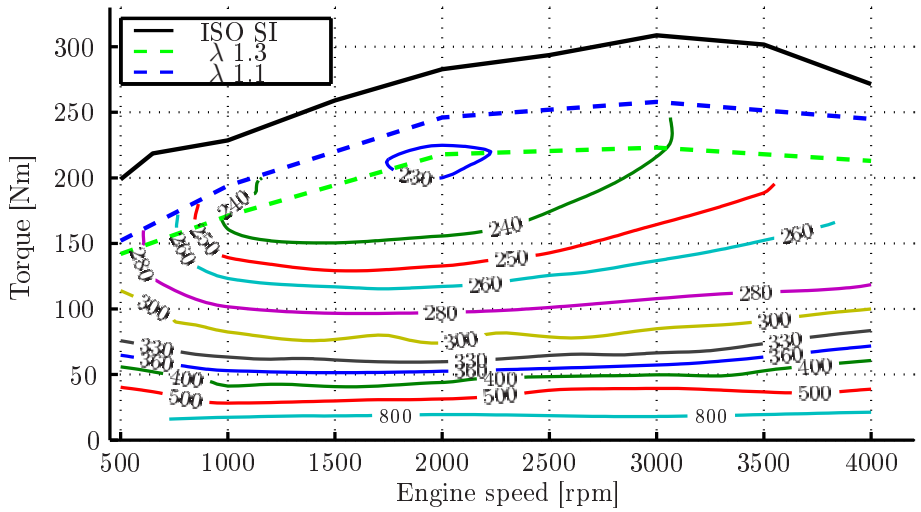

Figure 5.32: Brake Specific Fuel Consumption contours for a six cylinder SI engine operated in lean conditions.

obtain a more representative view of the difference the contours are compared to one another using the SI cases as references

$$\text{Improvement } [\%] = (1 - \frac{\text{BSFC}_{\text{SI}_{\text{lean}}}}{\text{BSFC}_{\text{SI}_{\text{stoichiometric}}}}) \cdot 100 \tag{5.5}$$

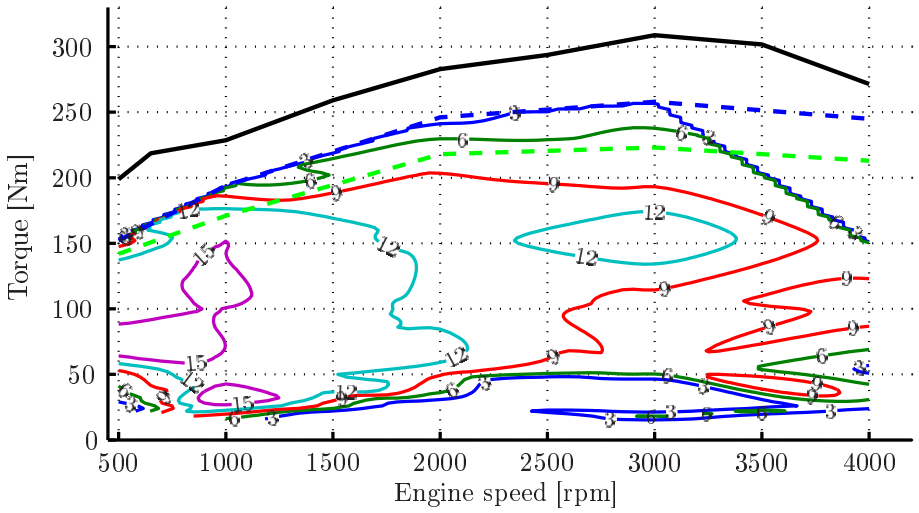

Figure 5.33: Lean versus stoichiometric operation improvement contours, as defined in equation 5.5, at various loads and speeds.

As mentioned earlier the lean operation leads to improvements, as indicated in figure 5.33 where the two modes are compared in terms of BSFC. So the potential benefits of lean operation on thermodynamic work described in chapter 2 appear to be plausible.

However, as for EGR, the dilution prolongs the combustion duration and for low load operation, where SI combustion in stoichiometric conditions already leads to excessively long combustion durations, the potential of adding excess air is inevitably reduced. Otherwise, the technique leads to significant improvement over a great operational area, but the real drawback of the technique is associated with the emissions (see figure 5.34).

Conventional stoichiometric SI operation leads to a significant amount of engine-out NO_X emissions, but the stoichiometric operation allows a three way catalyst to work flawlessly and ultra low NO_X emissions are possible, but only in stoichiometric conditions, not in lean conditions. The results seen in this study are consistent with those obtained in [97], in a comparison of lean SI and stoichiometric operation in terms of catalyst function; with lean operation the NO_X conversion efficiency of a three-way catalyst approaches zero. So, to summarize findings regarding lean SI operation, there is a significant fuel consumption improvement potential (which only requires minor modification of the hardware) if the NO_X emissions can be handled.

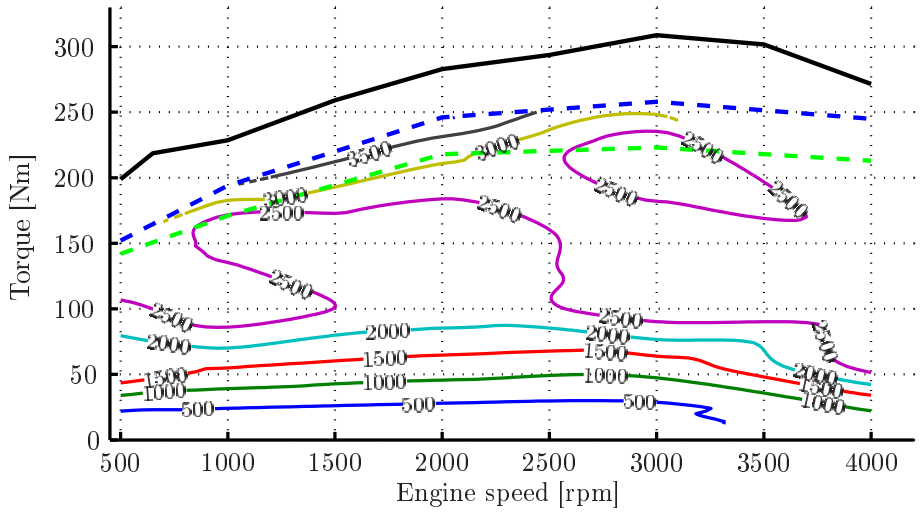

Figure 5.34: NO_X concentration contours for lean SI operation.

5.4.3 SGDI

In the previous section dilution with excess air was used and the air/fuel mixture was homogenously distributed. However, the air:fuel ratio (λ) will affect the laminar flame speed [22], since the flame will propagate more slowly if it propagates through a lean mixture rather than a stoichiometric one, and at a certain point flame propagation will not be possible if the flammability limit is reached [22]. Thus, there will be a limit for the amount of excess air that can be used for operating a lean SI engine, even if the prolonged combustion can be tolerated. One way of using globally lean mixtures, but not necessarily lean in the region where the flame propagates, is to use a stratified charge in which the flame propagates and excess air outside the stratified region. With this approach the global air equivalence ratio can be higher than the lean flammability limit since the flame propagates through a mixture that is more suitable for flame propagation and thus more excess air can be used. The same single-cylinder engine as used for the stoichiometric EGR study was set up for SGDI operation. The engine parameters can be seen in table 5.4.

The data presented are all based on results obtained in tests with identical injection duration and engine speed (2000 rpm). The aim was to achieve a load of 2 bar BMEP, but with constant duration the load varied slightly. Some settings led to increases in efficiency; those settings led to more work and vice versa for the settings leading to lower efficiency. Only single pulse injections were applied for simplicity. In figure 5.35 results can be seen in the form of contours obtai-

Table 5.4: Parameters for the single cylinder SGDI engine.

Parameter	Value	Unit/Parameter	Name/Value
Bore [mm]	84	Injector	Bosch HDEV 5.1
Stroke [mm]	90	Ignition coil	max70mJ@15.6V
Compression ratio [au]	10.5	Fuel	RF-02-03
Water and oil temperature [°C]	90	Spark plug	NGK
Fuel pressure [bar]	190	Pressure sensor	Kistler 6061B
IVO 0mm [CAD BTDC]	34	EVC 0mm [CAD ATDC]	26
Engine speed [rpm]	2000	Injected mass [g/s]	0.174-0.180
BMEP [bar]	1.4-2.3	Air equivalence ratio [λ]	3.8±0.1

ned in tests with different end of injections (EOI) and spark timings. Since the charge is prepared late in the cycle, compared to conventional SI combustion, both spark timing and injection timing will influence many parameters more strongly than in SI combustion, where the spark-timing has a predominant influence. From figure 5.35(a) it can be seen that the efficiency or BSFC of the engine can vary significantly at the tested settings and the system appears to be sensitive to settings, but the values are competitive compared to those of SI combustion. Within the tested span the BSFC varies over 100 g/kWh and the best values can be associated with early timings, in accordance with patterns reported in [99] and in [100] where experiments with an engine similar to the one used here were conducted. From the hydrocarbon emissions in figure 5.35(b) it can be seen that the combustion efficiency is also strongly influenced, however with the settings presented misfires occurred in varying intensity, depending on the settings which will naturally influence the hydrocarbon emissions. The NO_X emissions are clearly sensitive to the relationship between EOI and spark timing for the earlier timings, since the contours are curved. However, NO_X emissions generally correlate with the phasing of both EOI and spark timing; earlier timing leading to greater amounts of NO_X. SGDI operation was found to be prone to misfire when conditions were excessively lean [101], if swirl was not used, accordingly in this study sensitivity to misfire was also seen and misfire-free operation was only observed in a restricted domain.

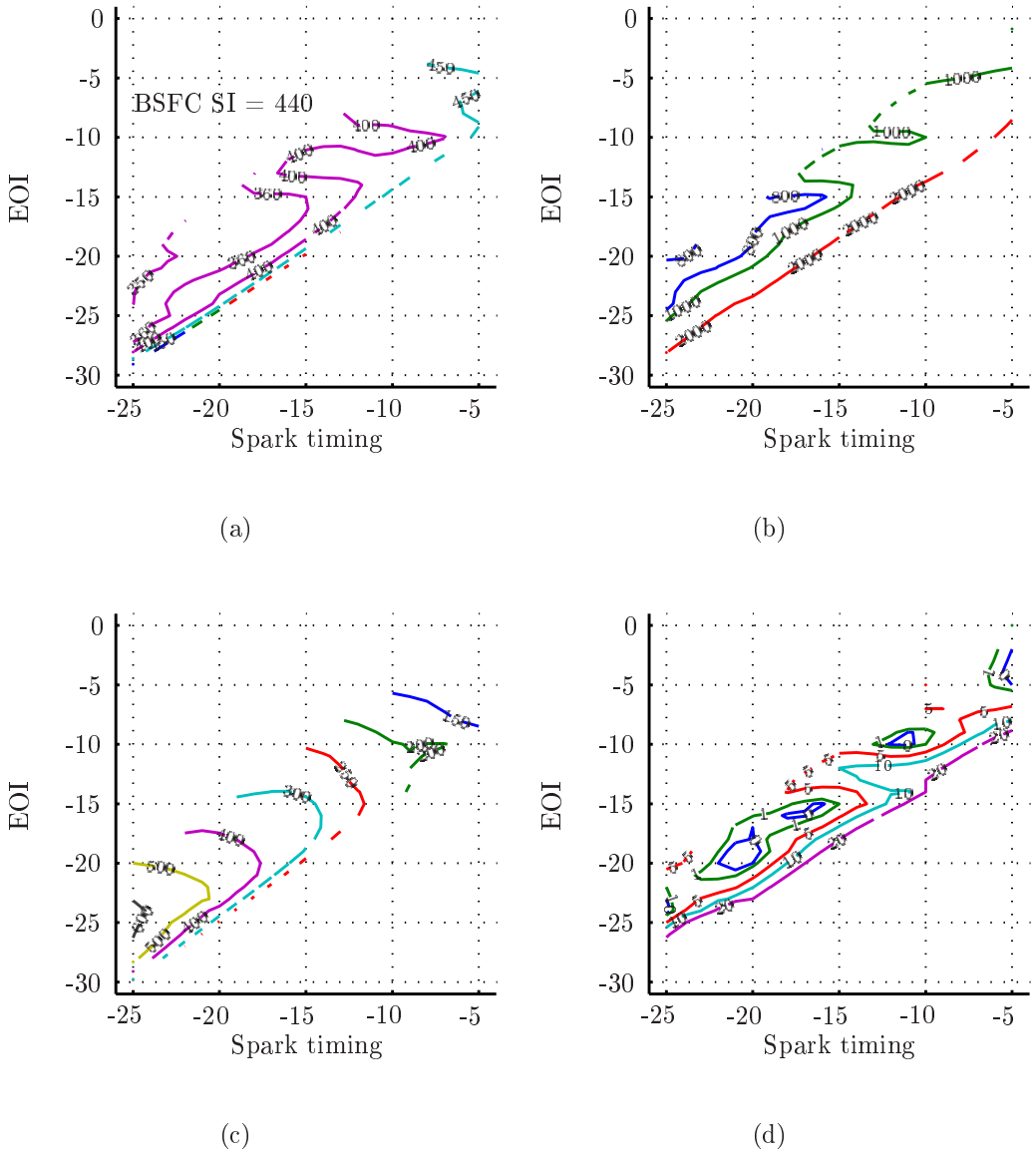

Figure 5.35: BSFC contours (and reference value for SI combustion) in g/kWh (a), HC in ppm (C3 calibrated) (b), NO_X in ppm (c) and misfires per 1000 cycles (d) obtained with different End Of Injection, EOI, and spark timings for SGDI operation at 2000 rpm and around 2 bar BMEP (with fixed injection duration).

In figure 5.36 the results for soot and combustion duration can be seen. Significant increases in PM concentrations were observed when their test engine was operated stratified compared to homogenous [102], and the concentrations were also higher for later injection timings during stratified operation. The same tendencies were

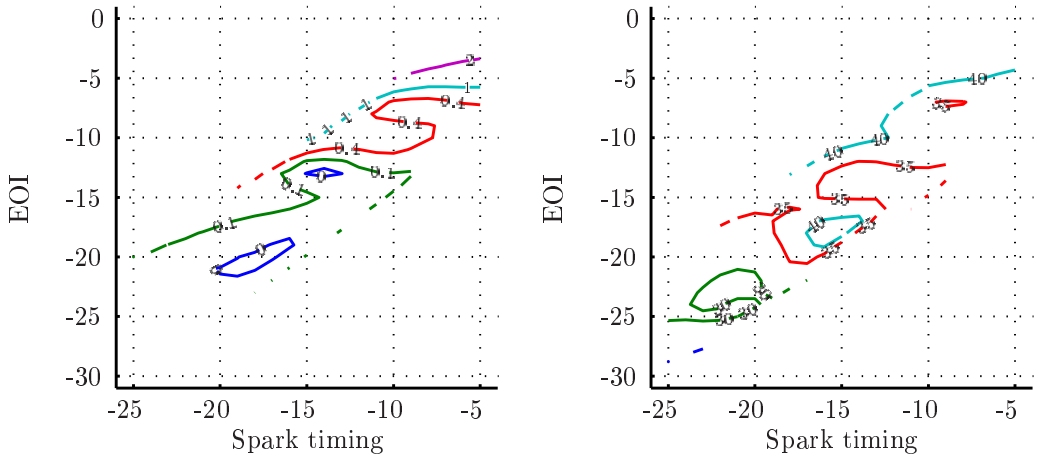

(a) (b)

Figure 5.36: Contours of soot (FSN) (a) and combustion duration (CA10-CA90) (b) obtained with different EOI and spark timings for SGDI operation at 2000 rpm and around 2 bar BMEP.

also seen here; generally the soot levels were high and the later phasing led to more soot. However there are regions with less soot, at least in the order of accuracy of the measurement equipment (AVL415 smoke meter), but those regions are small and soot emissions appear to be a cause of concern for SGDI engines. For the combustion duration, defined as CA10 to CA90, some correlation can be seen with shorter combustion duration and the BSFC. Earlier phasing is correlated with a shorter combustion duration, which is essential for efficiency.

In order to determine general trends for the measured parameters, lines were fitted to the data (see figure 5.37). As mentioned earlier, the BSFC was connected to the phasing and, accordingly, the BSFC trend line was correlated with the phasing, although some measurement points deviated strongly from the least square regression lines represented by

$$y = ax + b \tag{5.6}$$

which are plotted in figure 5.37(a), 5.37(c) and 5.37(d). This pattern differs from that of conventional SI combustion, in which a CA50 timing slightly after TDC leads to the most work.

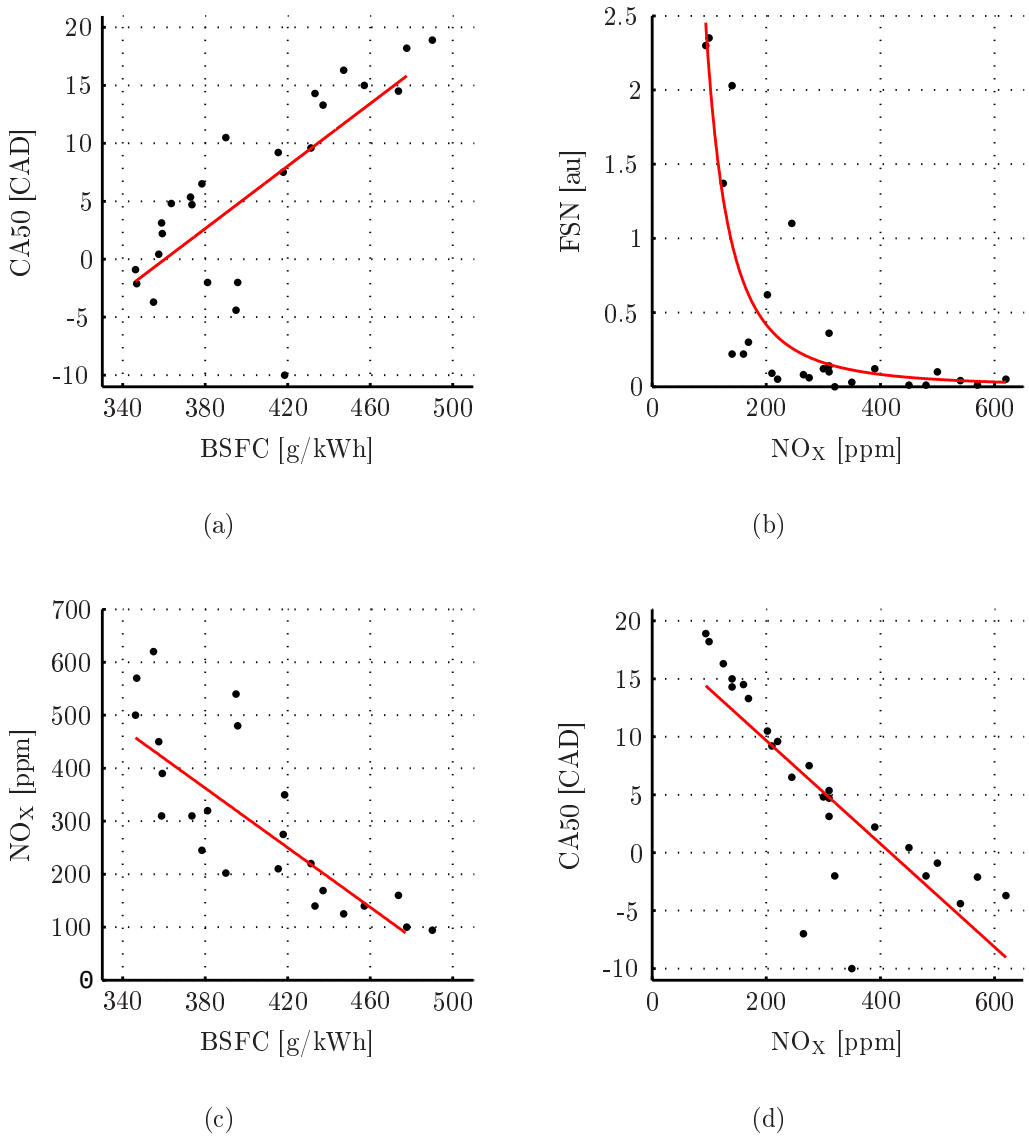

Figure 5.37: Correlations for SGDI operation at 2000 rpm and around 2 bar BMEP between combustion phasing (CA50) and BSFC (a), soot (FSN) and NO_X (b), NO_X and BSFC (c) and CA50 and NO_X (d).

The trend line for figure 5.37(b) is the least square fitted line of

$$y = ax^b \tag{5.7}$$

and the inverse correlation between soot and NO_X seen is normally associated with Diesel engines [11], and usually called the "Diesel dilemma". Obviously, the

goal is to achieve both low NO_X and low PM emissions, but the two parameters are connected with each other in this unfortunate fashion. The reason for this trend is assumed to be the same as in Diesel engines, where cases with high combustion temperatures lead to the formation of large amounts of NO_X, but high rates of oxidation of soot, and vice versa for cases with low combustion temperatures. The relationships between BSFC and NO_X, and between CA50 and NO_X, shown in figure 5.37(c) and 5.37(d), respectively, support the hypothesis that similar reasons underlie the relationship between soot and NO_X to those that apply in Diesel engines. The highest efficiencies were achieved at earlier phasing, which in turn increases the combustion temperature and thus the NO_X emissions.

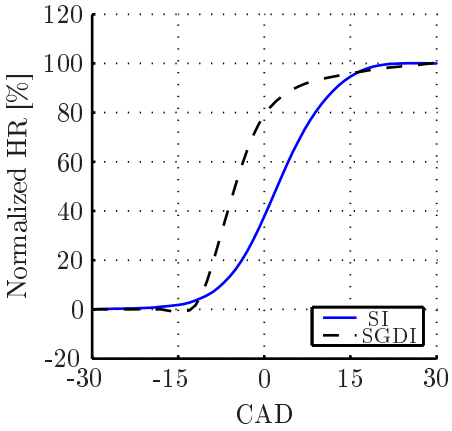

Figure 5.38: Examples of normalized accumulated heat release curves for both conventional SI combustion and SGDI combustion at 2000 rpm and 2 bar BMEP, each normalized with respect to its maximum value.

Illustrative heat release traces for SI and SGDI combustion can be seen in figure 5.38. Beside the obvious feature that the whole SGDI combustion is more advanced than the SI combustion, slight evaporation can be seen initially in the SGDI trace, followed by rapid heat generation which in the end decays slowly. This is in accordance with results presented in [103; 100]. It is not desirable to have combustion phased in this manner, and there might be further potential for reducing fuel consumption and NO_X emissions using the technique if the optimum phasing could be retarded. To obtain a rough estimate of the amount of thermodynamic work that is lost due to this unfavorable combustion phasing, the mathematical model used in earlier chapter was applied to replicate a measured case and then to explore the effects of varying the combustion phasing.

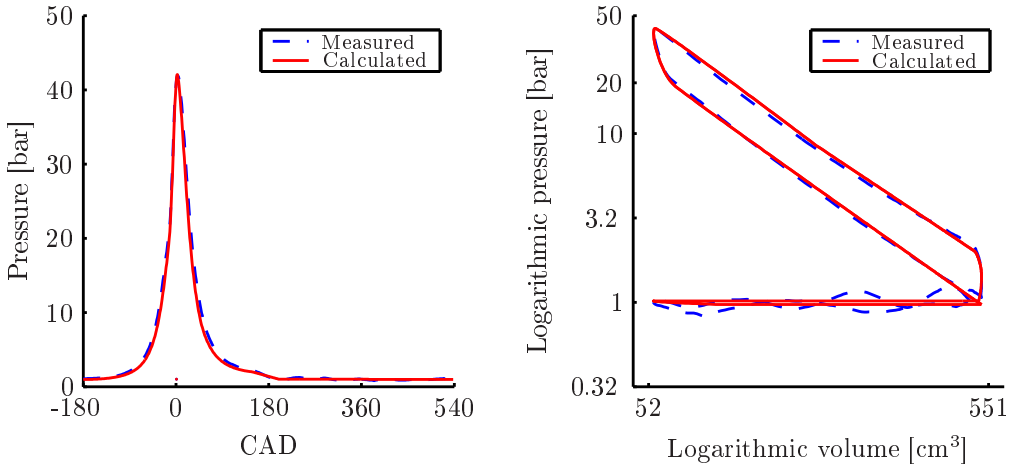

(a) (b)

Figure 5.39: Measured and calculated pressure traces for SGDI combustion at 2 bar BMEP and 2000 rpm, plotted against CAD (a) and logarithmic pressure versus the logarithmic volume (b).

From figure 5.39 it can be seen that the mathematical model can be used to replicate the measured pressure trace with only minor discrepancies, and table 5.5 shows that it provides similar to observed values of thermodynamic work. However, the pressure oscillations caused by the relatively large valve overlap are not captured by the simple representation of the gas exchange phase and thus the pump losses are slightly under-predicted, by ca. 0.06 bar in absolute terms. It was found that the behavior during expansion was not constantly polytropic throughout the whole expansion, the initial part showed an expansion with a higher polytropic constant than the later part. Thus, two constants were used for the expansion; starting with a value of 1.28 and ending with a value of 1.26.

In the measurements it was found that when the combustion was phased later than the optimum point (which was at very early phasing) the quality of the combustion was reduced leading to reduced efficiencies. However, according to the mathematical model identical rates and quality of combustion to that achieved at the optimum point (as illustrated in figure 5.39 and table 5.5) can be potentially obtained at any phasing. This indicates the amount of thermodynamic work that is lost due to the early phasing and the potential scope for further improvement of SGDI. In figure 5.40 the calculated results can be seen when the combustion phasing is changed (while all other parameters are held constant). The case with a CA50 phasing at -5 CAD (which replicates the measured case) shows the highest pressure, and all other cases show lower maximum values, which would probably

Table 5.5: Values used to replicate parameters measured for an SGDI combustion case by the model described in Chapter 2.

Parameter	Value - measured	Value - calculated
IMEP [bar]	2.813	2.806
PMEP [bar]	0.09	0.03
CA50 [CAD]	-5.1	-5.0
Intake pressure [bar]	0.991	0.991
Exhaust pressure [bar]	1.014	1.014
EVO [CAD ATDC]	136	136
EVC [CAD ATDC]	26	26
IVO [CAD BTDC]	34	34
IVC [CAD ATDC]	216	216
n during compression	-	1.32
n during expansion	-	1.28 and 1.26

lead to reduced NO_X emissions if the modeled phenomena were observed in a real engine. In figure 5.40(c) the pressure near TDC is presented and the effect of varying the combustion phasing on the thermodynamic work (the area enclosed by the pressure trace) can be seen. Around 1% more thermodynamic work could be obtained if total control of combustion phasing was possible, as indicated by figure 5.40(d). The consequence of this unfavorable combustion phasing on the thermodynamic work is thus weaker than may be intuitively expected, probably because the main part of the combustion occurs during a relatively short period. However, the consequence for NO_X emissions can only be speculated since emissions are not included in the model. To summarize findings regarding SGDI, it has significant potential to reduce fuel consumption, compared to SI combustion and the challenging aspects are soot, NO_X and misfire, all of which are likely to compromise some of the fuel consumption benefit.

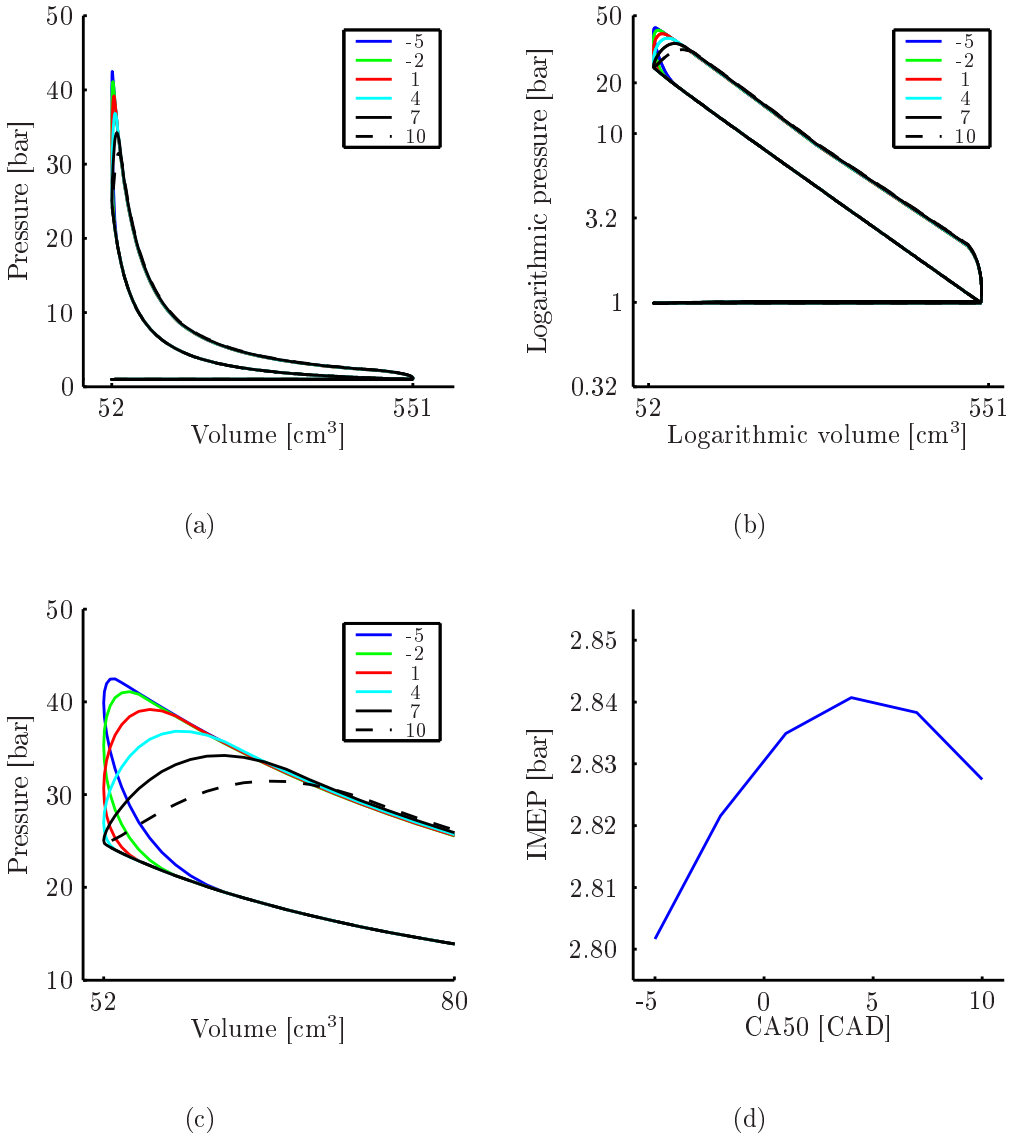

Figure 5.40: Calculated pressure traces for SGDI combustion using settings from table 5.5 but with different CA50 timings (-5 to 10 CAD), plotted against volume (a), logarithmic pressure versus logarithmic volume (b) logarithmic pressure versus logarithmic volume at volumes near the combustion (c) and the resulting thermodynamic work for each modeled phasing.

5.4.4 Discussion - dilute concepts

The different dilute concepts all show the possibility of increasing the efficiency of an engine. Lean or stoichiometric operation with EGR in an SI engine leads to improvements for basically the whole operational range of the engine, compared to HCCI and SGDI operation which leads to improvements over a limited area. But the effect over the limited area is on the other hand significantly higher. The conversion efficiency for NO_X emissions of a three-way catalyst at stoichiometric operation is far closer to unity than lean NO_X after-treatment systems. This means that if dilution with excess air is used then the amount of engine-out NO_X must be much lower than the levels of conventional SI combustion even if a lean NO_X after-treatment system is used. So from this point HCCI combustion appears competitive due to the low NO_X emissions and SI combustion with EGR due to proper three-way catalyst function for NO_X. For HCCI using NVO the exhaust gas temperature are in the regions that allow proper catalyst function for HC and CO conversion, which also is the case for the lean or stoichiometric operation with EGR in SI combustion. For SGDI combustion it can be assumed that some of the improvement seen will have to compromised to reduce the NO_X levels and increase exhaust gas temperature. To summarize, HCCI combustion is a competitive dilute concept in many senses if the combustion can be controlled.

5.5 Losses

All engines have an efficiency far lower than unity due to various kinds of losses; this section compares losses in HCCI combustion and SI combustion. As previously shown, HCCI combustion shows higher efficiency than SI combustion, and here the results for the two types of combustion at one operational setting are broken down to estimate and compare their losses. After this the thermodynamic model presented in Chapter 2 is used to further evaluate the differences between the two cases. Values for the key parameters of SI and HCCI combustion can be seen in table 5.6. As expected, HCCI combustion shows a lower BSFC value (22 %) than SI combustion, and thus provides the same mechanical work per unit fuel injected. What is not expected is that less thermodynamic work is needed for HCCI to achieve the same mechanical work, the HCCI combustion shows a lower indicated friction (FMEP defined as IMEP - BMEP) so the SI combustion requires a 5 % higher IMEP to achieve the same BMEP. The high intake air pressure required for HCCI leads to a significant reduction in pumping work (PMEP). Two benefits of keeping the general in-cylinder temperature high (as with NVO) are its positive effects on hydrocarbon emissions and car-

bon monoxide, otherwise HCCI combustion is associated with low combustion efficiencies, but for this case with NVO the combustion efficiency is high, with especially low values for CO emissions.

Table 5.6: Results of the comparison of energy losses in SI and HCCI combustion at 2 bar BMEP 2000 rpm.

Parameter	SI	HCCI
Engine speed	2000 rpm	2000 rpm
Torque	51 Nm	51 Nm
BMEP	2 bar	2 bar
BSFC	402 g/kWh	320 g/kWh
IMEP	2.78 bar	2.65 bar
Std IMEP	0.044 bar	0.042 bar
PMEP	0.539 bar	0.187 bar
FMEP	0.789 bar	0.644 bar
Injected fuel	52.6 kJ/s	41.8 kJ/s
Intake pressure	43.5 kPa	97.54 kPa
Intake temperature	309 K	303 K
Exhaust gas temperature	918 K	667 K
HC	641 ppm (C3)	554 ppm (C3)
CO	0.89 $\%_{\text{volume}}$	0.056 $\%_{\text{volume}}$
Air flow	0.0162 kg/s	0.0167 kg/s
Estimated internal EGR	$<5\%$	35%

If the different losses are related to the energy of the fuel supplied then they can be compared in proportion to one another. In figure 5.41 pie-charts for losses in SI and HCCI combustion are shown. A complete circle represents the energy of the fuel supplied for the SI combustion (the circle for HCCI is not complete since less fuel is injected due to the higher efficiency for this case). The losses in this representation are divided into the following classes: work (which is, of course, the intended output of the engine), FMEP, BMEP, PMEP, exhaust, fuel and other. FMEP, the indicated friction, is defined as the difference between the thermodynamic work and BMEP, and thus represents how efficiently the thermodynamic work is converted into mechanical work. PMEP is the work needed to pump the gas. The exhaust losses are simply defined as the difference in heat of the gas entering and leaving the engine. There is also chemical energy associated with the exhaust emissions, where hydrocarbon and carbon monoxide leaving with the exhaust gases represent losses, these are simply represented as fuel losses. Finally, other losses that could not be further classified for this study are pooled as "other losses", including heat losses from the engine either via heat losses through the cylinder walls or head, and friction leading to heat within the engine (some additional exhaust losses will also be found here since the exhaust

gases will be cooled in the exhaust port). When the losses for the two types of combustion are compared it can be seen that all the losses are smaller for HCCI combustion than for SI combustion, *i.e.* HCCI combustion is more efficient for multiple reasons. The increased intake air pressure reduces the pumping losses, the reduced exhaust gas temperature combined with similar mass flow (due to the NVO for HCCI) leads to reduced heat losses in the exhaust gases, the low engine-out emission levels lead to low losses in the form of unburnt fuel and the other heat losses are smaller.

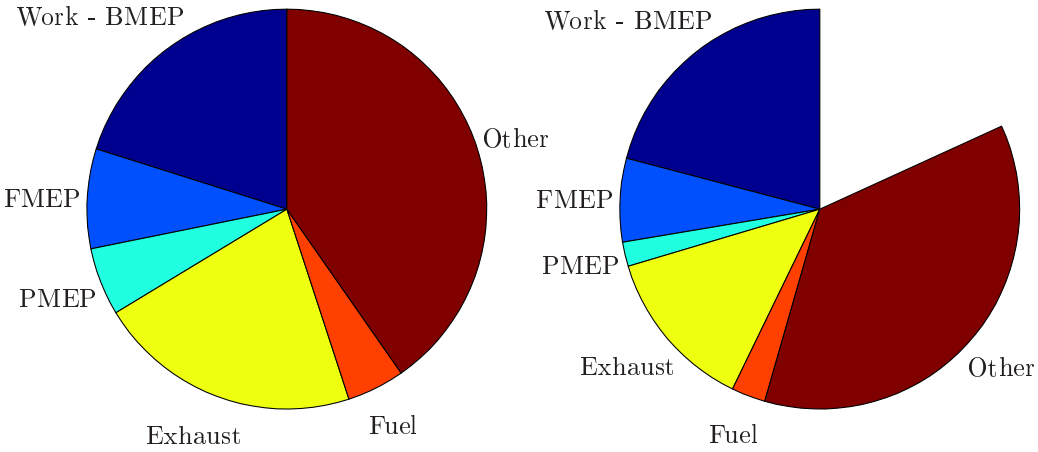

Figure 5.41: Proportional contributions of various kinds of losses of energy in SI (left) and HCCI (right) combustion.

5.5.1 Evaluation

From table 5.6 it can be seen that the thermodynamic work (IMEP) obtained from the two types of combustion only differs marginally in comparison to the difference in energy of the supplied fuel. Thus, a certain amount of fuel leads to a higher amount of thermodynamic work for the HCCI case. This can also be seen in figure 5.41 since the BMEP and FMEP areas are almost identical for HCCI and SI combustion, although ca. 25% less fuel was combusted for the HCCI case. This difference will be further investigated here using the thermodynamic model described in Chapter 2.

Pressure traces for the compression and expansion strokes observed in operation with SI and HCCI combustion can be seen in figure 5.42. Both the measured pressure traces for SI and HCCI could be replicated with only minor discrepancies using the simplified thermodynamic model. Here only the compression and

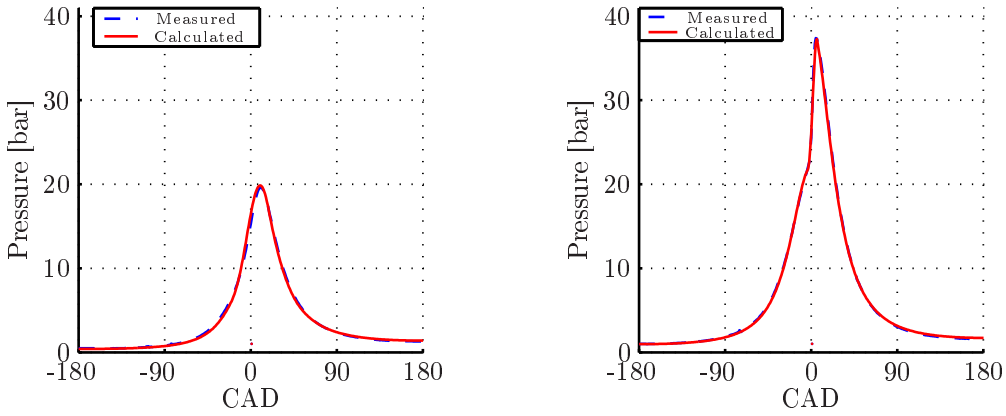

(a) (b)

Figure 5.42: Averaged pressure traces (dashed lines) from 300 cycles from six cylinders and calculated (solid lines) pressure traces for SI (a) and HCCI (b) combustion.

expansion are evaluated and the thermodynamic work achieved in this period is called $IMEP_{gross}$. In table 5.7 the input parameters used that led to a representation of the pressure traces with only minor deviations from measured values, and associated results can be seen. When $IMEP_{gross}$ is calculated the greater pumping losses for SI combustion (as seen in table 5.6 and figure 5.41) are apparent, and due to the greater pumping loss a greater amount of thermodynamic work is required during the compression and expansion. However, the difference in $IMEP_{gross}$ is around 14% and the difference in added fuel is around 25% between SI and HCCI combustion, thus the lower pumping losses can only partly explain the difference in thermodynamic work, and there must be additional contributors to the greater thermodynamic work.

Table 5.7: Calculated results and input parameters for the thermodynamic comparison of SI and HCCI combustion.

Parameter	SI	HCCI
$IMEP_{gross}$	3.29 bar	2.88 bar
Added fuel	526 J	418 J
Estimated in cylinder mass	0.173 g	0.268 g
Intake air pressure	45 kPa	97 kPa
Combustion duration	40 CAD	10 CAD

To evaluate how the different parameters influence the thermodynamic work, the HCCI case as in figure 5.42(b), which was tuned to a real case, was used

but with different parameters for combustion duration, the gas constant and in-cylinder mass with associated intake air pressure. The calculated pressure traces and associated $IMEP_{gross}$ values obtained with the different parameters can be seen in figure 5.43. The solid line with the highest $IMEP_{gross}$ value was obtained using the same parameters as in figure 5.42(b) and represents pure HCCI combustion, which is here called the base case (A). SI combustion showed a longer combustion duration and the dotted black line represents the base SI scenario, but with a combustion duration of 40 CAD instead of 10 CAD the longer combustion duration has adverse effects on thermodynamic work (compare A and B in figure 5.43(b)).

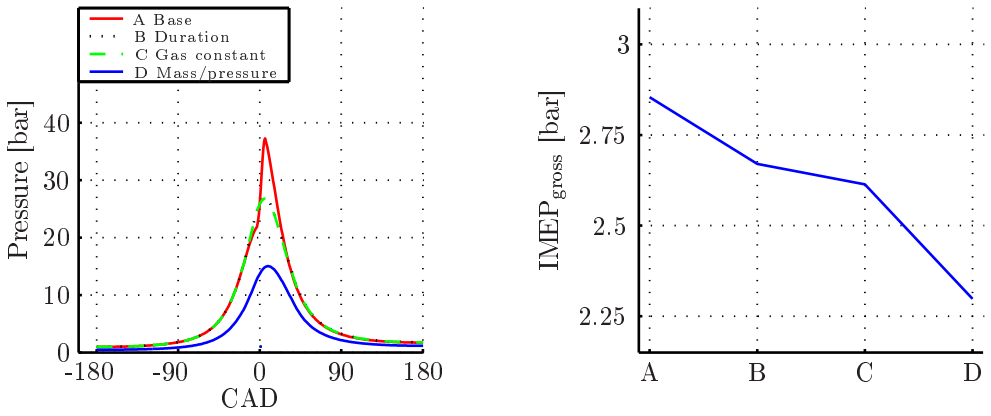

(a) (b)

Figure 5.43: Calculated pressure traces and IMEPgross values for HCCI combustion with variations of the indicated parameters.

In equation 2.18 the influence of the gas constant of the pumped medium on the thermodynamic work is highlighted, and since trapped residuals are used in the HCCI case the gas constant differs slightly compared to the SI case. This effect is indicated by the dashed line, which was obtained when the duration was prolonged and the gas constant was changed. There is only a marginal difference in gas constants between the two cases, but it leads to an additional slight decrease in thermodynamic work (see case C in figure 5.43(b)). As can be seen in equation 2.16, and mentioned in earlier chapter, the pressure at the start of compression will influence the thermodynamic work, but if the mass is proportional to the pressure then the pressure will have no influence in this context. For the case with NVO the trapped hot residuals combined with the valve timings leads to high pressure prior to compression, but the in-cylinder mass is not directly proportional to the pressure, which may be advantageous from a thermodynamic perspective. To evaluate how much less thermodynamic

work is achieved due to the greatly (less than half) reduced pressure (in addition to the effect on pumping work) and slightly (around 35% less) reduced in-cylinder mass in SI combustion, this lower pressure and mass is used (in addition to the long combustion duration and changed gas constant) in the thermodynamic model. The effects are indicated by the solid line with the lowest peak pressure in figure 5.43(a), and the associated thermodynamic work in figure 5.43(b) for case D. It should be noted that this simplified model does not take into account any changes in heat losses between the cases, and there will most likely be a great difference in heat loss between them and the base case, which was tuned to experimental data. This will lead to a less steep reduction than the drastic decline in thermodynamic work shown in figure 5.43(b) for real measurements. It should also be noted that the intention for this section is not to exactly describe all losses with perfect precision, but merely to highlight other factors, beside the pump losses, that contribute to the significantly increased thermodynamic efficiency of the HCCI mode.

5.5.2 Discussion - losses

The greater efficiency of HCCI using NVO is not due to merely reduced pump losses, which play a considerable role, but most types of other losses are also reduced. For instance, the reduced exhaust gas temperature leads to reduced heat losses in the exhaust gases. Furthermore, a greater amount of thermodynamic work is obtained from HCCI combustion for a given amount of fuel compared to SI combustion. This is partly due to the higher pump losses for SI combustion and partly to the reduced combustion duration. However, the trapped residuals have multiple effects since they influence the gas constant of the pumped medium besides allowing the pressure prior to combustion to be high relative to the in-cylinder mass, which has a positive effect on the thermodynamic work.

Chapter 6

Conclusions

There is an urgent need to reduce the CO_2 emissions of passenger cars to meet future emission requirements, especially for vehicles with SI engines. This can be done by using HCCI combustion for part load operation, since HCCI combustion has higher efficiency than SI combustion and the standardized drive cycles utilize mainly part load operation. HCCI can be achieved in SI engines by trapping residuals (NVO), however when using this method there is a low load and speed threshold, below which HCCI combustion is not possible. The proposed concept of combining initial flame propagation through a stratified charge with subsequent HCCI combustion, aims to provide control over HCCI combustion in such a manner that HCCI combustion can occur in this region.

The fundamentals of the concept have been optically verified by local air equivalence ratio measurements combined with chemiluminescence and conventional pressure measurements, *i.e.* the results show that it is possible to combine initial flame propagation through a stratified charge with subsequent HCCI combustion. When this control method was used it was found that the minimum load possible for HCCI could be reduced, while maintaining efficiency and similar NO_X emissions to those of conventional HCCI combustion.

Charge stratification was found to be important in many respects, it not only supplied a richer region in the vicinity of the sparkplug (which was required for the initial flame propagation), but also induced air motions and generated regions that were more prone to HCCI combustion. Charge stratification without any flame propagation was also found to beneficially influence parameters that restrict HCCI operation at its upper load limit.

Existing control methods for HCCI using NVO by pilot injection have been evaluated. Heat-generating reactions during the NVO caused by the pilot injection have been detected and mapped experimentally by both conventional and optical measurements. It was found that the effects of pilot injections on these reactions are a key factor in the overall effects of pilot injections (and hence the potential to control HCCI combustion using them).

The control methods developed will contribute to reducing the CO_2 emissions of a vehicle, since extending the operational range of HCCI will allow more time to be spent in more efficient combustion modes during drive cycle operation.

Chapter 7

Summary of papers

Paper I

Spark Assisted HCCI Combustion Using a Stratified Hydrogen Charge

by Andreas William Berntsson and Ingemar Denbratt

This paper describes initial experiments exploring the concept of initial flame propagation through a stratified charge combined with subsequent HCCI combustion. The objective was to investigate this hybrid concept, based on a combination of HCCI combustion of n-heptane and SI combustion of hydrogen. The basic idea was to initiate HCCI combustion with a spark-ignited stratified lean hydrogen mixture.

Photographs of OH chemiluminescence from the combustion were taken with the intention to verify that the combustion sequence consisted of flame front combustion followed by HCCI combustion, in the same cycle. Chemiluminescence images showed an expanding flame front initiated by the spark plug prior to the HCCI combustion. The hybrid combustion concept gave greater scope for controlling the combustion than the pure HCCI concept.

In this initial study it was assumed that low NO_X levels would only be possible if hydrogen was used for the stratified charge, since the wide flammability limits of hydrogen would allow a flame to propagate despite very lean conditions and

this could be used to keep the flame temperature low.

The paper was presented by the author at ICE2005, the 7th International Conference on Engines for Automobile in Capri, Italy, September 11-16, 2005. The author was the main author and carried out the experiments, analyzed and post-processed the data, wrote the post-processing scripts and wrote the paper.

Paper II

HCCI Combustion Using a Spark Ignited Stratified Charge

by Andreas William Berntsson and Ingemar Denbratt

This paper describes the second (published) step in experimental investigations of the concept of initial flame propagation through a stratified charge combined with subsequent HCCI combustion. In these studies both hydrogen and the main fuel were used for the stratified charge.

The combination of SI and HCCI combustion in the same cycle was investigated in a metallic engine rather than the optical engine used in the initial tests. Both hydrogen and a mixture of iso-octane and n-heptane were used as fuels for the stratification charge. The hybrid combustion concept was found to give better control of combustion timing and the CA50 could be controlled by varying the injection timing and stratification amount.

The studies indicated that there was potential scope to achieve low NO_X operation, even when the same fuel was used for the stratified and the main charge. This would naturally place less demands on the fueling system, thus the focus in the project was shifted towards using the same fuel for the stratified charge and the main charge in further investigations of the concept.

The paper was presented by the author at the 2006 JSAE Annual Congress, Yokohama, Japan, May 24-26, 2006. The author was the main author and carried out the experiments, analyzed and post-processed the data, wrote the post-processing scripts and wrote the paper.

During the experimental period (2005), the author noted some other interesting phenomena in addition to the combination of SI and HCCI. In some cases the charge stratification itself appeared to affect the combustion, even without spark-

assistance. At the time of the experiments the author was not aware of the work in a similar field [38]. Although the intention during the experimental period was to investigate the combination of SI and HCCI combustion, this "new" way of combustion control warranted further attention. Experiments were conducted in parallel with the main experiments and the data acquired were analyzed after the data related to the initial idea were analyzed, then presented in the following paper.

Paper III

HCCI Combustion Using Charge Stratification for Combustion Control

by Andreas William Berntsson and Ingemar Denbratt

This work documented the trends seen in addition to those related to the main foci in the previous measurements, regarding the effects of charge stratification *per se* on combustion phasing, the rate of heat release and emissions during HCCI combustion. Experiments were carried out in both optical and traditional single-cylinder engines and PRF50 was used as both stratification and main fuel.

It was found that a stratified charge alone can influence the combustion. Increasing the stratification amount or late injection timing of the stratified charge leads to an advanced CA50 timing. The optical results, obtained using a high speed CCD camera, showed that an increase in stratification leads to prolonged combustion and the maximum rate of heat release depends on the stratification amount - a larger amount gives a lower rate of heat release but the main heat release is advanced. Varying the injection timing results in variations in the phasing of the main heat releases.

The initial idea focuses on achieving control of HCCI combustion especially for the low load region. However, this approach also displays features that are suitable for the high load region, since too high rates of combustion are problematic at this boundary. So, the concept described in this paper could potentially be used to increase the HCCI operational range towards higher loads. This method was only briefly further investigated in this project, but was more thoroughly addressed in another project.

The paper was presented by the author at the SAE World Congress in Detroit, USA, April 16-19, 2007. The author was the main author and carried out the experiments, analyzed and post-processed the data, wrote the post-processing scripts and wrote the paper.

Paper IV

Optical study of HCCI Combustion using NVO and an SI Stratified Charge

by Andreas William Berntsson and Ingemar Denbratt

This was the first article describing experiments in which the author used LASER-based measurement techniques to investigate the combustion processes. The focus was again on combining SI combustion of a stratified charge and HCCI combustion. For these measurements the author collaborated with Lucien Koopmans at Volvo Cars, and the experiments were carried out on Volvo engine geometry using low lift short duration camshafts, to gain knowledge regarding HCCI combustion in SI engine-relevant geometry. The effects of using the proposed idea on HCCI combustion were investigated in engine experiments to identify ways to extend the operational range of HCCI combustion to lower loads.

For these experiments a piezo electric outward-opening injector was used and the engine was operated with negative valve overlap (NVO) to initiate HCCI combustion by increasing the exhaust gas recirculation (EGR) and thus retaining sufficient thermal energy to reach auto-ignition temperatures.

The paper describes two series of experiments with full factorial designs, to investigate how the tested parameters (amounts of fuel injected in pilot injections and main injections, stratification injection timing and spark-assistance) influenced the combustion (which is especially important since the proposed idea increases the number of influential variables).

In the optical study laser-induced fluorescence (LIF), from 3-pentanone was measured, to analyze the concentration and distribution of fuel vapor within the cylinder and to establish the concentrations in absolute terms for stratified cases by calibration with homogenous cases. In addition, formaldehyde was measured by using LIF to locate the low temperature reactions. Due to the simplicity of

addition, the chemiluminescence signals from OH radicals were also measured to locate the flame front and reaction zone.

The injection and ignition timing of the SI stratified charge were found to be the main parameters influencing the HCCI combustion phasing, and the NO_X emissions were found to be significantly affected by the use of a SI stratified charge, and its injection timing. When combining SI combustion of a stratified charge with HCCI combustion the operational range of HCCI combustion could be increased to lower loads, with very low NO_X emissions. The basic idea that a stratified charge should be present and that the flame should propagate through it was optically verified.

The paper was presented by the author at ICE2007, the 8th International Conference on Engines for Automobile in Capri, Italy, September 16-20, 2007. The author was the main author and carried out the experiments, set up the equipment, analyzed and post-processed the data, wrote the post-processing scripts and wrote the paper.

Since it was a simple addition all measurements techniques were used throughout whole revolutions, even during the NVO. The reactions occurring during the NVO were naturally interesting and the main hypothesis was that the pilot injection during the NVO mainly led to radical formation and, presumably, not to any high temperature reactions. However, the chemiluminescence of OH was measured during the NVO anyway since the author wished to see if any high temperature reactions did occur, and this could be done with only a limited amount of work for the setup. During the NVO implicit indications of high temperature reactions (signs of chemiluminescence of OH) were observed. This triggered some further investigation of the reactions occurring during the NVO.

Paper V

LIF for OH imaging in the Negative Valve Overlap of a HCCI Combustion Engine

by Andreas William Berntsson, Mats Andersson, Daniel Dahl and Ingemar Denbratt

This paper presented continuations of the previous work by the author indicating

that high temperature reactions occur during the NVO. However, these previous indications of high temperature reactions were based on chemiluminescence measurements, which compared to LIF measurements require long exposure times and can be misleading since other reactions with similar emission spectra may contribute to the signals. To limit this effect and more rigorously examine the reactions LIF of OH was measured. Since OH radicals are associated with high temperature reactions, OH radicals detected during the negative valve overlap strongly indicated that high temperature reactions did occur in the highly diluted environment of the trapped exhaust gases during the NVO. Reactions were identified from 20 CAD prior to TDC (during the NVO) to around 60 CAD after TDC, with an intensity peak at about TDC.

The experiments were executed under the assumption that the threshold for detection by the pressure transducer would be too high to register the reactions occurring during the NVO, however indications of reactions could be noted by pressure trace analysis and heat-generating reactions were observed during 40 CAD by pressure trace analysis.

The paper was presented by the author at INSA SIA The Spark Ignition Engine of the Future Conference - Technologies to meet the CO_2 challenge in Strasbourg, France, November 28-29, 2007. The author and Mats Andersson carried out the optical engine experiments and arranged the optical setup. The author was the main author and was responsible for setting up the optical engine. Daniel Dahl carried out the multi-cylinder experiments. The analysis and post-processing of all the data and writing the post-processing scripts was the author's responsibility. Mats Andersson was responsible for choosing the excitation wavelength and the simulation in LIFBASE. The paper was written by the author, apart from the section describing the experimental setup for OH, which was written by Mats Andersson.

The indications of heat-generating reactions observed in both optical experiments and conventional pressure trace analysis prompted the authors to further investigate this phenomenon, and acquired results were presented in the following paper.

Paper VI

A LIF-study of OH in the Negative Valve Overlap of a Spark-assisted HCCI Combustion Engine

by Andreas William Berntsson, Mats Andersson, Daniel Dahl and Ingemar Denbratt

In this study, the reactions during the NVO were further investigated. One of the crucial parameters to control in HCCI combustion is the combustion phasing, and one way of doing this is to vary the ratio of fuel injected in pilot and main injections. However, the fundamental reason for this was not completely understood so this study was intended to increase our understanding of the mechanism whereby this ratio affects combustion phasing (and hence provides opportunities to control it), by studying the reactions that occur in the highly diluted environment during the NVO when the load and pilot to main injection ratio is varied.

As in the previous study (Paper V), PLIF from OH radicals was analyzed in a series of experiments with an optical single-cylinder engine and a series of experiments was also performed using a multi-cylinder engine with varied NVO timings, to verify that similar effects occurred in a multi-cylinder engine using gasoline and in the optical engine using PRF. Data acquired from corresponding optical analysis showed the occurrence of OH radicals (and thus high temperature reactions) during the NVO in all tested operating conditions. The results also indicated that the extent of the high temperature reactions was influenced by both varied parameters (total fuel amount and the pilot to main injection ratio), since decreasing the relative amount of the pilot injection and/or increasing the total amount of fuel led to larger amounts of OH radicals. The contribution of heat generated during the NVO caused by the pilot injection led to increases in the temperature during the compression, and the changes in phasing caused by varying the pilot to main injection ratio were mainly due to the resulting temperature changes during the compression.

The paper was presented by the author at the SAE World Congress in Detroit, USA, April 14-17, 2008. The author and Mats Andersson carried out the optical engine experiments and arranged the optical setup. The author was the main author and was responsible for setting up the optical engine. Daniel Dahl carried out the multi-cylinder experiments. The analysis and post-processing of all the data and writing the post-processing scripts was the author's responsibility. Mats Andersson was responsible for choosing the excitation wavelength and the

simulation in LIFBASE. The paper was written by the author, apart from the section describing the experimental setup for OH, which was written by Mats Andersson.

Paper VII

Reducing Pressure Fluctuations at High Loads by Means of Charge Stratification in HCCI Combustion with Negative Valve Overlap

by Daniel Dahl, Mats Andersson, Andreas William Berntsson, Ingemar Denbratt and Lucien Koopmans

This paper further investigates the technique that was explored by the author in Paper III in another project. The technique described in Paper III has features that are suitable for high load while the focus of the author's project was on low load. Thus, this technique was further investigated in another project.

One constraint at high loads is that the combustion becomes too rapid, leading to excessive pressure-rise rates and large pressure fluctuations (ringing), causing noise. SCCI (Stratified Charge Compression Ignition) was used to address these issues. The approach was evaluated in tests with a single-cylinder metal research engine and a single-cylinder optical engine. The latter was used to characterize the combustion in laser-based analyses including LIF determinations of fuel tracer, OH and CH_2O (formaldehyde) distributions. A high speed camera was also used for direct imaging of chemiluminescence.

The effects of two main parameters were studied: the proportion of fuel injected late to create a stratified charge and the timing of the late injection. In addition, two fuels were used: a certification gasoline fuel and a blend of n-heptane, iso-octane and 3-pentanone. Both fuels were used in the metal engine for comparison. Use of a stratified charge allowed the maximum pressure-rise rates and ringing intensity to be reduced at the expense of increases in NO_X and CO emissions, regardless of fuel type. Optical results indicated that both the fuel distribution and combustion were not homogenous.

The author was a co-author of this paper which was presented by Daniel Dahl at the SAE 2009 International Powertrains, Fuels and Lubricants Meeting in

Florence, Italy, June 15-17, 2009. The author and Mats Andersson arranged the optical setup, which was set up for the measurements reported in Paper VIII and the same setup with small modifications performed by Mats Andersson and Daniel Dahl was used for the experiments described in this paper. The author was also responsible for setting up the optical engine and contributed by writing post-processing scripts.

Paper VIII

Simultaneous LIF of OH, HCHO, PIV and High Speed Video Imaging combined with Fuel Tracer LIF Measurements in a HCCI engine using Charge Stratification and Spark-assist

by Andreas William Berntsson, Mats Andersson and Ingemar Denbratt

The experimental period for this paper was intended to be the author's last measurement campaign in this project and the intention was to extend knowledge from previous studies regarding the combination of SI combustion through a stratified charge and subsequent HCCI combustion. The experimental setup and procedure designed to do this were established over an extended period by the author and Mats Andersson, and the measurements reported in this paper were actually carried out prior to those presented in Paper VII, but published later. The author came to the conclusion that if some parameters could be measured simultaneously at a certain time in one cycle and complemented by high speed video images prior to and after that time then this would be of great interest and provide knowledge that was complementary to information obtained in previous studies.

So, the concept of combining charge stratification and spark-assistance with HCCI to achieve a lower minimum load was again the focus, especially in this study the phenomena occurring near TDC. Several optical techniques were applied simultaneously in experiments with an optical engine, including LIF of OH, HCHO, PIV and High Speed Video imaging, combined with LIF measurements of the fuel tracer 3-pentanone together with conventional cylinder pressure and emission measurements. This procedure was applied to limit any misleading trends caused by averaging measurements acquired in different periods. Since flame propagation is highly stochastic and HCCI combustion is highly sensitive, this procedure provided greater knowledge.

The same conclusion could yet again be drawn, that the minimum low load limit could be reduced by using the proposed concept. It was found that the charge stratification, in addition to enriching the region near the sparkplug, induced air motions that enhanced the initial flame propagation and supplied a region with conditions more suitable for HCCI combustion, thus promoting the transition from flame propagation to HCCI. Hence, the proposed concept influences the conditions in more ways than merely providing a different thermal environment caused by the flame propagation.

The author was the main author for this paper which have been submitted for publication. The author and Mats Andersson carried out the optical engine experiments and arranged the optical setup. The author was responsible for setting up the optical engine. The analysis and post-processing of all the data and writing the post-processing scripts was the author's responsibility. Mats Andersson was responsible for choosing the excitation wavelength and the simulation in LIFBASE. The paper was written by the author, apart from the section describing the experimental setup for OH, which was written by Mats Andersson.

Bibliography

[1] S. Onishi, S. H. Jo, K. Shoda, P. D. Jo, and S. Kato, "Active Thermo-Atmophere Combustion (ATAC) - A New Combustion Process for Internal Combustion Engines," *SAE technical paper series 790501*, 1979.

[2] R. H. Thring, "Homogenous-Charge Compression-Ignition (HCCI) Engines," *SAE technical paper series 892068*, 1989.

[3] *Worldwide Emissions Standards Passenger Cars & Light Duty Trucks.* Delphi, 2008.

[4] *COM(2007) 856 final - Setting emission performance standards for new passenger cars as part of the Community's integrated approach to reduce CO_2 emissions from light-duty vehicles.* COMMISSION OF THE EUROPEAN COMMUNITIES, 2007.

[5] N. A. Otto, "Gas-Motor Engine," June 1887. US patent no. 365701.

[6] R. Diesel, "Method of and apparatus for converting heat into work," February 1895. US patent no. 542846.

[7] "*http* : *//www.volvocars.com*," June 2009.

[8] TÜV, *pkw2008CO2cd - excel document.* German TÜV, 2008.

[9] "*http* : *//www.dieselnet.com*," June 2009. Online information service on clean Diesel engines and Diesel emissions.

[10] "*http* : *//www.autoevolution.com*," June 2009.

[11] J. B. Heywood, *Internal Combustion Engine Fundamentals.* McGraw-Hill Inc., international ed., 1988.

[12] H. Alvarez, *Energiteknik Del 1.* Studentlitteratur, 1999.

[13] D. R. Lancaster, R. B. Krieger, and J. H. Lienesch, "Measurement and analysis of engine pressure data," *SAE paper 750026*, 1975.

[14] D. F. Caris and E. E. Nelson, "A new look at high compression engines," *SAE transactions*, vol. 67, pp. 112–122, 1959.

[15] S.-E. Mörtstedt and G. Hellsten, *Data och diagram*. Liber, 1999.

[16] E. Clapeyron, "Puissance motrice de la chaleur," *Journal de l'École Royale Polytechnique*, pp. 153–190, 1834.

[17] S. M. Aceves, D. L. Flowers, C. K. Westbrook, J. R. Smith, W. Pitz, R. Dibble, M. Christensen, and B. Johansson, "A Multi-Zone Model for Prediction of HCCI Combustion and Emissions," *SAE technical paper series 2000-01-0327*, 2000.

[18] V. Golovitchev, "*www.tfd.chalmers.se/ ∼ valeri*," June 2009.

[19] J. Warnatz, U. Maas, and R. W. Dibble, *Combustion : physical and chemical fundamentals, modelling and simulation, experiments, pollutant formation*. Springer, fourth ed., 2006.

[20] H. Zhao, *HCCI and CAI for the automotive industry*. CRC, 2007.

[21] N. Iida, Y. Yamasaki, and S. S., "The Key Points of HCCI Combustion Controls," *Which Fuels For Low CO_2 Engines*, pp. 29–44, 2004.

[22] I. Glassman, *Combustion*. Academic Press, third ed., 1996.

[23] P. M. Najt and D. E. Foster, "Compression-ignited homogeneous charge combustion," *SAE technical paper series 830264*, 1983.

[24] S. B. Fiveland, R. Agama, M. Christensen, B. Johansson, J. Hiltner, F. Maus, and D. N. Assanis, "Experimental and Simulated Results Detailing the Sensitivity of Natural Gas HCCI Engines to Fuel Composition," *SAE technical paper series 2001-01-3609*, 2001.

[25] D. Flowers, S. M. Aceves, J. Martinez-Frias, R. Smith, M. Au, J. Girard, and R. Dibble, "Operation of a Four-Cylinder 1.9L Propane Fueled Homogenous Charge Compression Ignition Engine: Basic Operating Characteristics and Cylinder-to-Cylinder Effects," *SAE technical paper series 2001-01-3609*, 2001.

[26] C. D. Marriott, S.-C. Kong, and R. B. Reitz, "Investigation of Hydrocarbon Emission from a Direct Injection-Gasoline Premixed Charge Compression Ignited Engine," *SAE technical paper series 2002-01-0416*, 2002.

[27] J. Martinez-Frias, S. M. Aceves, D. Flowers, R. J. Smith, and R. Dibble, "Thermal Charge Conditioning for Optimal HCCI Engine Operation," *Journal of Energy Resources Technology*, vol. 124, pp. 67–75, 2002.

[28] J. Hyvönen, G. Haraldsson, and B. Johansson, "Operating Conditions Using Spark Assisted HCCI Combustion During Combustion Mode Transfer to SI in a Multi-Cylinder VCR-HCCI Engine," *SAE technical paper series 2005-01-0109*, 2005.

[29] N. Milovanovic, D. Blundell, R. Pearson, J. Turner, and R. Chen, "Enlarging the Operational Range of a Gasoline HCCI Engine By Controlling the Coolant Temperature," *SAE technical paper series 2005-01-0157*, 2005.

[30] G. Haraldsson, P. Tunestål, B. Johansson, and J. Hyvönen, "HCCI Combustion Phasing in a Multi Cylinder Engine Using Variable Compression Ratio," *SAE technical paper series 2002-01-2858*, 2002.

[31] J. Hyvönen, G. Haraldsson, and B. Johansson, "Operating range in a Multi Cylinder HCCI engine using Variable Compression Ratio," *JSAE technical paper series 20030178*, 2003.

[32] U. Wagnar, R. Anca, A. Velji, and U. Spicher, "An Experimental Study of Homogenous Charge Compression Ignition (HCCI) with Various Compression Ratios, Intake Air Temperatures and Fuels with Port and Direct Fuel Injection," *SAE technical paper series 2003-01-2293*.

[33] G. Haraldsson, P. Tunestål, and B. Johansson, "Transient Control of a Multi-Cylinder HCCI Engine During a Drive Cycle," *SAE technical paper series 2005-01-0153*, 2005.

[34] M. Christensen, A. Hultqvist, and B. Johansson, "Demonstrating the Multi Fuel Capability of a Homogenous Charge Compression Ignition Engine with Variable Compression Ratio," *SAE technical paper series 1999-01-3679*, 1999.

[35] P. Strandh, J. Bengtsson, R. Johansson, P. Tunestål, and B. Johansson, "Cycle-to-Cycle Control of a Dual-Fuel HCCI Engine," *SAE technical paper series 2004-01-0941*, 2004.

[36] J.-O. Olsson, P. Tunestål, G. Haraldsson, and B. Johansson, "A Turbo Charged Dual Fuel HCCI Engine," *SAE technical paper series 2001-01-1896*, 2001.

[37] M. Richter, J. Engström, A. Franke, M. Aldén, A. Hultquist, and B. Johansson, "The Influence of Charge Inhomogeneity on the HCCI Combustion Process," *SAE technical paper series 2000-01-2868*.

[38] T. Aroonrisopon, P. Werner, J. O. Waldman, V. Sohm, D. E. Foster, T. Morikawa, and M. Iida, "Expanding the HCCI Operation With the Charge Stratification," *SAE technical paper series 2004-01-1756*, 2004.

[39] N. Iida, Y. Yamasaki, S. Sato, K. Kumano, and Y. Kojima, "Study on Auto-Ignition and Combustion Mechanism of HCCI Engine," *SAE technical paper series 2004-32-0095*, 2004.

[40] M. Sjöberg and J. E. Dec, "Smoothing HCCI Heat-Release Rates Using Partial Fuel Stratification with Two-Stage Ignition Fuels," *SAE technical paper series 2006-01-0629*, 2006.

[41] S. Tanaka, F. Ayala, J. C. Keck, and J. B. Heywood, "Two-stage ignition in HCCI combustion and HCCI control by fuels and additives," *Combustion and Flame*, vol. 132, pp. 219–239, 2003.

[42] M. Christensen and B. Johansson, "Homogenous Charge Compression Ignition with Water Injection," *SAE technical paper series 1999-01-0182*, 1999.

[43] L. Koopmans, R. Ogink, and I. Denbratt, "Direct Gasoline Injection in the Negative Valve Overlap of a Homogenous Charge Compression Ignition Engine," *JSAE technical paper series 20030195*, 2003.

[44] W. Z, J.-X. Wang, S.-J. Shuai, G.-H. Tian, X. An, and Q.-J. Ma, "Study of the effect of spark ignition on gasoline HCCI combustion," *Proceedings of the Institution of Mechanical Engineers, Part D: Journal of Automobile Engineering*, vol. 220, no. 6, pp. 817–825, 2006.

[45] J. Wijesinghe and G. Hong, "Experimental Investigation of Spark-Assisted Autoignition Combustion in a Small Two-Stroke Engine," *SAE technical paper series 2008-01-1665*, 2008.

[46] R. M. Wagner, S. C. Edward, K. D. adn Daw, J. B. Green, and B. G. Bunting, " On the Nature of Cyclic Dispersion in Spark-Assisted HCCI Combustion," *SAE technical paper series 2006-01-0418*, 2006.

[47] I. Denbratt, "Method of controlling the process of combustion in an internal combustion engine, and engine with means for controlling the engine valves," March 2003. US patent no. 6536407.

[48] L. Koopmans and I. Denbratt, "A Four Stroke Camless Engine, Operated in Homogenous Charge Compression Ignition Mode with Commercial Gasoline," *SAE technical paper series 2001-01-3610*, 2001.

[49] R. Ogink and V. Golovitchev, "Gasoline HCCI Modeling: Computer Program Combining Detailed Chemistry and Gas Exchange Processes," *SAE technical paper series 2001-01-3614*, 2001.

[50] "*http* : *//www.bmw.com*," June 2009.

[51] T. Urushihara, K. Hiraya, A. Kakuhou, and T. Itoh, "Expansion of HCCI Operating Region by the Combination of Direct Fuel Injection, Negative Valve Overlap and Internal Fuel Reformation," *SAE technical paper series 2003-01-0749*, 2003.

[52] L. Koopmans, R. Ogink, and I. Denbratt, "Visualisation (PLIF) of Intermediates Generated in the Negative Valve Overlap of an HCCI Operated Engine," *Proceedings of the Combustion Institute*, vol. 28, pp. 1563–1577, 2000.

[53] A. Berntsson and I. Denbratt, "Optical study of HCCI Combustion using NVO and an SI Stratified Charge," *SAE technical paper series 2007-24-0012*, 2007.

[54] A. Berntsson, W., M. Andersson, D. Dahl, and I. Denbratt, "LIF imaging of OH during the Negative Valve Overlap of a HCCI Combustion Engine," *Proceedings of The Spark Ignition Engine of the Future - Technologies to meet the CO_2 challenge conference*, 2007.

[55] A. Berntsson, W., M. Andersson, D. Dahl, and I. Denbratt, "A LIF-study of OH in the Negative Valve Overlap of a Spark-assisted HCCI Combustion Engine," *SAE technical paper series 2008-01-0037*, 2008.

[56] B.-E. Lindh, *Scania fordonshistoria 1891-1991.* 1992.

[57] "$http://www.mitsubishi-motors.com$," June 2009.

[58] M. Alt and U. Grebe, "Fuel Injection System Requirements to enable HCCI Combustion," *3rd International Automotive Workshop Direct Injection for Gasoline Engines - power point presentation*, 2007.

[59] A. Kulzer, W. Fischer, R. Karrelmayer, C. Sauer, T. Wintrich, and K. Benninger, "Homogenous Charge Compression Ignition on Gasoline Engines - The Potential of CO_2*Reduction*," *MTZ*, vol. 70, no. 1, pp. 32–39, 2009.

[60] A. Kulzer, J.-P. Hathout, C. Sauer, W. Fischer, R. Karrelmayer, A. Löffler, and A. Christ, "Das Verbrauchkonzept CAI - Verbrennung und Reglerung fü das CAI-Brennverfahren mit BDE-Technologie und vollvariablem Ventiltrieb," *Aachener Kolloquium Fahrzeug- und Motortechnik*, no. 16, pp. 1195–1218, 2007.

[61] H. Blaxill and A. Cairns, "Production-Feasible Controlled Auto-Ignition," *Auto Technology*, vol. 3, pp. 28–31, 2007.

[62] C. Jelitto, J. Willand, J. Jakobs, O. Magnor, M. Schultalbers, and E. Millich, "Challenge of a Gasoline Compression Ignition-Demonstrator," *VDI-berichte*, no. 1975, pp. 271–288, 2006.

[63] C. Jelitto, J. Willand, J. Jakobs, O. Magnor, M. Schultalbers, and M. Köller, "Potentials of the GCI-combustion process," *8th Stuttgart International Symposium*, 2008.

[64] C. Jelitto, J. Willand, J. Jakobs, O. Magnor, M. Schultalbers, and E. Millich, "Gasoline Compression Ignition Aus den Forschungslabors in die Anwendung," *Aachener Kolloquium Fahrzeug- und Motortechnik*, no. 16, pp. 1177–1194, 2007.

[65] W. A. Berntsson, M. Andersson, and I. Denbratt, "Characterization of a HCCI Engine Using Charge Stratification and Spark-Assist with Simultaneous PIV, Multi-Species LIF and High Speed Video," *International Journal of Engine Research*, vol. XX, no. XX, pp. XX–XX, 2009.

[66] T. Wilson, M. Haste, H. Xu, S. Richardson, D. Yap, and T. Megaritis, "In-cylinder Flow with Negative Valve Overlapping - Characterised by PIV Measurement," *SAE technical paper series 2005-01-2131*, 2005.

[67] R. Standing, N. Kalian, T. Ma, H. Zhao, M. Wirth, and A. Schamel, "Control of CAI Combustion Through Injection Timing in a GDI Engine With an Air- Assisted Injector," *SAE technical paper series 2005-01-0132*, 2005.

[68] B. Leach, H. Zhao, Y. Li, and T. Ma, "Control of CAI Combustion Through Injection Timing in a GDI Engine With an Air- Assisted Injector," *SAE technical paper series 2005-01-0134*, 2005.

[69] Y. Li, H. Zhao, N. Brouzos, T. Ma, and B. Leach, "Control of CAI Combustion Through Injection Timing in a GDI Engine With an Air- Assisted Injector," *SAE technical paper series 2006-01-0206*, 2006.

[70] H. Persson, A. Hultqvist, B. Johansson, and A. Remon, "Investigation of the Early Flame Development in Spark-Assisted HCCI Combustion Using High-Speed Chemiluminescence Imaging," *SAE technical paper series 2007-01-0212*, 2007.

[71] A. Berntsson and I. Denbratt, "Spark Assisted HCCI Combustion Using a Stratified Hydrogen Charge," *SAE technical paper series 2005-24-039*, 2005.

[72] A. Berntsson and I. Denbratt, "HCCI Combustion Using a Spark Ignited Stratified Charge," *Proceedings. JSAE Annual Congress*, vol. 24-06, pp. 23–28, 2006.

[73] D. Dahl, M. Andersson, W. A. Berntsson, I. Denbratt, and L. Koopmans, "Reducing Pressure Fluctuations at High Loads by Means of Charge Stratification in HCCI Combustion with Negative Valve Overlap," *SAE technical paper series 2009-01-1785*, 2009.

[74] A. G. Gaydon, *The Spectroscopy of Flames*. Chapman and Hall, second ed., 1974.

[75] A. Berntsson and I. Denbratt, "HCCI Combustion Using Charge Stratification for Combustion Control," *SAE technical paper series 2007-01-0210*, 2007.

[76] A. C. Eckbreth, *Laser Diagnostics for Combustion Temperature and Speices*. Combustion Science & Technology Book Series, Gordon and Breach Publishers, 1996.

[77] Y. Yamasaki and N. Iida, "Numerical Analysis of Autoignition and Combustion of n-Butane and Air Mixture in Homogenous-Charge Compression-Ignition Engine Using Elementary Reactions," *JSME International Journal*, vol. 46, no. 1, pp. 52–59, 2003.

[78] M. Richter, *Combustion Engine Characterization and Development by Means of Laser Diagnostics*. doctoral thesis ed., 2002.

[79] J. Luque and D. Crosley, *LIFBASE: Database and Spectral Simulation Program (Version 1.45)*. SRI International Report MP 98-021, 1998.

[80] F. Grossman, P. B. Monkhouse, M. Ridder, V. Sick, and J. Wolfrum, "Communication in the presence of noise," *Applied Physics B*, vol. 62, pp. 249–253, 1996.

[81] M. Aldén, *Optical Combustion Diagnostics*. CECOST-course material.

[82] C. Crowe, M. Sommerfeld, and Y. Tsuji, *Multiphase flows with droplets and particles*. CRC, 1998.

[83] J. G. R. Clift and M. Weber, *Bubbles, Drops and Particles*. Academic Press, London, 1978.

[84] L. Rabiner and O. Herrmann, "The Predictability of Certain Optimum Finite Impulse Response Digital Filters," *IEEE Transactions on Circuit Theory*, vol. CT-20, no. 4, pp. 401–408, 1973.

[85] C. E. Shannon, "Communication in the presence of noise," *Proc. Institute of Radio Engineers*, vol. 37, no. 1, pp. 10–21, 1949.

[86] "*http* : *//www.mathworks.com/*," June 2009. MATLAB and Simulink for Technical Computing.

[87] C. K. Westbrook, "Chemical kinetics of hydrocarbon ignition in practical combustion systems," *Joint Meeting of the Scandinavian-Nordic and Italian Sections of the Combustion Institute*, 2003.

[88] N. Graf, J. Gronki, C. Schulz, T. Beritaud, J. Cherel, P. Duret, and J. Lavy, "In-Cylinder Combustion Visualization in an Auto-Igniting Gasoline Engine using Fuel Tracer- and Formaldehyde-LIF Imaging," *SAE technical paper series 2001-01-1924*, 2001.

[89] J. Olofsson, H. Seyfried, M. Richter, M. Aldén, A. Vressner, A. Hultqvist, B. Johansson, and K. Lombaert, "High-Speed LIF Imaging for Cycle-Resolved Formaldehyde Visualization in HCCI Combustion," *SAE technical paper series 2005-01-0641*, 2005.

[90] H. Zhao, Z. Peng, and T. Ma, "Investigation of the HCCI/CAI Combustion Process by 2-D PLIF Imaging of Formaldehyde," *SAE technical paper series 2004-01-1901*, 2004.

[91] M. C. Weikl, F. Beyrau, A. Leipertz, A. Loch, C. Jelitto, and J. Willand, "Locally Resolved Measurement of Gas-Phase Temperature and EGR-Ratio in an HCCI-Engine and Their Influence on Combustion Timing," *SAE technical paper series 2007-01-0182*, 2007.

[92] L. Koopmans, H. Ström, S. Lundgren, O. Backlund, and I. Denbratt, "Demonstrating a SI-HCCI-SI Mode Change on a Volvo 5-Cylinder Electronic Valve Control Engine," *SAE technical paper series 2003-01-0753*, 2003.

[93] M. Tabata and T. Yamamoto, "Improving NOx and Fuel Economy for Mixture Injected SI Engine with EGR," *SAE technical paper series 950684*, 1995.

[94] K. K. Kuo, *Principles of Combustion.* Wiley-Interscience, 1986.

[95] G. L. Borman and K. W. Ragland, *Combustion Engineering.* McGraw-Hill Inc., first ed., 1998.

[96] R. Stone, *Introduction to Internal Combustion Engines.* Palgrave, third ed., 1999.

[97] D. Dahl, I. Denbratt, and L. Koopmans, "An Evaluation of Different Combustion Strategies for SI Engines in a Multi-Mode Combustion Engine," *SAE technical paper series 2008-01-0426*, 2008.

[98] J. R. Sodré and S. M. C. Soares, "Comparison of Engine Power Correction Factors for Varying Atmospheric Conditions," *Journal of the Brazilian Society of Mechanical Science & Engineering*, vol. 25, no. 3, pp. 279–285, 2003.

[99] F. Zhao, M. C. Lai, and D. L. Harrington, "Automotive spark-ignited direct-injection gasoline engines," *Progress in Energy and Combustion Science*, vol. 25, pp. 437–562, 1999.

[100] B. Xander, "Grundlegende Untersuchungen an einem Ottomotor mit direkteinspritzung und strahlgeführtem brennverfahren," *Disertation Thesis*, 2006.

[101] T. Ashizawa, K. Saitoh, Y. Tamura, and T. Sakai, "Development of a new in-line 4-cylinder direct-injection gasoline engine," *Proceedings of JSAE Fall convention*, 1988.

[102] M. M. Maricq, D. H. Podsiadlik, D. D. Brehob, and M. Haghgooie, "Particulate emissions from a direct-injection, spark ignition (DISI) engine," *SAE technical paper series 1999-01-1530*, 1999.

[103] U. Spicher, J. Reissing, J. M. Kech, and J. Gindele, "Gasoline Direct Injection (GDI) Engines - Development Potentials," *SAE technical paper series 1999-01-2938*, 1999.

Paper I

Spark Assisted HCCI Combustion Using a Stratified Hydrogen Charge

Andreas William Berntsson and Ingemar Denbratt

SAE Technical Paper

SAE NAPLES SECTION

2005-24-039

SAE TECHNICAL
PAPER SERIES

Spark Assisted HCCI Combustion Using a Stratified Hydrogen Charge

A. Berntsson and I. Denbratt
Chalmers University of Technology, Sweden

ICE2005
7th International Conference on Engines for Automobile

Capri, Naples
Italy
September 11-16, 2005

SAE International

2005-24-039

Spark Assisted HCCI Combustion Using a Stratified Hydrogen Charge

Andreas Berntsson and Ingemar Denbratt
Chalmers University of Technology

ABSTRACT

Future requirements for emission reduction from combustion engines in ground vehicles might be met by using the HCCI combustion concept. In this concept a more or less homogenous air fuel mixture is compressed to auto ignition. This gives good fuel consumption compared to a normal SI engine and its ability to burn lean mixtures at low temperatures has a positive impact on exhaust emissions. However, there are challenges associated with this concept, for instance its limited operating range and combustion control.

The objective of this work is to investigate a hybrid concept, based on a combination of HCCI combustion of *n*-heptane and SI combustion of hydrogen. The basic idea is to initiate HCCI combustion with a spark ignited stratified lean hydrogen mixture. To verify that the combustion sequence consists of flame front combustion followed by HCCI combustion, photographs of OH chemiluminescence from the combustion were taken. This was made in a single cylinder engine with optical access through a quartz window in the piston. The performance of the hybrid combustion was compared to that of pure HCCI combustion.

Chemiluminescence images show an expanding flame front initiated by the spark plug. It is shown that the flame front propagation through the hydrogen charge can be used to expand the operating range of HCCI combustion, especially towards lower loads. The hybrid combustion concept gives greater scope for controlling the combustion than the pure HCCI concept. By varying the amount of hydrogen the crank angle when 50% of the energy is burned, CA50, can be phased further away from TDC.

INTRODUCTION

The ever increasing demands to reduce emissions and fuel consumption reduction are prompting the development of more advanced combustion concepts. One promising concept is homogeneous charge compression ignition (HCCI). In an HCCI engine the combustion is chemically controlled [1], and it releases heat more rapidly than flame front combustion. In the ideal cycle for an SI engine the combustion occurs at constant volume and this cycle is the most efficient of the ideal cycles [2]. The rapid heat release of the HCCI combustion occurs at almost constant volume, which partly explains its low fuel consumption. Another advantage is its ability to burn lean mixtures, thereby reducing pump losses. At part load it can be operated unthrottled, resulting in greatly improved efficiency compared to SI combustion [3]. HCCI combustion gives low NOx and PM emissions [4] as a result of the lean mixture. The lean unthrottled operation gives higher mass, compared to throttled operation, and thus a lower cycle averaged temperature resulting in lower heat losses. A consequence of the combustion occuring in many places simultaneously is that cycle-to-cycle variations are small [5].

There are challenges associated with the HCCI concept which have to be overcome before it is commercialised. The control of ignition timing [6], the limited operating range [4] and limiting the rate of heat release [7] are such challenges. Cylinder-to-cylinder variation can be a problem in HCCI engines [4], since the temperature can vary between the different cylinders.

In this work a hybrid combustion concept was studied, combining HCCI combustion of n-heptane and stratified SI combustion of hydrogen. The hybrid concept's ability to increase the operating range and to improve the control of the combustion was also analysed.

EXPERIMENTAL APPARATUS

OPTICAL ENGINE

A single cylinder research engine with optical access was used for the chemiluminescence study. Its displaced volume corresponds to the size of a passenger car engine. This engine has an extended piston housing a mirror that provides in conjunction with a quartz window in the piston crown optical access. The combustion chamber in this system is optically accessible from below. The quartz window in the piston crown allows optical access to most of the combustion

chamber, the area covered can be seen in Figure 1. The cylinder pressure was measured using a piezoelectric pressure transducer. For all the measurements wide open throttle was used.

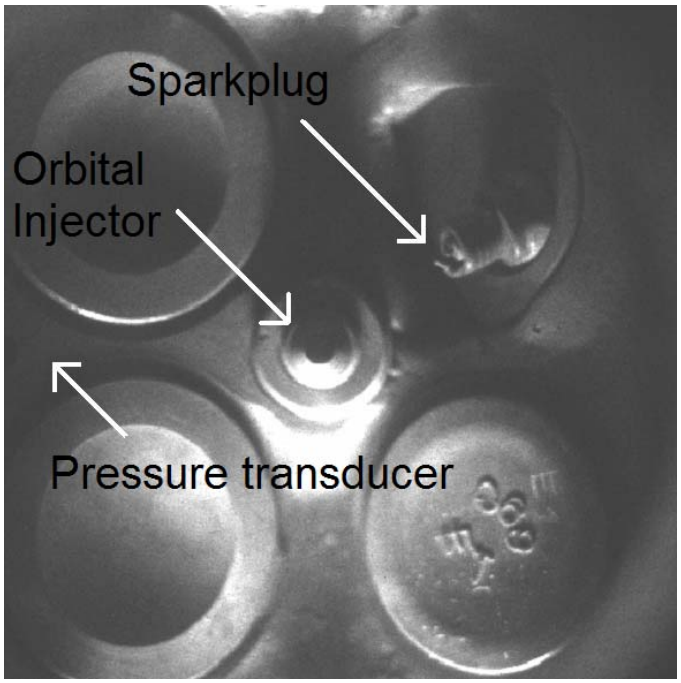

Figure 1The optically accessible combustion chamber. The optically covered diameter was 73 mm.

The optical piston had a flat piston crown, this in combination with a large included valve angle and large crevices between the piston and the liner limited the compression ratio. The arrangement with elongated piston and thereby heavier piston resulted in great friction losses, vastly greater than would be expected in a conventional engine. Thus, only indicated work values are considered in this paper. The main parameters for the engine can be seen in Table 1.

Table 1 Engine parameters.

Bore	83 mm
Stroke	90 mm
Swept volume	487 cm^3
Compression ratio	10.6:1
Conrod length	139.5 mm

CAMERA

An intensified LaVision DynaMight digital camera was used to capture the chemiluminescence images. To control the timing of the camera an AVL 4210 timing unit was used.The images presented in this paper are averaged from 20 cycles. This in order to represent images that are less affected by cycle-to-cycle variations and that corresponds to a typical chemiluminescence signal for a specific CAD. Both the gain and exposure time of 200 µs were kept constant in this study. The noise was calculated from areas in the image that should not have given a signal, e.g. the area outside the window. This noise was subtracted from the images. An unfiltered background image was added to the averaged filtered images. The resolution of the camera was 1024 by 1024 pixels, for the present setup equal to 14 pixels for each millimetre. A schematic sketch of the camera setup can be seen in figure 2.

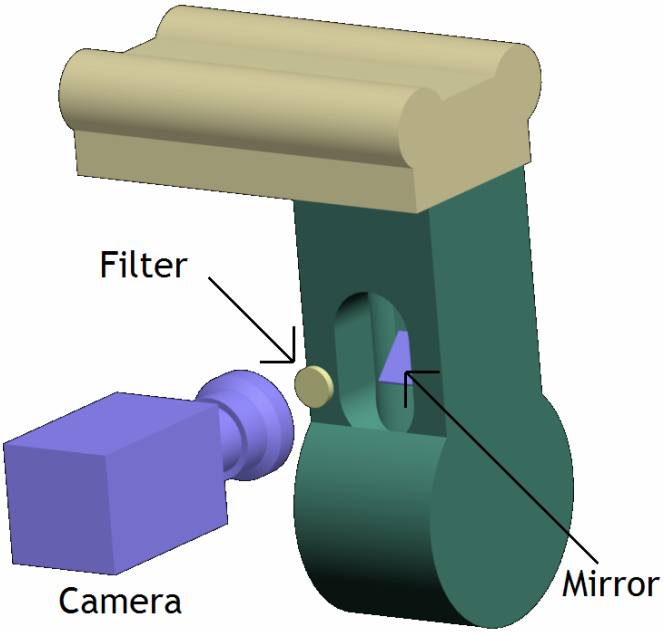

Figure 2 Schematic camera setup.

In order to study flame front propagation a filter was used to isolate the emitted light from the OH radicals. The specie of interest here is the OH radicals which can be associated with the reaction zone.

$H+OH=H_2O+hv$

The reaction gives intensity peaks for the emitted light at wavelengths between 306 and 309 nm [8]. The filter used was a narrowband filter with a centre wavelength of 310 nm, and its transmission spectrum is presented in Figure 3.

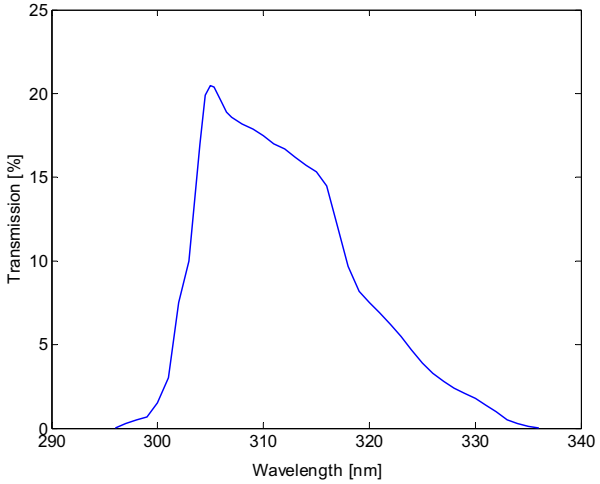

Figure 3 The filter's transmission spectrum.

In this study hydrogen was injected into a more or less homogeneous mixture of *n*-heptane and air, i.e. the stratified hydrogen charge consisted of hydrogen, n-heptane and air. This in combination with the spectral range of the filter lead to that the effect of the Vaidya hydrocarbon flame bands are present in the chemiluminescence measurement. The Vaidya bands correspond to the HCO reaction and intensity peaks at wavelengths of 301, 311, 319 and 330 nm [8] will pass through the filter. The emission from the OH reaction is one of the strongest features from most flame spectra [8] and is here considered to be the dominant one due to the enrichment of hydrogen in the stratified zone and the high transmission of the filter at 306 nm. Thus, the effect from the Vaidya emission is neglected in this study.

GAS INJECTION

In order to obtain a stratified hydrogen charge an Orbital injector was used, which was originally designed for use as an air-assisted, spray-guided direct injection device [9]. It uses pressurised air to break up the fuel spray. In this study the injector's gas function was used and the pressurised air was changed to pressurised hydrogen. Thus, it was only used as a gas injector. The pressure of the hydrogen was kept at 800 kPa.

FUEL INJECTION

Port injection was used for the *n*-heptane. The timing of the injections and ignition can be seen in Figure 4.

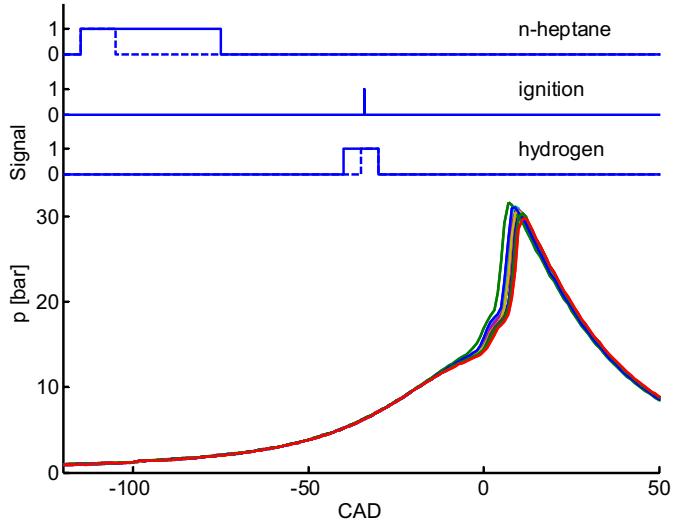

Figure 4 Timing of n-heptane injection, ignition and hydrogen injection for this study. Dashed lines indicates minimum duration of hydrogen or n-heptane and solid line indicates maximum duration. The cylinder pressure traces are from 10 different cycles with parameters as in Table 2.

INLET HEATER

Since the investigation was performed in an optical engine with high cooling losses the intake air was heated to extend the operational range to light loads. The peak pressure is preferably kept at a low value due to the sensitivity of the optical research engine. The heater decreases the amount of fuel needed to establish HCCI combustion and the reduction of fuel decreases the peak pressure. The intake air temperature was measured directly at the intake valve using a thermocouple.

IGNITION

In order to mount a gas injector centrally within the combustion chamber a modified cylinder head was used. One of the exhaust valves in the modified four valve pent-roof cylinder head was removed and replaced by a spark plug. The depth of the sparkplug's location was adjustable, but this feature was not used in this work. The ordinary sparkplug mounting was occupied by the Orbital injector, allowing it to point down, along the cylinder's axial direction, as shown in the schematic sketch in Figure 5.

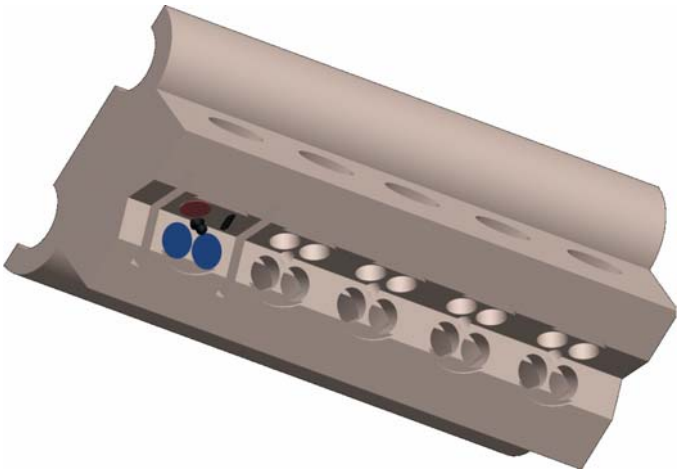

Figure 5 Schematic sketch of the modified cylinder head.

METAL ENGINE

The quartz window in the piston was replaced with a metallic window in order to make the research engine more rigid for all measurements that did not require optical access. With a metallic piston the engine could run with higher cylinder pressure and continuously. The knock sensitivity of the engine was dramatically decreased with the metallic piston.

RESULTS AND DISCUSSION

CHEMILUMINESCENCE IMAGES

Chemiluminescence images of HCCI combustion and flame front propagation are presented in Figure 6. All images were taken under identical operating conditions, the parameters of which can be seen in Table 2. The camera gain was identical for all images.

Table 2 Parameters used for chemiluminescence images.

Engine speed	1200 rpm
Liquid fuel	*n*-heptane 5400 J/s
Gaseous fuel	Hydrogen 880 J/s
Lambda	2.2
IMEP	3.2 bar
Intake air temperature	85 ºC

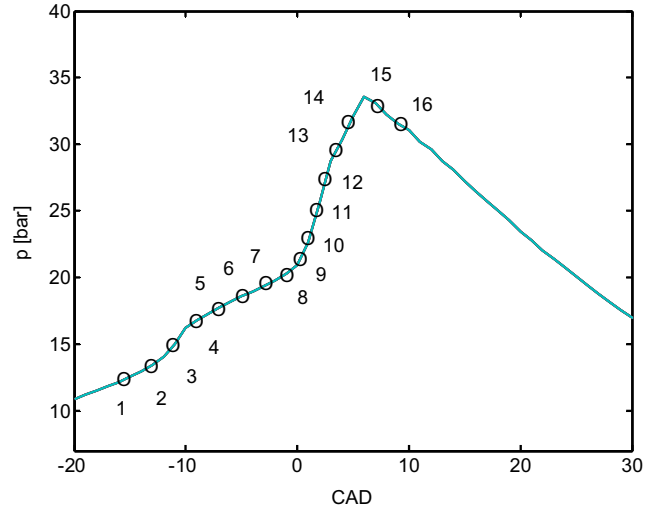

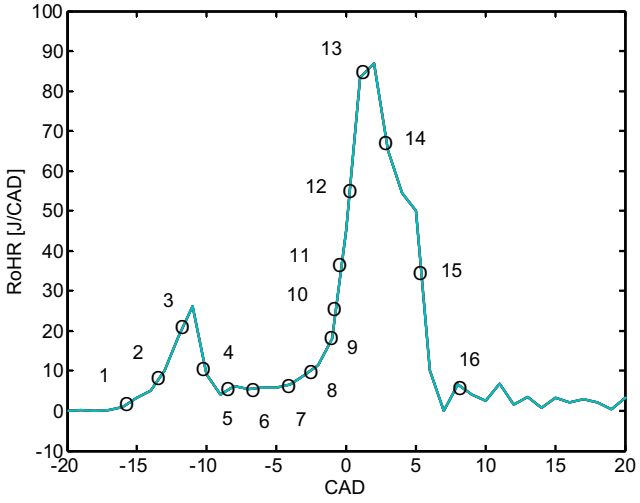

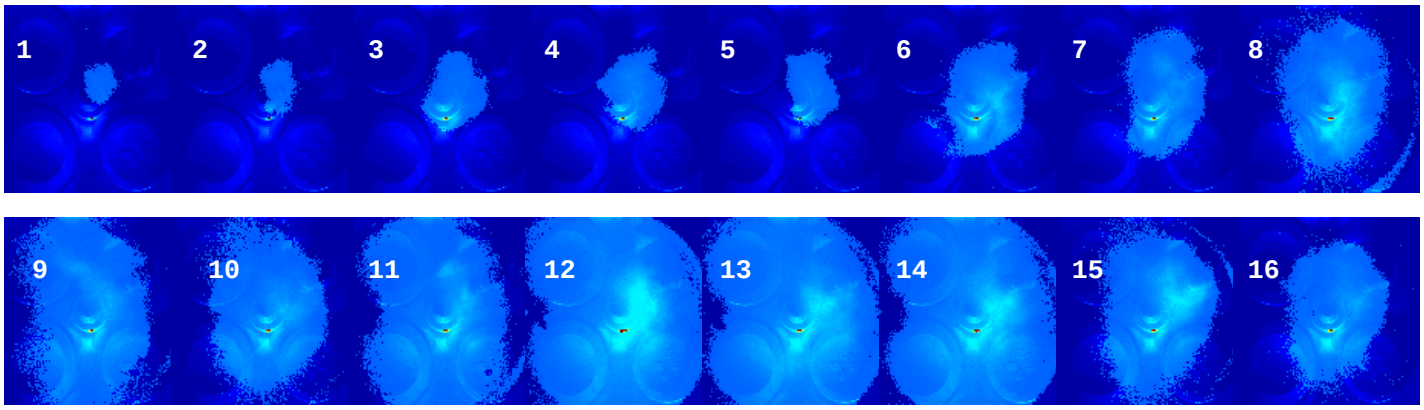

Figure 6 Chemiluminescence images of the combustion. The timing of the images is presented as circular symbols in the pressure trace and the rate of heat release. The pressure trace and rate of heat release are averages of 10 cycles.

The pressure trace and the rate of heat release for the conditions used in the chemiluminescence study are presented in Figure 6, in which the image timings are indicated by the circular symbols. The strongest signal in the chemiluminescence images coincided with the peak values of the main heat release. The signal strength prior to the main heat release is fairly constant in intensity; the signal merely occupies an increasingly large area. Without the stratified charge signals were only obtained during the main heat release, the same result was seen by Wagner et al. [6] and Kumano and Iida [10]. Thus the signal prior to the main heat release originates from flame front combustion. The chemiluminescence images show an expanding flame front, which is initiated by the sparkplug and expands from there. During the main heat release there is a strong signal covering almost the entire combustion chamber for a duration of approximately 5 CAD. This signal corresponds to HCCI combustion.

OPERATING RANGE

The scope for expanding the HCCI operating range, by using a spark ignited stratified hydrogen charge, is shown in Figures 7-9. Only one parameter was varied for establishing the pure HCCI operating range, i.e. only the fuel amount was varied. All other parameters were kept constant and the sparkplug was fired for all measurements, with or without hydrogen, in order to isolate the effect of the stratified charge. This gives a very narrow operating range for pure HCCI combustion. By increasing the fuel amount the peak cylinder pressure tends to move closer to TDC rather than just increasing the work output. The narrow HCCI operating range is expanded by replacing 600 or 1200 J/s of *n*-heptane by hydrogen. The operating range study was performed with three different intake air temperatures, see Table 3.

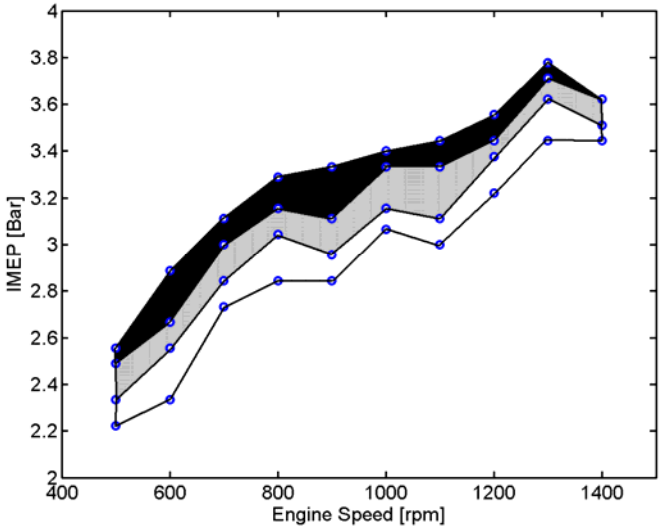

Figure 7 Operating range for 60 ºC intake air temperature. The dark region corresponds to pure HCCI. In the grey region 600 J/s of hydrogen is used and in the white region 1200 J/s is used.

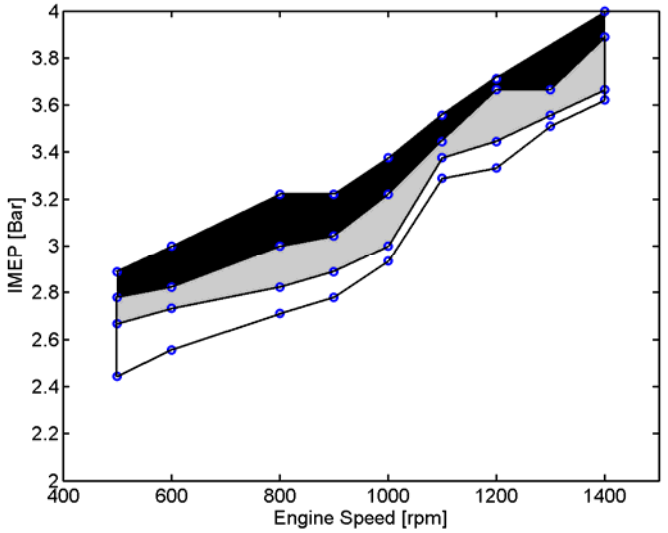

Figure 8 Operating range for 70 ºC intake air temperature. The dark region corresponds to pure HCCI. In the grey region 600 J/s of hydrogen is used and in the white region 1200 J/s is used.

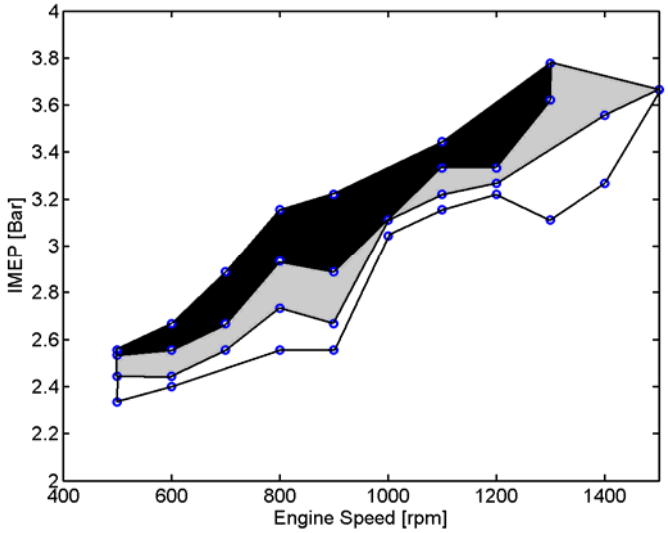

Figure 9 Operating range for 80 ºC intake air temperature. The dark region corresponds to pure HCCI. In the grey region 600 J/s of hydrogen is used and in the white region 1200 J/s is used.

Table 3 Parameters used the operating range study.

Liquid fuel	*n*-heptane 1700 to 7400 J/s
Gaseous fuel	hydrogen 0, 600 or 1200 J/s
Intake air temperature	60, 70 or 80 ºC

The HCCI operating range is increased by the use of the stratified hydrogen charge. The upper limit for the operating range is limited by knock due to the high pressure that evolves when the peak pressure moves closer to TDC. Naturally, the great rate of heat release of HCCI combustion also plays a role in producing such high pressure. Although some of the energy that should be combusted in an HCCI manner is replaced by flame front combustion, with a lower rate of heat release, the HCCI combustion dominates, limiting the expansion of the operating range towards higher loads. Use of experimental equipment that can deliver more energy in the form of a stratified hydrogen charge might increase the operating range of a combination of HCCI and flame front combustion. At the lower limit of the HCCI operating range, the cycle-to-cycle variations increase and the combustion quality deteriorates, resulting in increased HC emissions. The peak cylinder pressure also moves further from TDC. The stratified charge of hydrogen has a great impact in expanding the operating range towards lower loads.

CA50

The effect of combining flame front combustion of hydrogen with HCCI combustion of *n*-heptane on combustion control is presented in Figures 10-12. Combustion control involves the modulation of several parameters and in this analysis the parameter studied is CA50, more precisely the effect on CA50 of different proportions of HCCI combustion and flame front combustion, in terms of energy. The parameters used for this analysis are presented in Table 4.

Table 4 Parameters used in CA50 study.

Gaseous fuel	hydrogen 0, 5, 10 or 15 %
Liquid fuel	*n*-heptane 100, 95, 90 or 85 %
Engine speed	600, 700 and 800 rpm
Intake air temperature	60, 70 and 80 ºC

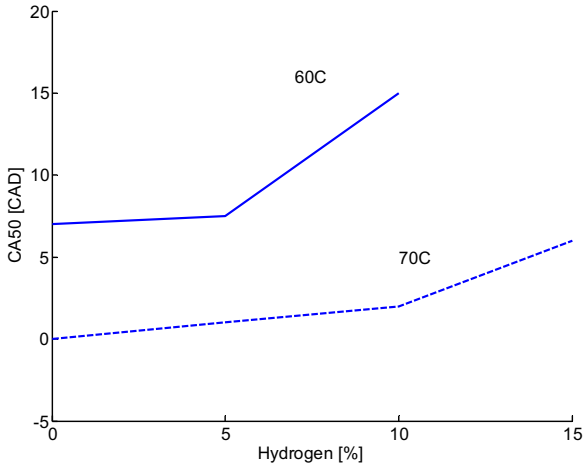

Figure 10 The CA50 at different proportions of hydrogen. Engine speed 600 rpm and indicated output 0.8 kW. For this engine speed an intake air temperature of 80 °C gave to advanced combustion timing.

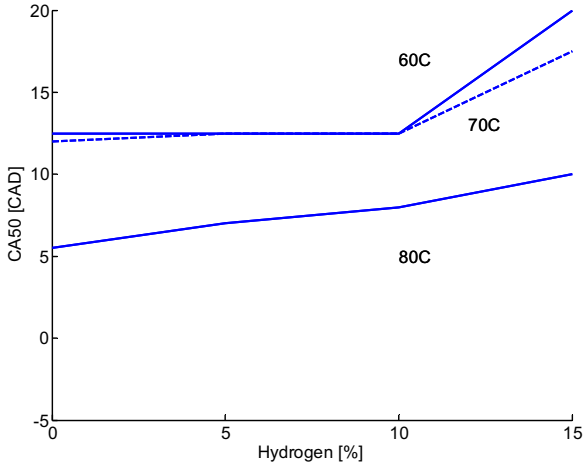

Figure 11 The CA50 at different proportions of hydrogen. Engine speed 700 rpm and indicated output 0.9 kW.

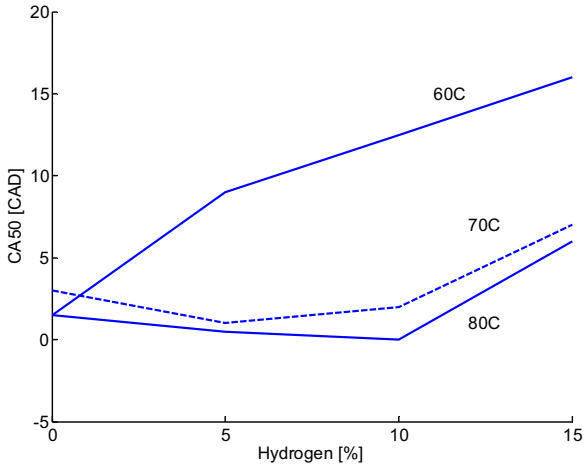

Figure 12 The CA50 at different proportions of hydrogen. Engine speed 800 rpm and indicated output 1 kW.

The general consequence of replacing some of the HCCI combustion with flame front combustion is that CA50 is retarded. The degree of combustion phasing depends on the different operational conditions and proportions of hydrogen. In order to retard the combustion for conditions resulting in CA50 close to TDC a greater amount of hydrogen is needed. For a constant engine speed and load a lower intake air temperature results in retarded combustion, and the necessary temperature needed for HCCI combustion is reached later in the cycle. The curves for an intake air temperature higher than 70 °C in figure 12 actually shows advanced combustion timing, if less than 10 % of the energy comes from hydrogen. The NO_x emissions were measured in the CA50 study and it was found that SI combustion of a lean stratified hydrogen charge did not increase the NO_x emissions. For most operational conditions, slightly lower NO_x values were obtained with increased amounts of hydrogen due to the lower average cycle temperature.

CONCLUSION

A chemiluminescence study of the hybrid combustion concept was performed in order to verify that it consisted of both HCCI combustion and SI combustion. It was shown that it is possible to combine HCCI combustion of *n*-heptane and SI combustion of a stratified hydrogen charge.

An SI stratified hydrogen charge can be used to enhance the operating range of HCCI combustion of *n*-heptane. The operating range was extended towards lower loads, which might reduce the need for a mode switch between HCCI operation and idle.

It was shown that a stratified hydrogen charge can be used to control HCCI combustion of *n*-heptane. By altering the amount of hydrogen it was possible to control the CA50 timing. It was seen that the CA50 timing can be retarded by using minor proportions of hydrogen for the operating conditions used in this study. The hydrogen appears not to compensate for the leaner mixture of *n*-heptane resulting in the retarded CA50 timing. The heat added during early flame front combustion does not compensate for the higher temperature requirements for HCCI combustion due to the leaner *n*-heptane-air mixture. This might be different if the ignition timing of the SI combustion is advanced. For some operating conditions a slight advance of the CA50 timing was observed, this phenomenon will be further investigated in future work.

ACKNOWLEDGMENTS

The authors wish to acknowledge STEM, Swedish Energy Agency, for funding this work and all co-workers at the division for their contribution to it.

REFERENCES

1. Koopmans, L., Strömberg, E., Denbratt, I., “The Influence of PRF and Commercial Fuels with High Octane Number on the Auto-Ignition Timing of an Engine Operated in HCCI Combustion Mode with Negative Valve Overlap”, SAE Technical Paper Series, SAE Paper 2004-01-1967.
2. Heywood, J. B. , “Internal Combustion Engines Fundamentals” 1988, Singapore: McGraw-Hill Inc.
3. Hultquist, A., Christensen, M., Johansson, B., Ricther, M., Nygren, J., Hult, J., Aldén, M., “The HCCI Combustion Process in a Single Cycle – High-Speed Fuel Tracer LIF and Chemiluminescence Imaging”, SAE Technical Paper Series, SAE Paper 2002-01-0424.
4. Lü, X-C., Chen, W., Huang, Z., “A fundamental study on the control of the HCCI combustion and emissions by fuel design concept combined with controllable EGR. Part 1. The basic characteristics of HCCI combustion”, Fuel, Volume 84, Issue 9, Pages 1074-1083 (June 2005).
5. Hultquist, A., Christensen, M., Johansson, B., Franke, A., Aldén, M., “A Study of the Homogenous Charge Compression Ignition Combustion Process by Chemiluminescence Imaging”, SAE Technical Paper Series, SAE Paper 1999-01-3680.
6. Wagner, U., Anca, R., Velji, A., Spicher, U., “An Experimental Study of Homogenous Charge Compression Ignition (HCCI) with Various Compression Ratios, Intake Air Temperatures and Fuels with Port and Direct Fuel Injection”, SAE Technical Paper Series, SAE Paper 2003-01-2293.
7. Lü, X-C., Chen, W., Huang, Z., “A fundamental study on the control of the HCCI combustion and emissions by fuel design concept combined with controllable EGR. Part 2. Effect of operating conditions and EGR on HCCI combustion”, Fuel, Volume 84, Issue 9, Pages 1084-1092 (June 2005).
8. Gaydon, A. G., ”The Spectroscopy of Flames”, Chapman and Hall, Second edition.
9. Cathcart, G., Tubb, J., “Application of Air Assisted Direct Fuel Injection to Pressure Charged Gasoline Engines”, SAE Technical Paper Series, SAE Paper 2002-01-0705.
10. Kumano, K., Iida, N., “Analysis of the Effect of Charge Inhomogeneity on HCCI Combustion by Chemiluminescence Measurement”, SAE Technical Paper Series, SAE Paper 2004-01-1902.

CONTACT

Corresponding author:
Andreas Berntsson
Chalmers University of Technology
Department of Applied Mechanics
Division of Combustion and Multiphase Flow
Hörsalsvägen 7
SE-412 96 Göteborg
Sweden
Email:andreas.berntsson@chalmers.se

DEFINITIONS, ACRONYMS, ABBREVIATIONS

HCCI: Homogenous Charge Compression Ignition.

CAD: Crank Angle Degree.

TDC: Top Dead Center.

CA50: Crank angle when 50% of the energy is burned.

WOT: Wide Open Throttle.

HC: Hydro Carbon.

SI: Spark Ignition.

NO_x: Nitrogen Oxides.

PM: Particulate Matter.

Paper II

HCCI Combustion Using a Spark Ignited Stratified Charge

Andreas William Berntsson and Ingemar Denbratt

Proceedings of the JSAE Annual Congress

114 HCCI Combustion Using a Spark Ignited Stratified Charge*

Andreas Berntsson [1] Ingemar Denbratt [2]

Requirements for further reductions for fuel consumption and emissions might be met by using HCCI combustion, provided that certain challenges can be overcome – the most important of which is to develop ways to control the combustion.

In this study a combination of SI and HCCI combustion was investigated, in which a SI stratified charge is used to initiate the HCCI combustion. Both hydrogen and a mixture of iso-octane and n-heptane were used as fuels for the stratification charge. The hybrid combustion concept was found to give better control of combustion timing and the CA50 could be controlled by varying the injection timing and stratification amount.

Keywords: **HCCI, Spark Assisted, Fuel Stratification**

1. INTRODUCTION

Increasingly strict requirements to reduce exhaust emissions and fuel consumption are prompting the development of more advanced combustion concepts. One promising concept is Homogeneous Charge Compression Ignition, HCCI. In an HCCI engine the combustion is controlled by chemical kinetics [1], and heat is released more rapidly than in normal flame front combustion. In the ideal air standard SI cycle the combustion occurs at constant volume and this cycle is therefore the most efficient of the ideal cycles [2]. The rapid heat release of HCCI combustion and its ability to burn lean mixtures, thereby reducing pump, exhaust and cooling losses due to less throttled operation results in greatly improved efficiency compared to SI combustion [3]. HCCI combustion gives low NO_X and PM emissions [4] as a result of the lean homogenous mixture. Also cycle-to-cycle variations are minor because the combustion occurs in a distributed fashion at many places simultaneously [5].

However several challenges associated with the HCCI concept must be overcome before it can be commercially applied, notably ways must be developed to control ignition timing [6], expand its limited operating range [4] and limit the rate of heat release [7] are such challenges. Cylinder-to-cylinder variations can also cause problems in HCCI engines [4], since the temperature can vary between the different cylinders. Chemiluminescence images have shown that it is possible to create a hybrid combustion, in which initial spark-ignited flame-front combustion is followed by HCCI combustion [8]. The SI combustion provides a potential means to control the HCCI combustion. Therefore, this study further explored the hybrid combustion concept, combining HCCI combustion of a mixture of n-heptane and iso-octane with SI combustion of a stratified charge of either hydrogen or the same fuel as for the HCCI combustion. The scope for improving combustion phasing control by using the combined combustion approach, and it's effects on NO_X and HC emissions, were evaluated.

2. EXPERIMENTAL APPARATUS

A single-cylinder research engine was used for this study, with a displaced volume corresponding to that of a typical passenger car engine. The main parameters of the engine are presented in Table 1, and a schematic diagram of its layout, in Figure 1. A primary reference fuel, PRF, consisting of a mixture of 50 $\%_{vol}$ n-heptane and 50 $\%_{vol}$ iso-octane was used as the main fuel for the homogenous mixture. This fuel and hydrogen were also used as fuels for the stratified charge.

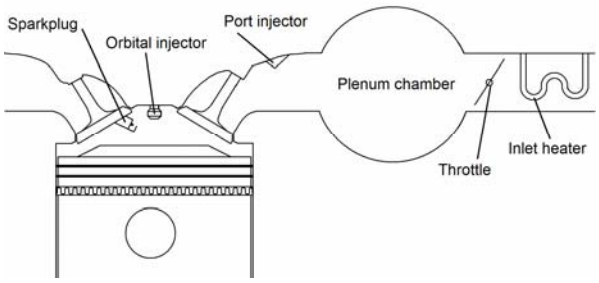

Fig. 1 Schematic diagram of the engine layout.

*Presented at 2006 JSAE Annual Congress

1) Chalmers University of Technology - E-mail; andreas.berntsson@chalmers.se

2) Chalmers University of Technology - E-mail; denbratt@chalmers.se

Table 1 Engine parameters

Bore	83 mm
Stroke	90 mm
Swept volume	487 cm^3
Compression ratio	14:1
Conrod length	139.5 mm
IVO	10 CAD BTDC
IVC	40 CAD ABDC
EVO	40 CAD BBDC
EVC	10 CAD ATDC

2.1. Fuel injection

An Orbital "air assisted" injector, originally designed for application in spray-guided direct-injection combustion systems, was used to deliver a stratified charge [9]. This injector generally uses pressurized air to atomize the fuel, but in these studies when hydrogen was used as the stratification fuel, only the injector's gas function was used and the pressurized air was changed to pressurized hydrogen. The pressure of the hydrogen was kept at 700 kPa. When PRF was used as the stratification fuel the injector was operated in a more conventional manner, using air as assisting media to atomize the stratification fuel.

Port injection was used for the main fuel in both cases, this in order to create an as homogenous air/fuel mixture as possible.

2.2 Inlet heater

An inlet heater was used to increase the inlet air temperature. The heater extended the load range to lower loads and allowed the combustion phasing to be initially adjusted. The intake air temperature was measured directly at the intake valve using a thermocouple.

2.3 Ignition

In order to mount the injector centrally within the combustion chamber a modified four-valve pent-roof cylinder head was used, in which one of the exhaust valves had been removed and replaced by a spark plug. The injector was mounted vertically at the original location of the spark plug. The protrusion of the sparkplug was adjustable, and after initial adjustments its position was kept constant for all measurements.

3. RESULTS AND DISCUSSION

3.1. PRF

The effects of varying the amount of stratification fuel can be seen in Figure 2. Operating conditions used in these experiments are presented in Table 2. Three different amounts of stratification fuel were used as well as HCCI combustion without any stratification. The dwell time between the end of injection (EOI) and spark timing (IGN) was kept constant at 10 CAD.

Table 2 Operating conditions used to assess the effects of varying the amounts of stratification fuel (PRF).

Injection timing	-60 CAD
IMEP	4 bar
λ	2.35 (overall)
Intake air pressure	87 kPa
Engine speed	1200 rpm
Stratification amount	0 450 900 1350 J/s
Main fuel	4750 4300 3850 3100 J/s
Dwell time (EOI-IGN)	10 CAD
Intake air temperature	100°C
Air assist amount	Case 1 1.4 l_N/min Case 2 2.1 l_N/min Case 3 2.8 l_N/min

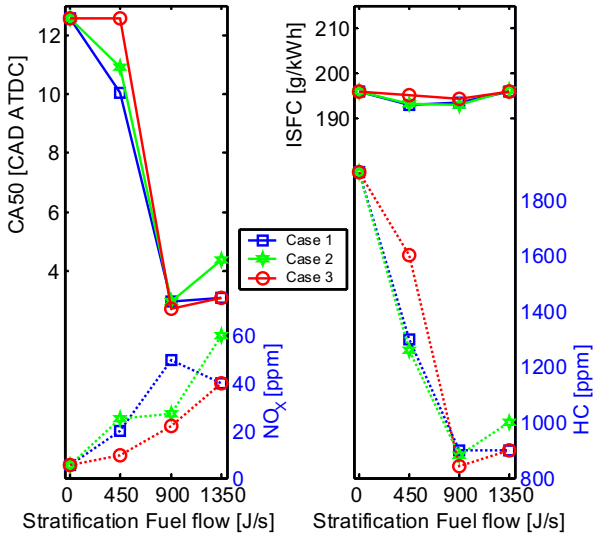

Fig. 2 CA50, ISFC and emissions obtained with different amounts of PRF as stratification fuel. Dotted lines indicate to emissions.

Under these conditions, the phasing of the combustion timing can be advanced by increasing the amount of stratification fuel up to, but not beyond, 900 J/s. Further increases may fail to yield further advances in phasing because only a fraction of the additional stratification fuel is consumed by the propagating flame, and the rest is combusted in HCCI mode after auto-ignition.

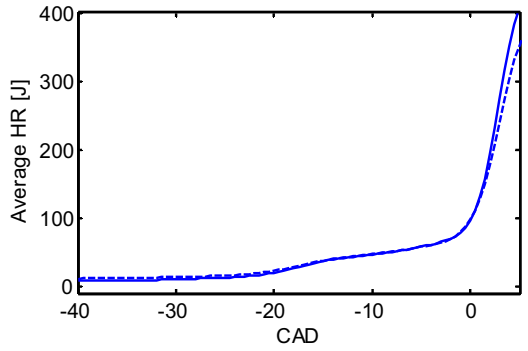

Fig. 3 Average heat release curve for case 1 in Table 2 during the early stage of the combustion. The solid and dashed lines correspond to stratification fuel flows of 900 J/s and 1350 J/s respectively.

As the heat release curves in Figure 3 show, increasing the stratification charge from 900 to 1350 J/s results in little or no additional heat release during the early stages of the combustion. Thus, the additional stratification fuel is not combusted in an SI mode during the early stages of combustion.

As shown in Figure 2, as CA50 phasing is advanced NO_X emissions tend to rise. Case 3, with the highest air-assisted flow, appeared to give the lowest NO_X emissions. The NO_X emissions in this case are probably lower because the stratified charge is diluted more (leaner) when the amount of assisting air is increased, and consequently the flame temperature is lower.

The advancement of the late HCCI combustion (CA50 at 12 CAD ATDC), observed under the basic settings with increasing amounts of stratification fuel appears to compensate for the increased compression work and heat losses due to the SI combustion when the amount of stratification is increased, since fuel consumption remains almost constant. HC emissions decrease as the stratification amount increases.

The effects of varying the injection and ignition timing using PRF as fuel for the stratified charge can be seen in Figure 4. Operating conditions for these tests can be found in Table 3.

The effects of varying injection timing were studied at four different operating conditions: two different engine speeds and two different dwell times for each speed. The dwell time was constant for each case, i.e. when the injection timing was changed the ignition timing was adjusted accordingly.

Table 3 Operating conditions used for assessing the effects of varying injection timing, using PRF as the stratification fuel.

Injection timing	-80 -70 -60 -50 CAD	
IMEP	4 bar	
λ	2.35 (overall)	
Intake air pressure	Case 1-2	84 kPa
	Case 3-4	90 kPa
Engine speed	Case 1-2	1000 rpm
	Case 3-4	1200 rpm
Stratification amount	Case 1-2	360 J/s
	Case 3-4	450 J/s
Main Fuel	Case 1-2	3500 J/s
	Case 3-4	4200 J/s
Dwell time (EOI-IGN)	Case 1	5 CAD
	Case 2	10 CAD
	Case 3	15 CAD
	Case 4	20 CAD
Intake air temperature	Case 1-2	87°C
	Case 3-4	97°C

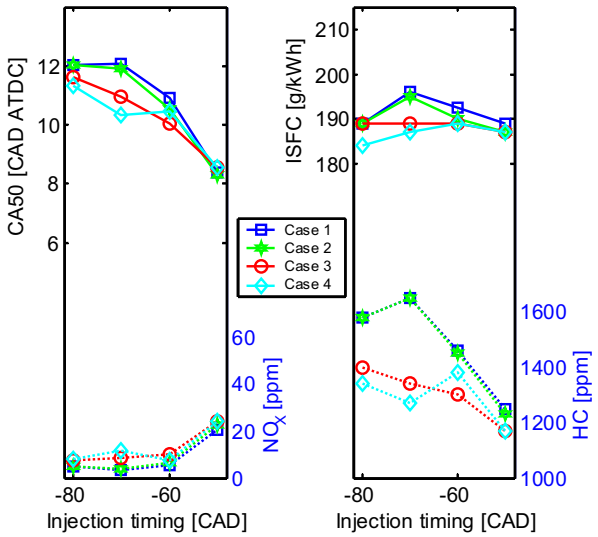

Fig. 4 CA50, ISFC and emissions obtained with different injection timings of the stratified charge using PRF as stratification fuel. Dotted lines indicate emissions.

A general effect of retarding the injection of the stratified charge is that the CA50 timing advances. The combustion phasing depends mainly on the injection timing and minor variations of spark timing (dwell) have no effect on combustion phasing. These tendencies were found at both the studied engine speeds and the possible control range of combustion phasing is around 4 CAD for each case.

The NO_X penalty for advancing the CA50 timing by around 4 CAD is only 20 ppm for all the operating conditions.

Varying the injection timing had no apparent effect on the fuel

conversion efficiency for cases 3 and 4, but for cases 1 and 2 slight increases in fuel consumption were observed with the -70 CAD ATDC injection timing. This might be explained by that for a low engine speed and a too early injection, before -70 CAD, it does not seem to be possible to sustain a premixed flame, the flame will probably quench and most of the stratification fuel will mix with the homogenous fuel and be combusted by the HCCI combustion. For later injections, premixed combustion occurs and thermal efficiency is slightly reduced due to heat losses, but after -70 CAD the CA50 timing is phased closer to TDC and the efficiency is restored.

Generally, the HC emissions follow the trend noted above, i.e. early combustion leads to more complete combustion, probably due to less quenching.

3.2. Hydrogen

Lower amounts of energy were supplied in the stratified charge when hydrogen was used as the stratification fuel, since low amounts of hydrogen would be used if it was produced on-board the vehicle (by fuel reformation). The effect of varying the amount of hydrogen used as fuel for the stratified charge can be seen in Figure 5. The operating conditions for the study can be found in Table 4.

Table 4 Operating conditions used for the study of different amounts of stratification with Hydrogen as stratification fuel.

Injection timing	-50 CAD
IMEP	Case 1 4.1 bar Case 2-3 4.2 bar
λ	Case 1 2.4 Case 2-3 2.1
Intake air pressure	Case 1 85 kPa Case 2-3 96 kPa
Engine speed	Case 1 1000 rpm Case 2-3 1200 rpm
Stratification amount	0 420 560 700 J/s
Main Fuel	Case 1-2 4200 J/s Case 3-4 5000 J/s
Dwell time (EOI-IGN)	Case 1,3 2 CAD Case 2 5 CAD
Intake air temperature	Case 1 80˚C Case 2-3 96˚C

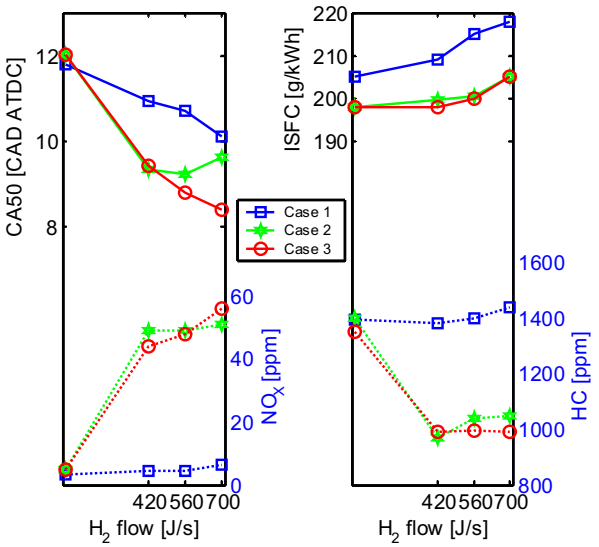

Fig. 5 CA50, ISFC and emissions obtained using different amounts of hydrogen as stratification fuel. Dotted lines indicate emissions.

In Figure 5 it can be seen that increasing the amount of hydrogen supplied as stratification fuel advances the phasing of the CA50 timing. However for the operating conditions in cases 2 and 3, the use of PRF as stratification fuel had a greater impact on CA50 timing for an equal NO_X increase, compare Figure 2. If hydrogen's very wide flammability limits are not used to combust a very lean mixture in SI mode, then the NO_X penalty for combining SI combustion with HCCI combustion will be of the same order as for the PRF fuel. If the hydrogen mixture on the other hand is too lean then the available energy for controlling the auto-ignition will be too low to have a significant impact on CA50.

With hydrogen it was only possible to use very short dwell times between EOI and IGN.

In Figure 6 the effect of varying injection and ignition timing when hydrogen was used as fuel for the stratified charge can be seen. Operating conditions are given in Table 5.

Table 5 Operating conditions used for the studying the effects of varying the injection timing with hydrogen as stratification fuel.

Injection timing	-70 -65 -55 -50 CAD
IMEP	4.1 bar
λ	2.4 (overall)
Intake air pressure	85 kPa
Engine speed	1000 rpm
Stratification amount	Case 1-2 420 J/s Case 3 560 J/s
Main fuel	4200 J/s
Dwell time (EOI-IGN)	Case 1 0 CAD Case 2-3 2 CAD
Intake air temperature	80˚C

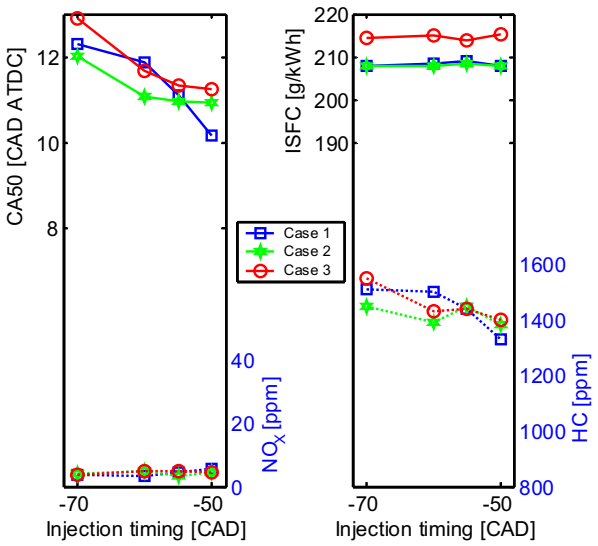

Fig. 6 CA50, ISFC and emissions obtained with different injection timings of the stratified charge using hydrogen as stratification fuel. Dotted lines correspond to emissions.

The observed trend is a slightly advanced CA50 timing when the injection timing is retarded. The flame temperature of the stratified hydrogen charge is kept low due to the leanness of the mixture, as can be seen from the very low NO_X increases. The CA50 timing can be advanced by about 2 CAD without any detectable NO_X penalty. The flame front is able to propagate through this lean hydrogen mixture due to hydrogen's wide flammability limits.

Injection timing has only minor (if any) effects on the fuel consumption and as when using PRF as stratification fuel the HC emissions are correlated with the CA50 timing, i.e. early combustion leads to more complete combustion.

4. CONCLUSION

A hybrid combustion concept, combining SI and HCCI combustion, was evaluated to investigate its potential for improving combustion control. The SI combustion of a stratified charge provides a means to control the HCCI combustion. It was shown that it is possible to influence and control the HCCI combustion by using SI combustion of a stratified charge.

The following conclusions can be drawn from the experiments:

(1) The CA50 timing could be advanced by up to 10 CAD with a NO_X penalty of only 20 ppm by varying the amount of stratification fuel supplied when PRF was used as stratification fuel.

(2) The CA50 timing could be advanced without any increase in fuel consumption.

(3) By optimizing the injection timing a further 4 CAD advancement of the CA50 timing could be obtained with a NOx penalty of 20 ppm.

(4) When hydrogen was used as the stratification fuel the CA50 timing could be advanced 4 CAD with the amounts of hydrogen that were tested here (equivalent to 13 % of the total supplied energy).

(5) With hydrogen it was possible to advance combustion phasing 2 CAD without any detectable NO_X penalty.

(6) A hybrid spark assisted combustion system allows the combustion phasing to be controlled from cycle to cycle (even after the inlet valve has been closed).

(7) A hybrid spark assisted combustion system can extend the useable HCCI load range to lower loads.

When hydrogen's wide flammability limits are exploited and the flame temperature is kept low (with low additional NO_X emissions), the impact of the stratified charge becomes too small to compensate for the increased complexity of adding hydrogen systems to a future vehicle.

For the operating conditions used in this study PRF appears to be the most suitable fuel for the stratified charge due to the larger range of combustion phasing it allows, and the fact that no separate fuel is needed for the stratified charge.

ACKNOWLEDGEMENT

The authors would like to thank STEM, the Swedish Energy Agency, for funding this work. The following members of the technical staff at the Division of Combustion and Multiphase Flow; Allan Sognell, Rolf Berg, Ingemar Johansson and Morgan Svensson are greatlfully acknowledged for their help with the experimental setup.

REFERENCES

[1] Koopmans, L., Strömberg, E., Denbratt, I., "The Influence of PRF and Commercial Fuels with High Octane Number on the Auto-Ignition Timing of an Engine Operated in HCCI Combustion Mode with Negative Valve Overlap", SAE Technical Paper Series, SAE Paper 2004-01-1967.

[2] Heywood, J. B. , "Internal Combustion Engines Fundamentals" 1988, Singapore: McGraw-Hill Inc.

[3] Hultquist, A., Christensen, M., Johansson, B., Richter, M., Nygren, J., Hult, J., Aldén, M., "The HCCI Combustion Process in a Single Cycle – High-Speed Fuel Tracer LIF and Chemiluminescence Imaging", SAE Technical Paper Series, SAE Paper 2002-01-0424.

[4] Lü, X-C., Chen, W., Huang, Z., "A fundamental study on the control of the HCCI combustion and emissions by fuel design concept combined with controllable EGR. Part 1. The basic characteristics of HCCI combustion", Fuel, Volume 84, Issue 9, Pages 1074-1083 (June 2005).

[5] Hultquist, A., Christensen, M., Johansson, B., Franke, A., Aldén, M., "A Study of the Homogenous Charge Compression Ignition Combustion Process by Chemiluminescence Imaging", SAE Technical Paper Series, SAE Paper 1999-01-3680.

[6] Wagner, U., Anca, R., Velji, A., Spicher, U., "An Experimental Study of Homogenous Charge Compression Ignition (HCCI) with Various Compression Ratios, Intake Air Temperatures and Fuels with Port and Direct Fuel Injection", SAE Technical Paper Series, SAE Paper 2003-01-2293.

[7] Lü, X-C., Chen, W., Huang, Z., "A fundamental study on the control of the HCCI combustion and emissions by fuel design concept combined with controllable EGR. Part 2. Effect of operating conditions and EGR on HCCI combustion", Fuel, Volume 84, Issue 9, Pages 1084-1092 (June 2005).

[8] Berntsson, A., Denbratt, I., "Spark Assisted HCCI Combustion Using a Stratified Hydrogen Charge", SAE Technical Paper Series, SAE Paper 2005-24-039.

[9] Cathcart, G., Tubb, J., "Application of Air Assisted Direct Fuel Injection to Pressure Charged Gasoline Engines", SAE Technical Paper Series, SAE Paper 2002-01-0705.

DEFINITIONS, ACRONYMS, ABBREVIATIONS

HCCI: Homogenous Charge Compression Ignition.

PRF: Primary Reference Fuel.

CAD: Crank Angle Degree.

TDC: Top Dead Center.

BDC: Bottom Dead Center.

EOI: End Of Injection.

IGN: Ignition.

CA50: Crank angle when 50% of the energy is burned.

HC: Hydrocarbon.

SI: Spark Ignition.

NO_X: Nitrogen Oxides.

HR: Heat Release.

PM: Particulate Matter.

ISFC: Indicated Specific Fuel Consumption.

Paper III

HCCI Combustion Using Charge Stratification for Combustion Control

Andreas William Berntsson and Ingemar Denbratt

SAE Technical Paper

SAE TECHNICAL PAPER SERIES

2007-01-0210

HCCI Combustion Using Charge Stratification for Combustion Control

Andreas W. Berntsson and Ingemar Denbratt
Chalmers University of Technology

Reprinted From: Homogeneous Charge Compression Ignition Engines, 2007 (SP-2100)

ISBN 0-7680-1636-3

2007 World Congress
Detroit, Michigan
April 16-19, 2007

SAE International™

400 Commonwealth Drive, Warrendale, PA 15096-0001 U.S.A. Tel: (724) 776-4841 Fax: (724) 776-0790 Web: www.sae.org

All SAE papers, standards, and selected books are abstracted and indexed in the Global Mobility Database.

ISSN 0148-7191

Printed in USA

2007-01-0210

HCCI Combustion Using Charge Stratification for Combustion Control

Andreas W. Berntsson and Ingemar Denbratt
Chalmers University of Technology

ABSTRACT

This work evaluates the effect of charge stratification on combustion phasing, rate of heat release and emissions for HCCI combustion. Engine experiments in both optical and traditional single cylinder engines were carried out with PRF50 as fuel. The amount of stratification as well as injection timing of the stratified charge was varied.

It was found that a stratified charge can influence combustion phasing, increasing the stratification amount or late injection timing of the stratified charge leads to an advanced CA50 timing. The NO_X emissions follows the CA50 advancement, advanced CA50 timing leads to higher NO_X emissions. Correlation between CA50 can also be seen for HC and CO emissions when the injection timing was varied, late injection and thereby advanced CA50 timing leads to both lower HC and CO emissions. This trend can not be seen when the stratification amount was varied, increased stratification amount leads to higher CO emission and for operating condition with late CA50 timing the HC emissions also increase with increasing stratification amount. Optical studies, with high speed CCD camera, show that an increase in stratification leads to poor combustion quality near the cylinder walls, due to leaner mixtures near the cylinder walls and this results in higher HC and CO emissions.

The maximum rate of heat release depends on stratification amount - a larger amount gives a lower rate of heat release but the main heat release is advanced. Varied injection timing results in different phasing of the main heat releases.

The use of charge stratification for HCCI combustion can lead to a larger operating range, due to its effect on combustion phasing and rate of heat release, since the upper load range is partly restricted by too high rates of heat release leading to high pressure oscillations and the lower load to late combustion phasing leading to high cycle-to-cycle variations.

INTRODUCTION

Increasingly strict requirements to reduce exhaust emissions and fuel consumption are prompting the development of more advanced combustion concepts. One promising concept is Homogeneous Charge Compression Ignition, HCCI. In an HCCI engine the combustion is controlled by chemical kinetics [1], and heat is released more rapidly than in normal flame front combustion. In the ideal air standard SI cycle the combustion occurs at constant volume and this cycle is therefore the most efficient of the ideal cycles [2]. The rapid heat release of HCCI combustion and its ability to burn lean mixtures, thereby reducing pump, exhaust and cooling losses due to less throttled operation results in greatly improved efficiency compared to SI combustion [3]. HCCI combustion gives low NO_X and PM emissions [4] as a result of the lean homogenous mixture. Cycle-to-cycle variations are also minor because the combustion occurs in a distributed fashion at many places simultaneously [5].

However several challenges associated with the HCCI concept must be overcome before it can be commercially applied, notably ways must be found to control ignition timing [6], expand its limited operating range [4] and limit the rate of heat release [7]. Cylinder-to-cylinder variations can also cause problems in HCCI engines [4], since the temperature can vary between the different cylinders and the ignition delay is highly dependent on the mixture temperature [8].

Combustion phasing control is one of the crucial parameters for controlling HCCI combustion and the timing when 50 % of the energy is combusted, CA50, is a good indicator of the phasing of the combustion process [9], the ability to rapidly control combustion phasing is necessary especially during transients.

There are numerous solutions to the challenges associated with combustion control. One solution is to adjust the inlet air temperature by heating the incoming air with air heaters [10-13] or by varying the coolant temperature [14]. However, thermal control of the combustion phasing has the drawback that the thermal inertia of the associated engine parts usually limits the

transient response time. Another way to influence the charge temperature, and thus control the combustion phasing is to adjust the compression ratio. Increasing the compression ratio will increase the pressure, which will decrease the autoignition temperature and increase the charge temperature [8]. Geometrically variable compression ratio have been used to control HCCI combustion by several authors [6, 15-18], but it is difficult to find a mechanism that is fast enough to cope with real vehicle transients.

Further factors that play important roles in the timing of autoignition are the properties of the fuel, since the ignition delay of different fuels at given pressures and temperatures varies dramatically. For this reason, several authors [17, 19] have used mixtures of two fuels with contrasting octane numbers and ignition temperatures (iso-octane and n-heptane or ethanol and n-heptane) that have appropriate ignition temperatures to allow correct phasing of the combustion.

The charge homogeneity has been found to have modest effect on the combustion process [21]. However, Aroonisopon et al [22] stabilized the combustion at the lower load limit for HCCI combustion by using charge stratification and Sjöberg et al [23] used stratification to achieve staged combustion, which smoothed the rate of heat release and thereby enabled the load to be increased. In a previous study, [24], SI combustion of a stratified charge in combination with HCCI combustion was investigated. Chemiluminescence images have shown that it is possible to create a hybrid combustion mode, in which initial spark-ignited flame-front combustion is followed by HCCI combustion. The SI combustion provides a potential way to control the HCCI combustion as shown in [25]. The study presented here explores the effect of charge stratification on HCCI combustion of a mixture of n-heptane and iso-octane. The possibilities for improving combustion phasing control by using charge stratification, and it's effects on NO_X and HC emissions and the rate of heat release, are evaluated.

EXPERIMENTAL APPARATUS

Experiments were carried out in a single-cylinder engine with and without optical access. Its displaced volume corresponds to that of a passenger car engine. For all experiments a modified cylinder head was used, in which one of the exhaust valves had been removed and replaced by a sparkplug. The engine parameters can be seen in table 1 and a schematic sketch of the layout can be seen in figure 3.

Table 1 Engine parameters

Bore	83 mm
Stroke	90 mm
Swept volume	487 cm^3
Compression ratio	10.6:1 conventional
	8:1 optical
Conrod length	139.5 mm
IVO	10 CAD BTDC
IVC	40 CAD ABDC
EVO	40 CAD BBDC
EVC	10 CAD ATDC

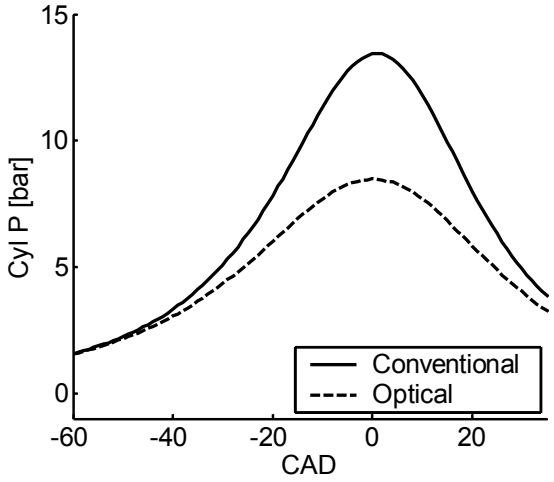

Figure 1 Motored pressure traces for the optical engine and the conventional engines.

OPTICAL ENGINE

A single cylinder research engine with optical access was used for the optical study. This engine has an extended piston housing a mirror that provides, in conjunction with a quartz window in the piston crown, optical access to most of the combustion chamber from below. The volume covered can be seen in Figure 2. The optical piston had a flat piston crown which, in combination with a large included valve angle and large crevices between the piston and the liner, unfortunately limited the compression ratio. The optical engine is restricted to low engine speeds and since comparisons between optical engine and metallic engine should be possible all measurements were made at low engine speeds. The main parameters for the engine can be seen in Table 1.

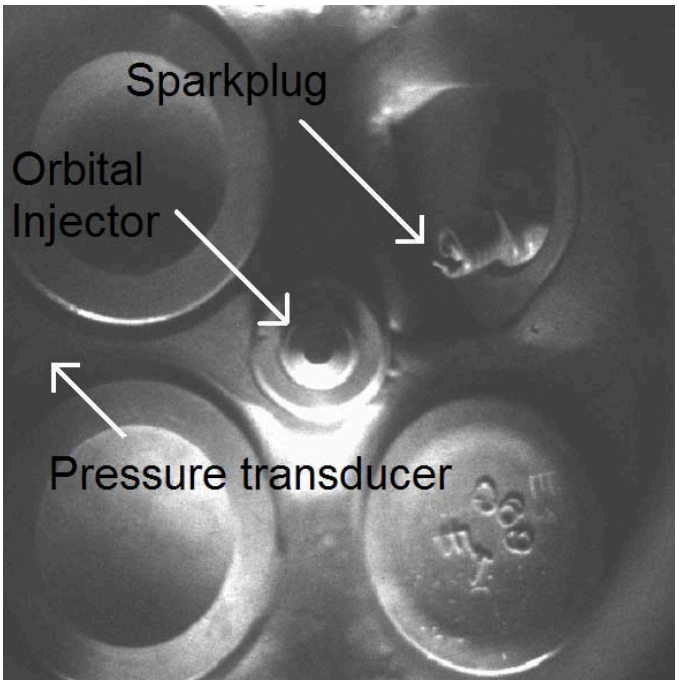

Figure 2 *The optically accessible combustion chamber. The diameter of the optically covered section is 73 mm. The Orbital fuel injector can be seen in the centre.*

CAMERA

A Phantom high speed CCD camera was used to capture the natural luminosity of the combustion by direct imaging. To control the timing of the camera an AVL 4210 timing unit was used. The images presented in this paper were obtained from single combustion cycles, and are shown in consequent order. This enables the combustion progress to be followed without any discrepancy caused by averaging a large number of cycles. Both the gain and exposure time of 160 µs were kept constant in this study. The resolution of the camera was 512 by 512 pixels, which is equivalent (for this setup) to 7 pixels per millimeter. Each frame corresponds to one CAD.

FUEL INJECTION

Port injection was used for the main fuel supply to create a homogenous air fuel mixture. In order to obtain a stratified charge an Orbital injector was used, which is designed as an air-assisted, spray-guided direct injection device [26]. It uses pressurised air to inject and break up the fuel spray. In this study the Orbital injector was used only to create a stratified charge. The fuel used, for both the stratified charge and the homogenous mixture, was a mixture of n-heptane and iso-octane with 50 $\%_{vol}$ of each component, PRF50.

INLET HEATER

Since some of the investigations were performed in an optical engine with high cooling losses and low compression ratio the intake air was heated to extend the operational range to light loads. The intake air temperature was measured directly at the intake valve using a thermocouple. By varying the inlet air temperature, for measurements in both the metallic and optical engines, it was possible to phase the combustion so that a reference condition would have the same combustion phasing.

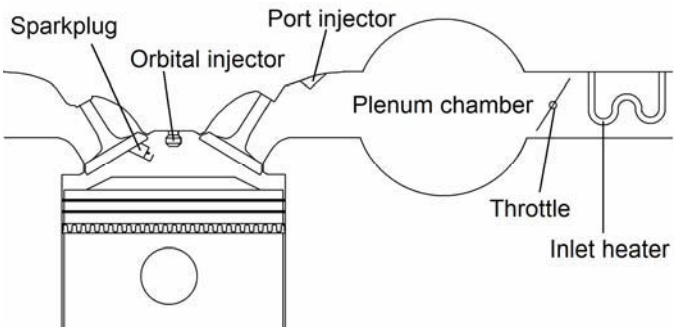

Figure 3 Schematic sketch of the engine layout.

RESULTS AND DISCUSSION

The results are presented and discussed in two main sections, one dealing with data obtained when the stratification amount was varied and one covering data obtained when the injection timing of the stratified charge was varied. For the study in which the stratification amount was varied, both optical and traditional measurements were carried out.

VARIATION OF STRATIFICATION FUEL AMOUNT

The effects of varying the amount of stratification fuel can be seen in figure 4. Operating conditions used in these experiments are presented in table 2. Three different amounts of stratification fuel were used for the study in the conventional engine and five different amounts for the optical engine. The total fuelling (stratification + main) was kept constant.

Table 2 Operating condition used for the study in which the stratification fuel amount was varied.

Engine speed	1000 rpm
IMEP	4.1 Bar
Injection timing stratification(EOI)	-70,-60,-50 CAD conventional
	-50 CAD optical
Inlet air temperature	75 °C conventional
	175 °C optical
Total fuel amount	87 mg/s
Intake pressure	95 kPa
Stratification amount	0 – 20 mg/s
λ	2.75 conventional
	2.5 optical

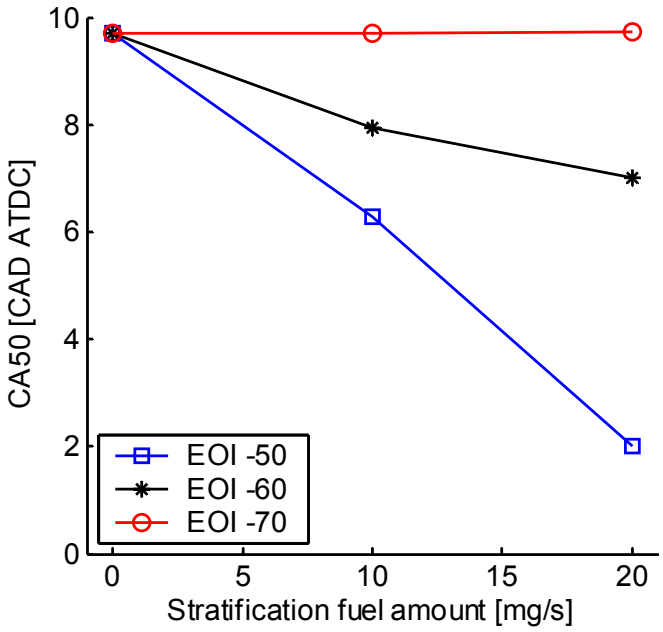

Figure 4 CA50 timing obtained with different stratification fuel amounts and three different injection timings.

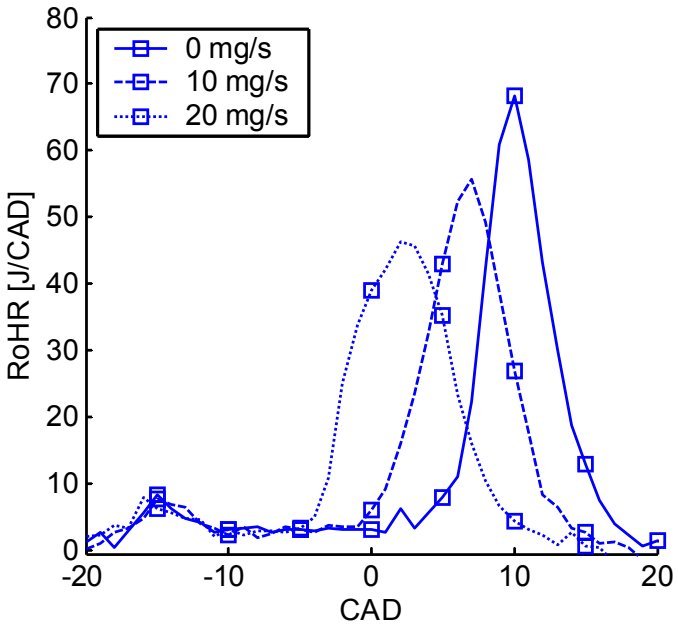

Figure 5 Rate of Heat Release traces for three different amounts of stratification with an injection timing (EOI) of the stratified charge of EOI -50 CAD.

Two different trends were observed when then stratification amount was varied. When the stratification fuel is injected early, EOI -70 CAD, the timing at which 50 % of the energy was combusted, CA50, was unaffected by any variation of stratification fuel amount. The combustion phasing remained at the same timing as for the HCCI combustion, when no fuel stratification was used. However when the injection timing of the stratified charge was retarded, EOI -60 or EOI -50, a trend of advanced CA50 timing can be seen. The latest injection timing led to the most significant change in combustion phasing. The scope for combustion phasing is around 2.5 CAD for the case with EOI -60 and around for the case with 8 CAD for EOI -50. When the injection is retarded the stratification is maintained and becomes sufficiently rich to display such a low ignition delay that it can lead to a staged combustion that starts in this richer zone, and thus affects the phasing of the combustion.

Figure 5 shows rate of heat release traces for the different stratification amounts with injection timing (EOI) of - 50 CAD. The solid line corresponds to no stratification fuel flow, i.e. pure HCCI combustion with the highest rate of heat release. The maximum rate of heat release decreases when the amount stratification is increased and the duration of the combustion is increased due to the staged combustion (caused by the local variation of equivalence ratio) prolonging the heat release. The main heat release is also advanced with increasing stratification. The phasing of the low temperature reactions is virtually unaffected and the rate of heat release trace shows no significant changes due to charge stratification prior to the start of combustion.

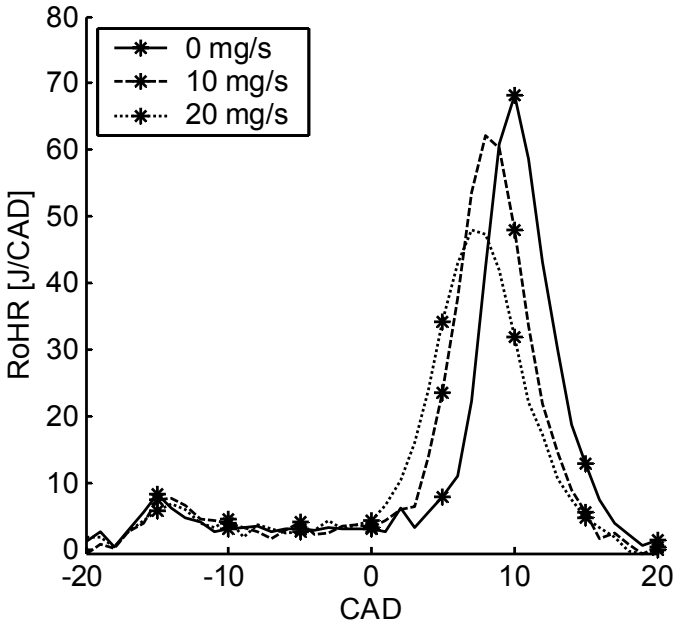

Figure 6 Rate of Heat Release traces for three different amounts of stratification with an injection timing (EOI) of the stratified charge of -60 CAD.

The same trend, i.e. the maximum rate of heat release declined when the stratification was increased, was observed with the injection timing (EOI) of -60 CAD (figure 6). However the effect of stratification on the phasing of the main heat release was significantly weaker than with the EOI of -50 CAD (figure 5). The

combustion duration for the main heat release was only slightly increased with increased amounts of stratification in this case. The slightly more advanced injection with EOI at – 60 CAD compared to - 50 CAD gives more time for the stratified charge to mix with the surroundings, resulting in less rich stratification. This leads to a longer ignition delay for the stratified charge compared to retarded timing and the stratified charge is ignited later in the cycle with less effect on the main charge, in terms of combustion phasing. However some of the effect on the maximum rate of heat release will be present since the combustion is somewhat staged and the combustion is only partly advanced.

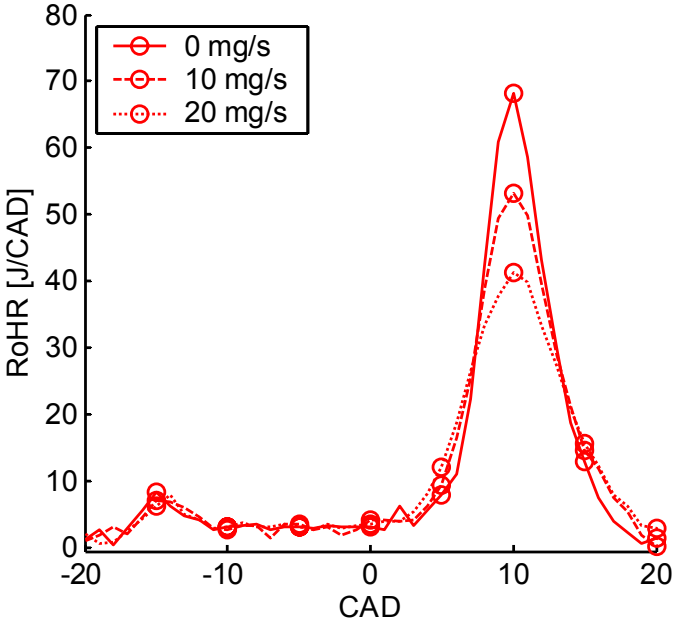

Figure 7 Rate of Heat Release traces for three different amounts of stratification with an injection timing (EOI) of the stratified charge of -70 CAD.

Figure 7 presents the rate of heat traces obtained with the EOI for the stratified charge at – 70 CAD can be seen. The correlation between the maximum heat release rate and charge stratification was also observed with this timing. However the phasing of the main heat release remained constant and the heat release peaked at the same CAD position with each amount of stratification. There was a slight increase in the duration of the main heat release when the charge was stratified, but its duration was not increased to the same extent when the stratification fuel flow was increased from 10 to 20 mg/s. When the stratification amount was increased to 20 mg/s the combustion quality appeared to deteriorate, i.e. the accumulated heat release declined, indicating lower combustion efficiency. This was probably due to quenching near the cylinder wall, due in turn to the mixture being too lean at the periphery caused by the charge stratification in combination with the late phasing.

This tendency for maximum rates of heat release to decline when the charge was stratified, as shown in figures 5-7, has also been reported in other studies [23].

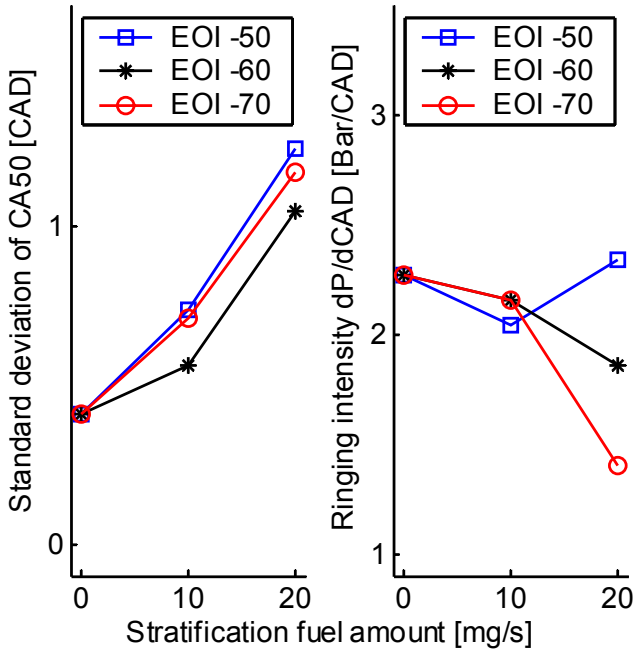

Figure 8 Standard deviations of CA50 and ringing intensity for different injection timings and stratification amounts.

The introduction of charge stratification leads to a larger cycle-to-cycle variations under the operating conditions used in this study, see figure 8. When no stratification was used the operating conditions led to very stable HCCI combustion with a standard deviation of 0.5 CAD of the CA50 timing. Increasing the stratification to a stratification fuel amount of 10 mg/s leads to a small increase in standard deviation and when it was increased further, to 20 mg/s, the standard deviation was approximately doubled compared to pure HCCI combustion. In [22] it was reported that the use of charge stratification led to more stable combustion, but the cited result was achieved at the low load limit for HCCI combustion where pure HCCI combustion is very unstable and then the charge stratification led to more stable combustion.

The ringing intensity of the cylinder pressure can be seen to the right in figure 8. The ringing intensity is an effect of the rate of heat release in combination with combustion phasing. An increase in ringing intensity was observed with the combination of 20 mg/s of stratified fuel and EOI of -50 CAD (due to the more advanced combustion phasing, which normally leads to a higher ringing intensity than later combustion), but not in any of the other tested cases.

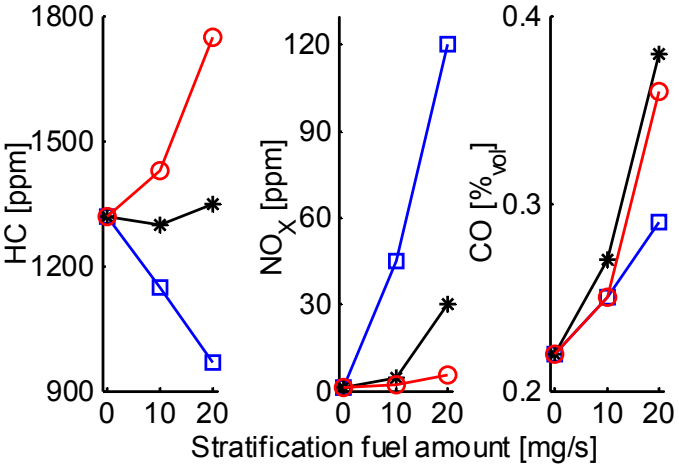

Figure 9 Emissions associated with different stratification fuel amounts. Squares correspond to EOI -50, circles to EOI -60 and stars to EOI -70.

In figure 9 the effect of stratification on emissions can be seen. Stratification leads to increasing HC emissions if the combustion is not advanced as a result of the stratification, as in the case when EOI was – 50 CAD. NO_X and CO emissions also increased when the stratification amount was increased, but their rates of increase differed dramatically. When the injection timing was retarded the increase in NO_X emissions caused by charge stratification is dramatic, due to the higher adiabatic reaction temperature. An advanced combustion phasing in it self will also cause an increase in NO_X emission as well as the increase in charge stratification. Stratification leads to reductions in combustion efficiency, especially with early injection. The increases in CO and HC emissions are probably caused by near-wall quenching. With increasing stratification the charge becomes leaner near the cylinder wall, which leads to increased quenching. The charge stratification also contributes to a more stratified temperature; the temperature is lower at the periphery and this will further enhance the negative effect of the leanness of the mixture near the walls.

OPTICAL RESULTS

The effects of varying the amount of fuel stratification were also studied in an optical engine, in which experiments with the operating conditions with an EOI of - 50 CAD were repeated. However, since the optical engine had lower compression ratio and higher heat losses due to the optical access some parameters were not completely identical, see tables 1 and 2 and figure 1. These drawbacks were compensated for by using a higher inlet air temperature and a richer mixture, and the timing of the combustion was adjusted so the CA50 timing for both the optical and conventional engines coincided at a stratified fuel injection rate of 10 mg/s.

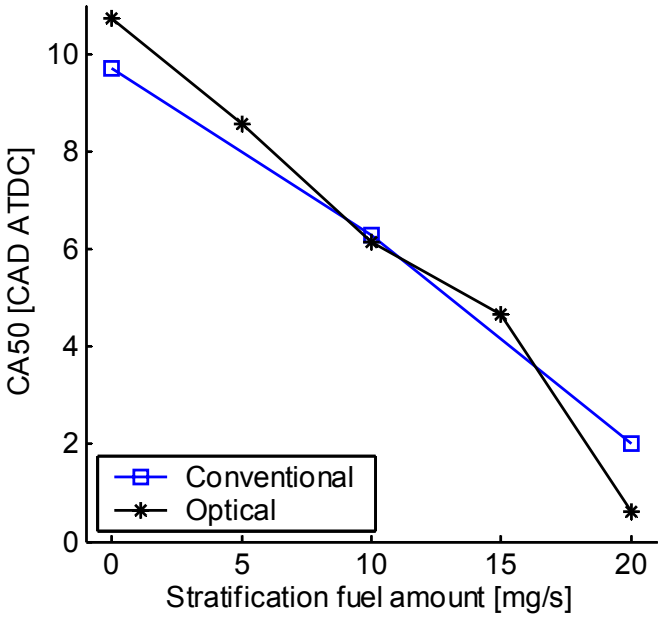

Figure 10 CA50 timing for different stratification fuel amounts for both the optical and the traditional engine with an injection timing (EOI) of the stratified charge of - 50 CAD.

In figure 10 the effect of charge stratification on CA50 timing can be seen for both the optical and conventional engines. In both engines CA50 timing clearly advanced when the stratification amount was increased and the behavior captured during the optical measurements is believed to mirror behavior in the traditional engine.

An overview of the photographs taken between – 3 to 22 CAD by direct imaging can be seen in figure 14. Each frame corresponds to one CAD, the first and fourth rows shows events with no stratification or HCCI combustion, the second and fifth events with 10 mg/s of stratification and the third and sixth events with 20 mg/s. Distinct differences in the point of start of ignition can be observed, the photographs for the case with 20 mg/s of stratification show that visible light (reactions) started 12 CAD prior to the HCCI case. In the HCCI case, the combustion chamber becomes filled with reaction zones covering the entire visible area within approximately 4 CAD. The ignition sequence of the HCCI combustion can be seen in figure 11. The first visible reaction corresponds to the initialization of the main heat release. Similar behavior was seen when the natural chemiluminescence of the OH radical was studied in HCCI combustion [24], i.e. signals were detected only during the main heat release.

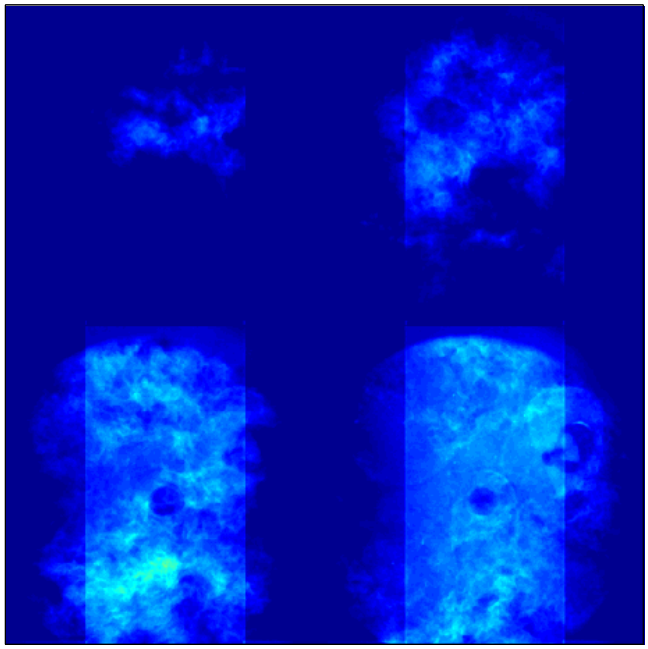

Figure 11 Ignition sequence of the HCCI combustion with no stratification.

The charge is initially ignited near the centre of the cylinder since the cold cylinder wall introduce a temperature gradient with lower temperature near the wall. The squish zones on the outer right and left sides have the largest surface to volume ratios, so the mixture is cooler and the ignition delay is longer in these zones.

The images of the combustion sequence when 10 mg/s of stratification was used, figure 12, show that the ignition process was longer than in pure HCCI combustion. The combustion starts in a smaller volume in the richer regions of the stratified charge and expands less rapidly. The ignition sequence from the points when there is no signal to the point at which there are signals from the entire chamber is approximately 3 – 4 CAD longer compared to HCCI combustion, although the combustion begins earlier and develops in a more self-stabilizing environment. Very small regions with high signal strength can be observed approximately 4 CAD after the first visual signs of reaction. These small regions might be due to unvaporized droplets. Since these small, intense regions emerged after the first signs of reaction and their lifespan was greater than the exposure time, and the initial reaction displays similar luminosity strength over a great area (compared to any eventual droplet), it is believed that the combustion is initiated in a premixed region.

The ignition sequence with stratification amount of 20 mg/s was both prolonged and dramatically phased, see figures 13 and 14. The charge stratification for this case was strong and the reaction zone was also stratified, the reaction was not evenly distributed in the combustion chamber. The high NO_X emissions associated with this amount of charge stratification are due to the large variations in equivalence ratio which led to large variations in local reaction temperatures.

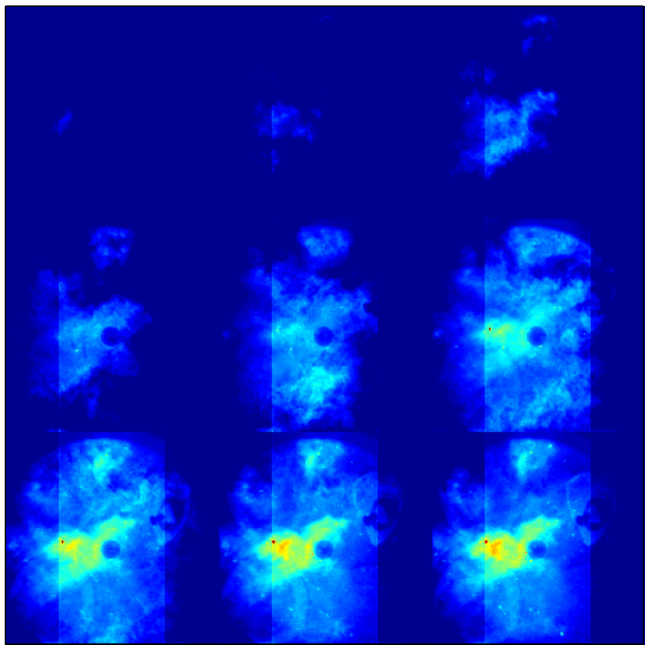

Figure 12 Ignition sequence when 10 mg/s of stratification was used.

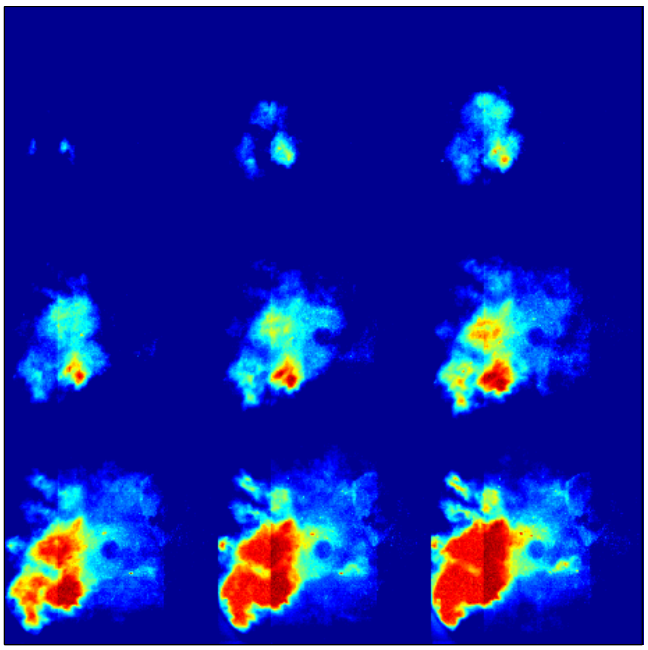

Figure 13 Ignition sequence when 20 mg/s of stratification was used.

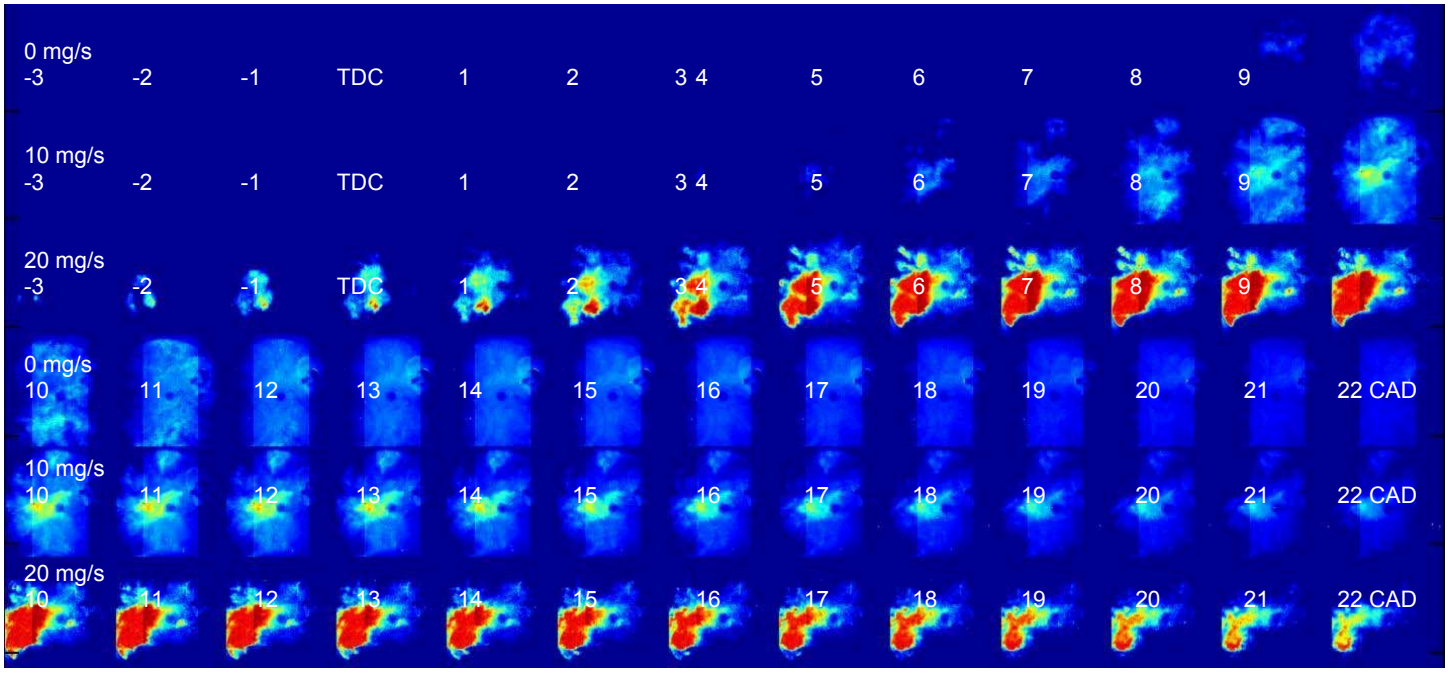

Figure 14 Images of the combustion with 0, 10 and 20 mg/s of stratification.

In figure 14 it can be seen that natural luminosity from the combustion is generally weaker near the cylinder walls when charge stratification is introduced, which will lead to increased quenching near the walls, as previously discussed. However the advanced phasing leads to the HC emissions is reduced and only the CO is increased due to the leaner charge near the wall.

The location of the initial reaction, i.e. the stratified regions, showed the strongest signal and continued to give the strongest signal from ignition throughout the complete main heat release. The temperature remained stratified throughout the combustion under the operating conditions used here, especially in the case with the highest stratification.

VARIATION OF INJECTION TIMING

The effects on combustion phasing of varying the injection timing (EOI), can be seen in figure 15. Operating conditions used in these experiments are presented in table 3. Events at three different engine speeds with different loads were studied, only the injection timing was varied for each speed. The amount of stratification was kept constant for each engine speed.

Table 3 Operating conditions used for the injection timing study.

Engine speed	750, 1000 and 1250 rpm
IMEP	3.2, 3.6 and 4.2 Bar
Injection timing (EOI)	-90, to -50 CAD conventional
Inlet air temperature	93, 88 and 80°C
Total fuel amount	52, 81 and 105 mg/s
Stratification amount	10, 14 and 15 mg/s
λ	3.1, 3.1 and 3
Intake pressure	88, 95 and 98 kPa

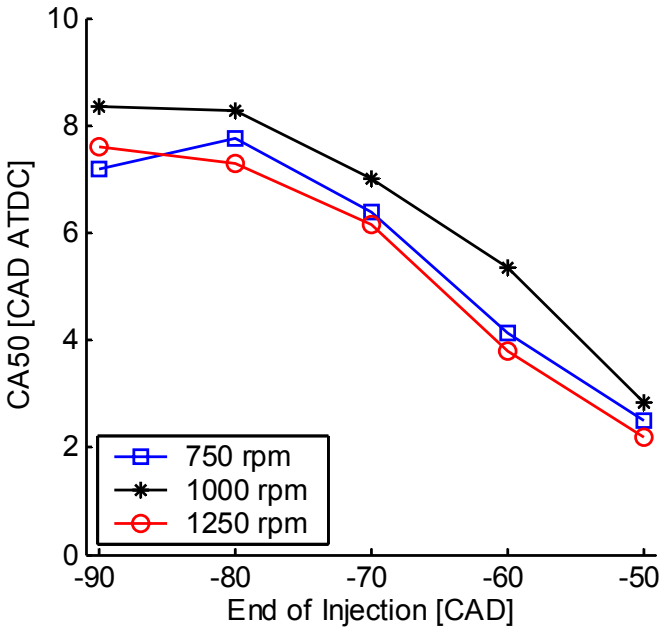

Figure 15 CA50 timing for different injection timings.

Retarding the injection timing led to advanced combustion phasing for all three engine speeds studied here, see figure 15. The early injection timing leads to the stratified charge having more time to mix with the surroundings and to distribute throughout a larger volume. This leads to the difference in equivalence ratio between the stratified charge and the surroundings is being smaller with the late injection timings. Thus, the ignition delay for the stratified charge is more similar to that of the surroundings, and the stratified charge ignites too late to influence the main combustion.

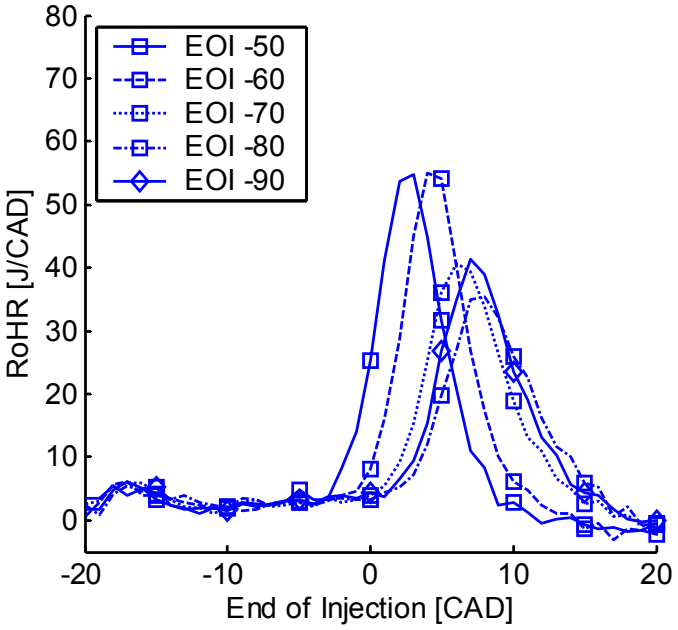

Figure 16 Rate of Heat Release traces obtained with an engine speed of 750 rpm and five different injection timings.

The rate of heat release traces in figure 16 show that the maximum heat release rate is increased when the injection timing is retarded. This is because the CA50 timing is advanced when the injection is retarded, promoting faster reactions due to the higher temperatures and pressures. The low temperature chemistry does not show any significant correlations with variations in the injection timing of the stratified charge.

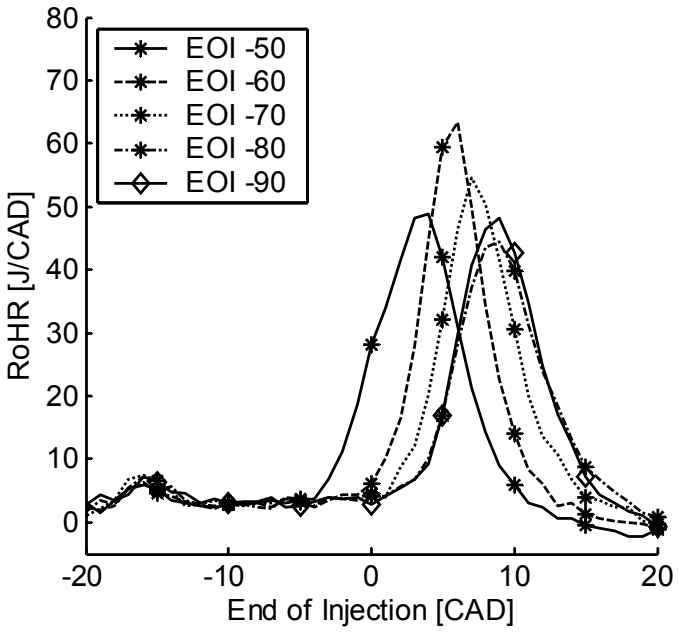

Figure 17 Rate of Heat Release traces obtained with an engine speed of 1000 rpm and five different injection timings.

For the case with an engine speed of 1000 rpm, figure 17, the trends were somewhat different from those observed with engine speeds of 750 and 1250 rpm (figures 16 and 18, respectively). The maximum rate of heat release stagnated at an injection timing of EOI - 60 CAD and was reduced when the EOI was - 50 CAD. The increases in the maximum rate of heat release were due to the advanced timing, leading to combustion in a more self stabilizing environment, and the initial phase of the main heat release showed a steep gradient in the rate of heat release. When the EOI is – 50 CAD the combustion becomes prolonged since the stratified charge has less time to mix with the surroundings, and the ignition delay becomes short enough in the richer regions to prolong the combustion, resulting in a less steep gradient of the rate of heat release of the main heat release and the maximum rate of heat release is thus reduced. This trend was not seen for the case with an engine speed of 1250 rpm, figure 18, where the shapes of the rate of heat release traces were similar when the injection timing was varied. Only minor variations associated with variations in the injection timing, except in the phasing of the main heat release of the combustion, were observed. The stratified charge in this case does not produce a prolonged combustion that increases the combustion duration or, therefore, reduce the maximum heat release rate, it only contributes as an initial ignition point that can influence the phasing of the combustion. If the amount of stratification fuel was increased then staged combustion would probably have been possible.

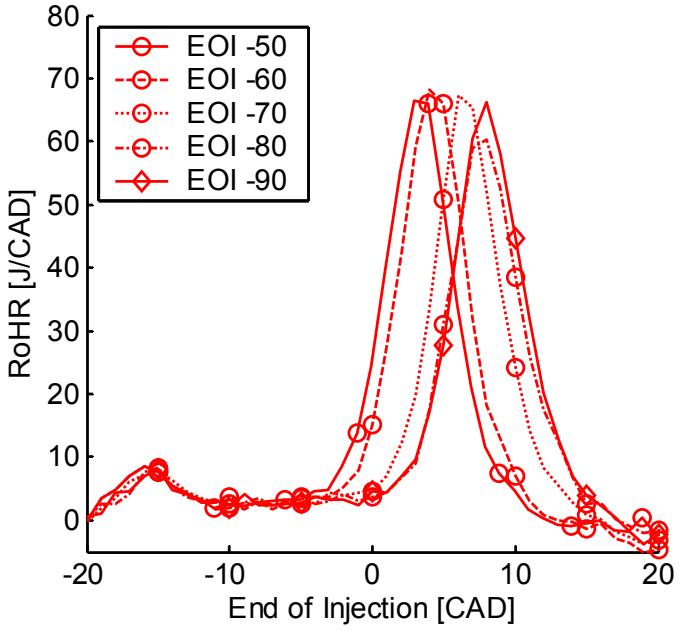

Figure 18 Rate of Heat Release traces obtained with an engine speed of 1250 rpm and five different injection timings.

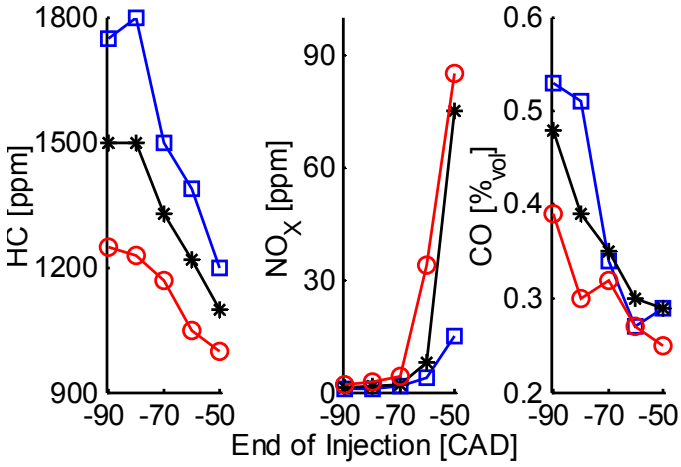

Figure 19 Emissions associated with different injection timings. Squares corresponds to 750 rpm and 3.2 bar IMEP, circles to 1000 rpm and 3.6 bar IMEP and stars to 1250 rpm and 4.2 bar IMEP.

The emissions for the three cases with varying injection timing can be seen in figure 19. The trend for NO_X emissions to increase with advanced combustion phasing was also seen when the injection timing was varied. Variations in injection timing had essentially the same effect on combustion phasing in all three cases, see figure 15. However there were distinct differences in the amounts of NO_X emissions. The operating conditions with high engine speed and load resulted in higher NO_X emissions. The HC emissions followed the CA50 phasing, i.e. advanced combustion led to lower emissions since there was more time for oxidation and the combustion occurred at higher pressure and temperature. The CO emissions showed similar trends. The load and engine speed also influence the emissions. Higher engine speeds gives less time for heat losses and less blow-by, which increase the compression temperature, this leads to an increased HC and CO oxidation.

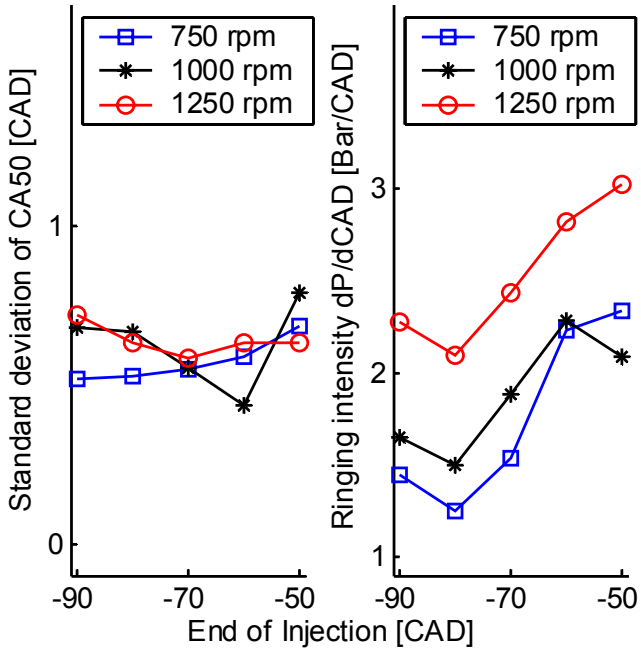

Figure 20 Standard deviations of CA50 and ringing intensity for different engine speeds and injection timings.

Cycle-to-cycle variations in combustion phasing did not appear to be affected by changes in the injection timing of the stratified charge, except for the case with an engine speed of 1000 rpm, where the standard deviation of the CA50 timing slightly decreased as the EOI was changed from -90 to -60 CAD, then increased as it was changed further to – 50 CAD see figure 20. The slight decreasing trend is due to the advancement of the combustion, which makes the environment more self-stabilizing while the sharp increase from -60 to -50 CAD is believed to be a result of the combustion becoming staged and the main heat release being influenced by this more unstable initial ignition.

CONCLUSIONS

An experimental study of the effect of charge stratification on HCCI combustion was performed to investigate its potential for improving combustion control. Controlling the charge stratification provides a means to control HCCI combustion. The result show that it is possible to influence and control the HCCI combustion by using charge stratification.

The following conclusions can be drawn from the experiments:

- The CA50 timing could be advanced by 4 CAD with a NO_X penalty of 25 ppm by varying the amount of stratification fuel amount, and by up to 8 CAD with a penalty of 120 ppm.
- By varying the injection timing up to 6 CAD advancement of the CA50 timing could be obtained with a NO_X penalty of 20 ppm.
- Charge stratification leads to lower combustion efficiency, due to the mixture being leaner near the cylinder wall and temperature stratification with higher temperature in the centre of the combustion chamber. This leads to increases in the HC and CO emissions, the phasing capabilities can however cope with the increased HC emissions for some operating conditions.
- The NO_X emissions must be closely monitored since they can rise rapidly if the stratified charge leads to local hot regions.
- The maximum rate of heat release could be lowered by staged combustion by varying the stratification fuel amount. Up to 35 % reductions were achieved for the operating condition studied here.
- The rate of heat release of the main heat release is smoother when the stratification amount is increased.
- Charge stratification results in staged combustion, which leads to lower ringing intensity unless the combustion phasing is strongly advanced.
- Direct imaging of the combustion shows that the initial sequence of the main heat release is staged and prolonged with stratification. In HCCI operation the ignition sequence of the main heat release occurs over 4 CAD from the point at which there is no visible reaction until reactions are taking place throughout the combustion chamber, while this process takes an additional 4 CAD with stratification.
- The ignition sequence of the main heat release is initiated in a premixed rich zone of the stratified charge.
- Varying the injection timing leads to different changes in the rate of heat release under different operating conditions, but the phasing of the combustion advances with retarded injection timing. With advanced injection timing the charge stratification decreases, accompanied by smaller difference in the ignition delay between the stratified charge and the surroundings, and the stratified charge is ignited late enough to only have a small effect on combustion phasing.
- When charge stratification is applied in stable HCCI operating conditions, the combustion becomes more unstable, the reason for this is the sensitivity of the small amounts injected by the direct injector.
- The positive features of charge stratification (i.e. reduced maximum rates of heat release and its phasing capabilities) may provide scope to increase the HCCI operating range.
- The equipment required for creating a stratified charge that could be used to control HCCI may become a standard feature of future direct injected vehicles and software modifications may be the only changes needed.
- Soot problems may be associated with the use of a stratified charge for controlling HCCI, but this was not studied in this investigation.

ACKNOWLEDGMENTS

The authors wish to acknowledge STEM, Swedish Energy Agency, for funding this work.

REFERENCES

1. Koopmans, L., Strömberg, E., Denbratt, I., “The Influence of PRF and Commercial Fuels with High Octane Number on the Auto-Ignition Timing of an Engine Operated in HCCI Combustion Mode with Negative Valve Overlap”, SAE Technical Paper Series, SAE Paper 2004-01-1967.
2. Heywood, J. B. , “Internal Combustion Engines Fundamentals” 1988, Singapore: McGraw-Hill Inc.
3. Hultquist, A., Christensen, M., Johansson, B., Ricther, M., Nygren, J., Hult, J., Aldén, M., “The HCCI Combustion Process in a Single Cycle – High-Speed Fuel Tracer LIF and Chemiluminescence Imaging”, SAE Technical Paper Series, SAE Paper 2002-01-0424.
4. Lü, X-C., Chen, W., Huang, Z., “A fundamental study on the control of the HCCI combustion and emissions by fuel design concept combined with controllable EGR. Part 1. The basic characteristics of HCCI combustion”, Fuel, Volume 84, Issue 9, Pages 1074-1083 (June 2005).
5. Hultquist, A., Christensen, M., Johansson, B., Franke, A., Aldén, M., “A Study of the Homogenous Charge Compression Ignition Combustion Process by Chemiluminescence Imaging”, SAE Technical Paper Series, SAE Paper 1999-01-3680.
6. Wagner, U., Anca, R., Velji, A., Spicher, U., “An Experimental Study of Homogenous Charge Compression Ignition (HCCI) with Various Compression Ratios, Intake Air Temperatures and Fuels with Port and Direct Fuel Injection”, SAE Technical Paper Series, SAE Paper 2003-01-2293.
7. Lü, X-C., Chen, W., Huang, Z., “A fundamental study on the control of the HCCI combustion and emissions by fuel design concept combined with controllable EGR. Part 2. Effect of operating conditions and EGR on HCCI combustion”, Fuel, Volume 84, Issue 9, Pages 1084-1092 (June 2005).
8. Glassman, I. , “Combustion” 1996, third edition, United States of America: Academic Press Ltd.
9. Olsson, J., Tunestål, P., Johansson, B., “Closed-loop control of an HCCI engine”, SAE Technical Paper Series, SAE Paper 2001-01-1031.

10. Marriott, C. D, Kong, S-C., Reitz, R. B., “Investigation of Hydrocarbon Emission from a Direct Injection-Gasoline Premixed Charge Compression Ignited Engine”, SAE Technical Paper Series, SAE Paper 2002-01-0416.
11. Flowers, D., Aceves, S. M., Martinez-Frias, J., Smith, R., Au, M., Girard, J., Dibble, R., “Operation of a Four-Cylinder 1.9L Propane Fueled Homogenous Charge Compression Ignition Engine: Basic Operating Characteristics and Cylinder-to-Cylinder Effects”, SAE Technical Paper Series, SAE Paper 2001-01-1895.
12. Fiveland, S. B., Agama, R., Christensen, M., Johansson, B., Hiltner, J., Maus, F., Assanis, D. N., “Experimental and Simulated Results Detailing the Sensitivity of Natural Gas HCCI Engines to Fuel Composition”, SAE Technical Paper Series, SAE Paper 2001-01-3609.
13. Martinez-Frias, J., Aceves, S. M., Flowers, D., Smith, R. J., Dibble, R., “Thermal Charge Conditioning for Optimal HCCI Engine Operation”, Journal of Energy Resources Technology, Volume 124, Pages 67-75 (March 2002).
14. Milovanovic, N., Blundell, D., Pearson, R., Turner, J., Chen, R., “Enlarging the Operational Range of a Gasoline HCCI Engine By Controlling the Coolant Temperature”, SAE Technical Paper Series, SAE Paper 2005-01-0157.
15. Haraldsson, G., Tunestål, P., Johansson, B., Hyvönen, J., “HCCI Combustion Phasing in a Multi Cylinder Engine Using Variable Compression Ratio”, SAE Technical Paper Series, SAE Paper 2002-01-2858.
16. Hyvönen, J., Haraldsson, Johansson, B., “Operating range in a Multi Cylinder HCCI engine using Variable Compression Ratio”, JSAE Technical Paper Series,JSAE Paper 20030178.
17. Haraldsson, G., Tunestål, P., Johansson, “Transient Control of a Multi Cylinder HCCI Engine During a Drive Cycle”, SAE Technical Paper Series, SAE Paper 2005-01-0153.
18. Christensen, M., Hultqvist, A., Johansson, B., “Demonstrating the Multi Fuel Capability of a Homogenous Charge Compression Ignition Engine with Variable Compression Ratio”, SAE Technical Paper Series, SAE Paper 1999-01-3679.
19. Strandh, P., Bengtsson, J., Johansson, R., Tunestål, P., Johansson, B., “Cycle-to-Cycle Control of a Dual-Fuel HCCI Engine”, SAE Technical Paper Series, SAE Paper 2004-01-0941.
20. Olsson, J-O., Tunestål, P., Haraldsson, G., Johansson, B, “A Turbo Charged Dual Fuel HCCI Engine”, SAE Technical Paper Series, SAE Paper 2001-01-1896.
21. Richter, M., Engström, J., Franke, A., Aldén, M., Hultquist, A., Johansson, B, “The Influence of Charge Inhomogeneity on the HCCI Combustion Process”, SAE Technical Paper Series, SAE Paper 2000-01-2868.
22. Aroonrisopon, T., Werner, P., Waldman, J. O., Sohm, V., Foster, D. E., Morikawa, T, Iida, M., “Expanding the HCCI Operation With the Charge Stratification”, SAE Technical Paper Series, SAE Paper 2004-01-1756.
23. Sjöberg, M., Dec, J. E., “Smoothing HCCI Heat-Release Rates Using Partial Fuel Stratification with Two-Stage Ignition Fuels”, SAE Technical Paper Series, SAE Paper 2006-01-0629.
24. Berntsson, A., Denbratt, I., “Spark Assisted HCCI Combustion Using a Stratified Hydrogen Charge”, SAE Technical Paper Series, SAE Paper 2005-24-039.
25. Berntsson, A., Denbratt, I., “HCCI Combustion Using a Spark Ignited Stratified Charge”, JSAE Technical Paper Series, JSAE Paper 20065424.
26. Cathcart, G., Tubb, J., “Application of Air Assisted Direct Fuel Injection to Pressure Charged Gasoline Engines”, SAE Technical Paper Series, SAE Paper 2002-01-0705.

CONTACT

Corresponding author:
Andreas Berntsson
Chalmers University of Technology
Department of Applied Mechanics
Division of Combustion and Multiphase Flow
Hörsalsvägen 7B
SE-412 96 Göteborg
Sweden
Email: andreas.berntsson@chalmers.se

DEFINITIONS, ACRONYMS, ABBREVIATIONS

HCCI: Homogenous Charge Compression Ignition.

PRF: Primary Reference Fuel.

CAD: Crank Angle Degree.

TDC: Top Dead Center.

BDC: Bottom Dead Center.

EOI: End Of Injection.

CA50: Crank angle when 50% of the energy is burned.

HC: Hydrocarbon.

SI: Spark Ignition.

NO_X: Nitrogen Oxides.

PM: Particulate Matter.

CO: Carbon monoxide.

APPENDIX

POST PROCESSING

Post processing of the measurement data was carried out for the cylinder pressure trace and for the images. MatLab was used for all post processing.

The pressure trace was recorded by a piezo electric pressure transducer, Kistler 6061b, with a sampling rate between 1 to 10 samples per CAD using an AVL Indimaster. The data was converted to ascii-format and imported to MatLab.

The rate of heat release was calculated by assuming that the combustion process is close to an adiabatic isentropic process.

$pV^{\gamma} = const$, and $\gamma = \frac{c_p}{c_v}$. Then the heat release can be written

$$\frac{dQ}{d\theta} = \frac{\gamma}{\gamma - 1} p \frac{dV}{d\theta} + \frac{1}{\gamma - 1} V \frac{dp}{d\theta}$$

if the convective heat transfer and the crevice volume is small. CA50, rate of heat release and heat release were all based on this equation with the assumption that γ remained constant. Calibration of the heat release calculation were carried with a motored pressure trace.

The images, taken by a Phantom camera, were post processed to reduce noise. Noise level subtraction were carried out by calculating the noise in areas where there should not be any signal (areas outside the optically covered area) due to combustion.

ACCURACY AND REPEATABILITY

Temperature, for instance intake air temperature, was measured with K-type thermocouples with an accuracy of +/- 2 K of the absolute temperature, however for repetitive measurement the accuracy is far better (K element displays effect of aging, however these temperature and the limited time for measurement makes aging negligible). Air pressure, temperature and relative humidity could play a certain role for the combustion due to changes in air density, so repetitions from day to day could play a small but perhaps not a negligible role. To minimize the effect of various conditions from day to day a certain studied trend in the test matrix was studied non stop, and the test matrix order was randomized to further decrease the effect of changes in atmospheric conditions during the measurements. Short term time trends, from the first to the last recorded cycle, were monitored (the time trend for CA50 were studied in MatLab for all operation conditions) to verify that the combustion had stabilized (and that averaging a number of cycles will give an average value of a stable combustion). For the optical engine small time trends can be present, due to that the optical engine could not be used continuously and thus not allowing it to thermally stabilize completely, but the optical engine were only studied in short periods of time and any small time trends during these measurements can be neglected. The Kistler 6061b, has a good accuracy both linearity and shift sensitivity and its accuracy in combination with the rate of heat release script in MatLab is believed to be accurate enough to capture the trends. If the pressure transducer is incorrectly phased to the location of the crankshaft, major discrepancies will result and thus the TDC location was calibrated. The accuracy for the emissions measurements is also good, however for NO_X measurements the calibration were carried out at much greater values than presented here and the accuracy of 0.5 % is valid for full scale, so for pure HCCI operation the NO_X levels will be equal in size as the measurement accuracy, the trends for the NO_X values is however valid. For all measurements lean mixtures were used, which in terms of measurement accuracy is non favorable, accuracy +/- 0.5 % at λ=1 and +/- 2 % at λ=1.6 but the values are good enough and the O_2 measurement with an accuracy of +/- 1 % could be used when the combustion had stabilized.

In total it is believed that the quality of the measurement equipment and the post processing of its data is high enough to correctly capture trends caused by charge stratification in a HCCI engine.

Paper IV

Optical study of HCCI Combustion using NVO and an SI Stratified Charge

Andreas William Berntsson and Ingemar Denbratt

SAE Technical Paper

SAE NAPLES SECTION

2007-24-0012

SAE TECHNICAL
PAPER SERIES

Optical study of HCCI Combustion using NVO and an SI Stratified Charge

A. W. Berntsson, I. Denbratt
Chalmers University of Technology, Sweden

ICE2007
8th International Conference on Engines for Automobile

Capri, Naples
Italy
September 16-20, 2007

SAE International

2007-24-0012

Optical study of HCCI Combustion using NVO and an SI Stratified Charge

Andreas W. Berntsson, Ingemar Denbratt
Chalmers University of Technology, Sweden

ABSTRACT

The effects of using an SI stratified charge in combination with HCCI combustion on combustion phasing, rate of heat release and emissions were investigated in engine experiments to identify ways to extend the operational range of HCCI combustion to lower loads.

In the experiments an optical single-cylinder engine equipped with a piezo electric outward-opening injector and operated with negative valve overlap (NVO) and low lift, short duration, camshaft profiles, was used to initiate HCCI combustion by increasing the exhaust gas recirculation (EGR) and thus retaining sufficient thermal energy to reach auto-ignition temperatures.

Two series of experiments with full factorial designs were performed, to investigate how the tested parameters (amounts of fuel injected in pilot injections and main injections, stratification injection timing and spark-assistance) influenced the combustion.

In the optical study fourth harmonic light (266 nm) from a Nd:YAG laser was used to induce fluorescence (LIF), from 3-pentanone added as a fuel tracer, to analyze the concentration and distribution of fuel vapor within the cylinder. In addition third harmonic light (355 nm) was used to study the concentration and distribution of formaldehyde in the cylinder, and chemiluminescence signals from OH radicals were used to locate the flame front.

It was found that the injection and ignition timing of the SI stratified charge were the main parameters influencing the HCCI combustion phasing. The NO_X emissions were found to be significantly affected by the use of a SI stratified charge, and its injection timing.

The results show that use of an SI stratified charge can extend the operational range of HCCI combustion to lower loads by advancing combustion phasing. In addition, use of NVO in combination with an SI stratified charge provides a useful, flexible means to control HCCI combustion.

INTRODUCTION

Increasingly strict requirements to reduce exhaust emissions and fuel consumption are prompting the development of more advanced combustion concepts. One promising concept is Homogeneous Charge Compression Ignition, HCCI. In an HCCI engine the combustion is controlled by chemical kinetics [1], and heat is released more rapidly than in normal flame front combustion. In the ideal air standard SI cycle the combustion occurs at constant volume and this cycle is therefore the most efficient of the ideal cycles [2]. The rapid heat release of HCCI combustion and its ability to burn lean mixtures, thereby reducing pump, exhaust and cooling losses due to less throttled operation results in greatly improved efficiency compared to SI combustion [3]. HCCI combustion yields low NO_X and PM emissions [4] as a result of the lean homogenous mixture. Cycle-to-cycle variations are also minor because the combustion occurs in a distributed fashion in many places simultaneously [5].

However, several challenges associated with the HCCI concept must be overcome before it can be commercially applied, notably ways must be found to control ignition timing [6], expand its limited operating range [4] and limit the rate of heat release [7]. Cylinder-to-cylinder variations can also cause problems in HCCI engines [4], since the temperature can vary between the different cylinders and the ignition delay is highly dependent on the mixture temperature [8].

Combustion phasing is one of the crucial parameters to control in HCCI combustion and the timing when 50 % of the energy is combusted, CA50, is a good indicator of the phasing of the combustion process [9].

The ability to rapidly control combustion phasing is especially important during transients.

There are numerous solutions to the challenges associated with combustion control. One is to adjust the inlet air temperature by heating the incoming air with air heaters [10-13] or by varying the coolant temperature [14]. However, thermal control of the combustion phasing has the drawback that the thermal inertia of the associated engine parts usually limits the transient response time. Another way to influence the charge temperature, and thus control the combustion phasing, is to adjust the compression ratio. Increasing the compression ratio will increase the pressure, which will decrease the autoignition temperature and increase the charge temperature [8]. Geometrically variable compression ratio have been used to control HCCI combustion by several authors [6, 15-18], but it is difficult to find a mechanism that is fast enough to cope with real vehicle transients.

Further factors that play important roles in the timing of autoignition are the properties of the fuel, since the ignition delay of different fuels at given pressures and temperatures varies dramatically. For this reason, mixtures of two fuels with contrasting octane numbers and ignition temperatures (iso-octane and n-heptane or ethanol and n-heptane) that have appropriate ignition temperatures to allow correct phasing of the combustion have been used in several studies [17, 19].

One promising way of initiating HCCI combustion is to retain large quantities of exhaust gases (EGR), thereby retaining sufficient thermal energy to initiate the HCCI combustion. Camshafts with short duration and low lift profiles, and negative valve overlap (NVO), have been used by Koopmans *et al* [20-23].

The charge homogeneity has been found to have modest effects on the combustion process [24]. However, Aroonisopon *et al* [25] stabilized the combustion at the lower load limit for HCCI combustion by using charge stratification and Sjöberg *et al* [26] used stratification to achieve staged combustion, which smoothed the rate of heat release and thereby enabled the load to be increased. Both lower maximum rates of heat release and phasing capabilities due to charge stratification have been observed in previous studies [27]. In another previous study, [28], the effect of combining SI combustion of a stratified charge and HCCI combustion was investigated. Chemiluminescence images showed that it is possible to create a hybrid combustion mode, in which initial spark-ignited flame-front combustion is followed by HCCI combustion. The SI combustion provides a potential way to control the HCCI combustion as shown in [29].

The study presented here explores the effect of an SI stratified charge on HCCI combustion initiated using NVO. The possibilities for improving combustion phasing control by using an SI stratified charge, and its effects on NO_X and HC emissions and the rate of heat release were studied in two full factorial experiments. The parameter study led to three different operating conditions that extended the HCCI operating range to lower loads and combustion phenomena under these three conditions have been optically studied.

EXPERIMENTAL APPARATUS

ENGINE AND VALVE TRAIN

Experiments were carried out in a single-cylinder engine with optical access. Its displaced volume corresponds to that of a passenger car engine. For all experiments a prototype cylinder head was used with geometry similar to that of a DI SI engine. The engine parameters can be seen in table 1 and a schematic sketch of the layout of the optical setup can be seen in figure 1.

Table 1: Engine parameters.

Bore	83 mm
Stroke	90 mm
Swept Volume	487 cm^3
Compression ratio	12.3:1
Conrod length	139.5 mm

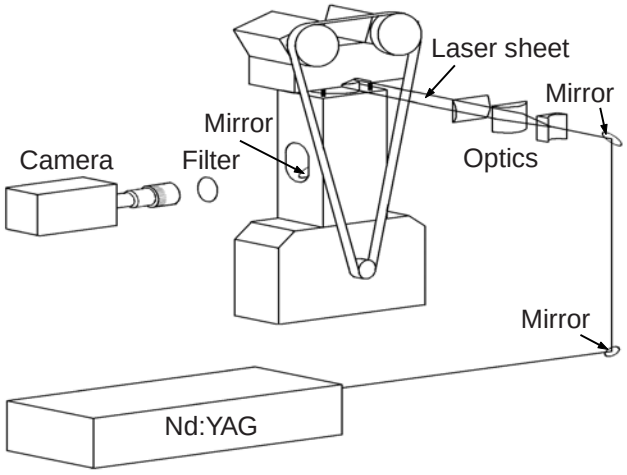

Figure 1: Schematic layout of the optical engine.

This engine has an extended piston housing a mirror that provides, in conjunction with a quartz window in the piston crown, optical access to most of the combustion chamber from below. The optically accessible volume can be seen in Figure 2.The optical engine is restricted to low engine speeds and since a Nd:YAG laser was used in the optical studies, all measurements were made at 1200 rpm, which corresponds to 10 Hz.

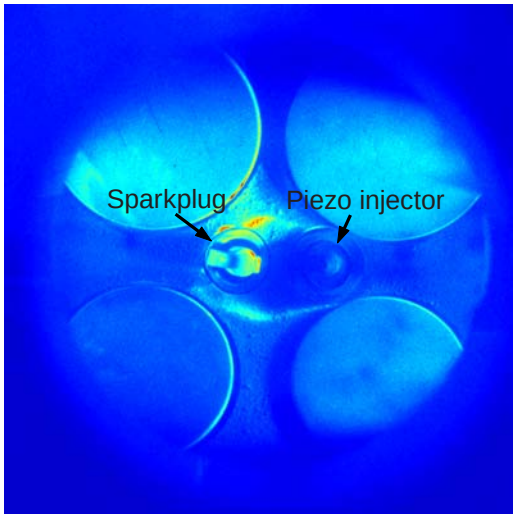

Figure 2: The optically accessible combustion chamber. The diameter of the optically covered zone was 73 mm.

The fuel was supplied using an outward opening hollow cone type piezo electric direct injector, with a fuel pressure of 200 bar, which is capable of multiple injections and has been shown to maintain fuel clouds in the vicinity of the sparkplug [30]. A 35 mJ ignition coil was used to ensure that sufficient ignition energy was supplied by the sparkplug. The locations of the injector and the sparkplug can be seen in figure 2.

The engine was operated with NVO to initiate HCCI combustion, since Koopmans [34] found that by increasing the NVO the auto-ignition timing could be advanced, due to the increased residual mass fraction, and thus one of the problems that must be overcome to extend the operating range of HCCI to lower loads (retarded combustion phasing) could be overcome. Furthermore, an injection prior to TDC in the NVO, here called a pilot injection, can influence the combustion phasing [23]. A main injection was injected after TDC during the NVO and during the compression stroke a further injection was added to create a stratified charge in the vicinity of the sparkplug, and thus allow flame propagation to occur in globally lean conditions. Illustrative injection timings, valve lift profiles and motored pressure traces obtained when conventional valve timing and NVO were used can be seen in figure 3. The short duration for the camshafts and the timing led to compression of the trapped exhaust during the gas exchange phase, allowing the temperature during the NVO to be increased to such a degree that reactions could occur when a pilot injection was used. The valve timing was symmetrical around TDC, since unsymmetrical timing would lead to increased pumping work. Log-log P-V diagrams for both conventional valve timing and valve timing with NVO are shown in figure 4.

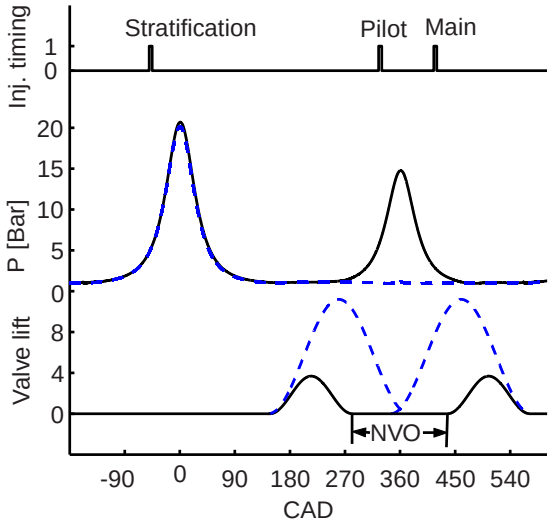

Figure 3: Valve lift profiles, injection timings, and motored pressure traces obtained with both conventional valve timing (dashed lines) and NVO (solid lines).

Since the investigations were performed in an optical engine with higher cooling losses than in a metal engine the intake air was heated to allow similar settings. The intake air temperature was measured directly at the intake valve using a thermocouple and the temperature was kept at 90 °C for all measurements. The cylinder head used was a prototype cylinder head without any cooling, the cylinder was water cooled and the temperature was set to 90 °C. To achieve a condition that was similar to a traditional engine in terms of surface temperature, the engine was operated in a SI stratified mode until the cylinder head was 130 °C and then the settings that should be studied were used. This procedure was carried out for all measurements to achieve high repeatability accuracy.

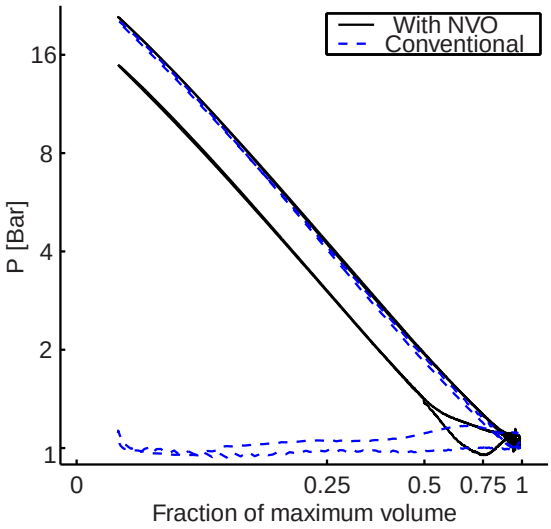

Figure 4: Motored pressure for trace when NVO is used and when conventional valve timings are used for WOT.

FACTORIAL EXPERIMENTS

Table 2: A 2^{IV} factorial design scheme, four variables are all tested at two different states with all its different combinations.

Case	A	B	C	D
1	+	+	+	+
2	-	-	+	-
3	-	-	-	+
4	-	+	-	-
5	+	-	-	-
6	-	-	+	+
7	-	+	+	+
8	+	-	+	-
9	+	-	-	+
10	+	+	+	-
11	+	+	+	-
12	+	-	+	+
13	+	+	-	-
14	+	+	-	+
15	+	+	+	-
16	-	-	-	-

The most efficient way to examine the effects of multiple variables experimentally is to apply an appropriate factorial design [31]. The assumptions that underlie these factorial designs are that the measurements are independent of each other, the variation is in the same order within the measurement span and that the measurements are normally distributed. Furthermore, the span of the measurements must be sufficiently large (relative to the measurement accuracy and/or inherent variation in the data) to capture major trends but sufficiently small to capture local trends and to ensure that the order of the variation of the measurements is not affected. Conclusions can only be drawn within the span of each variable, so attention was focused on the spans for each of the variables prior to executing the factorial experiments. Some parameters were fixed, in accordance with previous work, mainly performed by Koopmans *et al* [23], to limit the variables to four, allowing two 2^{IV} full factorial designs (in which all permutations of four variables in two different states are tested) to be applied, since reduced experiments often require prior experience of the studied variables and considerable knowledge of the system in order to make reductions without sacrificing too much statistical power. The NVO was set at 160 CAD, and the timing of the pilot injection and main injection at selected values similar to those used by Koopmans for the lower part of the HCCI operation range. The same fuel components that were used for the optical study were used in the parameter study to minimize fuel-related effects on variations in the results.

The initial study focused on the effects of the tested variables when the load was constant, while in the later study operating conditions with different loads were investigated since the ultimate objective was to reduce the lower load limit of HCCI operation by using an SI stratified charge. Table 2 shows how the variables were varied in the two experimental series (for convenience designated Experiment 1 and Experiment 2). The variables chosen and their different states can be seen in table 3 and 4. The load was kept constant in Experiment 1 by changing the relative amounts of fuel injected in the pilot, main and stratification injections, while keeping the total amount of fuel injected constant, while in Experiment 2 the relative amounts injected in the pilot and main injections, and the total amount of fuel, were varied. Charge stratification in it self has been shown to influence combustion in experiments with PRF50 as fuel [27] so, as shown in the table, this was included as one of the test parameters, with and without spark assistance.

Table 3: Test matrix for experiment 1.

Fuel	
	80 % iso-octane
	10 % n-heptane
	10 % 3-pentanone
Valve timing	
IVO	440 CAD
IVC	570 CAD
EVO	150 CAD
EVC	280 CAD
Experimental variable	State + / -
A Pilot injection amount	Large / Small
B Main injection amount	Large / Small
C Stratification injection timing	Early / Late
D Spark ignition	Yes / No
Results	
Pressure trace	CA50
	RoHR
NO_X emissions	ppm and $ISNO_X$
HC emissions	ppm and ISHC

OPTICAL MEASUREMENTS

LIF

In the optical studies fourth harmonic (266 nm) light from a Nd:YAG Spectra Physics laser was used to induce fluorescence (Laser-Induced Fluorescence, LIF) from the fuel tracer 3-pentanone, in order to analyze the concentration and distribution of fuel vapor within the cylinder, and third harmonic (355 nm) light to excite formaldehyde, in order to analyze the location of low temperature reactions during early combustion phases [32]. A planar laser sheet located 5 mm beneath the sparkplug was used, in combination with the quartz window, to visualize the combustion chamber from below. The images were taken using an image intensified LaVision Dynamight camera, providing up to 1024x1024 resolution equipped with LaVision DaVis 6.2 software. However, all postprocessing of the images was carried out using MatLab. For

Table 4: Test matrix for experiment 2.

Fuel	
	70 % iso-octane
	15 % n-heptane
	15 % 3-pentanone
Valve timing	
IVO	440 CAD
IVC	570 CAD
EVO	150 CAD
EVC	280 CAD
Experimental variable	State + / -
A Pilot injection amount	Large / Small
B Main injection amount	Large / Small
C Stratification injection timing	Early / Late
D Spark ignition	Yes / No
Results	
Pressure trace	CA50
	RoHR
NO_X emissions	ppm and $ISNO_X$
HC emissions	ppm and ISHC

the LIF fuel vapor study a Schott BG25 bandpass filter with a peak transmission at 390 nm, and for the formaldehyde study a Melles Griot 03FIV028 narrow band filter with a center wavelength of 455 nm and FWHM of 40 nm were used. 15 $\%_{vol.}$ of fuel tracer was used for the fuel vapor study.

CHEMILUMINESCENCE OF OH

In order to study flame front propagation a filter was used to isolate the emitted light from the OH radicals, which are associated with the reaction zone.

$$H + OH = H_2O + h\nu \quad (1)$$

The reaction gives intensity peaks for the emitted light at wavelengths between 306 and 309 nm [33]. An image intensified Dynamight camera was used to capture chemiluminescence from the OH radicals thus generated, in conjunction with a Melles Griot 03FIV119 narrowband filter with a centre wavelength of 310 nm and a FWHM of 14 nm.

RESULTS AND DISCUSSION

FACTORIAL EXPERIMENT 1

Table 5: Main effects from the factorial Experiment 1 with a fixed load.

Effect	Result				
L_{AHC}	238 ppm	L_{ANO_X}	-30 ppm	L_{ACA50}	-2.5 CAD
L_{BHC}	-557 ppm	L_{BNO_X}	38 ppm	L_{BCA50}	1.6 CAD
L_{CHC}	130 ppm	L_{CNO_X}	65 ppm	L_{CCA50}	-4.5 CAD
L_{DHC}	510 ppm	L_{DNO_X}	54 ppm	L_{DCA50}	-16.3 CAD
$\overline{HC}$	2087 ppm	$\overline{NO_X}$	103 ppm	$\overline{CA50}$	5.8 CAD
σ_{HC}	150 ppm	σ_{NO_X}	30 ppm	σ_{CA50}	2.73 CAD

Effects on combustion phasing

Table 5 shows the main effects of the tested variables on combustion phasing when the load was kept constant. The variable that had the strongest effect on combustion phasing was D, using spark ignition or not, which advanced the combustion by 16 CAD on average, equivalent to ca. six standard deviations of the mean CA50. Thus, its effect was extremely statistically significant. The standard deviation for CA50 was averaged from the calculated standard deviation value for the CA50 for all recorded pressure traces from experiment 1. The combustion phasing also appeared to be affected by the timing of the stratification injection (the ignition timing followed the injection timing of the stratified charge with a fixed dwell time of 4 CAD). The variable A also affected the combustion phasing; increasing the relative amount of fuel injected in the pilot injection caused the combustion phasing to advanced. This phenomenon has also been observed by Koopmans [23] and is attributable to the increased reactions during the NVO. However the statistical significance of the effects of this variable on combustion phasing in the operating conditions applied in Experiment 1 is fairly low; confidence limit calculations indicate that there is only a ca. 80 % probability that it had an effect.

Effects on emissions

Increasing the relative amount of fuel injected in the pilot injection increased HC emissions, apparently because it increased the amount of wall wetting. Furthermore, the low density during the NVO also led to long spray penetration (sufficiently long for the spray to reach the piston top). The opposite trend was seen when the relative amount of fuel injected in the main injection was increased, and thus the pilot amount was reduced, since the piston was further down and there was less time for the fuel to reach the walls and the crevices. Advancing the combustion generally increases HC emissions since it leads to increases in pressures and, thus, in the density of the gas trapped in the crevices, due to the increased temperature difference between the gas in the crevices and the gas in the combustion chamber. Hence, introducing a spark in HCCI combustion also had a significant effect on HC emissions. The NO_X emissions were mainly influenced by the parameter C, the timing of the stratified charge and its ignition, and parameter D, the use (or not) of spark assistance. The initial flame propagation and all subsequent combustion phases, and (thus) increased NO_X emissions.

Effects on rate of heat release

By analyzing the averaged rate of heat release traces for the different cases in experiment 1, further information were gained and in figure 5 the trend of the

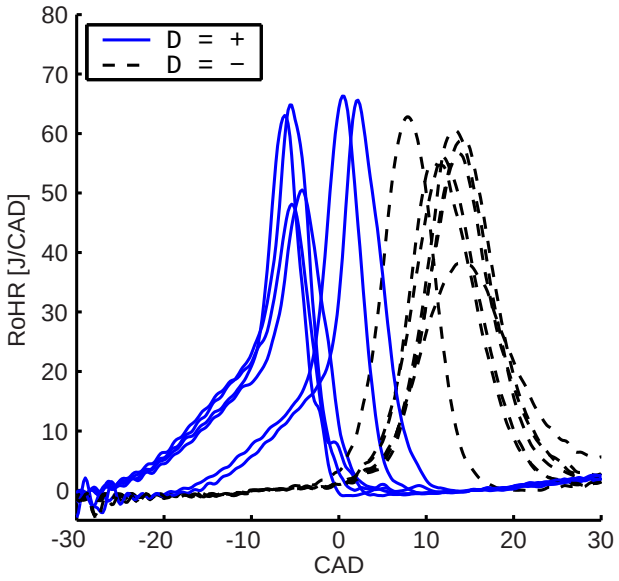

Figure 5: The averaged rate of heat release for experiment 1 when spark ignition was used (blue solid line) and when it was not used (dashed black line).

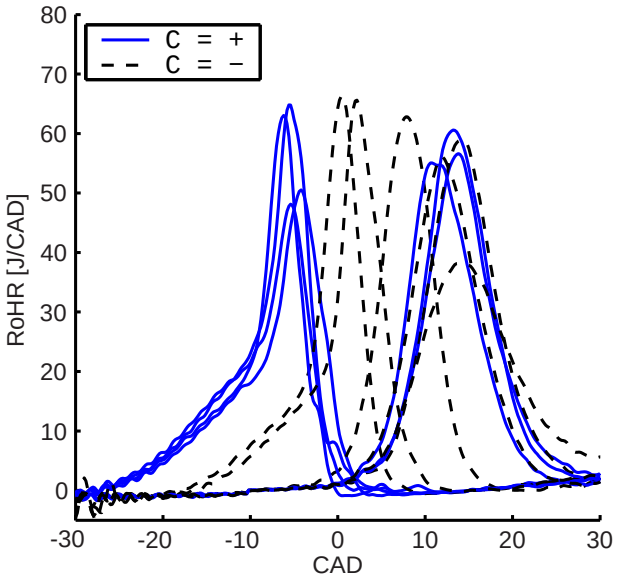

Figure 6: Averaged rate of heat release for experiment 1 when the stratification injection was injected early (solid blue lines) and late (dashed black lines).

greatly advanced combustion due to the introduction of the spark can be seen when the averaged traces for the different cases are plotted together. The initial stages of the combustion consists of initial flame propagation and subsequently of HCCI combustion, which can be seen in the rate of heat release traces for the cases that used the SI stratified charge. The gentle initial slope for those traces corresponds to SI combustion and the sudden increase in rate of heat release corresponds to the increased rate due to the transition to the more rapid HCCI combustion. This initial heat addition cause by early flame propagation increased the temperature and pressure within the combustion chamber enough to achieve such a low ignition delay for the remaining mixture that it self ignited and thus there were a transition to a chemically kinetically controlled combustion. This have been seen by the authors in previous studies [27,28].

More detailed information on the effects of injection timing (and thus ignition timing for the cases in which a spark was used, since the dwell time between the end of injection and spark timing was constant) can be seen in the rate of heat release traces in figure 6. The effects were not as clear as those of variable D, use (or not) of spark assistance. However, in the cases where spark-assistance was used the effect of injection timing is clearer, see figure 7. The combustion phasing was clearly influenced by the injection timing of the stratified charge in those cases; the initial flame propagation was initiated at an earlier stage when this charge was injected early, leading to advanced combustion, so the effect of variable C shown in table 5 was mainly due to the advance in combustion when spark assistance was used. The effects on combustion phasing of varying the injection timing of the stratified charge in cases without spark assistance seen in previous studies by the authors [27] were not observed in the operational conditions used in this study.

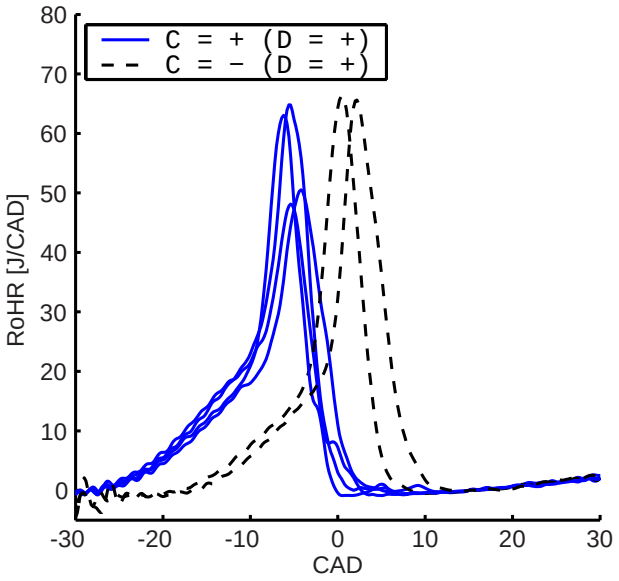

Figure 7: Averaged rate of heat release curves obtained in Experiment 1 when the stratification injection was injected early (solid blue lines) or late (dashed black lines) and spark assistance was used.

Increases in the relative amount of fuel injected in the pilot injection (parameter A), slightly advanced the combustion phasing, but more strongly in cases without spark assistance than in cases with spark assistance, in which the effect of SI combustion was dominant. In figure 8 the effect of increasing the relative size of the pilot injection on the pure HCCI cases can be seen, the additional reactions during the NVO in-

creased the temperature during the compression and thus the combustion advanced.

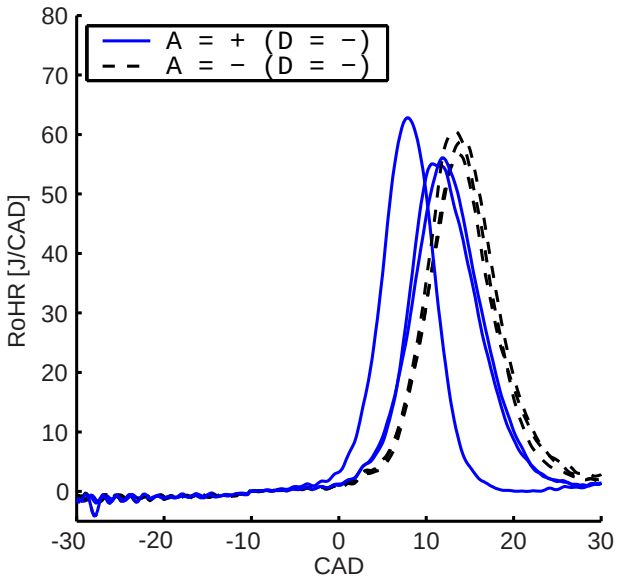

Figure 8: Averaged rate of heat release curves obtained in Experiment 1 for cases without spark assistance with different relative amounts of pilot injections.

Table 6: Combustion phasing and standard deviations for cases without spark assist and different amounts of pilot injection.

Case	CA50	σ_{CA50}
2 (A = -)	15.1 CAD	2.97 CAD
4 (A = -)	15.2 CAD	2.60 CAD
11 (A = -)	14.7 CAD	2.92 CAD
5 (A = +)	8.4 CAD	1.55 CAD
10 (A = +)	12.8 CAD	2.81 CAD
13 (A = +)	13.1 CAD	2.65 CAD

In table 6 the CA50 timing and its standard deviation for the pure HCCI cases can be seen, corresponding to the cases in figure 8. The average CA50 was advanced when the relative amount of fuel injected in the pilot injection was increased, but the standard deviation of these timings needed to be thoroughly studied before it could be definitively concluded that the pilot injection influenced the phasing.Calculated confidence intervals indicated that there was a significant advance in combustion phasing in case 5 (in which the pilot injection was relatively large) compared to cases 2, 4 and 11 (with relatively low pilot injections). However, similar calculations indicate that the statistical support was much weaker for the increased size of the pilot injection having a significant effect in cases 10 and 13 (again relative to cases 2, 4 and 11).

FACTORIAL EXPERIMENT 2

In the initial factorial experiment the effects of the tested variables were examined when the load was kept constant since the load influences most of the combustion parameters. However, the ultimate objective of the work was to identify settings that allow the HCCI operation range to be extended, and thus it was important to study the effects of the variables at different loads. This was done in the second factorial experiment (Experiment 2).

Table 7: Main effects from factorial Experiment 2.

Effect	Result				
L_{AHC}	-7 ppm	L_{ANO_X}	57 ppm	L_{ACA50}	-0.9 CAD
L_{BHC}	-130 ppm	L_{BNO_X}	124 ppm	L_{BCA50}	2.7 CAD
L_{CHC}	86 ppm	L_{CNO_X}	53 ppm	L_{CCA50}	-2.4 CAD
L_{DHC}	498 ppm	L_{DNO_X}	51 ppm	L_{DCA50}	-13.1 CAD
$\overline{HC}$	2819 ppm	$\overline{NO_X}$	104 ppm	$\overline{CA50}$	3.8 CAD
σ_{HC}	150 ppm	σ_{NO_X}	30 ppm	σ_{CA50}	2.23 CAD

Effects on combustion phasing

The main effects of the tested variables on combustion phasing are presented in table 7. As in Experiment 1, the variable with the strongest effect was variable D (spark assistance), which shifted combustion phasing (CA50) by ca. six standard deviations, and thus had an extremely statistically significant effect. The pilot injection was found to have little or no effect on combustion phasing in general (L_{ACA50}, in the order of half a standard deviation, especially when an SI stratified charge was used, since its phasing effects were so much stronger.

Effects on emissions

As in the constant load tests in Experiment 1, HC emissions were affected by parameter D in Experiment 2, where loads were varied. This was because the combustion was dramatically advanced by spark assistance, resulting in most of the combustion occurring close to or prior to TDC and (thus) greater amounts of the gas being trapped in the crevices. In cases without any spark assistance, and thus later combustion phasing, less gas was trapped in the crevices since the combustion temperatures were lower so the difference between the crevice gas temperature and the combustion temperature was smaller. This effect, of lower HC emissions in cases with retarded combustion phasing, would probably be weaker in a traditional engine since the crevice volume would be smaller.

Since the load was varied in Experiment 2 the NO_X emissions were not necessarily expected to show the same trends with respect to parameters A and B as those observed in Experiment 1. Accordingly, high states of those variables increased loads (by 0.14 and 0.35 kW, respectively), and thus increased NO_X emissions. For parameters C and D, the trends were the same as those seen in Experiment 1, and for the same reasons since they did not affect the load.

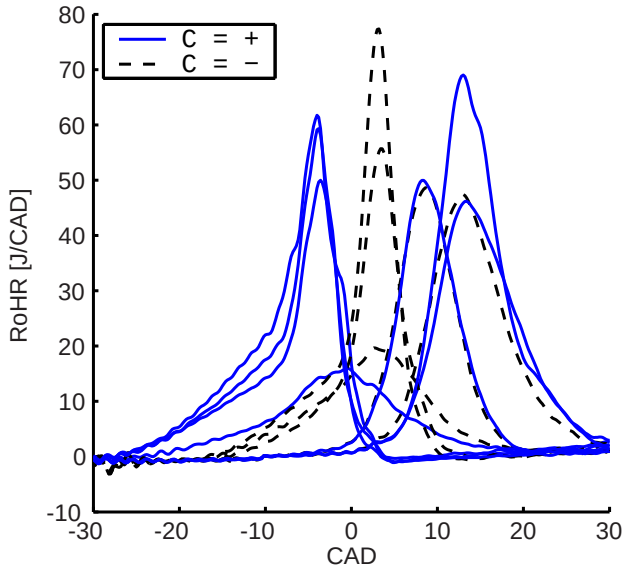

Figure 9: Averaged rate of heat release curves obtained in Experiment 2 when the stratification injection was injected early (solid blue lines) and late (dashed black lines).

Effects on rate of heat release

As shown in table 7 there is an indication that the injection timing of the stratified charge influences the combustion phasing, and its effect on the average rate of heat release can be seen in figure 9. As in Experiment 1 the change in phasing caused by varying the injection timing was due to the change in phasing of the SI stratified charge, see figure 10, thus the combination of spark assistance and varying the injection timing was the reason for the combustion phasing.

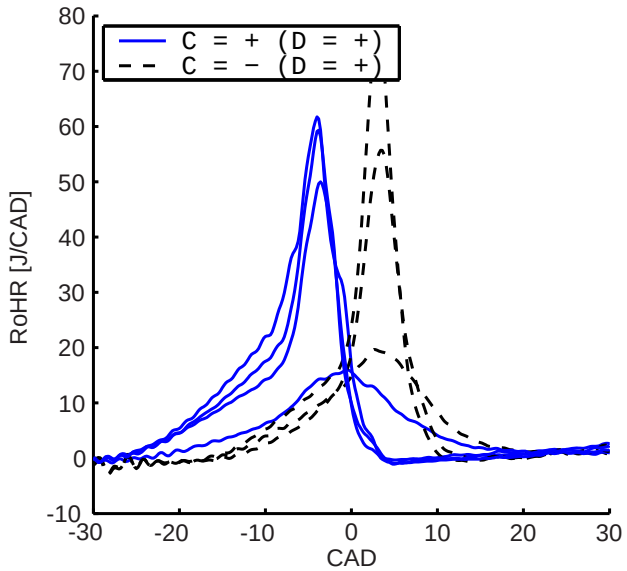

Figure 10: Averaged rate of heat release curves obtained in Experiment 2 when the stratification injection was injected early (solid blue lines) and late (dashed black lines) with spark assistance.

For the operation conditions used for this study, the timing of the stratified charge did not in itself have any significant effect on combustion phasing.

The effect of pilot injection on combustion phasing was found to be minor, however in cases where SI was not used, i.e. pure HCCI combustion, effects of the pilot injection were detected, as shown in figure 11. The four selected cases presented had similar loads, so the effects on phasing are not due to differences in load, but solely to the relative size of the pilot injection.

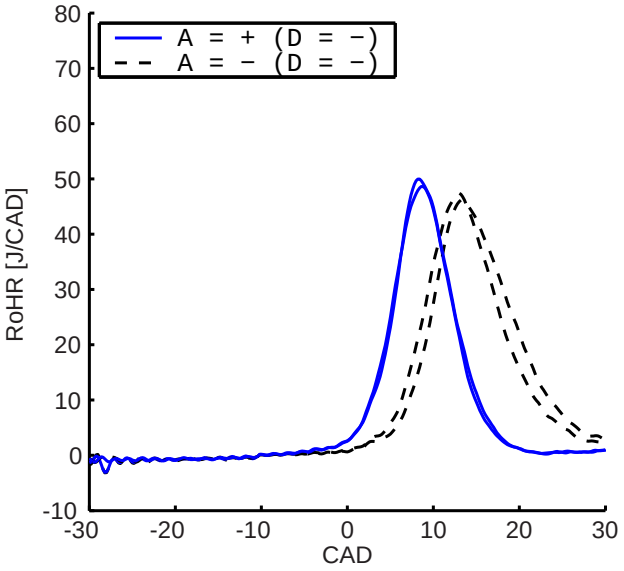

Figure 11: Averaged rate of heat release curves obtained in Experiment 2 for the cases without spark assistance and different relative amounts of pilot injections.

OPTICAL RESULTS

Three operational conditions were chosen for the optical studies, in which the operation range for HCCI combustion were expanded towards lower loads, see figure 12. The lower limit for HCCI operation range found by Koopmans [34] is also be seen. The inlet air temperature for the optical engine was adjusted so that its behavior was similar to that of a conventional engine and, thus, the load for pure HCCI combustion were identical to that found at 1200 rpm by Koopmans, i.e. case A.

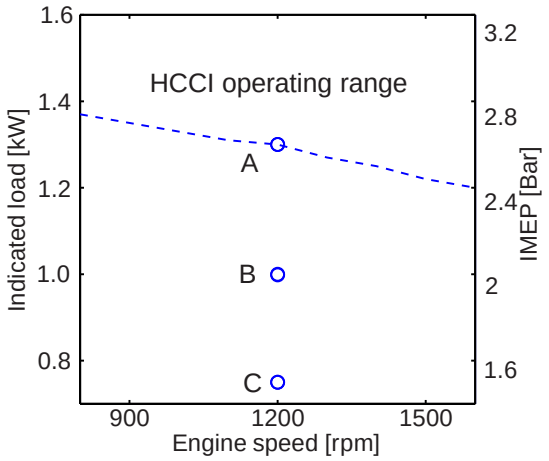

Figure 12: The loads in the three operating conditions used in the optical studies.

The parameters and some results obtained in these three operating conditions can be seen in table 8. Case A corresponds to pure HCCI combustion and thus no spark was used. In addition, no injection intended to create a stratified charge was used in this case, since such an injection may also have affected the behavior of the combustion and the purpose of this study was to evaluate the effects of spark ignition and charge stratification. In cases B and C an SI stratified charge was used to extend the HCCI operating range to lower loads, by creating a combustion mode in which normal flame front propagation combustion was followed by HCCI combustion. The amount of fuel injected in the pilot injections was identical in cases B and C, but the amounts injected in both the main injection and the stratification differed. The injection timing also differed between them. Equivalence ratios in all three operating conditions were lean, 1.3 or more, which is essential for reactions to occur during the NVO, since oxygen must be present for such reactions.

The fuel consumption values for the three operating conditions were similar, although the indicated fuel consumption was slightly higher for the pure HCCI combustion than for the other, spark-assisted cases. The levels of unburned HC emissions were also highest for the pure HCCI combustion, as usually found at the lower end of the HCCI operation range. It should be noted that absolute values of HC emissions from optical engines are not directly comparable to those from conventional engines, but trends are more directly applicable. NO_X emissions were very low in all of the cases, even those in which the initial mode of combustion was flame front propagation, and the combustion efficiencies were high, even though an optical engine was used in the tests.

Table 8: Operating conditions and results from the optically studied cases.

Case	Pilot inj.	Main inj.	Strat. inj.	Spark tim.
A	330/1.5	-300/1.2	—	—
B	330/1.1	-300/1.1	-50/0.9	-46
C	330/1.1	-300/0.7	-30/1.0	-26

Case	Load	λ	ISFC
A	1.3 kW	1.3	265 g/kWh
B	1.0 kW	1.4	239 g/kWh
C	0.75 kW	1.55	246 g/kWh

Case	HC	NO_X	CO	$\eta_{combustion}$
A	3100 ppm	20 ppm	0.6 $\%_{vol.}$	0.983
B	2100 ppm	44 ppm	0.4 $\%_{vol.}$	0.988
C	1700 ppm	18 ppm	0.6 $\%_{vol.}$	0.983

Figure 13 shows averaged pressure traces for the three cases. The rise in pressure during the NVO can also be seen.

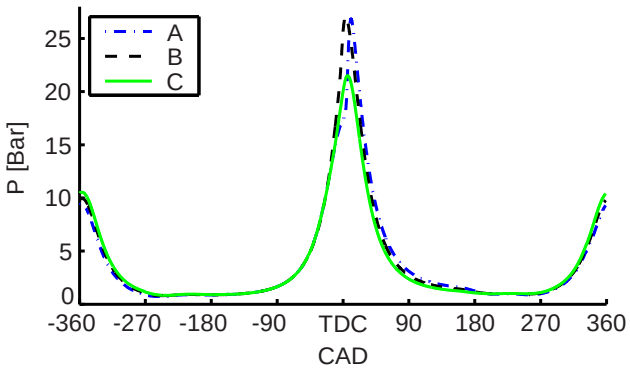

Figure 13: Averaged pressure traces for the three cases that were optically studied.

Averaged rate of heat release traces for the three cases can be seen in figure 14. The traces show that combustion phasing was retarded in the pure HCCI combustion, in which combustion was short and rapid, while in case B the heat release during the initial SI combustion, followed by a distinct change in rate to the HCCI combustion, are clearly visible. However, the averaged rate of heat release trace for case C, in which the load was lowest, was highly unrepresentative since the combustion displayed great cycle-to-cycle variations and thus an averaged trace is not presented. Instead rate of heat release traces for several separate cycles are displayed for case C, in which the initial SI combustion can be located and the later HCCI combustion can be seen, but less distinctly than in the trace for case B, and the timings also differ.

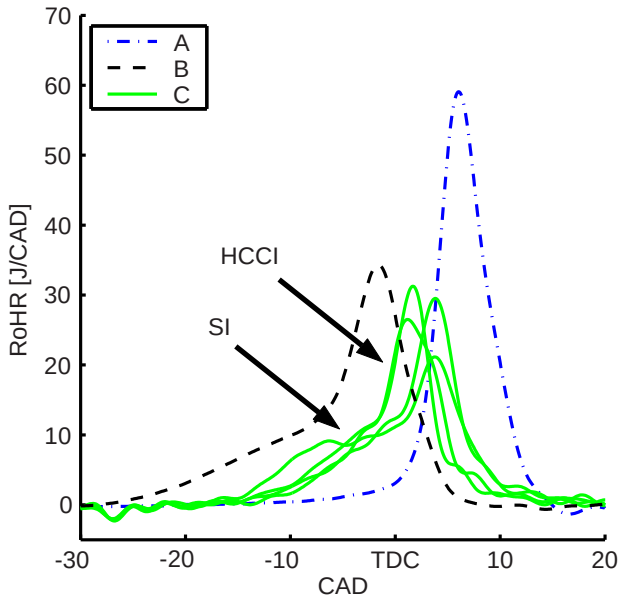

Figure 14: Averaged rate of heat release traces for cases A and B and multiple traces for case C.

LIF - FUEL DISTRIBUTION

Figure 15 shows images (and corresponding timings) of average LIF signals from the fuel tracer 3-pentanone, indicating fuel vapor concentrations, acquired for case A. The images show that the fuel concentration was heterogeneously distributed in the cylinder shortly after additions of fuel in both the pilot injection and the main injection. However, during compression the fuel was sufficiently mixed and showed an evenly distributed and homogenous pattern. Furthermore, effects of the rising pressure and temperature could be seen during the compression. The increasing pressure leads to a reduction in signal strength, due to greater amounts of quenching since the molecules collide more frequently and the excited electrons fluoresce less, since some of their energy is dispersed during the collisions. The increased pressure also leads to greater absorption which, in turn, reduces the numbers of molecules that are excited further in the combustion chamber and thus reduces the intensity of the signals on the left side of the image. The combustion was initiated at various spatial locations near the center of the combustion chamber, and thus the averaged signal is weaker near the center at TDC since the fuel tracer was combusted. After the pilot injection and during the NVO at 340 and 350 CAD the intensity of the fuel tracer signal varied, partly because the fuel had not been evenly distributed and partly because the reactions that occurred during the NVO consumed some of the fuel. The fuel concentrations at 340 CAD were highest near the center of the combustion chamber and at the periphery, as can be seen in the top right corners of the images.

The fuel distribution in case B can be seen in figure 16. During the NVO and after the pilot injection the trend of a stratified charge with richer regions as for the case A could be seen, however it's spatial location and intensity varied. The intensity was expected to change due to the lower amount of fuel injected in the pilot injection. A slightly richer core near the center and another slightly richer area to the right can be identified in the images, again partly because the fuel had not yet been evenly distributed and partly because of the reactions that occurred during the NVO. Prior to the stratification the fuel was evenly distributed and displayed a homogenous pattern, as seen in the image for -60 CAD in figure 16. After the stratification charge (which was injected at -50 CAD) an enriched zone could be identified and slightly later in the cycle the flame front from the SI combustion could be seen as it consumed the stratified charge.

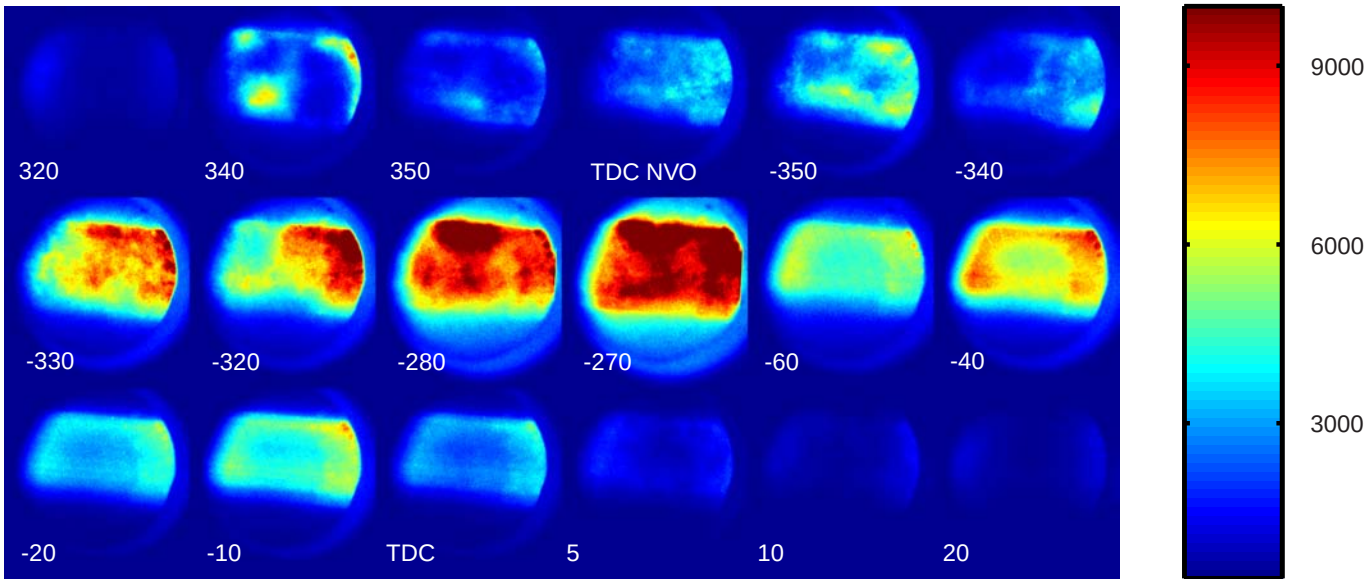

Figure 15: Averaged images (from 10 separate cycles) (and corresponding timings) for case A of LIF from the fuel tracer 3-pentanone.

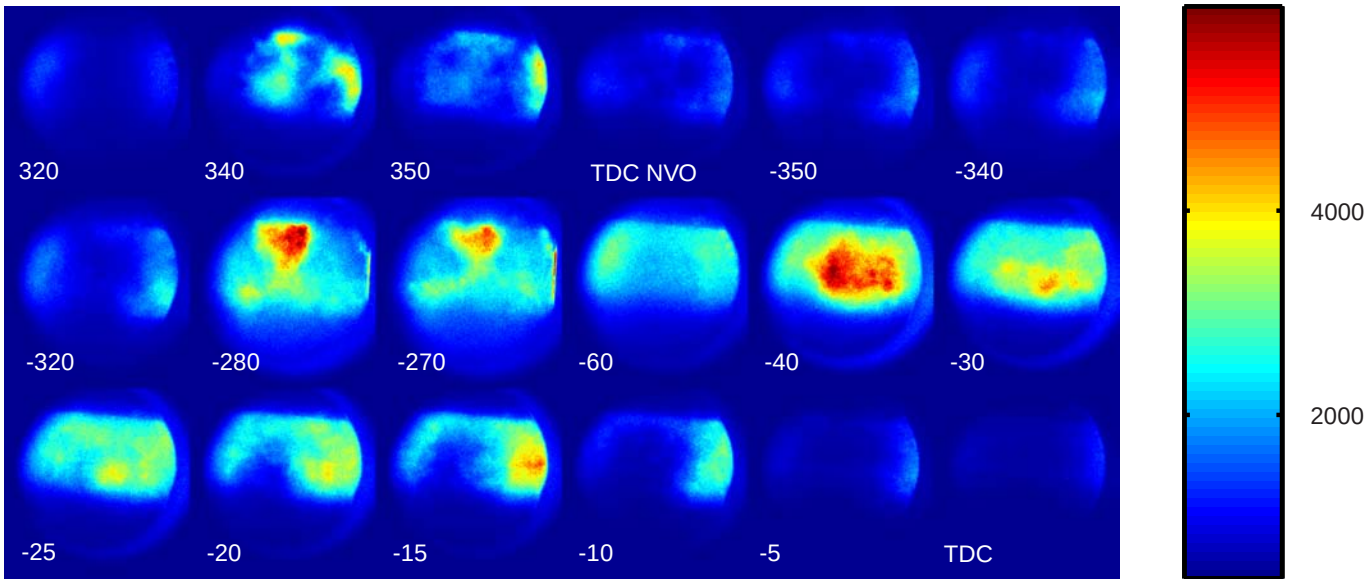

Figure 16: Average images (from 10 separate cycles) (and corresponding timings) of LIF from the fuel tracer 3-pentanone in case B.

The images presented in figure 16 are averaged images and the spatial location of the flame front (where there is a sharp drop in signal strength) varied. However the temporal trend of an expanding region of low signal strength can be easily seen. The purpose of the stratification injection was to enrich the vicinity near the sparkplug to such a degree that the charge became close enough to stoichiometric to allow normal flame propagation. The global air equivalence ratio could easily be determined by the use of a lambda sensor. The local air equivalence ratio were determined by using the LIF images of the fuel tracer for the case B and by comparing to reference images.

Reference images were taken during the compression on pure HCCI combustion that displayed evenly distributed fuel tracer signals. Images were taken at different periods in time in the cycle and the lambda were varied, and thus reference images with known air equivalence ratio at the different pressures during the compression were achieved.

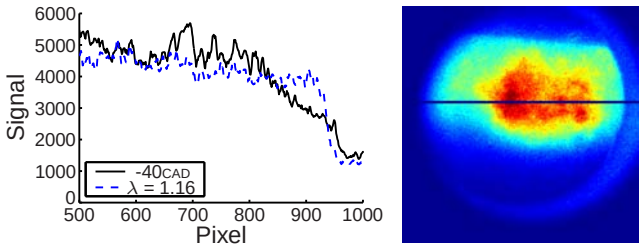

Figure 17: Average image for case B at -40 CAD (LIF with 3-pentanone as fuel tracer) and its signal strength.

In figure 17 the average image obtained of the fuel concentration at -40 CAD (10 CAD after the stratification injection), with the stratified charge near the center of the combustion chamber, can be seen. When the signal strength was studied more in detail, and the intensity of the stratified charge in particular, by plotting the intensity of a line through the image, the local signal strength could be seen. The images were taken with a spatial resolution of 1024x1024 and a pixel number of around 500 in the plot corresponds to the center of the combustion chamber. The dashed blue line shows the signal strength of a reference image with the closest signal strength, at the same position or height (in order to minimize effects of possible variations in intensity within the laser plane). The global air equivalence ratio for this operation condition were 1.4 and the local air equivalence ratio was slightly richer, ca. 1.16.

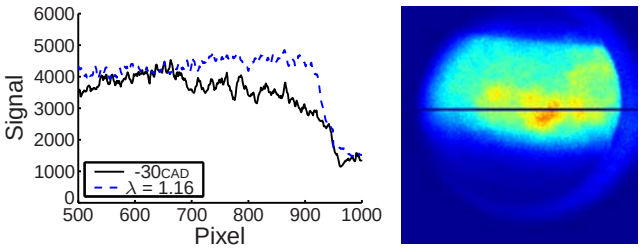

Figure 18: Average image for case B at -30 CAD, LIF with 3-pentanone as fuel tracer and its signal strength.

The fuel concentration at -30 CAD can be see in figure 18, 20 CAD after the stratification. Here, the edges around the stratified charge observed at -40 CAD are not as sharp, but an increase in signal strength near the center can be identified. For this case and timing SI combustion had been initiated, but the flame had only propagated a very short distance and the average image did not display any region near the center

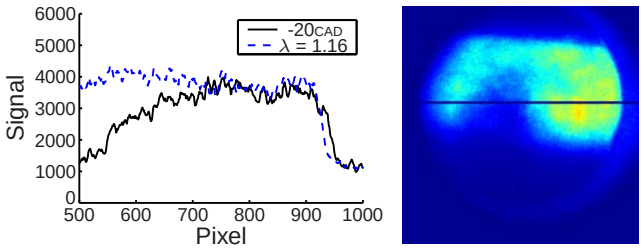

Figure 19: Average image for case B at -20 CAD, LIF with 3-pentanone as fuel tracer and its signal strength.

with low signal strength. Near the center of the combustion chamber the local air equivalence ratio was 1.16.

Figure 19 and 21 show the fuel concentrations at -20 and -10 CAD, respectively. At these timings the flame had propagated through the charge and its propagation can easily be seen. When the fuel concentration was studied, as above, a richer unburned region to the right of the images was identified. The drop in signal strength caused by the flame could be seen when the signal strengths were plotted, and the drop was naturally sharper in single images than in the average image since the location of the flame differs slightly from image to image. At -20 CAD the air equivalence ratio for the stratified charge was still around 1.16 and at -10 CAD the charge was somewhat leaner, around 1.18.

All the images presented were taken at the same height, 5 mm beneath the sparkplug since the aim was to create a stratified charge in the vicinity of the sparkplug in order to allow the initiation and propagation of a normal flame, and at this height all images show that the stratification injection enriches the region where the flame will propagate, and thus allows the flame to propagate. It should be noted that to avoid sacrificing the advantage of low NOx generation associated with HCCI combustion when introducing this SI stratified charge in order to increase combustion control the stratified charge was kept fairly lean, as shown in figure 17, 18, 19 and 21.

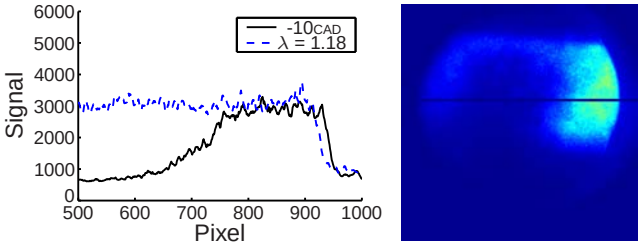

Figure 21: Average image for case B at -10 CAD, LIF with 3-pentanone as fuel tracer and its signal strength.

The fuel distribution in case C can be seen in figure 20. As for cases A and B the signal from the fuel tracer was inhomogenous during the NVO and the intensity of the signal was of the same order as for case B, since equal amounts of fuel were injected in the pilot injections. A slightly richer core near the center, and another slightly richer area to the right of the images, can be seen in the images acquired at 340 and 350 CAD, (as for case B, and for the same reasons). After TDC the signal shows a region with reduced signal strength as seen for cases A and B, but at a slightly different location. For case C the stratification injection was injected later than for case B, and the image directly after the stratification injection displays a clear stratified charge near the center of the combustion chamber which occupies a spatially smaller region than the corresponding region in case B. The images thereafter displayed a larger region with higher concentration and the propagating flame could be located as it consumed the stratified charge.

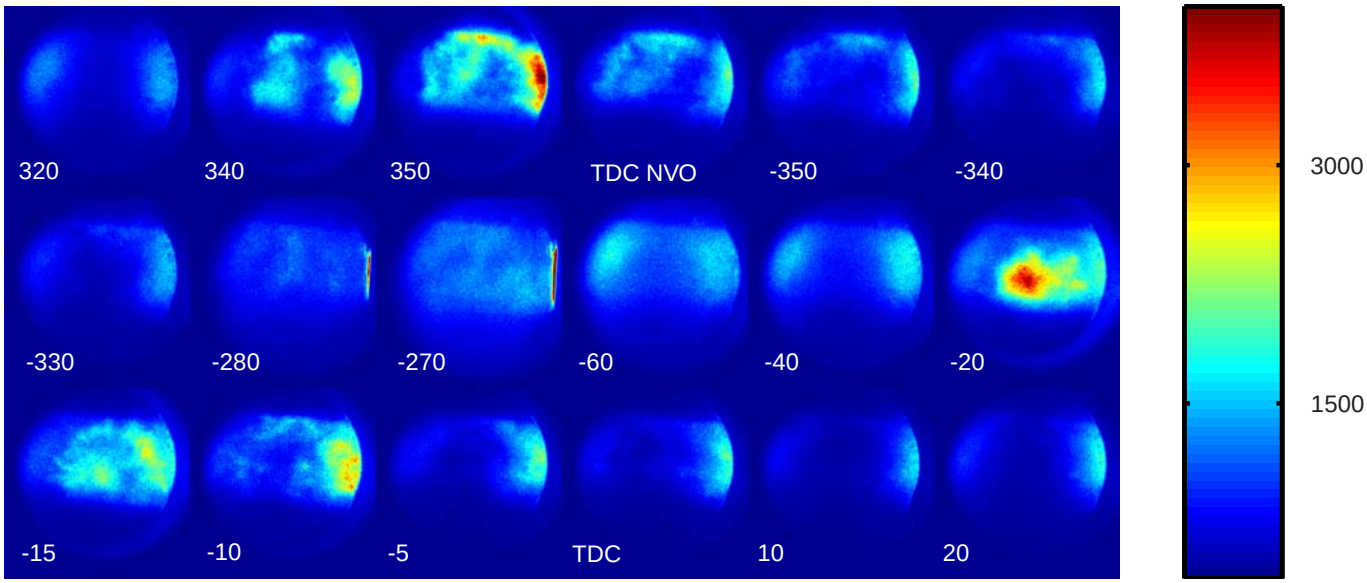

Figure 20: Average images (from 10 separate cycles) (and corresponding timings) for case C of LIF from the 3-pentanone fuel tracer.

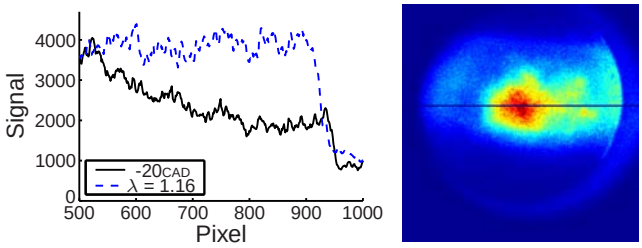

Figure 22: Average image for case C at -20 CAD, of LIF from the 3-pentanone fuel tracer and its signal strength.

Figure 22 shows the average image for the fuel concentration at -20 CAD (10 CAD after the stratification injection) for case C. The distribution of signal strengths shows there was a clearly stratified charge, peaking in intensity near the location of the sparkplug. At this timing the concentration reached an equivalence ratio of 1.16 in the center and rapidly decreased from there to the value corresponding to the global air equivalence ratio of 1.55. This decline in concentration occurs within 200 pixels, which corresponds to 17 mm. This sharper gradient in concentration was due to the global concentration being lower for case C compared to case B and to the larger amount and later injection timing of the stratified charge. Later in the cycle the stratified charge was distributed over a larger area, and at -10 CAD the stratified charge had been somewhat consumed by the flame, as illustrated in figure 24. The remaining stratified charge near the cylinder wall displayed an air equivalence ratio of around 1.18.

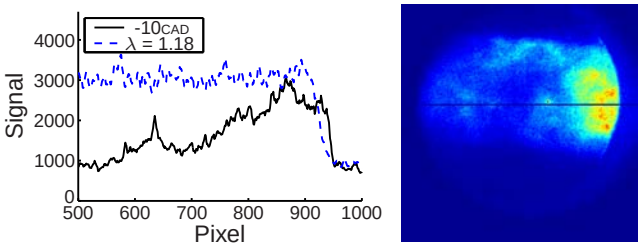

Figure 24: Average image for case C at -10 CAD, of LIF from the 3-pentanone fuel tracer and its signal strength.

LIF-FORMALDEHYDE

In figure 23 average images of the LIF from formaldehyde for case A can be seen. During the NVO the concentration of formaldehyde varied within the combustion chamber, and the same regions with low intensity as those observed in the LIF images of the fuel tracer could be seen at 330 and 340 CAD. After TDC the intensity of the formaldehyde signals increased, low temperature reactions occurred throughout almost the entire combustion chamber, and after the main injection mie-scattering could be seen in the spray. The formaldehyde intensity decreased as the fuel was mixed with the surrounding gas and remained weaker until the later part of the compression, when (as the temperature increased) the rates of low temperature chemistry again rose and were then superseded by high temperature reactions during the combustion. Thus, formaldehyde was present throughout the period between the pilot injection and the main combustion. During the main combustion the period in which the formaldehyde signals declined

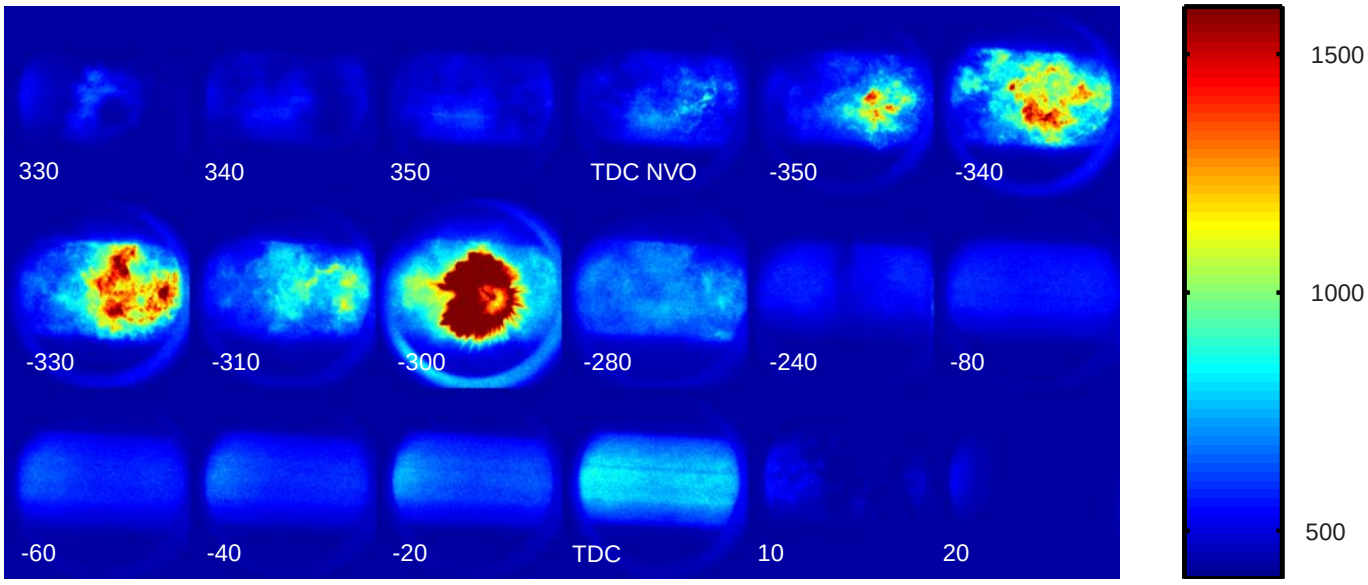

Figure 23: Average images (from 10 separate cycles) (and corresponding timings) for case A of LIF from formaldehyde.

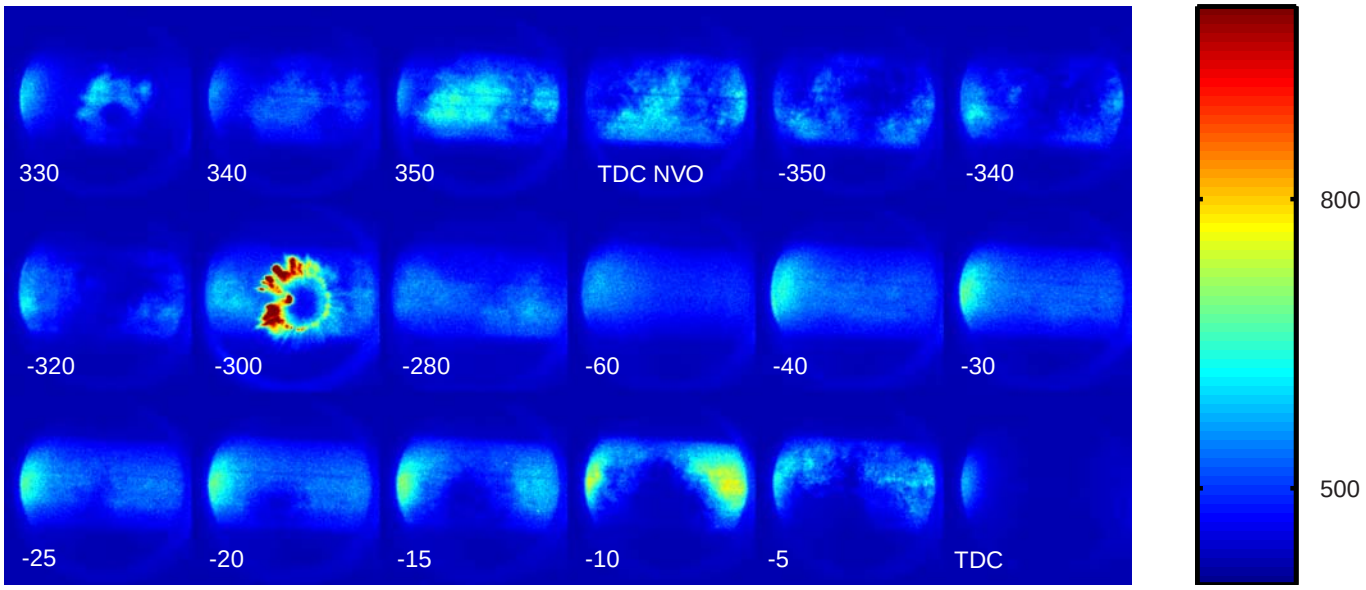

Figure 25: Average images (from 10 separate cycles) (and corresponding timings) for case B of LIF from formaldehyde.

was very short; within just 5 CAD the average images showed a transition from strong signals occupying the entire combustion chamber to weak signals at the periphery.

In figures 25 and 26 the signals from the formaldehyde within the combustion chamber can be seen for cases B and C, respectively. The amount of fuel injected in the pilot injection was lower for cases B and C than for case A, see table 8. This led to lower rates of low temperature reactions during the NVO, and consequently weaker formaldehyde signals see figure 23, figure 25 and 26.The rates of low temperature reactions prior to the compression were significantly lower for cases B and C, since less reactions occurred during the NVO and less heat was retained in the exhaust from the previous cycle due to the lower loads for cases B and C. During -310 CAD for case C any formaldehyde reactions could not be identified.

During the compression the SI combustion could easily be detected as the propagating flame consumed the formaldehyde, leaving an area with reduced signal strength, and later in the cycle the main combustion (HCCI) could be detected as the signal strength was reduced throughout the entire combustion chamber.

As for case A, the formaldehyde signals for cases B and C were weak in some regions after the pilot injection, partly because the fuel had not been evenly distributed and partly because of the high temperature reactions that occurred during the NVO.

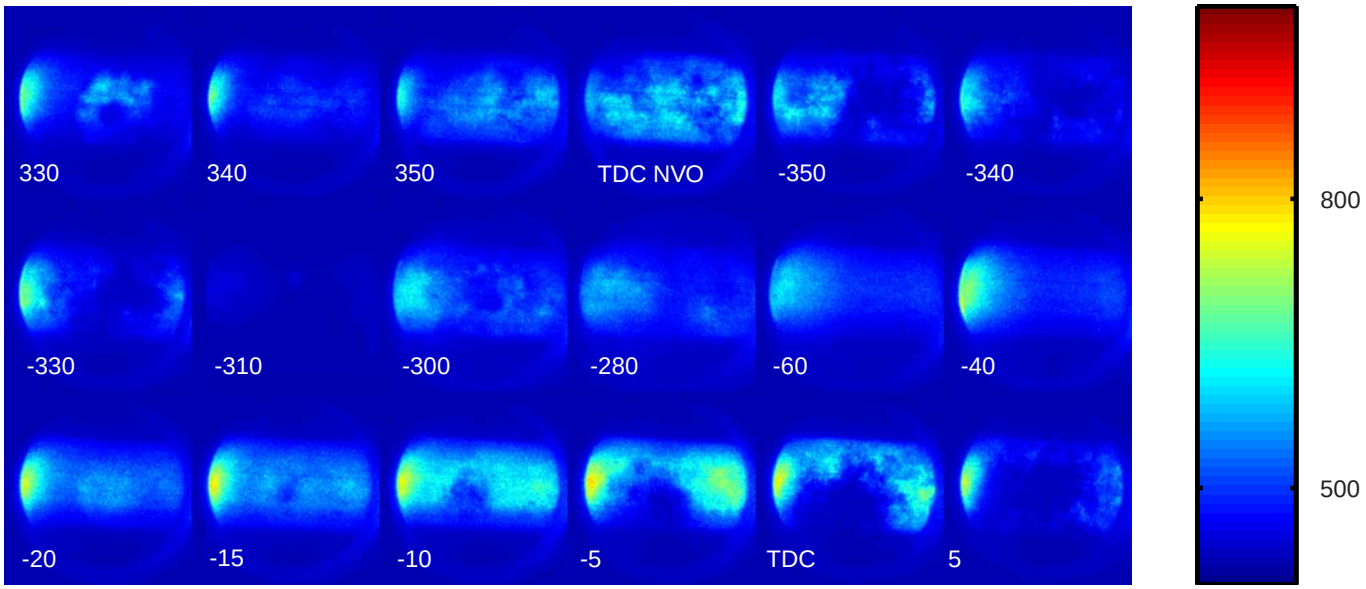

Figure 26: Average images (from 10 separate cycles) (and corresponding timings) for case C of LIF from formaldehyde.

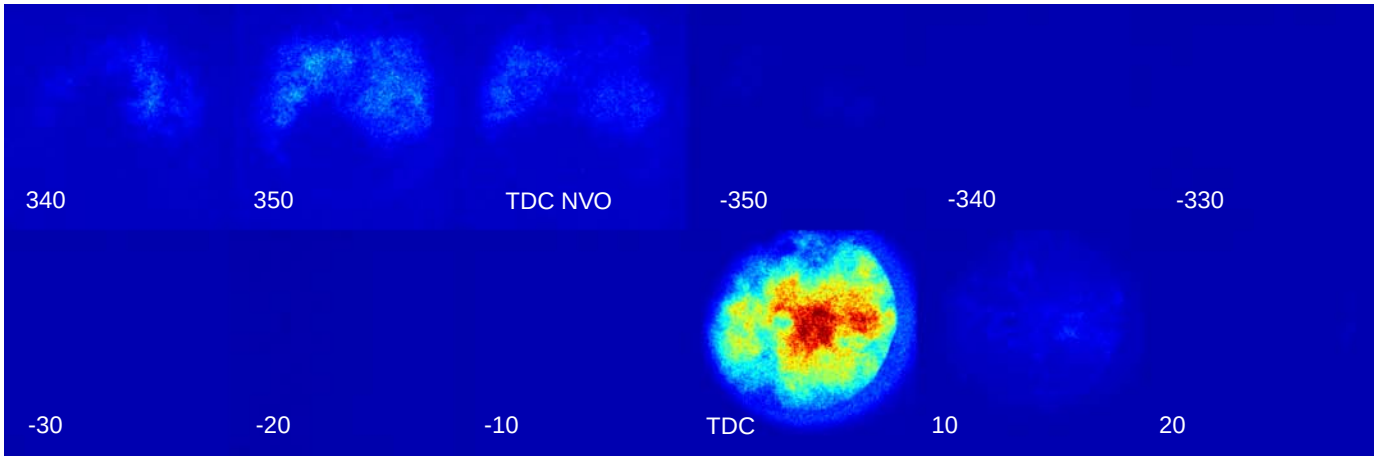

Figure 27: Average images (from 10 separate cycles) (and corresponding timings) for case A of the chemiluminescence of OH.

CHEMILUMINESCENCE OF OH

In figure 27 averaged images of the chemiluminescence from OH radicals can be seen. The chemiluminescence of OH is generally associated with reaction zones and in HCCI combustion the formation of OH radicals only occurs during the phase when the rate of heat release is rising, as seen in figure 14. However, during the NVO reactions were also observed and the location of the reactions corresponds to the location where the LIF from both formaldehyde and the fuel tracer declined. Thus, the reduced LIF signals were not due to lean regions caused by the fuel being unevenly distributed but to the fuel being consumed by the high temperature reactions that occurred during the NVO.

The chemiluminescence signal from the OH radicals in cases B and C can be seen figure 28 and figure 29, respectively. The presence of the initial flame front can easily be seen as an expanding region with high signal strength. When the SI stratified charge was used this evidence of high temperature reactions could be detected slightly before any rate of heat release in the pressure traces, just before -30 CAD for case B and just before -15 CAD for case C.

The spatial location of the chemiluminescence signal during the NVO correlate with regions that showed reduced signal strengths just after the pilot injections in the LIF images for both the fuel tracer and formaldehyde, as for case A, despite the fact that the chemiluminescence images were taken along the line of sight of the combustion and the fuel vapor and formaldehyde images were taken by LIF, and thus were restricted to the spatial location of the laser plane. This was probably possible because the images were acquired close to TDC and thus the depth of the images was small. The formaldehyde concentrations in cases B and C were lower than in case A, and the chemiluminescence signal showed a slight reduction at 350 CAD when the load was decreased, however at TDC during the NVO the signal was stronger. The total amount of high temperature reactions during the NVO was not decreased when the load was decreased by using the SI stratified charge.

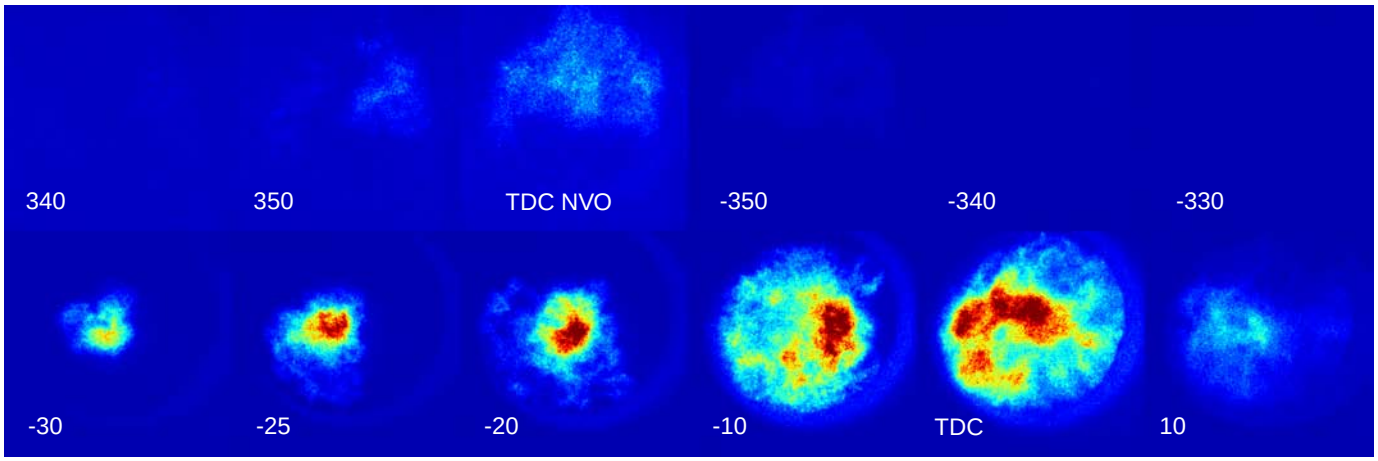

Figure 28: Average images (from 10 separate cycles) (and corresponding timings) for case B of the chemiluminescence of OH.

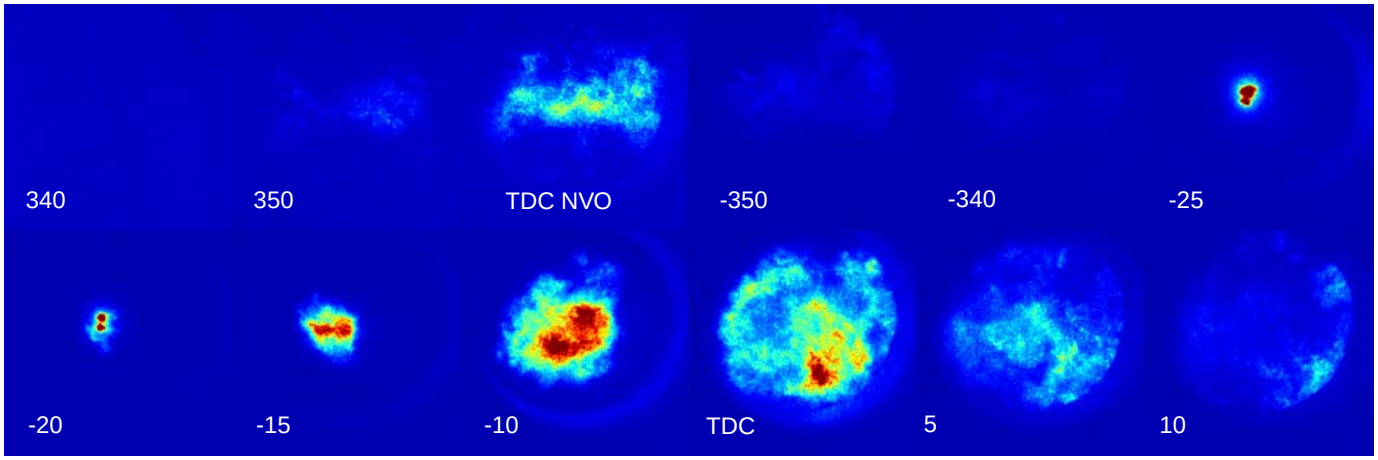

Figure 29: Average images (from 10 separate cycles) (and corresponding timings) for case C of the chemiluminescence of OH.

CONCLUSIONS

An experimental study of the effects of using a SI stratified charge in HCCI combustion using NVO was performed to investigate its potential for extending the operational range of HCCI to lower loads. Factorial designs were performed to identify parameters that influenced the combustion, and the results from the factorial designs led to the identification of three operation conditions that lowered the minimum load for HCCI combustion. These three operation conditions were optically studied and LIF was used to study the fuel vapor concentration and low temperature reactions and chemiluminescence of OH to locate the high temperature reactions.

When the load range of HCCI combustion was decreased by using a SI stratified charge, the concentrations of formaldehyde during the NVO, and between the NVO and compression, declined, indicating that the low temperature reactions were significantly reduced in these phases. However, the high temperature reactions (as indicated by the strength of the chemiluminescence signals) that occurred during the NVO did not decrease when the load was decreased.

The stratified charge was created by using an outward opening piezo electric injector, and images of LIF from the fuel tracer 3-pentanone indicate that an enriched region was created in the vicinity of the sparkplug, in which evidence of normal flame propagation prior to the HCCI combustion could seen. Local λ values for the stratified charge were estimated using LIF signals from the fuel tracer, calibrated with reference images for operating conditions with known, homogenous λ values.

The use of a SI stratified charge provided a means to control the combustion phasing, which could be substantially advanced, thereby allowing the load to be decreased. The injection and ignition timing of the stratified charge affected the degree of phasing. Varying the size of the pilot injection provided a further means to control the combustion phasing, but with significantly less impact than the use of the stratified charge. The HCCI operational range was expanded towards lower loads, from 2.7 bar IMEP to 1.5, without sacrificing indicated fuel consumption, combustion efficiency or low NO_X emissions.

ACKNOWLEDGEMENT

The authors wish to acknowledge STEM, the Swedish Energy Agency, for funding this work.

REFERENCES

1. Koopmans, L., Strömberg, E., Denbratt, I., "The Influence of PRF and Commercial Fuels with High Octane Number on the Auto-Ignition Timing of an Engine Operated in HCCI Combustion Mode with Negative Valve Overlap", SAE Technical Paper Series, SAE Paper 2004-01-1967.

2. Heywood, J. B. , "Internal Combustion Engines Fundamentals" 1988, Singapore: McGraw-Hill Inc.

3. Hultquist, A.,Christensen, M., Johansson, B., Ricther, M., Nygren, J., Hult, J., Aldén, M., "The HCCI Combustion Process in a Single Cycle - High-Speed Fuel Tracer LIF and Chemiluminescence Imaging", SAE Technical Paper Series, SAE Paper 2002-01-0424.

4. Lü, X-C., Chen, W., Huang, Z., "A fundamental study on the control of the HCCI combustion and emissions by fuel design concept combined with controllable EGR. Part 1. The basic characteristics of HCCI combustion", Fuel, Volume 84, Issue 9, Pages 1074-1083 (June 2005).

5. Hultquist, A., Christensen, M., Johansson, B., Franke, A., Aldén, M., "A Study of the Homogenous Charge Compression Ignition Combustion Process by Chemiluminescence Imaging", SAE Technical Paper Series, SAE Paper 1999-01-3680.

6. Wagner, U., Anca, R., Velji, A., Spicher, U., "An Experimental Study of Homogenous Charge Compression Ignition (HCCI) with Various Compression Ratios, Intake Air Temperatures and Fuels with Port and Direct Fuel Injection", SAE Technical Paper Series, SAE Paper 2003-01-2293.

7. Lü, X-C., Chen, W., Huang, Z., "A fundamental study on the control of the HCCI combustion and emissions by fuel design concept combined with controllable EGR. Part 2. Effect of operating conditions and EGR on HCCI combustion", Fuel, Volume 84, Issue 9, Pages 1084-1092 (June 2005).

8. Glassman, I. , "Combustion" 1996, third edition, United States of America: Academic Press Ltd.

9. Olsson, J., Tunestål, P., Johansson, B., "Closed-loop control of an HCCI engine", SAE Technical Paper Series, SAE Paper 2001-01-1031.

10. Marriott, C. D, Kong, S-C., Reitz, R. B., "Investigation of Hydrocarbon Emission from a Direct Injection-Gasoline Premixed Charge Compression Ignited Engine", SAE Technical Paper Series, SAE Paper 2002-01-0416.

11. Flowers, D., Aceves, S. M., Martinez-Frias, J., Smith, R., Au, M., Girard, J., Dibble, R., "Operation of a Four-Cylinder 1.9L Propane Fueled Homogenous Charge Compression Ignition Engine: Basic Operating Characteristics and Cylinder-to-Cylinder Effects", SAE Technical Paper Series, SAE Paper 2001-01-1895.

12. Fiveland, S. B., Agama, R., Christensen, M., Johansson, B., Hiltner, J., Maus, F., Assanis, D. N., "Experimental and Simulated Results Detailing the Sensitivity of Natural Gas HCCI Engines to Fuel Composition", SAE Technical Paper Series, SAE Paper 2001-01-3609.

13. Martinez-Frias, J., Aceves, S. M., Flowers, D., Smith, R. J., Dibble, R., "Thermal Charge Conditioning for Optimal HCCI Engine Operation", Journal of Energy Resources Technology, Volume 124, Pages 67-75 (March 2002).

14. Milovanovic, N., Blundell, D., Pearson, R., Turner, J., Chen, R., "Enlarging the Operational Range of a Gasoline HCCI Engine By Controlling the Coolant Temperature", SAE Technical Paper Series, SAE Paper 2005-01-0157.

15. Haraldsson, G., Tunestål, P., Johansson, B., Hyvönen, J., "HCCI Combustion Phasing in a Multi Cylinder Engine Using Variable Compression Ratio", SAE Technical Paper Series, SAE Paper 2002-01-2858.

16. Hyvönen, J., Haraldsson, Johansson, B., "Operating range in a Multi Cylinder HCCI engine using Variable Compression Ratio", JSAE Technical Paper Series,JSAE Paper 20030178.

17. Haraldsson, G., Tunestål, P., Johansson, "Transient Control of a Multi Cylinder HCCI Engine During a Drive Cycle", SAE Technical Paper Series, SAE Paper 2005-01-0153.

18. Christensen, M., Hultqvist, A., Johansson, B., "Demonstrating the Multi Fuel Capability of a Homogenous Charge Compression Ignition Engine with Variable Compression Ratio", SAE Technical Paper Series, SAE Paper 1999-01-3679.

19. Strandh, P., Bengtsson, J., Johansson, R., Tunestål, P., Johansson, B., "Cycle-to-Cycle Control of a Dual-Fuel HCCI Engine", SAE Technical Paper Series, SAE Paper 2004-01-0941.

20. Koopmans, L., Denbratt, I.,"A Four Stroke Camless Engine, Operated in Homogenous Charge Compression Ignition Mode with Commercial Gasoline", SAE Technical Paper Series, SAE Paper 2001-01-3610.

21. Koopmans, L., Backlund, O., Denbratt, I., "Cycle to Cycle Variations: Their Influence on Cycle Resolved Gas Temperature and Unburned Hydrocarbons from a Camless Gasoline Compression Ignition Engine", SAE Technical Paper Series, SAE Paper 2002-01-0110.

22. Koopmans, L., Ström, H., Lundgren, S., Backlund, O., Denbratt, I., "Demonstrating a SI-HCCI-SI Mode Change on a Volvo 5-Cylinder Electronic Valve Control Engine", SAE Technical Paper Series, SAE Paper 2003-01-0753.

23. Koopmans, L., Ogink, R., Denbratt, I., "Direct Gasoline Injection in the Negative Valve Overlap of a Homogenous Charge Compression Ignition Engine", JSAE Technical Paper Series, JSAE Paper 20030195.

24. Richter, M., Engström, J., Franke, A., Aldén, M., Hultquist, A., Johansson, B, "The Influence of Charge Inhomogeneity on the HCCI Combustion Process", SAE Technical Paper Series, SAE Paper 2000-01-2868.

25. Aroonrisopon, T., Werner, P., Waldman, J. O., Sohm, V., Foster, D. E., Morikawa, T, Iida, M., "Expanding the HCCI Operation With the Charge Stratification", SAE Technical Paper Series, SAE Paper 2004-01-1756.

26. Sjöberg, M., Dec, J. E., "Smoothing HCCI Heat-Release Rates Using Partial Fuel Stratification with Two-Stage Ignition Fuels", SAE Technical Paper Series, SAE Paper 2006-01-0629.

27. Berntsson, W. A., Denbratt, I., "HCCI Combustion Using Charge Stratification for Combustion Control", SAE Technical Paper Series, SAE Paper 2007-01-0210.

28. Berntsson, A., Denbratt, I., "Spark Assisted HCCI Combustion Using a Stratified Hydrogen Charge", SAE Technical Paper Series, SAE Paper 2005-24-039.

29. Berntsson, A., Denbratt, I., "HCCI Combustion Using a Spark Ignited Stratified Charge", JSAE Technical Paper Series, JSAE Paper 20065424.

30. Skogsberg, M., Dahlander, P., Denbratt, I., "Spray shape and atomization quality of an outward-opening piezo gasoline DI injector", SAE Technical Paper Series, SAE Paper 2007-01-1409.

31. Box, G. E. P. , Hunter, W. G., Hunter, J. S., "Statistics for experimenters" 1978, Canada: John Wiley & Sons, Inc.

32. Olofsson, J., Seyfried, H., Richter, M., Aldén, M., Vressner, A., Hultqvist, A., Johansson, B., Lombaert, K., "High-Speed LIF Imaging for Cycle-Resolved Formaldehyde Visualization in HCCI Combustion", SAE Technical Paper Series, SAE Paper 2005-01-0641.

33. Gaydon, A. G., "The Spectroscopy of Flames" 1974, Great Britain: Chapman and Hall, Second edition.

34. Koopmans, L., "HCCI Combustion by Retaining Residuals" 2005, PhD Thesis, Department of Applied Mechanics, Chalmers University, Sweden.

CONTACT

Corresponding author:
Andreas Berntsson
Chalmers University of Technology
Department of Applied Mechanics
Division of Combustion
Hörsalsvägen 7B SE-412 96
Göteborg Sweden
Email: andreas.berntsson@chalmers.se

DEFINITIONS, ACRONYMS, ABBREVATIONS

HCCI: Homogenous Charge Compression Ignition.

NVO: Negative valve overlap, the time between exhaust valve closing and intake valve opening.

SI: Spark Ignition.

EGR: Exhaust gas recirculation.

LIF: Laser induced fluorescence.

NO_X: Nitrogen Oxides.

PM: Particulate Matter.

CA50: Crank angle when 50% of the energy is burned.

HC: Hydrocarbon.

DISI: Direct injection spark ignition.

TDC: Top Dead Center.

CAD: Crank Angle Degree.

RoHR: Rate of heat release.

APPENDIX

POST PROCESSING

Post processing of the measurement data for the cylinder pressure traces and for the images was carried out using MatLab. The pressure trace were recorded using a Kistler 6061b piezo electric pressure transducer, with a sampling rate of 5 or 10 samples per CAD using an AVL Indimaster and an AVL Indicom and the pressure trace for 100 cycles were recorded for all the different cases. The data were converted to ASCII-format and imported to MatLab. The rate of heat release was calculated by assuming that the combustion process is close to an adiabatic isentropic process.

$$pV^{\gamma} = const \tag{2}$$

and

$$\gamma = \frac{c_p}{c_v} \tag{3}$$

Then the heat release can be written

$$\frac{dQ}{d\theta} = \frac{\gamma}{\gamma - 1} p \frac{dV}{d\theta} + \frac{1}{\gamma - 1} V \frac{dp}{d\theta} \tag{4}$$

if the convective heat transfer and the crevice volume is small (compared to the combustion chamber volume). CA50, rate of heat release and heat release were all based on this equation with the assumption that γ remained constant. Calibration of the heat release calculation was carried out with a motored pressure trace.

ACCURACY AND REPEATABILITY

Temperature, for instance intake air temperature, was measured with K-type thermocouples with an accu-

racy of +/- 2 K of the absolute temperature. However, for repetitive measurement the accuracy is far better (the K element is affected by aging, but at the temperatures and short measurement times used here these effects are negligible). Air pressure, temperature and relative humidity could influence the combustion due to changes in air density, so variations in these parameters from day to day could have small but perhaps not negligible effects. To minimize the effects of variations in conditions from day to day trends in the test matrix were continuously examined, and the test matrix order was randomized to further decrease the effect of changes in atmospheric conditions during the measurements. In addition, short term time trends, from the first to the last recorded cycle, were monitored (the time trends for CA50 were evaluated in MatLab for all operation conditions) to verify that averaging a number of cycles will give an average value for a fairly stable combustion and thus provide a representative value. For an optical engine small time trends will be present, since it cannot be used continuously and thus will not be able to thermally stabilize completely, but the optical engine was only used for short periods of time and any minor time trends during these measurements can be neglected. The Kistler 6061b piezo electric pressure transducer has high accuracy in terms of both linearity and shift sensitivity, and is believed to be sufficiently accurate when used in combination with the rate of heat release script in MatLab to capture the trends. If the pressure transducer is incorrectly phased to the location of the crankshaft, major discrepancies will result and thus the TDC location was calibrated.

For the exhaust gas analysis an ECO Physics CLD 700 ELht was used to determine the NO_X which was calibrated with a reference gas with a concentration of 90 ppm, the HC emission was measured by a J.U.M FID instrument and calibrated with Propane with a concentration of 2500 ppm and the CO was measured with a Maihak UNOR 611 instrument and calibrated with a reference gas with 0.45 $\%_{vol}$ in CO. The accuracy of the emissions measurements is also good, however for NO_X measurements the calibration was carried out at much greater values than presented here, and its accuracy at full scale is $\pm$ 0.5 %, so for pure HCCI operation the NO_X levels will be equal in size to the measurement accuracy. However, the trends for the NO_X values are valid. The λ was measured by using a Horiba MEXA-110λ and for all measurements lean mixtures were used, which in terms of measurement accuracy is not favorable but the conditions used were close enough to stoichiometric to be in the range where the measurement accuracy is acceptable ($\pm$ 0.5 % at λ=1 and $\pm$ 2 % at λ=1.6), so the values are good enough.

The operating conditions used to acquire the reference images for the LIF from the fuel tracer were chosen to be as identical as possible to those used in the optically studied cases, but with an homogenous mixture with known λ values. However, even if reference images are taken at identical pressures with similar masses the homogenous mixture will give a larger amount of absorption and a decreasing signal strength the further in in the combustion chamber would be achieved. The differences in load due to differences in lambda could also result in different amounts of O_2 and H_2O, which could in turn influence the amount of quenching (although similar amounts of fuel were injected in the pilot injections to reduce this effect). However, lambda values were strongly correlated with the signal strength, and differences in λ values of 0.02 could be detected by analyzing the signal intensity. Thus, it was possible to estimate fuel concentrations with sufficient accuracy for our purposes using reference images taken at the respective timings, but the local temperature will also contribute to a measurement error. Locally rich regions will experience higher amount of evaporation and thus those areas will be colder and when images with charge stratification were compared to reference images with a homogenous air fuel mixture the local temperature would result in an measurement error. The rich regions would probably be richer than what is indicated when they were compared to reference images. The signal strengths observed in the LIF fuel tracer images were highly dependent on the condition and settings for the equipment, so any differences in the shape of the laser plane, intensity or wear of the dichorit mirrors would influence the results. The images must be taken during the same measurement campaign in order to make valid comparisons between images. The laser intensity was always measured before any images were taken and all repetitions were evaluated in MatLab to verify that no incorrect images were included when the images were averaged.

The Vaidya bands correspond to the HCO reaction and intensity peaks at wavelengths of 301, 311, 319 and 330 nm [33], which will pass through the filter that was used for the chemiluminescence study. However, the emission from the OH reaction is one of the strongest features of most flame spectra [33] and is here considered to be the dominant one. However, the aim of the study of the chemiluminescence of the OH radical was to locate the high temperature reaction and the HCO will also be present during the high temperature reaction and thus not affect this aim.

Overall, the authors believe that the quality of the measurement equipment and the post processing of the data is sufficiently high to correctly capture trends caused by the SI stratified charge in a HCCI engine.

Paper V

LIF imaging of OH during the Negative Valve Overlap of a HCCI Combustion Engine

Andreas William Berntsson, Mats Andersson and Ingemar Denbratt

Proceedings of The Spark Ignition Engine of the Future Conference - SIA

LIF imaging of OH during the Negative Valve Overlap of a HCCI Combustion Engine

A. W. Berntsson[1], M. Andersson[1], D. Dahl[1], I. Denbratt[1]

1: Chalmers University of Technology, Hörsalsvägen 7B SE 412 96 Göteborg Sweden

Abstract: Future requirements for emission reduction from combustion engines in ground vehicles might be met by using the HCCI combustion concept. In this concept a more or less homogenous air fuel mixture is compressed to auto-ignition. This gives a good fuel economy compared to a normal SI engine and it has a positive impact on exhaust emissions. In the study presented here negative valve overlap (NVO) was used to initiate HCCI combustion by increasing the exhaust gas recirculation (EGR) and thus retaining sufficient thermal energy to reach auto-ignition temperatures, and raising the temperature during the NVO sufficiently to allow reactions to occur when a pilot injection was made prior to the NVO. The focus of the investigation was on the resulting high temperature reactions.

Since OH radicals are associated with high temperature reactions, the reactions were followed by monitoring planar laser-induced fluorescence (PLIF) of OH, using a dye laser and an intensified LaVision Dynamight camera. The presence of OH radicals detected during the negative valve overlap indicates that high temperature reactions do occur in the highly diluted environment of the trapped exhaust gases during the NVO. Reactions were identified from 20 CAD prior to TDC (during the NVO) and to around 60 CAD after TDC, with the intensity peak at about TDC.

Keywords: HCCI, NVO, OH LIF

1. Introduction

Future requirements to reduce exhaust emissions and fuel consumption are prompting the development of more advanced combustion concepts. One such concept is Homogeneous Charge Compression Ignition, HCCI, in which the combustion is controlled by chemical kinetics [1], and it releases heat more rapidly than in normal flame front combustion. In the ideal air standard SI cycle the combustion occurs at constant volume and this cycle is therefore the most efficient of the ideal cycles [2]. However, the rapid heat release of HCCI combustion and its ability to burn lean mixtures, thereby reducing pump, exhaust and cooling losses due to less throttled operation results in greatly improved efficiency compared to SI combustion [3]. The lean homogenous mixture leads to low NO_X and PM emissions [4]. Cycle-to-cycle variations are also minor because the combustion occurs in a distributed fashion in many places simultaneously [5].

However, there are challenges associated with the HCCI concept that must be overcome before it can be commercially applied, notably ways must be found to control ignition timing [6], expand its limited operating range [4] and limit the rate of heat release [7]. Cylinder-to-cylinder variations can also cause problems in HCCI engines [4], since the temperature can vary between the different cylinders and the ignition delay is highly dependent on the mixture temperature [8].

Combustion phasing is one of the crucial parameters to control in HCCI combustion and the timing when 50 % of the energy is combusted, CA50, is a good indicator of the phasing of the combustion process [9]. The ability to rapidly control combustion phasing is especially important during transients.

There are numerous solutions to the challenges associated with combustion control. Adjusting the inlet air temperature by heating the incoming air with air heaters [10-13] or by varying the coolant temperature [14] are some examples. However, thermal control of the combustion phasing has the drawback that the thermal inertia of the associated engine parts usually limits the transient response time. Another way to influence the charge temperature, and thus control the combustion phasing, is to adjust the compression ratio. Increasing the compression ratio will increase the pressure, which will decrease the auto-ignition temperature and increase the charge temperature [8]. Geometrically variable compression ratio have also been used to control HCCI combustion by several authors [6, 15-18], but it is difficult to find a mechanism that is fast enough to cope with real vehicle transients.

Further factors that play important roles in the timing of auto-ignition are the properties of the fuel, since the ignition delay of different fuels at given pressures and temperature varies dramatically. For this reason, mixtures of two fuels with contrasting octane

numbers and ignition temperatures (iso-octane and n-heptane or ethanol and n-heptane) that have appropriate ignition temperatures to allow correct phasing of the combustion have been used in several studies [17, 19].

The ability to create stratified charges in DI engines also allows various control methods to be adopted to increase the control of HCCI combustion. In [20-22] a stratified charge was created in which a flame (initiated by a spark) first propagated, and subsequently the combustion consisted of HCCI combustion. The initial SI combustion allowed the later HCCI combustion to be controlled. In [23, 24] the effect of the stratified charge *per se* was studied and it was found that charge stratification influenced the maximum rate of heat release as well as the combustion phasing for fuels which displayed low temperature reactions.

One promising way of initiating HCCI combustion is to retain large quantities of exhaust gases (EGR), thereby retaining sufficient thermal energy to initiate the HCCI combustion. Camshafts with short duration and low lift profiles, and negative valve overlap (NVO), have been used by Koopmans *et al* [25-28] for this purpose. Koopmans [25, 29] found that by increasing the NVO the auto-ignition timing could be advanced, due to the increased residual mass fraction, and thus one of the problems that must be overcome to extend the operating range of HCCI to lower loads (retarded combustion phasing) could be overcome. Furthermore, an injection prior to TDC in the NVO, here called a pilot injection, could influence the combustion phasing if the ratio between the pilot and main injection (injected after TDC in the NVO) was varied, as corroborated by several authors [28, 29]. Previous studies have found that during the NVO large amounts of formaldehyde can be formed [24], and high temperature reactions have also been manifested in the form of OH chemiluminescence.

The study presented here focused on the high temperature reactions (detected by monitoring the associated OH radicals) that occurred during the NVO in a spark-assisted HCCI engine operated with short duration and low lift camshafts. Planar laser-induced fluorescence (PLIF) of OH was used to determine the concentration and location of the OH since it is difficult to study the high temperature reactions by solely studying pressure traces, and thus optical techniques were required to detect them. This was performed for different operation condition that used pilot injections prior to the TDC during the NVO. In addition the effects of varying the injection parameters on the performance parameters of a multi-cylinder engine were analyzed and compared to the optical engine results to confirm that phenomena and trends observed in the optical engine could be validly compared to those that occur in traditional engines.

2. Experimental apparatus

The optical experiments were carried out in an AVL optical engine, and parameters of a multi-cylinder engine with no optical access were examined at several of the same operation points to confirm that the behavior observed in the optical engine was similar to that of more traditional engines. Furthermore, several operating variables were varied to confirm that trends reported in the literature were replicated in this study, and thus that the results obtained could be validly compared to findings reported by other authors using different engines (optical or traditional).

2.1 Multi-cylinder engine

Table 1: Specifications for the multi-cylinder engine.

Bore	84 mm
Stroke	96 mm
Swept volume	3192 cm^3
Compression ratio	11.5:1
Inlet air temperature	Ambient air
Fuel	RF-02-03, 99 RON
EOI Main	- 310 CAD
EOI Pilot	310 CAD
Camshaft duration intake	130 CAD
Camshaft duration exhaust	110 CAD
Intake valve lift	3 mm
Exhaust valve lift	2 mm
Spark-assist	- 30 CAD

The multi-cylinder engine used in the experiments was a 6 cylinder, 3.2 liter Volvo engine. Its specifications can be seen in table 1. Cam profile switching (CPS) and variable cam timing (VCT) were used on both the intake and exhaust. The CPS system allows two different cam profiles to be used: a low lift, short duration profile (permitting the high levels of internal EGR needed to initiate HCCI combustion) and a high lift, long duration profile (for use when operating the engine in SI mode). However, SI engine experiments were beyond the scope of this study. The VCT system allowed the cam timings, to be varied within ranges of 60 CAD on the intake cam and 40 CAD on the exhaust cam. The possible valve-timing options for the VCT/CPS system are illustrated in figure 1. Since only HCCI combustion using NVO was studied only the short lift and duration profiles were used. The engine had a fully programmable control unit controlled with a PC. The system made it possible to control spark timing, injection timing, injection pressure, injection amount, throttle and the VCT/CPS system in real time.

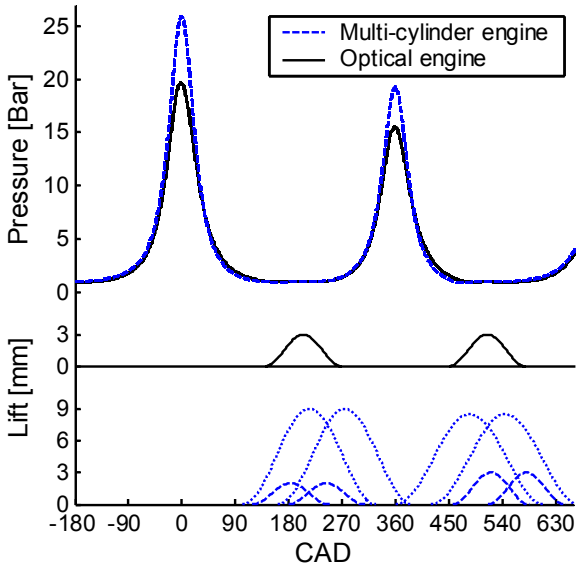

Figure 1: Motored pressure traces and valve lift profiles for the optical and multi-cylinder engine. Solid lines correspond to the optical engine and dashed lines to the multi-cylinder engine.

For the multi-cylinder engine experiments the fuel (a gasoline-like reference fuel) was supplied using a multi-hole direct injector, which was capable of multiple injections.

2.2 Optical engine

Table 2 Specifications for the optical engine.

Bore	83 mm
Stroke	90 mm
Swept volume	487 cm^3
Compression ratio	10:1
Inlet air temperature	90°C
Fuel	Iso-octane 85 %
	n-heptane 15 %
EOI Main	- 310 CAD
EOI Pilot	310 CAD
Camshaft duration	130 CAD
Valve lift	3 mm
Spark-assist	- 30 CAD

For the optical experiments a prototype cylinder head was used with similar geometry to that of the multi-cylinder engine. The engine parameters for the optical engine can be seen in table 2 and a schematic sketch of the layout of the optical setup can be seen in figure 2. The parameters for the optical engine and the multi-cylinder engine were not identical but similar, and since an optical engine has higher cooling losses than a metal engine the intake air was heated to make its behavior more similar to engines in real applications with similar settings. The intake air temperature was measured directly at the intake valve using a thermocouple and maintained at 90°C in all of the experiments, in contrast to the multi-cylinder engine, which was supplied with air at ambient temperature. A two-component fuel consisting of iso-octane and n-heptane was used (Table 2), to minimize disturbances since the fuel has similar combustion parameters to gasoline, but neither of the components fluoresce at the chosen excitation wavelength. The optical engine had an extended piston housing a mirror that provides, in conjunction with a quartz window in the piston crown, optical access to most of the combustion chamber from below. The optical engine was restricted to low engine speeds and since the Dye laser was pumped by a Nd:YAG laser, all measurements were made at 1200 rpm, which corresponds to 10 Hz.

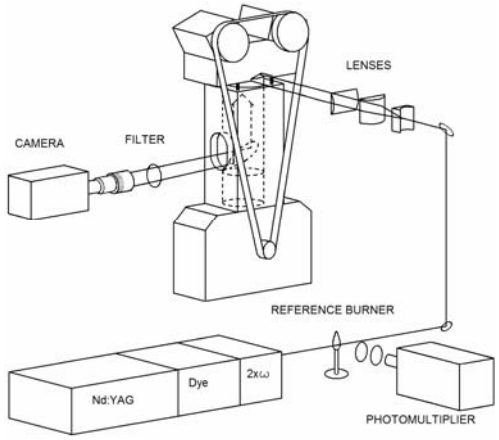

Figure 2: Schematic layout of the equipment used for the optical measurements.

The fuel was supplied using a multi-hole direct injector, which was capable of multiple injections. An AVL 4210 instrument controller was used to control the timings of the injections and the ignition in the optical engine, and a 35 mJ ignition coil to ensure that sufficient ignition energy was supplied by the sparkplug.

2.3 Optical setup

Excitation: Planar laser-induced fluorescence was used to detect and image the OH molecules. The Q1(6) transition in the A(v=1) - X(v=0) band at a wavelength of 283 nm was used for excitation. This transition was used since it provides high signal strength and relatively low dependence on rotational population changes due to temperature variations. The $Q_1(6)$ transition overlaps several weaker transitions in the Q_2, Q_{12} and Q_{21}-branches. This contributes to the signal strength, although these excitations are from low rotational states and their

relative strengths weaken somewhat at higher temperatures. An absorption spectrum was simulated with LIFBASE [30]. In order to avoid scattered laser light entering the detectors, fluorescence light from the A(v=0) - X(v=0) and A(v=1) - X(v=1) bands in the 300-320 nm-range was used for detection.

The tuneable UV-light was generated by a nanosecond dye laser pumped by the 2nd harmonic light of a Nd:YAG laser. The Rhodamine 6G dye provided light in the 560-600 nm wavelength range, the frequency of which was subsequently doubled to obtain the desired wavelength. The pulse energy of the UV light was about 12 mJ. In order to calibrate the wavelength of the laser, the beam could be sent through a propane flame and fluorescence from OH molecules in the flame was detected by a photomultiplier tube. Three cylindrical lasers were used to form a 50 mm wide horizontal laser plane passing 5 mm below the spark plug. A schematic layout of the set-up is shown in figure 2.

Detection: The LIF images of the OH molecule were taken using an intensified LaVision Dynamight camera, with a resolution of 1024x1024 operated by LaVision DaVis 6.2 software. However, all post-processing of the images was carried out using MatLab. To isolate the emission from the OH molecule a narrow-band filter with a center wavelength of 310 nm was used. The use of an intensifier led to the possibility to use short exposure times and thus any chemiluminescence from the OH radical captured by the camera becomes negligible, due to the far weaker signal of the chemiluminescence. Of resonance images were captured to evaluate this effect as well as to verify that any scattered laser light was eliminated by the filter. To control the timing of the camera an AVL 4210 timing unit was used. Both the gain and exposure time of 2.5 µs were kept constant in this study.

3. Results and discussion

3.1 Multi-cylinder engine results

As observed by Koopmans et. al. [28, 29], increasing the amount of fuel injected in pilot injections before TDC in the NVO (while keeping the total amount of fuel injected per combustion cycle constant) consistently advanced the combustion phasing (figure 3).

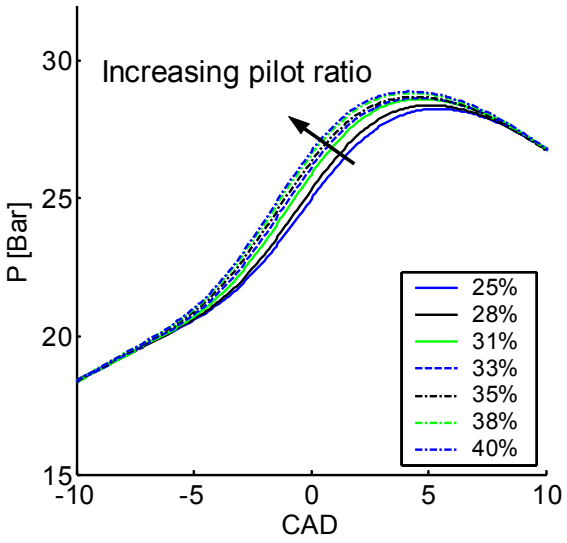

Figure 3: Pressure traces for various pilot to main ratios in the multi-cylinder engine.

In addition, the injection of fuel at this time led to reactions occurring during the NVO, as also seen in previous studies [20] under similar conditions, and in experiments with similar fuel and n-heptane by Koopmans *et. al.* [31]. Both of the cited studies indicated that formaldehyde was formed in large quantities during the NVO, and weak but detectable OH chemiluminescence signals were detected in [20] during the NVO. These reactions were believed to have been responsible for the observed advances in combustion phasing, the strong LIF signal from formaldehyde was attributed to the low temperature reactions that occurred, and the OH chemiluminescence signals were regarded as indications that high temperature reactions also occurred under the test conditions. However, since the chemiluminescence signals were weak and long exposure times were required (compared to the exposure times used for LIF measurements), there were considerable uncertainties regarding them. For instance, the Vaidya bands [32] caused by HCO can influence such chemiluminescence signals. Thus, to eliminate some of the uncertainties and to obtain a clearer understanding of the phenomena involved, higher-resolution measurements were needed, prompting the present study using PLIF to study the distribution of the OH radicals.

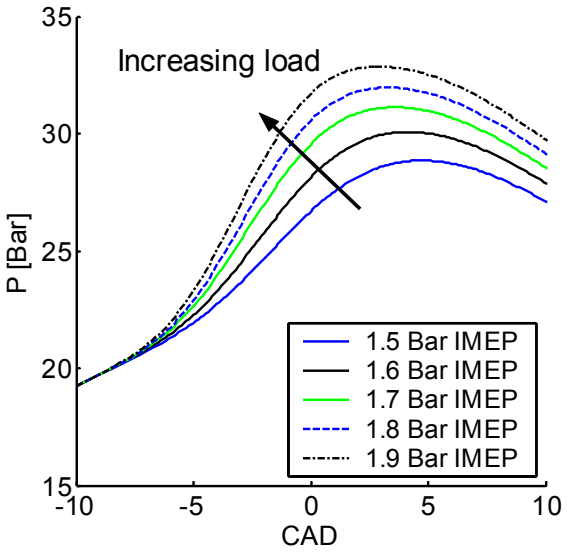

Figure 4: Pressure traces obtained at various loads in the multi-cylinder engine.

The trend of a load increase on cylinder pressure can be seen in figure 4, the amount of fuel injected as pilot injection was constant and only the main injection was increased. The results show the obvious trend off an increased peak pressure and a slight advanced combustion phasing.

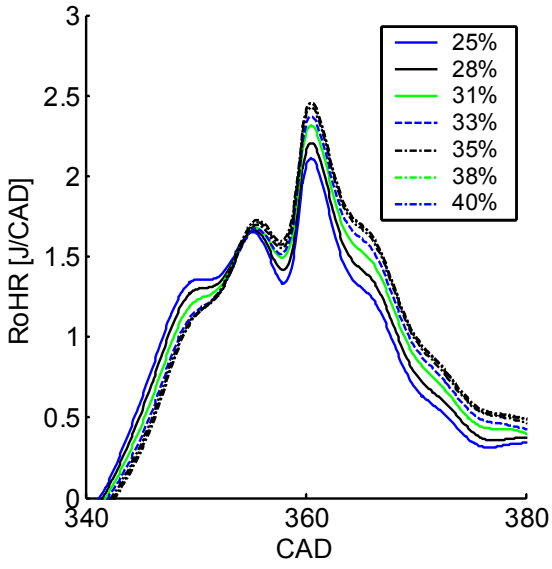

Figure 5: Rate of heat release traces resulting from reactions that occurred during the NVO with various pilot to main injections ratios (while keeping total amounts injected constant) in the multi-cylinder engine.

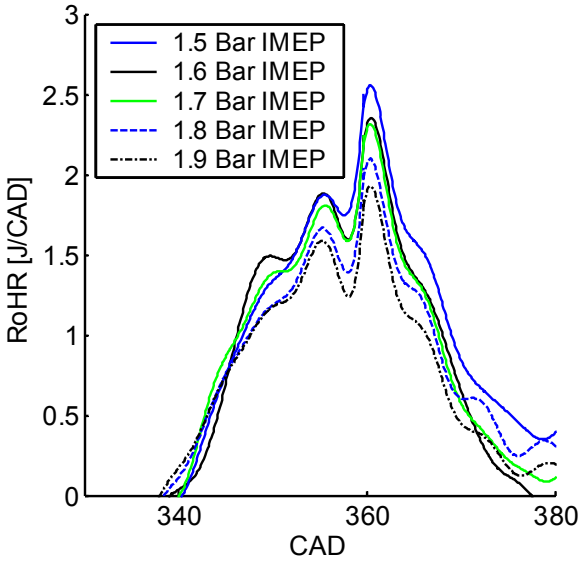

Figure 6: Rate of heat release traces resulting from the reactions that occurred during the NVO with various loads in the multi-cylinder engine.

The rates of heat release observed during the NVO can be seen in figures 5 and 6. The amounts of heat generated during the NVO were only small fractions of the heat generated during the main combustion, but they were sufficient to cause detectable increases in pressure, and thus significant amounts of heat-generating reactions did occur. Reactions started at around 340 CAD and continued for around 40 CAD. We attributed most of this heat generation to the relatively intense low temperature reactions noted in the previously mentioned optical experiments. However, the objective of this study was to investigate if this heat generation was due solely to the low temperature reactions or if high temperature reactions contributed to it, by examining whether or not any OH radicals were present during the time the heat was generated during the NVO.

3.2 Optical engine results

The multi-cylinder engine experiments showed that varying the selected parameters led to trends observed in the literature under various operating conditions, and for the optical experiments three different operating conditions (with different loads and pilot to main injection ratios, designated A, B and C here for convenience) were selected for further analysis of the combustion reactions by LIF of OH. As mentioned above, the intake air temperature was adjusted for the optical engine so that its behavior was similar to that of the multi-cylinder engine at similar settings. Pressure traces obtained at the three optically studied operational conditions can be seen in figure 7.

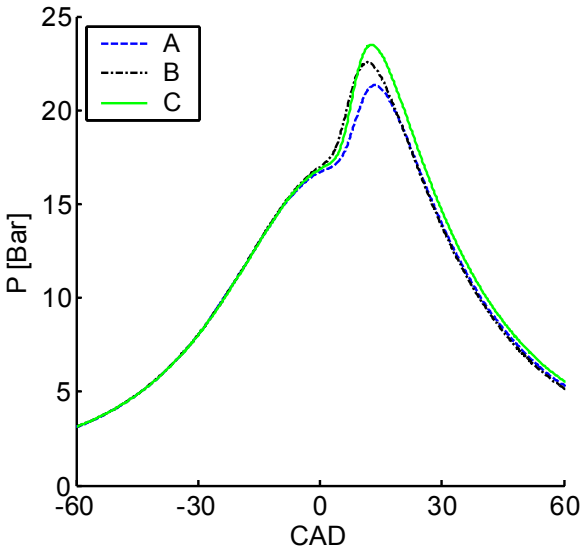

Figure 7: Pressure traces for the optically studied cases.

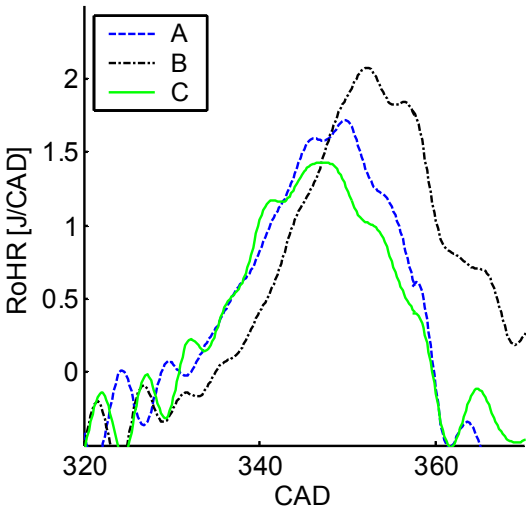

Figure 8: Rate of heat release traces during the NVO for the optically studied cases.

Rate of heat release traces for the three cases can be seen in figure 8. They show that heat-generating reactions occurred during the NVO at similar timings to those seen in the multi-cylinder engine, and both the durations and peak values were similar too, but the shapes of the curves obtained for the two engines were not completely identical. Thus, adjusting the temperature of the optical engine's intake air fulfilled its main purpose. There were however discrepancies between the engines during the main combustion, due to differences in their geometric parameters and heat losses, but these deviations were not relevant to this study, since the focus was on events during the NVO.

LIF signals from the OH radicals during the NVO can be seen in figure 9. The images presented here were averaged from 10 different filtered images. MatLab was used for all post-processing of the images, which involved filtering, averaging, threshold comparisons and intensity summation. Post-processing was essential, since LIF signals obtained from OH using dye lasers require high amounts of intensification, leading to high noise levels. Furthermore, post-processing was required to investigate the spatial distribution of the signal as well as its intensity. OH radicals were detected from 320 to 420 CAD, or from 40 CAD prior to TDC during the NVO to 60 CAD after it, but the first pronounced signals were observed at 340 CAD, and the first detectable LIF OH signals occurred ca. 10 CAD prior to the time evidence of reactions could be discerned

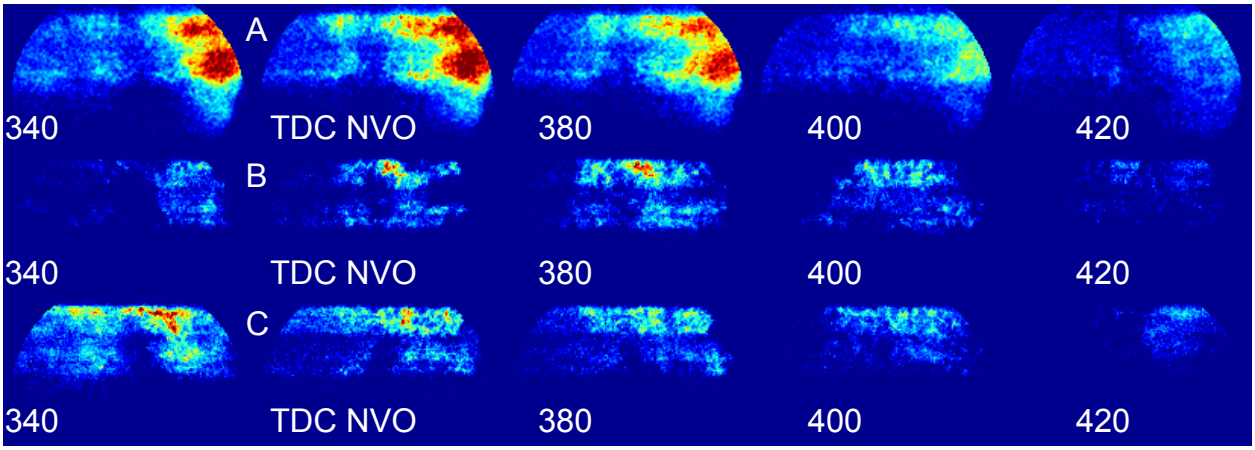

Figure 9: LIF images of OH for three operational conditions during the NVO.

in the pressure traces. These findings indicate that not only low temperature reactions (associated with formaldehyde formation) occurred during the NVO, but also high temperature reactions associated with highly reactive OH radicals. Thus, the assumption that previously observed chemiluminescence signals [20] were initiated by the formation OH appears to be valid. However, the LIF signals were present for longer times than the recorded chemiluminescence signals, since the LIF signals began with the initial formation of OH and continued as long as OH was present. Furthermore, the LIF signals lasted longer than the periods of heat generation noted in the pressure trace analysis, see figures 8 and 9. This was partly because LIF signals occurred not only during the formation of OH (which led to heat generation) but also when OH was present, and partly because the main causes of the heat generation were low temperature reactions. Furthermore, the threshold for detecting heat generation by pressure analysis was naturally higher than the threshold for detecting heat-generating reactions by LIF analysis.

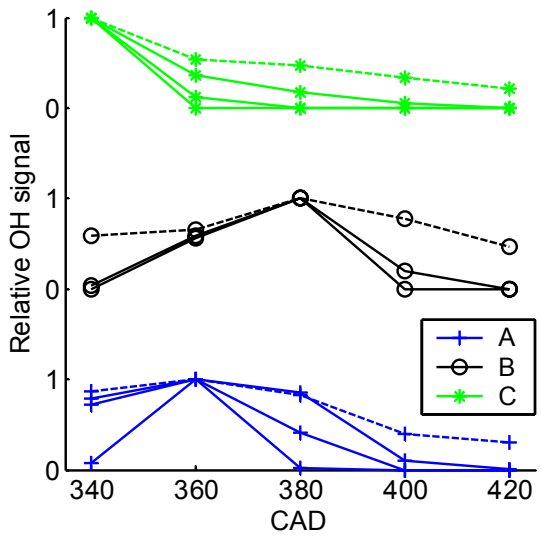

Figure 10: Relative OH signals obtained by comparing the intensity of the LIF images to threshold values (solid lines) or by summing the intensity at different timings.

Figure 10 provides more detailed information regarding the strengths of the signals resulting in the images presented in figure 9. The strengths of the signals in each pixel were converted to values exceeding various thresholds to map the OH distributions more precisely at each of the tested timings. The solid lines correspond to thresholds for weak, medium and strong OH signals and the dashed lines to summed intensities. The OH signals peaked between 340 and 380 CAD and the patterns were very similar, regardless of which of the thresholds or summed intensities was used. The timing of the intensity peak followed the phasing of the reactions that occurred during the NVO (cf. figures 8 and 10), i.e. the intensity peaked earlier in cases where the reactions appeared early, than in cases where the reactions where they appeared later.

4. Conclusion

An experimental study of a spark-assisted HCCI engine using NVO was performed to investigate the reactions occurring in the trapped residuals during NVO, especially the high temperature reactions, in an optical engine. Experiments with a multi-cylinder engine were also performed to confirm that the optical engine behaved similarly to a traditional one and that the engines followed trends reported in the literature. Patterns observed in the literature were replicated in both the optical engine and the multi-cylinder engine, thus results obtained with both of the engines could be validly compared with previous work.

Heat-generating reactions (lasting ca. 40 CAD) were noted to occur during the NVO when pressure trace analysis was performed for various operational conditions in both the optical and multi-cylinder engines. Just prior to detectable heat generation (by pressure trace analysis), OH radicals were identified by using LIF. The OH signals also lasted longer than the heat generation signals. This was mainly attributed to the main contributors to the heat generation being the low temperature reactions. However, the presence OH was detected in all of the studied operation conditions and thus if coexisted with the low temperature reactions.

5. Acknowledgement

The authors acknowledge the Swedish Energy Agency, STEM, for funding this work and Dr. Lucien Koopmans at Volvo Cars Corporation for supplying experimental equipment and support.

6. References

[1] Koopmans, L., Strömberg, E., Denbratt, I.: "*The Influence of PRF and Commercial Fuels with High Octane Number on the Auto-Ignition Timing of an Engine Operated in HCCI Combustion Mode with Negative Valve Overlap* ", SAE Technical Paper Series, SAE Paper 2004-01-1967.

[2] Heywood, J. B.: "*Internal Combustion Engines Fundamentals*", McGraw-Hill Inc., Singapore, 1988.

[3] Hultquist, A., Christensen, M., Johansson, B., Richter, M., Nygren, J., Hult, J., Aldén, M.: "*The*

HCCI Combustion Process in a Single Cycle - High-Speed Fuel Tracer LIF and Chemiluminescence Imaging", SAE Technical Paper Series, SAE Paper 2002-01-0424.

[4] Lü, X-C., Chen, W., Huang, Z.: "*A fundamental study on the control of the HCCI combustion and emissions by fuel design concept combined with controllable EGR. Part 1. The basic characteristics of HCCI combustion*", Fuel, Volume 84, Issue 9, Pages 1074-1083 (June 2005).

[5] Hultquist, A., Christensen, M., Johansson, B., Franke, A., Aldén, M.: "*A Study of the Homogenous Charge Compression Ignition Combustion Process by Chemiluminescence Imaging*", SAE Technical Paper Series, SAE Paper 1999-01- 3680.

[6] Wagner, U., Anca, R., Velji, A., Spicher, U.: "*An Experimental Study of Homogenous Charge Compression Ignition (HCCI) with Various Compression Ratios, Intake Air Temperatures and Fuels with Port and Direct Fuel Injection*", SAE Technical Paper Series, SAE Paper 2003-01- 2293.

[7] Lü, X-C., Chen, W., Huang, Z.: "*A fundamental study on the control of the HCCI combustion and emissions by fuel design concept combined with controllable EGR. Part 2. Effect of operating conditions and EGR on HCCI combustion*", Fuel, Volume 84, Issue 9, Pages 1084-1092 (June 2005).

[8] Glassman, I.: "*Combustion*", Academic Press Ltd., third edition, United States of America, 1996.

[9] Olsson, J., Tunestål, P., Johansson, B.: "*Closed loop control of an HCCI engine*", SAE Technical Paper Series, SAE Paper 2001-01-1031.

[10] Marriott, C. D, Kong, S-C., Reitz, R. B.: "*Investigation of Hydrocarbon Emissions from a Direct Injection-Gasoline Premixed Charge Compression Ignited Engine*", SAE Technical Paper Series, SAE Paper 2002-01-0419.

[11] Flowers, D., Aceves, S. M., Martinez-Frias, J., Smith, R., Au, M., Girard, J., Dibble, R.: "*Operation of a Four-Cylinder 1.9L Propane Fueled Homogenous Charge Compression Ignition Engine: Basic Operating Characteristics and Cylinder-to-Cylinder Effects*", SAE Technical Paper Series, SAE Paper 2001-01-1895.

[12] Fiveland, S. B., Agama, R., Christensen, M., Johansson, B., Hiltner, J., Maus, F., Assanis, D. N.: "*Experimental and Simulated Results Detailing the Sensitivity of Natural Gas HCCI Engines to Fuel Composition*", SAE Technical Paper Series, SAE Paper 2001-01-3609.

[13] Martinez-Frias, J., Aceves, S. M., Flowers, D., Smith, R. J., Dibble, R.: "*Thermal Charge Conditioning for Optimal HCCI Engine Operation* ", Journal of Energy Resources Technology, Volume 124, Pages 67-75 (March 2002).

[14] Milovanovic, N., Blundell, D., Pearson, R., Turner, J., Chen, R.: "*Enlarging the Operational Range of a Gasoline HCCI Engine By Controlling the Coolant Temperature*", SAE Technical Paper Series, SAE Paper 2005-01-0157.

[15] Haraldsson, G., Tunestål, P., Johansson, B., Hyvönen, J.: "*HCCI Combustion Phasing in a Multi Cylinder Engine Using Variable Compression Ratio*", SAE Technical Paper Series, SAE Paper 2002-01-2858.

[16] Hyvönen, J., Haraldsson, Johansson, B.: "*Operating range in a Multi Cylinder HCCI engine using Variable Compression Ratio*", JSAE Technical Paper Series, JSAE Paper 20030178.

[17] Haraldsson, G., Tunestål, P., Johansson, B.: "*Transient Control of a Multi Cylinder HCCI Engine During a Drive Cycle*", SAE Technical Paper Series, SAE Paper 2005-01-0153.

[18] Christensen, M., Hultqvist, A., Johansson, B.: "*Demonstrating the Multi Fuel Capability of a Homogenous Charge Compression Ignition Engine with Variable Compression Ratio*", SAE Technical Paper Series, SAE Paper 1999-01-3679.

[19] Strandh, P., Bengtsson, J., Johansson, R., Tunestål, P., Johansson, B.: "*Cycle-to-Cycle Control of a Dual-Fuel HCCI Engine*", SAE Technical Paper Series, SAE Paper 2004-01-0941.

[20] Berntsson, W. A., Denbratt, I.: "*Optical study of HCCI Combustion using NVO and an SI Stratified Charge*", SAE Technical Paper Series, SAE Paper 2007-24-0012.

[21] Berntsson, A., Denbratt, I.: "*Spark Assisted HCCI Combustion Using a Stratified Hydrogen Charge*", SAE Technical Paper Series, SAE Paper 2005-24-039.

[22] Berntsson, A., Denbratt, I.: "*HCCI Combustion Using a Spark Ignited Stratified Charge*", JSAE Technical Paper Series, JSAE Paper 20065424.

[23] Berntsson, W. A., Denbratt, I.: "*HCCI Combustion Using Charge Stratification for Combustion Control*", SAE Technical Paper Series, SAE Paper 2007-01-0210.

[24] Sjöberg, M., Dec, J. E.: "*Smoothing HCCI Heat-Release Rates Using Partial Fuel Stratification with Two-Stage Ignition Fuels*", SAE Technical Paper Series, SAE Paper 2006-01-0629.

[25] Koopmans, L., Denbratt, I.: "*A Four Stroke Camless Engine, Operated in Homogenous Charge Compression Ignition Mode with Commercial Gasoline*", SAE Technical Paper Series, SAE Paper 2001-01-3610.

[26] Koopmans, L., Backlund, O., Denbratt, I.: "*Cycle to Cycle Variations: Their Influence on Cycle Resolved Gas Temperature and Unburned Hydrocarbons from a Camless Gasoline Compression Ignition Engine*", SAE Technical Paper Series, SAE Paper 2002-01-0110.

[27] Koopmans, L., Ström, H., Lundgren, S., Backlund, O., Denbratt, I.: "*Demonstrating a SI-HCCI-SI Mode Change on a Volvo 5-Cylinder Electronic Valve Control Engine*", SAE Technical Paper Series, SAE Paper 2003-01-0753.

[28] Koopmans, L., Ogink, R., Denbratt, I.: "*Direct Gasoline Injection in the Negative Valve Overlap of a Homogenous Charge Compression Ignition Engine*", JSAE Technical Paper Series, JSAE Paper 20030195.

[29] Koopmans, L.: "*HCCI Combustion by Retaining Residuals*", PhD Thesis, Department of Applied Mechanics, Chalmers University, Sweden, 2005.

[30] Luque, J., Crosley, D.R.: "*LIFBASE: Database and Spectral Simulation Program (Version 1.45)*", SRI International Report MP98-021, 1998.

[31] Koopmans, L., Wallesten, J., Ogink, R., Denbratt, I.: "*Location of the First Auto-Ignition Sites for Two HCCI Systems in a Direct Injection Engine*", SAE Technical Paper Series, SAE Paper 2004-01-0564.

[32] Gaydon, A. G.: "*The Spectroscopy of Flames*", Chapman and Hall, Second edition.

8. Glossary

HCCI: Homogenous Charge Compression Ignition
LIF: Laser-Induced Fluorescence
NVO: Negative Valve Overlap
EGR: Exhaust Gas Recirculation
SI: Spark Ignited
OH: Hydroxyl
PLIF: Planar Laser-Induced Fluorescence
NO_X: Nitrogen Oxides
PM: Particulate Matter
CA50: Crank angle when 50% of the energy is burned
DI: Direct Injection
TDC: Top Dead Center
CAD: Crank Angle Degree
CPS: Cam Profile Switching
VCT: Variable Cam Timing
P: Pressure
EOI: End of Injection
Nd:YAG: Neodymium: Yttrium Aluminum Garnet
IMEP: Indicated Mean Effective Pressure
COV: Coefficient Of Variation
RoHR: Rate of Heat Release

Paper VI

A LIF-study of OH in the Negative Valve Overlap of a Spark-assisted HCCI Combustion Engine

Andreas William Berntsson, Mats Andersson, Daniel Dahl and Ingemar Denbratt

SAE Technical Paper

SAE TECHNICAL PAPER SERIES

2008-01-0037

A LIF-study of OH in the Negative Valve Overlap of a Spark-assisted HCCI Combustion Engine

Andreas W. Berntsson, Mats Andersson, Daniel Dahl and Ingemar Denbratt
Chalmers University of Technology, Sweden

Reprinted From: Homogeneous Charge Compression Ignition Engines, 2008 (SP-2182)

ISBN 978-0-7680-1639-0

9 780768 016390

**2008 World Congress
Detroit, Michigan
April 14-17, 2008**

SAE International™

400 Commonwealth Drive, Warrendale, PA 15096-0001 U.S.A. Tel: (724) 776-4841 Fax: (724) 776-0790 Web: www.sae.org

All SAE papers, standards, and selected books are abstracted and indexed in the Global Mobility Database.

ISSN 0148-7191

Printed in USA

2008-01-0037

A LIF-study of OH in the Negative Valve Overlap of a Spark-assisted HCCI Combustion Engine

Andreas W. Berntsson, Mats Andersson, Daniel Dahl and Ingemar Denbratt
Chalmers University of Technology, Sweden

ABSTRACT

Future requirements for emission reduction from combustion engines in ground vehicles might be met by using the HCCI combustion concept. In this study, negative valve overlap (NVO) and low lift, short duration, camshaft profiles, were used to initiate HCCI combustion by increasing the internal exhaust gas recirculation (EGR) and thus retaining sufficient thermal energy for chemical reactions to occur when a pilot injection was introduced prior to TDC, during the NVO.

One of the crucial parameters to control in HCCI combustion is the combustion phasing and one way of doing this is to vary the relative ratio of fuel injected in pilot and main injections. The combustion phasing is also influenced by the total amount of fuel supplied to the engine, the combustion phasing is thus affected when the load is changed. This study focuses on the reactions that occur in the highly diluted environment during the NVO when load and pilot to main ratio are changed.

To monitor these reactions, planar laser-induced fluorescence (PLIF) from OH radicals was analyzed in a series of experiments with an optical single-cylinder engine, since these radicals are known to be associated with high temperature reactions. A series of experiments was also performed using a multi-cylinder engine with varied NVO timings, which showed that the combustion phasing was influenced by both the ratio between the pilot and main injection amounts and the total amount of fuel. Data acquired from corresponding optical analysis showed the occurrence of OH radicals (and thus high temperature reactions) during the NVO in all tested operating conditions. The results also indicate that the extent of the high temperature reactions was influenced by both varied parameters, since decreasing the relative amount of the pilot injection and/or increasing the total amount of fuel led to larger amounts of OH radicals.

INTRODUCTION

Future requirements to reduce exhaust emissions and fuel consumption are prompting the development of more advanced combustion concepts. One promising concept is Homogeneous Charge Compression Ignition, HCCI. In an HCCI engine the combustion is controlled by chemical kinetics [1], and heat is released more rapidly than in normal flame front combustion. In the ideal air standard SI cycle the combustion occurs at constant volume and this cycle is therefore the most efficient of the ideal cycles [2]. The rapid heat release of HCCI combustion and its ability to burn lean mixtures, thereby reducing pump, exhaust and cooling losses due to less throttled operation results in greatly improved efficiency compared to SI combustion [3]. HCCI combustion yields low NO_X and PM emissions [4] as a result of the lean homogenous mixture. Cycle-to-cycle variations are also minor because the combustion occurs in a distributed fashion in many places simultaneously [5].

However, several challenges associated with the HCCI concept must be overcome before it can be commercially applied, notably ways must be found to control ignition timing [6], expand its limited operating range [4] and limit the rate of heat release [7]. Cylinder-to-cylinder variations can also cause problems in HCCI engines [4], since the temperature can vary between the different cylinders and the ignition delay is highly dependent on the mixture temperature [8].

Combustion phasing is one of the crucial parameters to control in HCCI combustion and the timing when 50 % of the fuel is combusted, CA50, is a good indicator of the phasing of the combustion process [2]. The ability to rapidly control combustion phasing is especially important during transients.

There are numerous solutions to the challenges associated with combustion control. One is to adjust the

inlet air temperature by heating the incoming air with air heaters [9-12] or by varying the coolant temperature [13]. However, thermal control of the combustion phasing has the drawback that the thermal inertia of the associated engine parts usually limits the transient response time. Another way to influence the charge temperature, and thus control the combustion phasing, is to adjust the compression ratio. Increasing the compression ratio will increase the pressure, which will decrease the auto-ignition temperature and increase the charge temperature [8]. Geometrically variable compression ratio have been used to control HCCI combustion by several authors [6, 14-17], but it is difficult to find a mechanism that is fast enough to cope with real vehicle transients.

Further factors that play important roles in the timing of auto-ignition are the properties of the fuel, since the ignition delay of different fuels at given pressures and temperatures vary dramatically. For this reason, mixtures of two fuels with contrasting octane numbers and ignition temperatures (iso-octane and n-heptane or ethanol and n-heptane) that have appropriate ignition temperatures to allow correct phasing of the combustion have been used in several studies [16, 18].

The ability to create charge stratification in DI engines allows various control methods to be adopted to increase the control of HCCI combustion, in [19- 21] a hybrid combustion mode has been described in which spark-initiated combustion of a stratified charge is followed by HCCI combustion. The initial SI combustion allowed the later HCCI combustion to be controlled. In [22, 23] the effect of the stratified charge per se was studied, and the charge stratification was shown to affect the maximum rate of heat release as well as combustion phasing for fuels which displayed low temperature reactions.

One promising way of initiating HCCI combustion is to retain large quantities of exhaust gases (EGR), thereby retaining sufficient thermal energy to initiate the HCCI combustion. Short duration and low valve lift profiles, and negative valve overlap (NVO), have been used for this purpose by Koopmans *et al* [24-27]. Koopmans [24, 28] found that by increasing the NVO the auto-ignition timing could be advanced, due to the increased residual mass fraction, and thus one of the problems that must be overcome to extend the operating range of HCCI to lower loads (retarded combustion phasing) could be overcome. Furthermore, an injection prior to TDC in the NVO, here called a pilot injection, could influence the combustion phasing if the ratio between the pilot and main (injected after TDC in the NVO) injections was varied, as found by various authors [27, 28]. Previous studies have detected large amounts of formaldehyde during the NVO [19], and evidence of high temperature reactions, manifested by OH chemiluminescence. For instance, chemiluminescence of OH was found between 20 CAD prior to TDC (during the NVO) and to TDC, with their intensity peaking at TDC.

The study presented here focused on the high temperature reactions that occurred during the NVO in a spark-assisted HCCI engine operated with short duration and low lift camshafts. The effects of varying the ratio between pilot and main injection amounts, and the total amount of fuel injected, on the high temperature reactions were studied in an optical engine, and the high temperature reactions have been associated with the presence of OH radicals. Planar laser-induced fluorescence (PLIF) of OH was used to determine its intensity and location since it is difficult to study the high temperature reactions by solely studying pressure traces, and thus optical studies were required to detect them. Furthermore, the effects of different injection parameters on engine behavior were studied in both a multi-cylinder engine and the optical single cylinder engine to confirm that the behavior observed in the optical engine could be validly compared to that of a normal engine, and to explain the observed trends, especially the advances in combustion phasing associated with increases in the relative amount of fuel injected in the pilot injection. Furthermore, to verify that the behavior observed in previous studies using NVO was replicated, and that the responses and trends observed in this study could be validly compared to those.

EXPERIMENTAL APPARATUS

Both engines in the experiments used NVO which led to compression of the trapped residuals during the NVO and the temperature during the NVO was increased to such a degree that reactions could occur when a pilot injection was injected prior to the TDC during the NVO as seen in previous studies [19]. Illustrative injection timings, valve lift profiles and motored pressure traces obtained when conventional valve timing and NVO were used can be seen in figure 1, 0 CAD was set as TDC in the main combustion and 360 CAD as TDC during the NVO.

The multi cylinder engine used for the experiments was a 6 cylinder, 3.2 liter Volvo engine. The engine was equipped with cam profile switching (CPS) and variable cam timing (VCT) on both intake and exhaust. The CPS system made it possible to have two different cam profiles, one with low lift and one with high lift. The VCT system made it possible to phase the opening and closing times of the valves 60 CAD on the intake side and 40 CAD on the exhaust side. The possible valve-timing options for the VCT/CPS system are illustrated in figure 2. However, this study was restricted to an analysis of HCCI combustion using NVO, and thus only the short lift and duration profiles were used. The engine had a fully

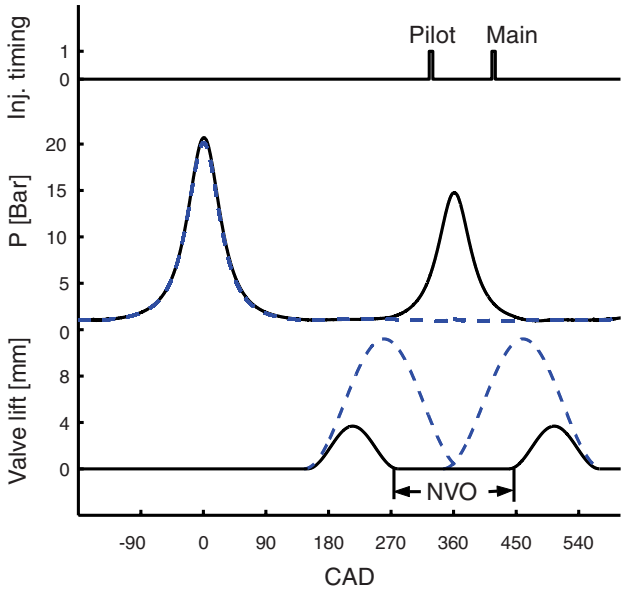

Figure 1: Valve lift profiles, injection timings, and motored pressure traces obtained with both conventional valve timing (dashed lines) and NVO (solid lines) in the optical engine.

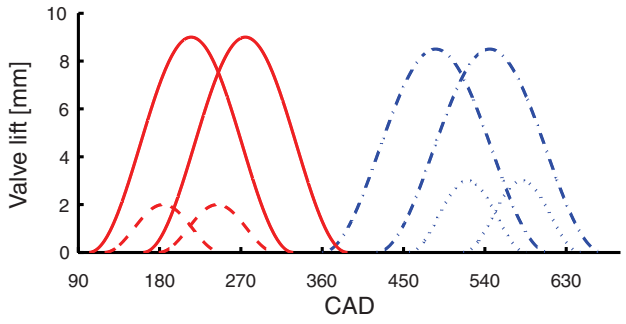

Figure 2: Valve lift profiles for the multi cylinder engine and its phasing capabilities.

programmable control unit controlled with a PC. The system made it possible to control spark timing, injection timing, injection pressure, injection amount, throttle and the VCT/CPS system in real time.

The optical experiments were carried out in a single-cylinder engine with optical access. For all experiments a prototype cylinder head was used with geometry similar to that of the multi-cylinder engine. The engine parameters for both the optical engine and the multi-cylinder engine can be seen in table 1 and a schematic sketch of the layout of the optical setup can be seen in figure 3. The parameters for the optical engine and the multi-cylinder engine were not identical but had similar values, and since the investigations were performed in an optical engine with higher cooling losses and lower compression ratio than in a metal engine, its intake air was heated to ensure that its behavior was similar to that of a real engine with similar settings. The temperature of its intake air was measured directly at the intake valve using a thermocouple and maintained at 90°C for all measurements, while in contrast the multi-cylinder engine was supplied with air at ambient temperature. To achieve a condition that was similar to the multi-cylinder engine in terms of surface temperature, the engine was operated in reference mode until the cylinder head was 130 °C and then the settings that should be studied were used. This procedure was carried out for all measurements in the optical engine to achieve high repeatability accuracy. Furthermore, the fuel used for the different engines differed; in the optical engine a two-component fuel consisting of iso-octane and n-heptane was used since neither of these components fluoresce significantly at the chosen excitation wavelength. For the multi cylinder engine a certification fuel was used that displayed similar behavior to conventional petrol.

Table 1: Engine parameters.

OPTICAL ENGINE	
Bore	83 mm
Stroke	90 mm
Swept Volume	487 cm ^{3}
Compression ratio	10:1
Inlet air temperature	90 °C
Fuel	iso-octane 85 $\%_{vol}$
	n-heptane 15 $\%_{vol}$
MULTI-CYLINDER	ENGINE
Number of cylinders	6
Bore	84 mm
Stroke	96 mm
Swept Volume	3192 cm ^{3}
Compression ratio	11.5:1
Inlet air temperature	Ambient air
Fuel (CEC legislative fuel)	RF-02-03, 99.5 RON
ENGINE SETTINGS	
EOI Main	-310 CAD
EOI Pilot	310 CAD
Camshaft duration	
Intake	130 CAD
Exhaust	130 CAD optical engine
	110 CAD multi-cylinder
Valve lift	
Intake	3 mm optical engine
	3 mm multi-cylinder
Exhaust	3 mm optical engine
	2 mm multi-cylinder
Spark-assist	-30 CAD

This optical engine has an extended piston housing a mirror that provides, in conjunction with a quartz window in the piston crown, optical access to most of the combustion chamber from below. The optically accessible volume can be seen in figure 4. The optical engine is restricted to low engine speeds and since the Dye laser was pumped by a Nd:YAG laser in the optical studies, all measurements were made

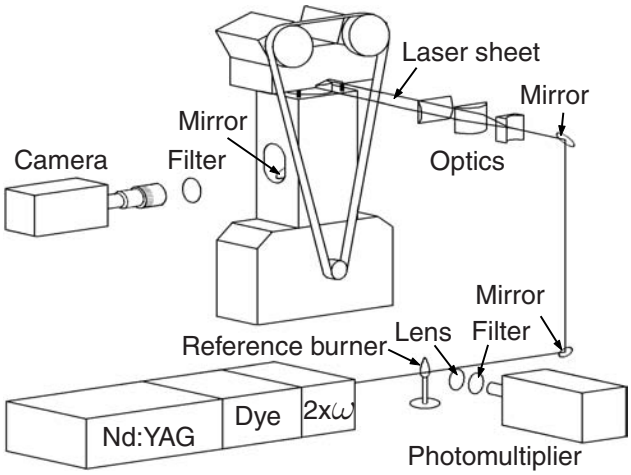

Figure 3: Schematic layout of the optical engine.

at 1200 rpm, which corresponds to 10 Hz, which led to a temperature stable operation condition for the Nd:YAG laser.

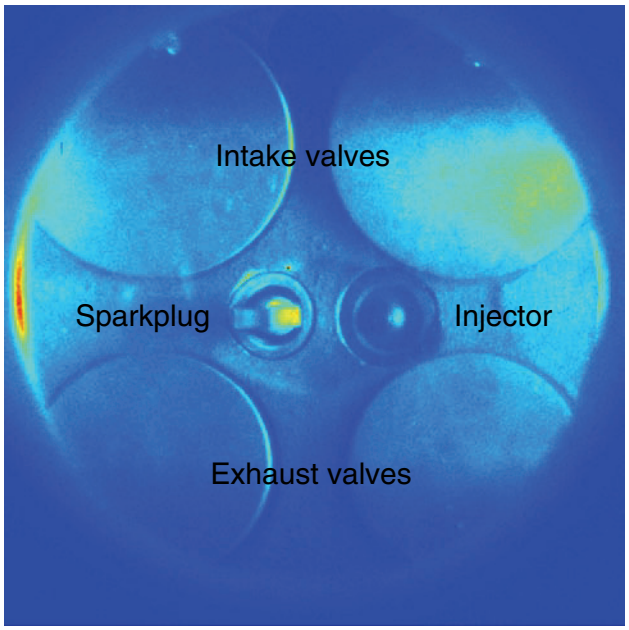

Figure 4: The optically accessible combustion chamber. The diameter of the optically covered zone was 73 mm.

For all experiments the fuel was supplied using a multi-hole direct injector, which was capable of multiple injections. To control the timings of the injections and the ignition in the optical engine an AVL 4210 instrument controller was used and a 35 mJ ignition coil was used to ensure that sufficient ignition energy was supplied by the sparkplug. The locations of the injector and the sparkplug can be seen in figure 4.

Two series of experiments were performed in both the multi-cylinder engine and the optical engine and the effects of these parameters were studied for two different NVO's in the multi-cylinder engine and for a single NVO in the optical engine, see table 2.

Table 2: Test matrix.

MULTI-CYLINDER	
Engine speed	1200 rpm
NVO	160 and 180 CAD
Experiment 1	
Pilot/Main ratio	25 - 40 %
Load	Constant 1.5 Bar IMEP
$\lambda_{180\ NVO}$	Constant 1.31$\pm$0.01
$\lambda_{160\ NVO}$	Constant 1.59$\pm$0.03
Experiment 2	
Pilot/Main ratio	37 - 43 %
Load	1.6 - 1.85 Bar IMEP
$\lambda_{180\ NVO}$	1.27 - 1.35
$\lambda_{160\ NVO}$	1.47 - 1.63
OPTICAL ENGINE	
Engine speed	1200 rpm
NVO	180CAD
Experiment 1	
Pilot/Main ratio	31 - 40 %
Load	Constant 1.5 Bar IMEP
λ	Constant 1.29$\pm$0.01
Experiment 2	
Pilot/Main ratio	37 - 43 %
Load	1.5 - 1.9 Bar IMEP
λ	1.22 - 1.3

OPTICAL EQUIPMENT

Planar laser-induced fluorescence was used to detect and image the OH molecules. The Q1(6) transition in the A(ν=1) - X(ν=0) band at a wavelength of 283 nm was used for excitation. This transition was used since it provides a high signal strength and has relatively low dependence on rotational population changes due to temperature variations. The Q1(6) transition overlaps with several weaker transitions in the Q_2, Q_{12} and Q_{21}-branches. This contributes to the signal strength, although these excitations are from low rotational states and their relative strengths decline somewhat at higher temperatures. An absorption spectrum was simulated by LIFBASE [29] which can be seen in figure 5. In order to avoid scattered laser light entering the detectors, fluorescence light from the A(ν=0) - X(ν=0) and A(ν=1) - X(ν=1) bands in the 300-320 nm-range was used for detection.

The tunable UV-light was generated by a nanosecond dye laser pumped by the 2nd harmonic light of a Nd:YAG laser. The Rhodamine 6G dye provided light in the 560-600 nm wavelength range, the frequency of which was subsequently doubled to obtain the desired wavelength. The pulse energy of the UV light was about 12 mJ. In order to calibrate the wavelength of the laser, the beam could be sent through a propane flame and fluorescence from OH molecules in the flame could be detected by a photomultiplier

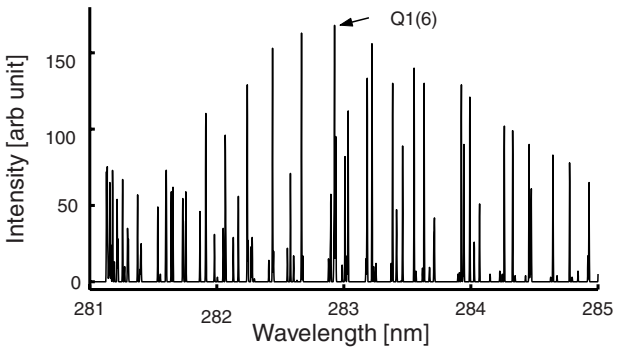

Figure 5: Simulated excitation spectrum for OH.

tube. Three cylindrical lenses were used to form a 50 mm wide horizontal laser plane passing 5 mm beneath the spark plug. A schematic diagram of the set-up is shown in figure 3.

DETECTORS AND FILTERS

The images were taken using an image intensified LaVision Dynamight camera, providing up to 1024x1024 resolution equipped with LaVision DaVis 6.2 software. However, all post-processing of the images was carried out using MatLab. A narrow-band filter with a center wavelength of 310 nm was used to isolate the emission from the OH radicals. Due to the short exposure times used (2.5 μs) and filtering any chemiluminescence from OH captured by the camera were negligible. Off-resonance images were captured to evaluate these effects and to verify that scattered laser light was effectively eliminated by the filter. To control the timing of the camera the AVL 4210 timing unit was used. Both the gain and exposure time of 2.5 μs were kept constant in this study.

RESULTS AND DISCUSSION

MULTI CYLINDER ENGINE RESULTS

The effects of varying the ratio between pilot and main injections while keeping the load constant can be seen in figure 6. The presented traces from the multi-cylinder engine was averaged from 200 consecutive revolutions for the whole engine, thereby from 100 cycles from each of the six cylinders. The combustion phasing was advanced when the relative amount of pilot injection was increased, by varying degrees depending on the cam settings (*i.e.* NVO), in accordance with observations in previous studies by the authors [19] and Koopmans *et. al.* [27]. For the cases with a NVO of 180 CAD, less advancement of the combustion was noted, which was attributed to the lower, and consequently less excess air during the NVO, allowing less reactions to occur. When a longer NVO was used the maximum rate of heat release was increased and the combustion duration decreased.

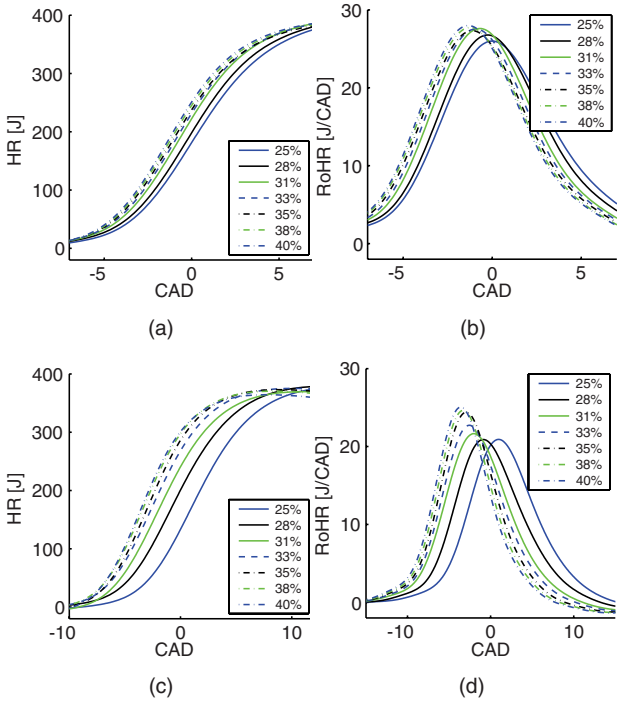

Figure 6: Averaged cumulative heat release and rate of heat release for 180 CAD NVO, (a) and (b), and for 160 CAD NVO, (c) and (d) for different pilot to main ratios during the main combustion.

The lower maximum rate of heat release for the cases with a NVO of 160 CAD could be partly explained by the fact that the combustion was less stable than in cases with a NVO of 180 CAD and partly due to the higher λ that led to lower reaction rates. Indications of the combustion instability can be seen in figure 7, in which the standard deviation of the CA50 timing is shown. The greater instability gave a smoother

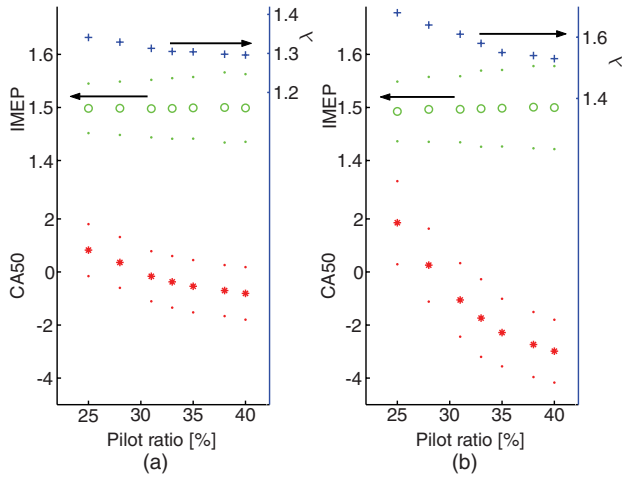

Figure 7: IMEP, air equivalence ratio and combustion phasing for 180 NVO, (a) and for 160 NVO (b), for different pilot to main ratios. Standard deviation is represented as dots.

rate of heat release when it was averaged over the different cycles. However, the combustion was stable in absolute terms, displaying a COV in IMEP of around 1.5 %, and the load for the different pilot to main injection ratios could be considered to be constant. The air equivalence ratio was slightly affected by the pilot to main injection ratio, but the load was kept constant by varying the total amount of fuel and thus there were only small differences in λ. The effects of the pilot to main injection ratio on combustion phasing were significant for the cases with a NVO of 160 CAD, since the average CA50 timing with 25 and 40 % pilot ratios differed by more than its standard deviations. Thus, it was statistically unlikely that the differences in combustion phasing were due to random effects. The combustion phasing was also advanced slightly by the higher pilot to main injection ratio with a 180 CAD NVO, but the statistical significance of the effect was weaker.

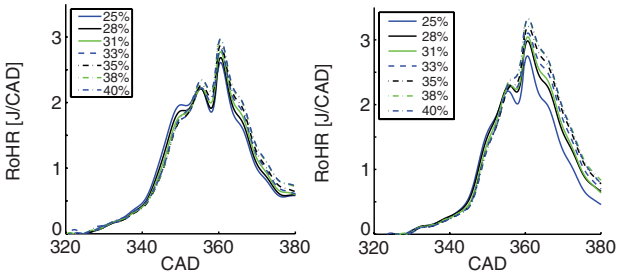

Figure 8: Rate of heat release during the NVO for 180 NVO, (a) and for 160 NVO, (b) for different pilot to main ratios.

Further investigations based on pressure trace analysis were performed to investigate if the heat generated by the reactions that occurred during the NVO was a major factor responsible for the finding that increasing the relative amount of the pilot injection advanced the combustion phasing. Other factors that may have influenced the phasing include the possibility that radicals were formed during the NVO that subsequently influenced the phasing of the main combustion and that higher pilot ratios led to an increase in these radicals. The rates of heat release observed during the NVO when the pilot to main injection ratio was varied can be seen in figure 8. Generally, the maximum rate of heat release during the NVO was much smaller than the maximum rate of heat release during the main combustion, as seen previously in figure 6. Evidence of reactions could be seen after ca. around 330 CAD as the rate of heat release started to increase, and peaked slightly after TDC during the NVO, after which it decreased. These trends were observed for all operation conditions studied in the multi cylinder engine. The cases with low pilot to main injection ratios initially displayed higher rates of heat release than those with higher pilot injection proportions. However, later in each cycle this trend reversed, and cases with higher pilot injection proportions showed higher rates of heat release. This was probably because the higher amounts of fuel injected prior to TDC in the cases with high pilot injection proportions led to increased evaporation and, hence, reductions in the temperature. Thus, the reactions that occurred during the NVO were initially slightly delayed in these cases, but in the later part of the combustion the relatively high amount of fuel injected during the NVO led to a higher accumulated heat release.

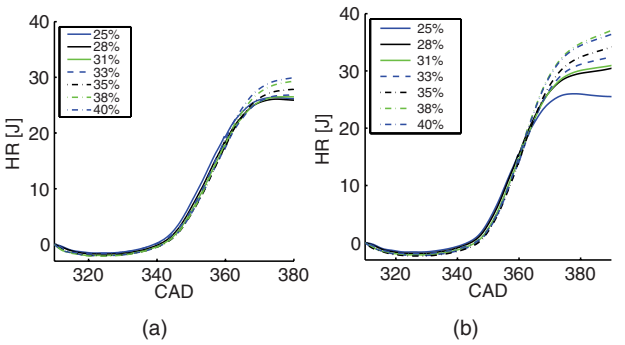

Figure 9: Heat release during the NVO for 180 NVO, (a) and for 160 NVO, (b) for different pilot to main ratios.

Figure 9 shows accumulated heat release curves during the NVO obtained with various pilot to main injection ratios. The evaporation of the pilot injection was manifested by a reduction in the accumulated heat release when it was injected (310 CAD), and at around 330 CAD the heat release gradient became positive, as previously indicated by the rate of heat release traces, see figure 8. Increasing the pilot injection proportion led to a slightly increased evaporation, as indicated by the finding that the accumulated heat release was lowest, at around 330 CAD, in the cases with the highest pilot injection proportions. However, the effects of the evaporation following the pilot injection were subsequently strongly compensated by the heat generating reactions, and the total accumulated heat release curves show there was a positive addition of heat during the NVO. The combustion efficiency, during the NVO $\eta_{\text{combustion,NVO}}$ was naturally far lower than unity, and only fractions of the fuel introduced in the pilot injections were combusted during the NVO, due to the very high levels of EGR during it (since mainly trapped residuals were compressed during the NVO) and of course the intention of the combustion during the NVO was only to control the main combustion. $\eta_{\text{combustion,NVO}}$ varied from 18 to 25 % when 180 CAD NVO was used, and between 23 and 27 % when 160 CAD was used. However, the $\eta_{\text{combustion,NVO}}$ values were lowest for the higher proportions of pilot injection. For cases with 160 CAD NVO the total amounts of heat generated during the NVO were greater than in the cases with 180 CAD, due (as discussed above) to the higher λ, which the $\eta_{\text{combustion,NVO}}$ indicated.

To investigate if the trend of advanced phasing with increasing pilot ratios was due to increases in the temperature of the gas during the compression, the influence of the heat added during the NVO caused by the pilot injection on the charge temperature during the compression was calculated. This was done using polytropic calculations, as further described in the Appendix. In figure 10 the pressure and calculated mass-averaged temperature can be seen for two cases: one with 25 % and one with 40 % pilot injections, both with an NVO of 160 CAD; the maximum and minimum pilot injection proportions tested at 160 CAD NVO. Those cases showed a difference in CA50 timing of around 5 CAD, see figures 6(c), 6(d) and 7(b), and the heat released during the NVO for those cases differed by ca. 10 J, see figure 9(b). The mass-averaged temperature was calculated by using the pressure and heat release values measured during the NVO for the two cases. Due to the low density and mass of the trapped residuals during the NVO the heat generated by the reactions that occurred led to a significant increase in temperature during the NVO, although the evaporation of the pilot injection temporary mitigated the temperature increase during the compression of the trapped residuals. During the NVO the temperature difference between the maximum values obtained with the different pilot injection proportions was of the order of 50 K, with the highest temperature achieved in the case with 40 % of pilot injection. This higher temperature for the case with higher amount of pilot injection led to a higher temperature during the compression (for the main combustion) compared to the case with the lower amount of pilot injection. The difference in temperature 10 CAD prior to TDC between the cases was in the order of 45 K. Weikl *et. al.* [30] studied the gas-phase temperature during HCCI combustion by using Coherent Anti-Stokes Raman Spectroscopy (CARS), for HCCI combustion with similar amounts of EGR, but at slightly higher loads. The cited authors found that a difference in temperature at TDC of 7 K would change the combustion phasing (CA50) by around 1 CAD. Similar ratios of changes in the CA50 timing to changes in temperature were found in this study, and thus it was concluded that the heat generated by the pilot injection was a major contributor to the combustion phasing. Furthermore was the temperature difference at the start of combustion (SOC) for the two cases analyzed in the order of 5 K, the case with 40 % of pilot injection displayed a slightly higher temperature, but 5K is in the order of the accuracy of the measurement.

The effects of a load change on the heat release and rate of heat release can be seen in figure 11. The load was increased by increasing the amount of fuel introduced in the main injection while keeping the pilot injection constant and, as seen by many authors, increasing the load in HCCI combustion led to an increase in the maximum rate of heat release and a

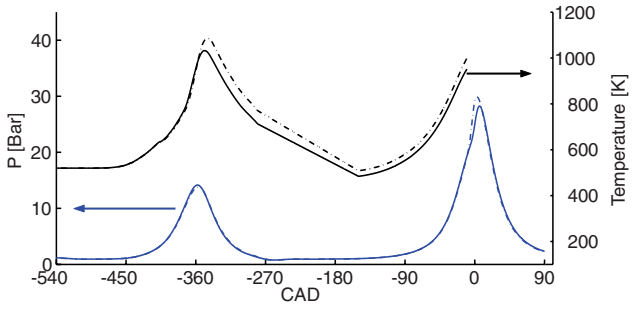

Figure 10: Pressure traces and calculated mass averaged temperatures for 25% and 40% of pilot injection when 160 CAD NVO was used. Dashed lines corresponds to 40% pilot and solid lines to 25%.

slightly advanced combustion. The combustion phasing and combustion duration were less affected by increases in the main fuel amount in the 180 CAD NVO cases than the 160 CAD NVO cases. These differences were partly due to the decreased cycle-to-cycle variations (see figure 12) when the load was increased, which led to the averaged rate of heat release traces displaying a shorter combustion duration and higher maximum rate of heat release, and partly to the fact that the shorter NVO led to a higher λ value, and thus more reactions could occur during the NVO and subsequently influence the combustion phasing. Since the influence on combustion phasing was stronger, the maximum rate of heat release increased more when the load was increased with

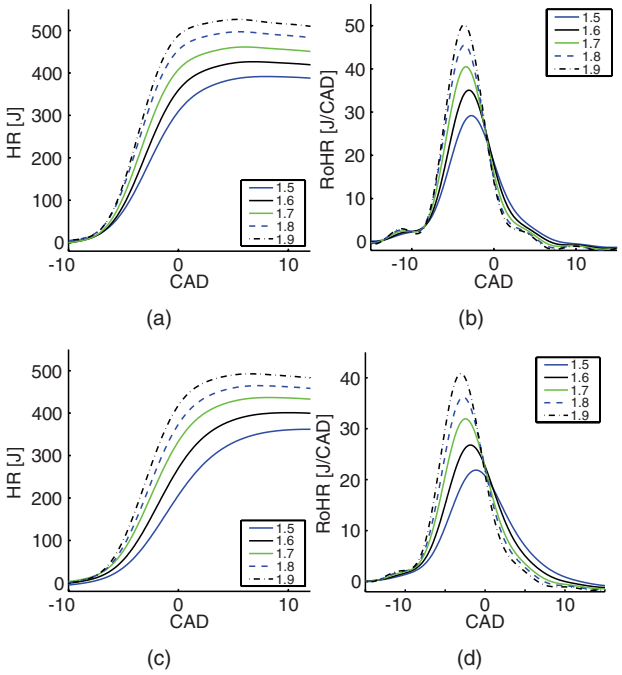

Figure 11: Averaged cumulative heat release and rate of heat release for 180 NVO, (a) and (b), and for 160 NVO, (c) and (d) for different loads (from 1.5 to 1.9 Bar IMEP).

160 CAD NVO than with 180 CAD NVO. In addition, changing the load from 1.5 to 1.9 bar IMEP had a statistically significant effect on the CA50 timing on the case with 160 CAD of NVO, but in the case with 180 CAD NVO according to the means and standard deviations of the measured values no statistically clear trends could be seen.

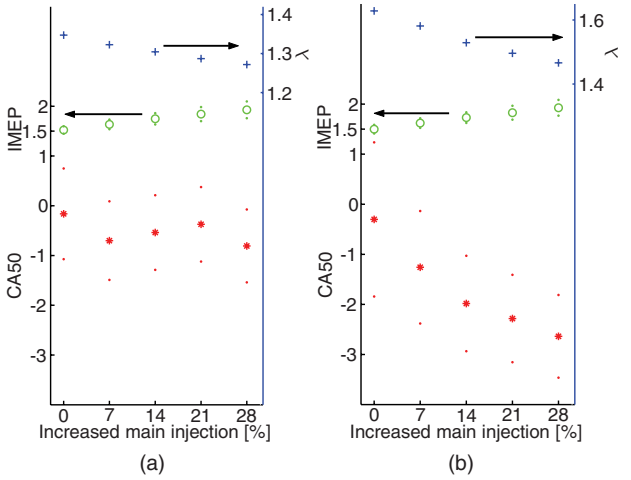

Figure 12: IMEP, air equivalence ratio and combustion phasing for 180 NVO, (a) and for 160 NVO (b), for different total fuel amounts. Standard deviation is represented as dots.

The rate of heat release curves during the NVO obtained when the load was varied can be seen in figure 13 and, as for the cases with varying pilot to main injection ratios, the maximum rate of heat release during the NVO was only a fraction of the maximum rate of heat release during the main combustion. Further similarities were also noted in the timing and duration of signs of reactions. The maximum rates of heat release were lower when the load was increased, presumably because the higher load led to a lower λ and thus less excess O_2 during the NVO, so less reactions could occur despite the elevated temperature of the trapped residuals caused by the increase in load. In the experiments with varying load (figure 13) the cases with higher load showed higher rates of heat release initially in the cycles, but later in the cycles the rates of heat release were highest in the lowest load cases. This was probably because increases in the load reduced the air equivalence ratio (figure 12), leaving less oxygen for the reactions during the NVO. Thus, despite a higher total amount of fuel being injected at the higher loads, less reactions occurred during the later parts of the combustion in the NVO. The total amount of fuel injected in the pilot injection was constant, and only the main injection was increased when the load was increased, so the pilot to main injection ratio decreased when the load was increased. The initially higher rates of heat release in the cases with higher loads may have been due to the higher load leading to higher temperatures during the compression in the NVO, thus allowing the reactions to start earlier, while later in the cycles the greater excess of oxygen at the lower loads led to higher maximum rates of heat release in those cases. The accumulated heat release traces (figure 14) show that the total amount of heat generated during the NVO was decreased when the load was increased. For the case with 180 CAD NVO, the reactions during the NVO were more strongly reduced when the load was increased than when 160 CAD NVO was used, so the reduction in accumulated heat due to the increase in load was higher, presumably because the longer NVO led to larger amounts of EGR, and thus lower λ values.

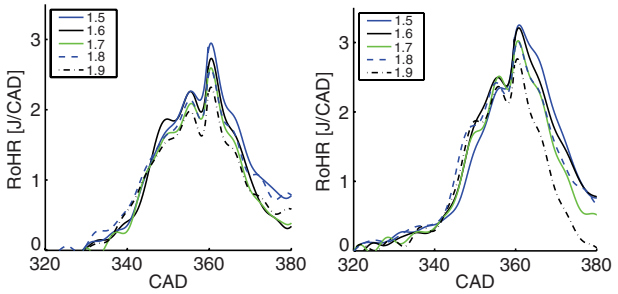

Figure 13: Rate of heat release during the NVO for 180 CAD NVO, (a) and for 160 CAD NVO, (b) for different loads (from 1.5 to 1.9 Bar IMEP).

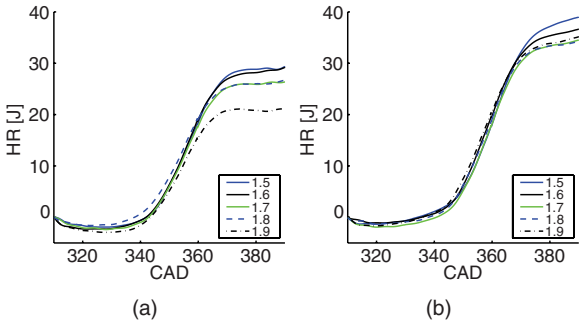

Figure 14: Heat release during the NVO for 180 NVO, (a) and for 160 NVO, (b) for different loads (from 1.5 to 1.9 Bar IMEP).

OPTICAL ENGINE RESULTS

The effects of varying the pilot to main injection ratio on heat release in the optical engine can be seen in figure 15. The response to increases in the pilot injection proportions was advanced combustion, as seen in the multi cylinder engine experiments. There were, of course, discrepancies between the two; the lower compression ratio and higher cooling losses of the optical engine led to slightly different results despite the similarity of the settings. However, it was encouraging that the correlation between advanced combustion and increases in the pilot to main injection ratio was observed, since investigating this trend and the effects of increased load were the main objectives of the study. The heat release was calculated and averaged over just 50 cycles because longer data acquisition periods led to unacceptable time trends due to increases in the temperature of the combustion chamber surfaces, which gradually advanced the combustion phasing. This was because it was not possible to thermally stabilize the optical engine. The observed changes in combustion phasing caused by increasing the pilot to main injection ratio from 31 to 40 % in the optical and multi cylinder engines were similar, but the combustion was generally advanced more in the multi cylinder engine.

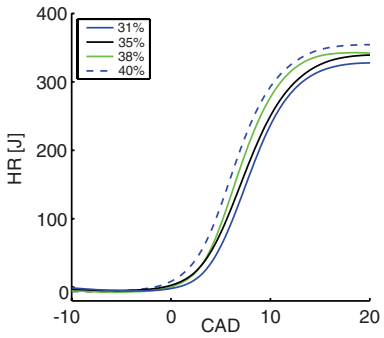

Figure 15: Average accumulated heat release traces for different pilot to main rations.

When the load was increased in the optical engine experiments less effect on the combustion phasing was seen than in the multi cylinder engine experiments, as shown in figure 16, which displays the heat release traces obtained when the load was increased. The influence on combustion phasing was probably weaker because the optical engine was run under reference conditions until the temperature of the cylinder head had reached 130°C, and then the settings for the case to be studied were applied and data were recorded for the following 50 cycles. In contrast, the multi cylinder engine was run continuously at the settings determined by the experimental matrix, and at higher loads the temperature of the combustion chamber surface became higher in the multi cylinder engine. Hence, the load had a stronger influence on the combustion phasing than in the optical engine, in which the temperature of the combustion chamber surface was less strongly influenced by the load.

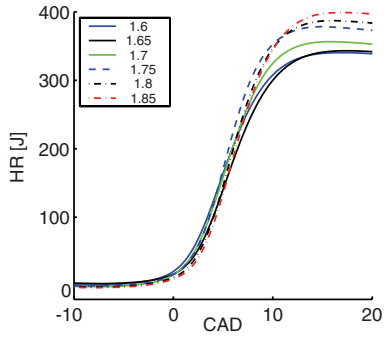

Figure 16: Average accumulated heat release traces for different total amounts of fuel, *i.e.* different loads (1.6 to 1.85 Bar IMEP).

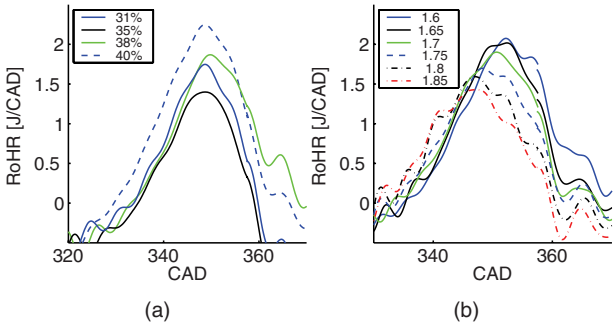

(a) (b)

Figure 17: Averaged rate of heat release traces during the NVO for different pilot to main ratios, (a) and for different loads (b).

When the pressure traces for the optical engine were analyzed, evidence of reactions during the NVO was detected, as shown in figure 17. Reactions were found to start at around 330 CAD, slightly earlier than in the multi cylinder engine, and continued until around TDC. When the load was increased the maximum rate of heat release decreased, as seen in the multi cylinder engine. The maximum rates of heat release were also of the same order of magnitude for both engines, although the traces obtained for the optical engine were calculated from just one cylinder and 50 cycles, but from six cylinders and 100 cycles from each cylinder for the multi cylinder engine. Thus, the effects of the shortcomings of the optical engine (notably that it was not thermally stabilized during the measurements and thus did not allow long data acquisition periods), on its responses were modest, comparisons between the two engines could be made, and trends observed in the optical engine could apparently be validly compared to those in traditional engines.

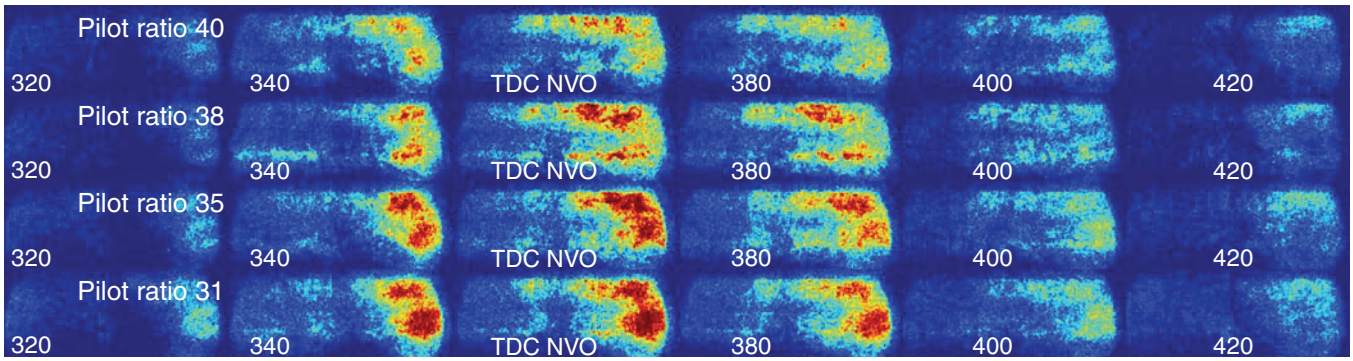

Figure 18: Averaged LIF images from OH for different amounts of pilot injection and for different timings.

As observed by the authors in previous studies OH was present during the NVO [19], and the OH signal appeared slightly before any evidence of reactions was noted in the rate of heat release traces (see figures 17, 18 and 20). Furthermore, the OH signals continued for a longer time (ca. 100 CAD, with an intensity peak at TDC) than the heat-generating reactions appeared to last in the rate of heat release traces during the NVO, especially for the cases with smaller relative pilot injections. The excitation wavelength was chosen to give a signal that was insensitive to any temperature change during the NVO, however many other factors influence LIF signals, for instance O_2 or H_2O contents can strongly affect the quenching. The pressure also affects the signal, however the pressure difference between the cases for the studied interval were minor, and both the consumption of O_2 and production of H_2O in the combustion during the NVO were only modest, so differences observed between the cases were believed to be mainly due to changes in operational settings. Each of the images presented in figure 18 were averaged from 10 separate images from 10 different cycles and all of the images were filtered. The spatial locations of the OH reactions were time dependent and initial signs were found at the periphery on the right side of the combustion chamber. Later in the cycle OH radicals were present throughout the whole combustion chamber until the signal decayed and the last signs were noted at the same location that the initial signs were noted. The intensity of the LIF signals varied for the different pilot injection amounts, it was found that increasing the relative amount of fuel introduced in the pilot injection for the same load led to a decreased OH signal. The signal to noise ratio of LIF obtained using dye lasers from OH is known to be generally poor, and thus great care was taken when analyzing the OH signal strength and its dependency on the studied parameters. These aspects of the investigation, and the filtering process, are described in more detail in the Appendix.

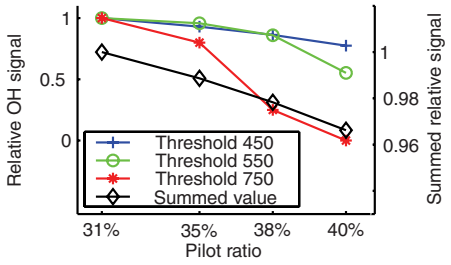

Figure 19: Variations in LIF signals from OH with relative pilot ratios, obtained using three threshold values, and summed values.

To investigate the spatial distribution of OH in the combustion chamber the images were studied in detail and different threshold values were used to determine how many pixels in the images could be associated with a significant signal from OH. In figure 19 the results can be seen when each of the pixels in the images from 320 CAD to 420 CAD were compared to different threshold values, providing indications of the areas covered by the optical field in the combustion chamber that were emitting weak (Threshold 450), moderate (Threshold 550) or strong (Threshold 750) OH signals. From the signals, of all strengths, in figure 19 it can be seen that an increase in the pilot to main injection ratio reduces the OH signal. For instance, in the case with a 40 % ratio no strong signals were detected from 320 to 420 CAD. Furthermore, the intensities were summed for all pixels and normalized, and the same trend as that discerned using the threshold values was seen. Thus, it gave a further indication that the OH intensity decreases with increasing pilot ratio.

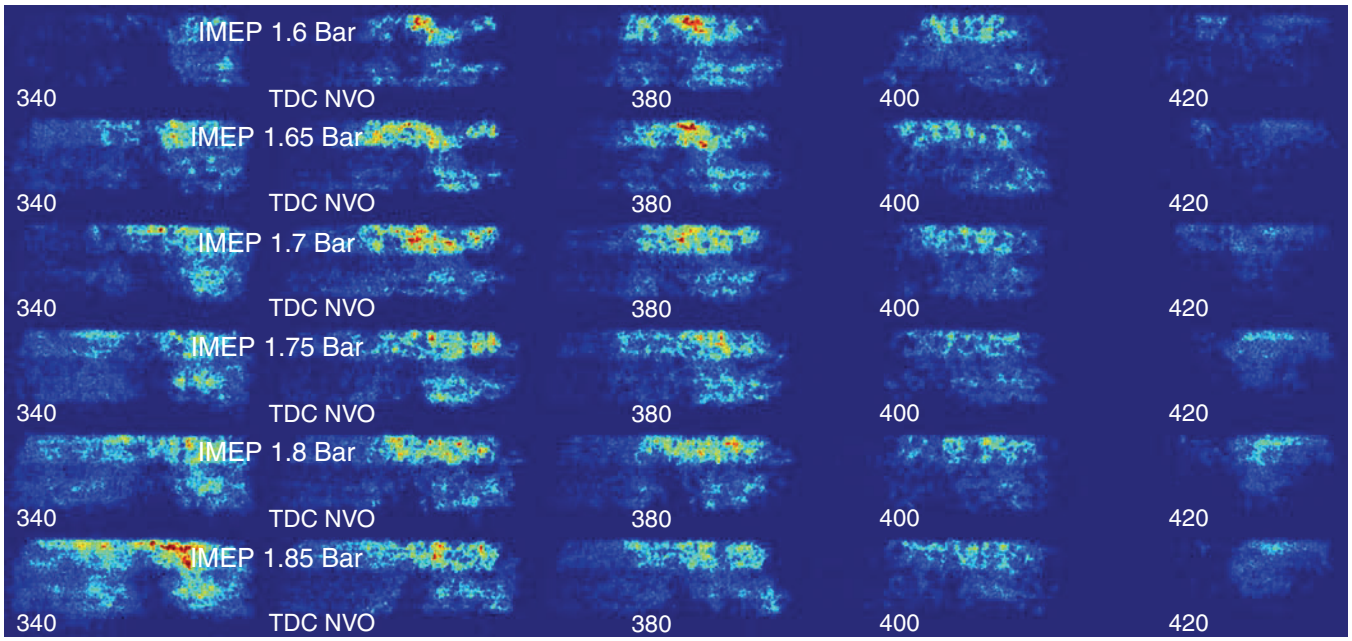

Figure 20: Averaged LIF images from OH for different loads and different timings.

As in the experiments with varying amounts of pilot injection, OH signals were detected between 320 and 420 CAD in the experiments when the load was varied. Averaged LIF images obtained between 340 and 420 CAD for various loads can be seen in figure 20. The OH intensity peaked at around TDC and slowly decreased for later timings. Increases in the total amount of fuel were accompanied by increased amounts of OH and, as in the experiments in which the pilot to main injection ratio was varied, the duration of the OH signal was unaffected by the changes in settings, only the intensity and/or spatial distribution of the signal were affected. Signals were consistently detected during the same time interval, but with varied intensity. This signal dependency on the total amount of fuel was also studied by setting different threshold values and summing the intensity for all pixels, and the results can be seen in figure 21. For low and medium threshold values the trends were clear; OH was present over a larger area in the cases with higher loads. However, with the high intensity threshold there was a deviation from this trend for some operational conditions. The deviation from this trend detected in some of the cases with the high intensity threshold might have been due to greater cycle-to-cycle variations in the spatial location of the OH signals, resulting in more evenly distributed averaged images with smaller regions of high intensity signals. However, the correlation between the intensity of the OH signals and load was still present in the summed values for all pixels. Of course, the conditions during the NVO changed when the load was varied, since increases in load led to reductions in λ and the increased amount of combustion to a reduction in O_2 and increased production of H_2O. These changes would also affect the levels of quenching of the LIF signal. However, the changes in O_2 concentrations would have a stronger impact on the level of quenching than the changes in H_2O concentrations, so the changes in quenching-associated conditions would probably have contrary effects to the observed increases in signal strength with increases in load. Thus, the detected trend would presumably have been even stronger with similar levels of quenching.

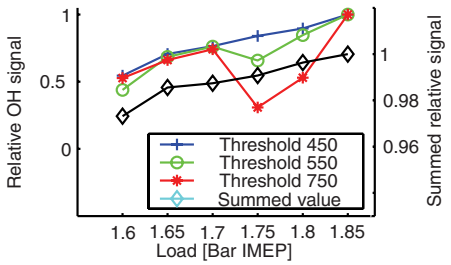

Figure 21: Variations in LIF signals from OH with load (1.6 to 1.85 bar IMEP), obtained using three threshold values, and summed values.

DISCUSSION

The experiments with the multi-cylinder engine showed similar results to those observed in previous studies by both the present authors and other authors, and that the phasing capacity of increasing the pilot to main injection ratio was due to increases in compression temperatures due to the generation of heat during the NVO.

In both series of experiments with the optical engine, the strength of the OH signals increased in cases that gave a reduced maximum rate of heat release (cf. figures 17, 19 and 21). Reductions in the amount of fuel introduced in the pilot injection led to lower maximum rates of heat release during the NVO, but increases in the amounts of OH, and when the load was increased the maximum rate of heat release during the NVO was decreased and the amount of OH was increased. Thus, the high temperature reactions contributed to the heat released during the NVO, but they were not the major factors. Indications of the occurrence of high temperature reactions under similar conditions during the NVO have been previously detected in the form of OH chemiluminescence [19], together with large amounts of formaldehyde indicating extensive low-temperature reactions. The heat released during the NVO was probably mainly due to these low temperature reactions. However, the first OH signals were detected at a similar time to the point when the rate of heat release started to rise, thus these reactions presumably contributed to the heat generation during the NVO. The correlation between increases in the amount of OH radicals and increases in the load were due to the associated increases in the temperature of the trapped residual gas during the NVO, which led to greater amounts of high temperature reactions. In terms of the high temperature reactions the increased residual gas temperature compensated for reductions in the amount of excess O_2 available for combustion during the NVO caused by the increases in load, but for the low temperature reactions the reductions in the amount of O_2 led to a reduction in reaction rates.

In the experiments in which the pilot to main injection ratios were varied, the increased evaporation caused by the increased amount of fuel injected prior to TDC during the NVO reduced the temperature in the cases with larger pilot injections. The reduced temperature of the trapped residuals in those cases led to reduced amounts of high temperature reactions and thus reduced the OH intensity. However, the equal amounts of excess O_2, and the higher amount of fuel in the cases with larger pilot injections led to the noted increases in maximum rates of heat release, as shown in figure 17(b). In both experiments fairly large relative amounts of pilot injections were used and it was beyond the scope of this study to evaluate the effects of load changes or variations in pilot to main injection ratios with small proportions of pilot injections on the high temperature reactions.

Since similar behavior was seen in both engines, it was concluded that the results from the optical engine could be validly compared to the phenomena seen in the multi-cylinder engine studies (and to the previously seen results), and in the multi-cylinder engine study it was found that the heat generation during the NVO was the source of the phased combustion, but the OH signal was not proportional to the amount of phasing so it was concluded that the low temperature reactions that occurred during the NVO were the main sources of heat generation that led to the phasing of the combustion.

CONCLUSIONS

An experimental study of the effects of varying the pilot to main injection ratio and the total amount of fuel in a spark-assisted HCCI engine using NVO was performed to investigate the effects of these parameters on the reactions that occurred during the NVO, and other engine variables, in both a multi cylinder engine and an optical engine. The trends observed in the two engines were very similar, and in both of them increases in the proportion of the pilot injection led to advanced combustion phasing, and increases in the total amount of fuel led to slight reductions in the combustion duration with higher maximum rates of heat release.

The pilot to main injection ratio influenced the maximum rate of heat release from the reactions that occurred in the trapped residuals during the NVO; increases in the proportion of the pilot injection leading to higher maximum rates. The excess O_2 was combusted to a greater extent because greater amounts of fuel were combusted during the NVO. The contribution of heat generated during the NVO caused by the pilot injection led to increases in the temperature during the compression, and the phasing caused by varying the pilot to main injection ratio was mainly due to the resulting temperature changes during the compression. When the load was increased by increasing the total amount of fuel, the maximum rate of heat release during the NVO was decreased due to the reductions in λ and, hence, in excess O_2.

Evidence of high temperature reactions was detected in the form of LIF signals from OH radicals slightly prior to any signs of heat release in the pressure traces, and OH signals were detected during the NVO in all operation conditions. The high temperature reactions were not the major source of heat generation during the NVO since the LIF OH signals were stronger in the cases with lower rates of heat release during the NVO. Higher loads led to increasing amounts of OH during the NVO due to the higher temperature of the trapped residuals. Greater proportions of pilot injection led to more evaporation, which reduced the temperature during the NVO and thus reduced the amount of OH radicals.

ACKNOWLEDGEMENT

The authors wish to acknowledge STEM, the Swedish Energy Agency, for funding this work and Dr. Lucien

Koopmans at Volvo Cars for supplying experimental equipment and support.

REFERENCES

1. Koopmans, L., Strömberg, E., Denbratt, I., "The Influence of PRF and Commercial Fuels with High Octane Number on the Auto-Ignition Timing of an Engine Operated in HCCI Combustion Mode with Negative Valve Overlap", SAE Technical Paper Series, SAE Paper 2004-01-1967.

2. Heywood, J. B. , "Internal Combustion Engines Fundamentals" 1988, Singapore: McGraw-Hill Inc.

3. Hultquist, A.,Christensen, M., Johansson, B., Ricther, M., Nygren, J., Hult, J., Aldén, M., "The HCCI Combustion Process in a Single Cycle - High-Speed Fuel Tracer LIF and Chemiluminescence Imaging", SAE Technical Paper Series, SAE Paper 2002-01-0424.

4. Lü, X-C., Chen, W., Huang, Z., "A fundamental study on the control of the HCCI combustion and emissions by fuel design concept combined with controllable EGR. Part 1. The basic characteristics of HCCI combustion", Fuel, Volume 84, Issue 9, Pages 1074-1083 (June 2005).

5. Hultquist, A., Christensen, M., Johansson, B., Franke, A., Aldén, M., "A Study of the Homogenous Charge Compression Ignition Combustion Process by Chemiluminescence Imaging", SAE Technical Paper Series, SAE Paper 1999-01-3680.

6. Wagner, U., Anca, R., Velji, A., Spicher, U., "An Experimental Study of Homogenous Charge Compression Ignition (HCCI) with Various Compression Ratios, Intake Air Temperatures and Fuels with Port and Direct Fuel Injection", SAE Technical Paper Series, SAE Paper 2003-01-2293.

7. Lü, X-C., Chen, W., Huang, Z., "A fundamental study on the control of the HCCI combustion and emissions by fuel design concept combined with controllable EGR. Part 2. Effect of operating conditions and EGR on HCCI combustion", Fuel, Volume 84, Issue 9, Pages 1084-1092 (June 2005).

8. Glassman, I., "Combustion" 1996, third edition, United States of America: Academic Press Ltd.

9. Marriott, C. D, Kong, S-C., Reitz, R. B., "Investigation of Hydrocarbon Emissions from a Direct Injection-Gasoline Premixed Charge Compression Ignited Engine", SAE Technical Paper Series, SAE Paper 2002-01-0419.

10. Flowers, D., Aceves, S. M., Martinez-Frias, J., Smith, R., Au, M., Girard, J., Dibble, R., "Operation of a Four-Cylinder 1.9L Propane Fueled Homogenous Charge Compression Ignition Engine: Basic Operating Characteristics and Cylinder-to-Cylinder Effects", SAE Technical Paper Series, SAE Paper 2001-01-1895.

11. Fiveland, S. B., Agama, R., Christensen, M., Johansson, B., Hiltner, J., Maus, F., Assanis, D. N., "Experimental and Simulated Results Detailing the Sensitivity of Natural Gas HCCI Engines to Fuel Composition", SAE Technical Paper Series, SAE Paper 2001-01-3609.

12. Martinez-Frias, J., Aceves, S. M., Flowers, D., Smith, R. J., Dibble, R., "Thermal Charge Conditioning for Optimal HCCI Engine Operation", Journal of Energy Resources Technology, Volume 124, Pages 67-75 (March 2002).

13. Milovanovic, N., Blundell, D., Pearson, R., Turner, J., Chen, R., "Enlarging the Operational Range of a Gasoline HCCI Engine By Controlling the Coolant Temperature", SAE Technical Paper Series, SAE Paper 2005-01-0157.

14. Haraldsson, G., Tunestål, P., Johansson, B., Hyvönen, J., "HCCI Combustion Phasing in a Multi Cylinder Engine Using Variable Compression Ratio", SAE Technical Paper Series, SAE Paper 2002-01-2858.

15. Hyvönen, J., Haraldsson, Johansson, B., "Operating range in a Multi Cylinder HCCI engine using Variable Compression Ratio", JSAE Technical Paper Series, JSAE Paper 20030178.

16. Haraldsson, G., Tunestål, P., Johansson, B., "Transient Control of a Multi Cylinder HCCI Engine During a Drive Cycle", SAE Technical Paper Series, SAE Paper 2005-01-0153.

17. Christensen, M., Hultqvist, A., Johansson, B., "Demonstrating the Multi Fuel Capability of a Homogenous Charge Compression Ignition Engine with Variable Compression Ratio", SAE Technical Paper Series, SAE Paper 1999-01-3679.

18. Strandh, P., Bengtsson, J., Johansson, R., Tunestål, P., Johansson, B., "Cycle-to-Cycle Control of a Dual-Fuel HCCI Engine", SAE Technical Paper Series, SAE Paper 2004-01-0941.

19. Berntsson, W. A., Denbratt, I., "Optical study of HCCI Combustion using NVO and an SI Stratified Charge", SAE Technical Paper Series, SAE Paper 2007-24-0012.

20. Berntsson, A., Denbratt, I., "Spark Assisted HCCI Combustion Using a Stratified Hydrogen Charge", SAE Technical Paper Series, SAE Paper 2005-24-039.

21. Berntsson, A., Denbratt, I., "HCCI Combustion Using a Spark Ignited Stratified Charge", JSAE Technical Paper Series, JSAE Paper 20065424.

22. Berntsson, W. A., Denbratt, I., "HCCI Combustion Using Charge Stratification for Combustion Control", SAE Technical Paper Series, SAE Paper 2007-01-0210.

23. Sjöberg, M., Dec, J. E., "Smoothing HCCI Heat-Release Rates Using Partial Fuel Stratification with Two-Stage Ignition Fuels", SAE Technical Paper Series, SAE Paper 2006-01-0629.

24. Koopmans, L., Denbratt, I.,"A Four Stroke Camless Engine, Operated in Homogenous Charge Compression Ignition Mode with Commercial Gasoline", SAE Technical Paper Series, SAE Paper 2001-01-3610.

25. Koopmans, L., Backlund, O., Denbratt, I., "Cycle to Cycle Variations: Their Influence on Cycle Resolved Gas Temperature and Unburned Hydrocarbons from a Camless Gasoline Compression Ignition Engine", SAE Technical Paper Series, SAE Paper 2002-01-0110.

26. Koopmans, L., Ström, H., Lundgren, S., Backlund, O., Denbratt, I., "Demonstrating a SI-HCCI-SI Mode Change on a Volvo 5-Cylinder Electronic Valve Control Engine", SAE Technical Paper Series, SAE Paper 2003-01-0753.

27. Koopmans, L., Ogink, R., Denbratt, I., "Direct Gasoline Injection in the Negative Valve Overlap of a Homogenous Charge Compression Ignition Engine", JSAE Technical Paper Series, JSAE Paper 20030195.

28. Koopmans, L., "HCCI Combustion by Retaining Residuals" 2005, PhD Thesis, Department of Applied Mechanics, Chalmers University, Sweden.

29. Luque, J., Crosley, D.R.,"LIFBASE: Database and Spectral Simulation Program (Version 1.45)", SRI International Report MP 98-021 (1998).

30. Weikl, M. C., Beyrau, F., Leipertz, A., Loch, A., Jelitto, C., Willand, J.,"Locally Resolved Measurement of Gas-Phase Temperature and EGR-Ratio in an HCCI-Engine and Their Influence on Combustion Timing", SAE Technical Paper Series, SAE Paper 2007-01-0182.

CONTACT

Corresponding author:
Andreas Berntsson
Chalmers University of Technology
Department of Applied Mechanics
Division of Combustion
Hörsalsvägen 7B SE-412 96
Göteborg Sweden
Email: andreas.berntsson@chalmers.se

DEFINITIONS, ACRONYMS, ABBREVIATIONS

LIF: Laser Induced Fluorescence.

HCCI: Homogenous Charge Compression Ignition.

NVO: Negative Valve Overlap, the time between the exhaust valve closing and the intake valve opening.

EGR: Exhaust Gas Recirculation.

SI: Spark Ignition.

OH: Hydroxyl.

PLIF: Planar Laser Induced Fluorescence.

SI: Spark Ignited.

NO_X: Nitrogen Oxides.

PM: Particulate Matter.

CA50: Crank Angle when 50% of the energy is burned.

DI: Direct Injected.

TDC: Top Dead Center.

CAD: Crank Angle Degree.

CPS: Cam Profile Switching.

VCT: Variable Cam Timing.

P: Pressure.

EOI: End Of Injection.

Nd:YAG: Neodymium: Yttrium Aluminum Garnet.

IMEP: Indicated Mean Effective Pressure.

COV: Coefficient Of Variation.

RoHR: Rate of Heat Release.

SOC: Start Of Combustion.

APPENDIX

POST PROCESSING - PRESSURE TRACES

Post processing of the measurement data for the cylinder pressure traces was carried out using MatLab. The pressure traces were recorded using a Kistler 6053 piezo electric pressure transducer, with a sampling rate of five samples per CAD in the optical engine and ten samples per CAD in the multi cylinder engine using an AVL Indimaster and an AVL Indicom. The data were converted to ASCII-format and imported to MatLab. The rate of heat release was calculated by assuming that the combustion process was close to an adiabatic isentropic process. Estimates of CA50, the rate of heat release and the heat release were all based on this equation with the assumption that γ remained constant. Calibration of the heat release calculation was carried out with motored pressure traces. The rate of heat release values obtained for reactions that occurred during the NVO were, as expected, small. However, the consistency of responses to changes in the settings and the fact that reactions were noted in all cases, even in the optical engine, suggest that the trends are plausible.

The temperature calculations were performed by assuming a polytropic process and the polytropic coefficient, was less than γ, since the polytropic compression and expansion could not be assumed to be close to adiabatic and isentropic due to the slower (and thus non-adiabatic) rate of change compared to the combustion. The accuracy in absolute terms was naturally sensitive to the values of the different parameters, but the intention of the temperature calculations was to investigate the temperature difference between the two compared cases rather than to obtain highly accurate values of the absolute temperature. The influence of different settings for polytropic coefficient, trapped mass, total mass, exhaust temperature and γ on the temperature differences between the cases was analyzed and the obtained differences were robust to changes.

POST PROCESSING - LIF IMAGES

The LIF images obtained by the intensified cameras displayed high amounts of noise, due to the high intensification of the weak signals, and thus post-processing of the images was essential. This was performed by using MatLab, and the effect of the filtering process was thoroughly studied in order to verify that the filter worked properly and thus reduced the extremely high gradients in the images while maintaining the proper signals. The noise or sharp gradients in intensity caused by the image intensification was studied in images on- and off-resonance as well as in regions in the combustion chamber and regions outside the optically accessible region to obtain knowledge about these disturbances. In figure 22, the filter's effects can be seen. The figure shows a filtered image and an unfiltered one, and the intensity along lines that start in a region with OH signals, around 500 in pixel number, and ends in an area without any OH signal, around 550 in pixel number. An intensity threshold of 500 would give the same result for both the filtered and unfiltered images. However, when the images were averaged, if there was a region that only had a significant signal in one of the images the reduced variation in the filtered images led to those reactions being detectable in the averaged images. The average value and the standard deviation of the intensity for the pixels within and outside the region with OH signals can be seen for both the filtered and the unfiltered images in figure 22. The solid lines correspond to the mean and mean +/- one standard deviation.

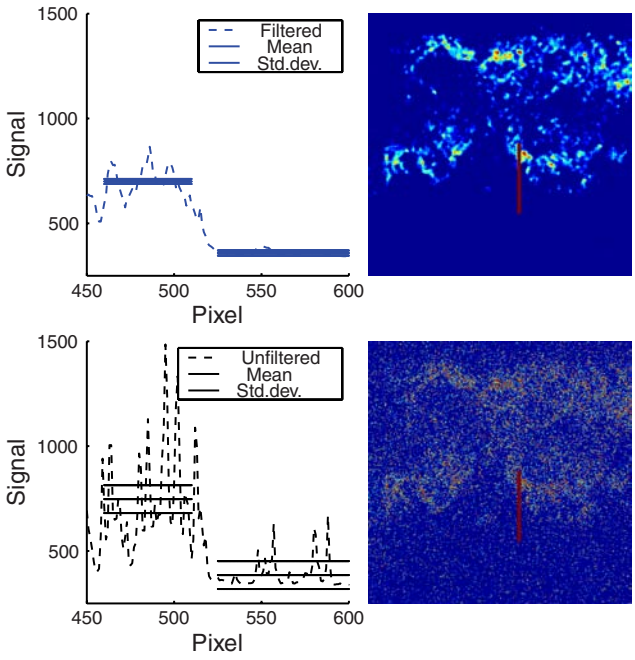

Figure 22: Filtered and unfiltered images.

Different threshold values were applied to locate OH reactions in the averaged images, to locate reactions that did not appear in all repetitions at the same location, or both weak and strong signals caused either by reactions located at spatially similar locations in the repetitions, or solely strong signals. This threshold analysis was complemented by summing the intensities for the whole images and the mean values (see figure 22) showed similar values, thus the summation of the intensities would identify correct trends.

ACCURACY AND REPEATABILITY

The frequency-doubled, triangular laser beam generated by the dye laser used as the excitation source provided a non-homogenous laser sheet, in terms of intensity, and thus the LIF signals obtained from

spatially different location in the combustion chamber could have been affected by the differences in laser intensity. However, this study did not involve any comparisons of the intensity of spatially different locations within the combustion chamber. Thus, the absorption did not play any major role in this analysis, although if the absorption had been strong enough to reduce the laser intensity sufficiently to make LIF analysis of OH impossible, then comparisons between different cases would have been greatly affected. But for the cases where the signal was limited to regions from which the laser sheet entered the combustion chamber (see figure 18 for the signals obtained at 320 CAD) the absorption would be the lowest due to the lower pressure and lower amounts of OH at those timings. So, despite the non-homogeneity of the laser sheet and absorption in the LIF images, it was believed that the analysis of the images using thresholds or summing intensity would be sufficient to identify correct trends. The dye laser's intensity was greatly affected by the pump laser's intensity, which could be influenced by variables such as the condition of the dichorit mirrors and the aging of the dye, so the intensity of the dye laser could vary over time. Nevertheless, since the laser's intensity was not critical, provided it was sufficient to induce LIF of OH, it was believed the repeatability of the optical study was adequate for our purposes.

To verify that the excitation wavelength corresponded to the resonance wavelength for OH, images were taken with wavelengths off resonance to assure that no significant signal was obtained for those wavelengths (see figure 23). This also verified that appropriate filters had been selected and that any reflection or scattered light at the excitation wavelength was deleted. The resonance wavelength for OH was tested in both a reference burner and in the combustion within the combustion chamber.

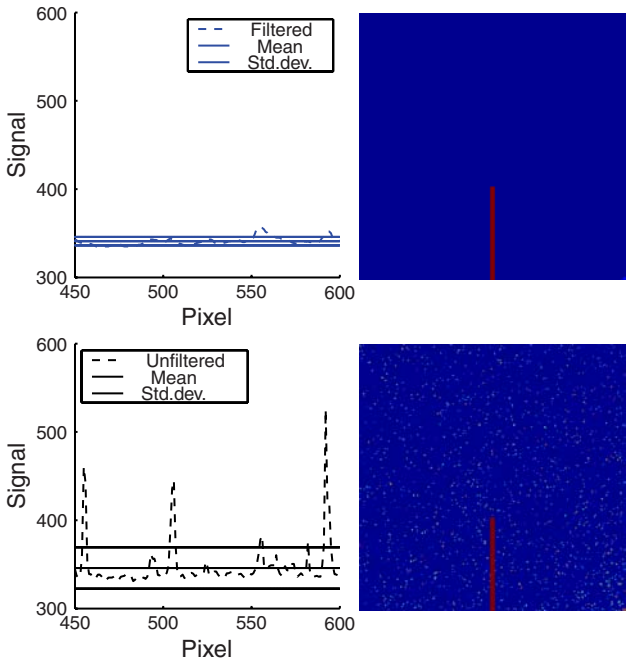

Figure 23: Filtered and unfiltered images taken with a off resonance wavelength during the NVO.

Paper VII

Reducing Pressure Fluctuations at High Loads by Means of Charge Stratification in HCCI Combustion with Negative Valve Overlap

Daniel Dahl, Mats Andersson, Andreas William Berntsson, Ingemar Denbratt and Lucien Koopmans

SAE Technical Paper

2009-01-1785

Reducing Pressure Fluctuations at High Loads by Means of Charge Stratification in HCCI Combustion with Negative Valve Overlap

Daniel Dahl, Mats Andersson, Andreas Berntsson and Ingemar Denbratt
Chalmers University of Technology

Lucien Koopmans
Volvo Car Corporation

ABSTRACT

Future demands for improvements in the fuel economy of gasoline passenger car engines will require the development and implementation of advanced combustion strategies, to replace, or combine with the conventional spark ignition strategy. One possible strategy is homogeneous charge compression ignition (HCCI) achieved using negative valve overlap (NVO). However, several issues need to be addressed before this combustion strategy can be fully implemented in a production vehicle, one being to increase the upper load limit. One constraint at high loads is the combustion becoming too rapid, leading to excessive pressure-rise rates and large pressure fluctuations (ringing), causing noise.

In this work, efforts were made to reduce these pressure fluctuations by using a late injection during the later part of the compression. A more appropriate acronym than HCCI for such combustion is SCCI (Stratified Charge Compression Ignition). The approach was evaluated in tests with a single-cylinder metal research engine and a single-cylinder optical engine. The latter was used to characterize the combustion in laser-based analyses including laser-induced florescence (LIF) determinations of fuel tracer, OH and CH_2O (formaldehyde) distributions. A high speed camera was also used for direct imaging of chemiluminescence.

The effects of two main parameters were studied: the proportion of fuel injected late to create a stratified charge and the timing of the late injection. In addition, two fuels were used: a certification gasoline fuel and a blend of n-heptane, iso-octane and 3-pentanone. Both fuels were used in the metal engine for comparison. Use of a stratified charge allowed the maximum pressure-rise rates and ringing intensity to be reduced at the expense of increases in NO_X and CO emissions, regardless of fuel type. Optical results indicated that both the fuel distribution and combustion were not homogenous.

INTRODUCTION

By 2015, European automakers will have to reduce their fleet average CO_2 emissions of new cars sold in the EU to 120 g/km (by measures such as the use of biofuels, gear-shift indicators and tyre-pressure monitoring) or risk penalties [1]. In 2005, the average emissions from new European cars amounted to 160 g/km, so a further 25% reduction was required [2]. In addition to upcoming regulations, increases in the environmental concern of customers and rising fuel prices are also prompting a need to improve the fuel efficiency of cars. There are numerous ways to reduce cars' CO_2 emissions, including reducing their mass, rolling resistance and aerodynamic drag coefficients, and improving the energy efficiency of components such as power steering systems, air-conditioning systems, water pumps and generators. Unfortunately, however, cars are tending to become heavier rather than lighter, due partly to the extra weight of additional safety equipment and other accessories, and partly because cars are simply becoming larger due to customer preferences for increased comfort, roominess etc. This means that more effort is required to improve the efficiency of their

The Engineering Meetings Board has approved this paper for publication. It has successfully completed SAE's peer review process under the supervision of the session organizer. This process requires a minimum of three (3) reviews by industry experts.

ISSN 0148-7191

SAE Customer Service: Tel: 877-606-7323 (inside USA and Canada)
Tel: 724-776-4970 (outside USA)
Fax: 724-776-0790
Email: CustomerService@sae.org
SAE Web Address: http://www.sae.org

Printed in USA

propulsion systems, especially in the premium car segment where weight is of greatest concern.

The first 4-stroke gasoline engine was run in 1876 [3] and today, over 130 years later, this type of engine is still the dominant prime mover for passenger cars. Furthermore, the spark ignition (SI) combustion strategy used in the gasoline engine has not been seriously challenged for most of its history, due in large part to its relative simplicity. However, other more complex strategies have been developed recently that are competitive because of the low efficiency of the SI strategy, especially in part load, which is mainly due to pumping losses caused by throttling of the intake air flow, large heat losses from the high temperature combustion and long burn durations.

One of the new strategies under development is the homogeneous charge compression ignition (HCCI) strategy. In contrast to SI combustion, in which a spark is used to initiate combustion, auto-ignition is used in the HCCI strategy. A close-to-homogenous charge of air, fuel and residuals from the previous cycle is compressed until the temperature is sufficiently high for auto-ignition of the mixture to occur.

One way of realizing HCCI combustion is by closing the exhaust valve early so that some of the hot residuals are retained in the cylinder, which helps to further increase the temperature during the compression stroke of the following cycle, as explained by Willand *et al*. [4], patented by Denbratt [5] and applied by Koopmans *et al*. [6]. By controlling the time when the exhaust valves close, one also affects the temperature of the mixture, and hence the ignition timing. The intake valve is opened late and a negative valve overlap between exhaust valve closing and intake valve opening is created. A pilot injection in the gas exchange phase can also be used to increase and control the temperature of the mixture, and thus adjust the ignition timing, as discussed by Koopmans *et al.* [7]. HCCI can run with wide open throttle (WOT), significantly reducing pumping losses. Wall heat losses are high in this type of HCCI combustion due to the high mean temperature over the cycle caused by the compression in the negative valve overlap. Nevertheless, although the mean cycle temperature is high, peak temperatures are lower than in conventional strategies, due to the large dilution ratio, and thus NO_X emissions are low in HCCI combustion [6, 7]. In addition, burn durations are significantly shorter in HCCI than in SI combustion, so it more closely resembles the ideal Otto-cycle, which further increases its efficiency.

The operating regime for HCCI combustion in a 4 stroke Otto engine is mainly limited to low loads and speeds. At high loads the range of possible operating parameter settings is reduced, because of misfires or very rapid burning [8]. Rapid combustion leads to high pressure-rise rates and, eventually, pressure oscillations causing noise, similar to knocking combustion in SI engines [9], as illustrated in Figure 1.

There are several ways in which knock can be classified in an engine by analyzing pressure traces (some of which are described by Burgdorf *et al.* [10]). One way is to define the knock intensity (KI) as the maximum amplitude of the high-pass filtered pressure signal. This method is used in this work, but to avoid discussions about the validity of using the term “knock”, the results presented here are expressed in more appropriate terms of ringing intensity (RI). An example is shown in Figure 2, in which an unfiltered and high-pass filtered signal for an HCCI cycle with severe ringing is plotted. In this example the ringing intensity is 3.4 bar (cut-off frequency, 4000 Hz).

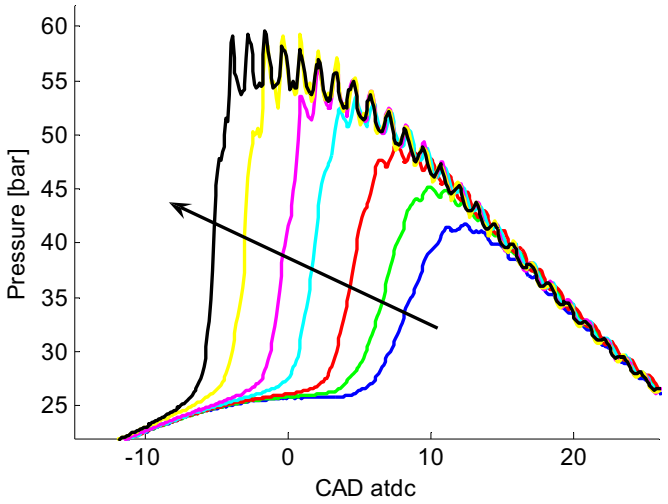

Figure 1. Traces showing typical load and pressure-rise increases caused by increasing fuel amounts (in arrowed direction) in HCCI combustion.

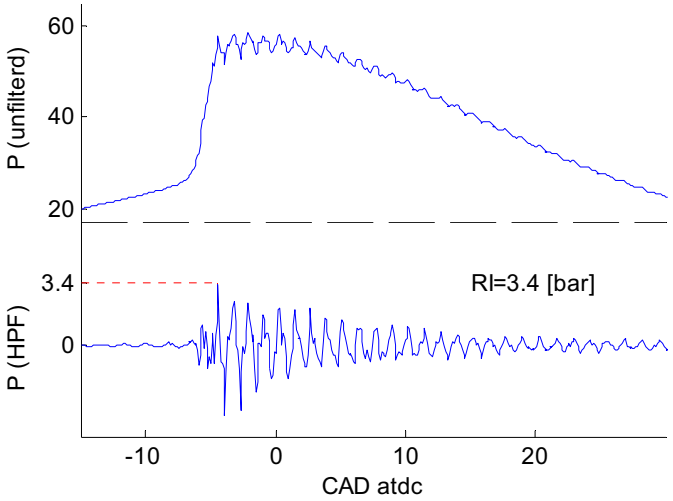

Figure 2. Unfiltered pressure trace (top) and high-pass filtered (HPF) pressure trace (bottom).

The effects of charge inhomogeneity on various relevant variables, e.g. combustion phasing, ROHR and emissions, have been widely studied [11-28]. Dec *et al.* [16] argue that using fuel stratification to control the combustion phasing is most effective for fuels with two-

stage ignition characteristics, such as n-heptane, and its effects are modest for fuels with single stage ignition characteristics, such as iso-octane and (often) gasoline. Sjöberg *et al.* also showed that fuel stratification with a primary reference fuel (PRF) including n-heptane can effectively smooth the heat release rate and lower the pressure-rise rate, [24]. Many studies have shown that the rate of heat release (ROHR) can be reduced by using a more inhomogeneous mixture, [19, 20, 22, 23, 25]. However, a typical single-stage ignition fuel was used in few of these studies (in which cases it was gasoline) [19 & 20]. Leach *et al.* [19] used NVO to control internal EGR rates, but they did not focus on the high load limit.

The study reported here investigated the possibilities to use a stratified charge to reduce the maximum pressure-rise rates and ringing intensity in an HCCI engine with NVO operating at high loads with engine geometry typical of gasoline engines for passenger cars. The stratified charge was created by adding a late injection, in the later part of the compression stroke, to the main injection in the early part of the intake stroke, see Figure 3. When introducing a stratified charge it is clearly contradictory to call the combustion HCCI. A more appropriate acronym is SCCI, for Stratified Charge Compression Ignition.

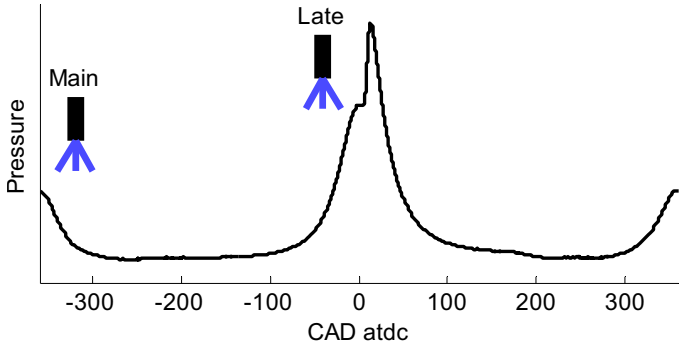

Figure 3. Illustration of the SCCI strategy.

A metal engine was used to study the effects of varying the amount and timing of the late injection on pressure trace-based combustion characteristics and emission levels, and an optical engine was used to observe the combustion phenomena when fuel stratification was introduced. This was done by high speed video (HSV) imaging of natural chemiluminescence and LIF of fuel tracer, OH and CH_2O. The PRF fuel used in the optical experiments was also used in the metal engine experiments (in addition to gasoline) for comparison.

EXPERIMENTAL SETUP & EQUIPMENT

ENGINE – A single cylinder AVL research engine was used for both metal engine and optical engine experiments. The geometry of the combustion chamber was similar in both setups, with a flat piston and pentroof head. The main difference was in the location of the injector. In the metal engine setup the injector was centrally placed perpendicular to the piston, while in the optical setup the injector was offset from the center by a small angle, see Figure 4. A multi-hole injector giving a horse-shoe shaped spray pattern was used for the metal engine setup while a hollow-cone piezo electric injector was used for the optical setup. Since the hollow-cone injector creates a more equally distributed spray than the multi-hole injector the authors believe that it also creates a more homogenous charge. The fuel pressure was set to 150 bar in the metallic engine and 190 bar in the optical engine. For the metal engine measurements two different compression ratios were used to account for the difference in the fuels' octane numbers (keeping auto-ignition timing at around TDC with approximately the same valve-timings in tests with both fuels). Detailed engine parameters can be seen in Table 1.

MEASURING EQUIPMENT - The emission measuring instruments consisted of a flame ionization detector for unburned HC, non-dispersive infrared radiation detectors for CO and CO_2, a chemiluminescence analyzer for NO_X, and a paramagnetic susceptibility analyzer for O_2. Propane was used to calibrate the HC instrument. Soot/particles were measured using an AVL 415 smoke meter. The fuel flow was measured using a Micro Motion meter, which obtains estimates of the fuel flow by measuring the Coriolis force. Equivalence ratios were measured using a lambda meter from Horiba. In-cylinder pressure was measured during 299 cycles at a resolution of 0.1 CAD around TDC and 1 CAD otherwise, using a cooled Kistler 6061b pressure transducer and a Kistler 6053 pressure transducer for the metal and optical engine measurements, respectively, connected (in both cases) to a Kistler 5044 charge amplifier. For data acquisition and real-time combustion analysis an AVL Indimaster 670 system connected to a PC with AVL IndiCom® 1.1 software was used. For the post-processing combustion analysis presented in this work an in-house MatLab® code was used.

METAL ENGINE MEASUREMENTS – Since charge stratification affects the combustion phasing, and the combustion phasing affects the heat-release rate, it was decided to keep the location of 50% burned (CA50) constant. The most convenient method to achieve this was to regulate the temperature of the incoming air with an electrical heater.

To obtain comparable starting points in each experiment the engine was first run in HCCI mode, with only a main injection, for each fuel. The duration of this injection was increased until the load peaked (due to too much fuel being injected, causing too early combustion phasing and thus negative work on the piston). Efforts were made to ensure that starting conditions for tests with the two fuels were similar in terms of variables such as IMEP, CA50, lambda, intake temperature and RI. The adverse effects of ringing are greater at higher loads. Therefore, the compression ratio and NVO were chosen not to maximize the load but rather to facilitate ringing. This gave a wider range of operating conditions and

facilitated analysis of the problem since quite high ringing intensity values could be tolerated.

The temperature of the engine coolant and oil was kept constant at 90°C, with a conditioning system. A reference point was used during the experimental campaign to check for abnormalities in the engine's behaviour by comparing IMEP, location of 50% heat release (CA50), temperature values, emission levels etc. to those obtained in an earlier reference test. All the measurements in the metal engine runs were repeated, in random order, to eliminate time trends and to obtain indications of the spread/deviation of the measurements. Each measurement covered 299 cycles.

The effects of two parameters were investigated in the metal engine tests: the proportion of fuel injected in the late injection and the timing of this injection. The amount of fuel injected in the late injection was 0, 2, 25 35 and 50% (w/w) of the total fuel amount, as approximated using the Coriolis meter in single injections into a motored engine at a cylinder pressure between that of the main and late injections. The end of injection (EOI) of the first injection was at 330 CAD bTDC, and two settings for the end of the late injection were used; 30 and 50 CAD bTDC, see Figure 3. Increasing the proportion of fuel and retarding the EOI of the late injection reduces the time available for mixing and should thus lead to a more stratified mixture.

OPTICAL SETUP – The cylinder head used for the optical measurements provided optical access through two pentroof quartz windows. The laser planes entered through one side, exited through the other, and were parallel to the piston. An extended piston with a quartz window in the center provided optical access to the combustion chamber from below, where a 45° mirror was mounted, as schematically shown in Figure 4. The lines in the left image indicate boundaries of the laser planes, which entered from the left.

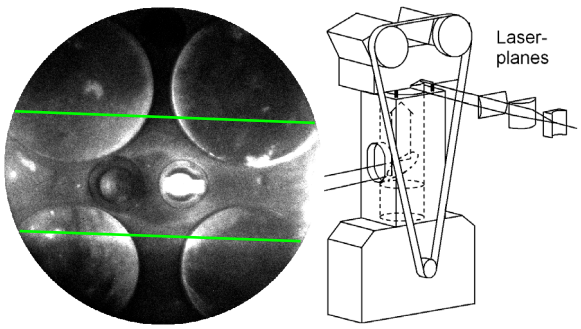

Figure 4. Left: optical view of the combustion chamber through the piston. Lines show boundaries of the laser planes. Right: Schematic view of the optically accessible engine.

The optical methods were used simultaneously in the following combinations:

HSV – formaldehyde LIF – OH LIF
HSV – formaldehyde LIF – fuel-tracer LIF
HSV – fuel-tracer LIF – OH LIF

Two laser systems were used: the third harmonic light from a Nd:YAG-laser (λ = 355 nm) to excite formaldehyde molecules, and a dye-laser with Rhodamine 590 pumped by the second harmonic of the Nd:YAG-laser, generating tunable light with wavelengths around 570 nm. This light was then frequency-doubled to UV-light in the range 280-286 nm. To detect OH molecules the light was tuned to the $Q_1(6)$ transition in the A(ν=1) – X(ν=0) band, at 282.93 nm. The dye-laser light was also used to excite 3-pentanone, which was added as a tracer for fuel distribution imaging. The two laser beams were spatially overlapped by dichroic mirrors, and formed into a horizontal sheet passing through the cylinder a few mm below the injector nozzle. To avoid interference between light generated by the two lasers, they were triggered a few microseconds apart from each other. Images of fluorescent light and emissions from the combustion were acquired through the piston window via a mirror reflecting UV and visible light. Two intensified CCD-cameras were used to detect fluorescent light. OH-fluorescence was detected in the 0-0 and 1-1 vibrational transitions around 305-315 nm, using a dichroic mirror with maximum reflectivity at 308 nm to split OH-fluorescence to the first camera, while an interference filter for transmission of light at 310±5 nm was placed in front of the camera. When this camera was used to detect fluorescence from the fuel tracer, a semi-transparent mirror was used to split off a fraction of the light and a long-pass WG360 filter was placed in front of the camera. The second camera was used to detect the fluorescence from formaldehyde using a long pass GG420 filter, or from the fuel tracer using the WG360 filter. In addition to the intensified CCD-cameras, a high-speed video (HSV) CMOS-camera was used to record the visible and near-infrared light emitted by the flame. HSV images were recorded every 2 CAD.

OPTICAL ENGINE MEASUREMENTS – Since the optical accessible head was not cooled, it made little sense to attempt to regulate the combustion phasing by varying the intake temperature. Each measurement, which took approximately 30 seconds started with the cylinder head temperature at ~100°C and ended at ~130-140°C, hence there was a time trend within each measurement. During this time, pressure traces were recorded continuously while LIF images and HSV were recorded every 23 cycles for 10 cycles in total. Formaldehyde/OH and fuel-tracer/OH measurements were performed at -10 to 10 CAD aTDC, at 5 CAD intervals, while formaldehyde/fuel-tracer measurements were performed at -35 to 5 CAD aTDC at 10 CAD intervals.

Three cases were examined in the optical engine: single injection in the early part of the intake stroke (EOI=330 CAD bTDC), referred to as the homogenous case; and split injections with 50% of the injection duration late, at 30 or 50 CAD bTDC (this was considered to equal approximately 50% of the fuel amount in both cases, since the fuel pressure was high compared to the cylinder pressures at each of the EOIs).

Table 1. Engine parameters and test data

Parameter	Metal Engine (Gasoline)	Metal Engine (PRF fuel)	Optical Engine (PRF fuel)
Intake valve opening [CAD aTDC(gas exchange)]	80	78	75
Exhaust valve closing [CAD bTDC (gas exchange)]	76	78	75
Intake valve duration [CAD]	120	120	120
Exhaust valve duration [CAD]	120	120	120
Bore [mm]	84	84	83
Stroke [mm]	90	90	90
Compression ratio	11.3	9	10.2
IMEPnet	4	3.9	3
Engine Speed [rpm]	1200	1200	1200
CA50 [CAD aTDC]	2 ±0.3	1.1 ±0.4	~0-6
Fuel	Gasoline: CEC legislative fuel, RF-02-03, 99.5 RON	50% n-heptane 40% Iso-octane 10% 3-pentanone	50% n-heptane 40% Iso-octane 10% 3-pentanone

RESULTS AND DISCUSSION

In this section results from the metal engine measurements are first presented, then results from the optical measurements.

METAL ENGINE – The results from the metal engine tests indicate that it is possible to reduce the maximum pressure-rise rate and the ringing intensity by using a late injection close to TDC. This was done keeping the combustion phasing constant and is valid for both PRF fuel and gasoline (Figure 5). The maximum pressure-rise rate was calculated by taking the maximum slope of filtered individual cycles and averaging these values for each measurement. The ringing intensity, RI, was calculated by taking the maximum amplitude of the high pass filtered (4000 Hz) pressure traces for each cycle then averaging this value over all cycles. In all tests, except when using the primary reference fuel with EOI at 50 CAD bTDC, both the ringing intensity and maximum pressure rise rate consistently decreased, almost linearly, with increases in the proportion of fuel in the late injection. For PRF with an EOI of 50 CAD bTDC the effects were strongest with a late injection amount corresponding to 25% of the total amount. Increasing the stratification further seems to increase both RI and the pressure rise rate.

Figure 6 shows the influence of varying the charge stratification on the burn duration. It clearly illustrates that the burn duration increases with increasing amounts of fuel in the late injection (except, again, when using PRF with an EOI of 50 CAD bTDC; in this case the burn duration is longest at ca. 25% stratification). Combining the results displayed in Figure 5 and Figure 6 one can conclude that an increase in burn duration decreases the ringing intensity.

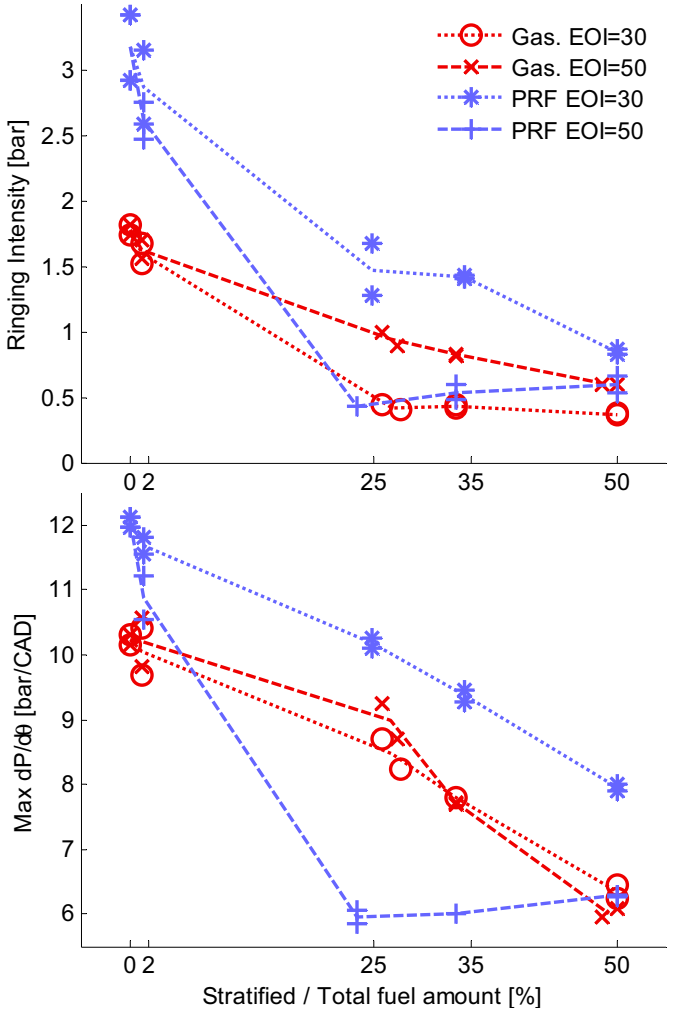

Figure 5. RI & maximum pressure-rise rate in tests using gasoline (Gas.) and primary reference fuel (PRF) with stratification EOIs at 30 and 50 CAD bTDC. Lines join average data points obtained from repeated measurements.

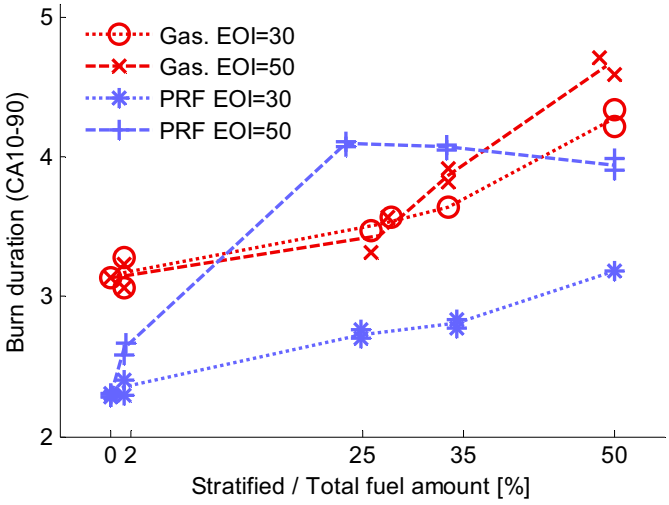

Figure 6. Burn duration (CA10-90) in tests using gasoline (Gas.) and primary reference fuel (PRF) with stratification EOIs at 30 and 50 CAD bTDC. Lines join average data points obtained from repeated measurements.

To assess whether a stratified mixture yields the same ringing intensity as a homogenous mixture with the same burn duration the ringing intensity was plotted against the burn duration of individual cycles, as shown in Figure 7 and Figure 8 for gasoline and PRF tests, respectively. For each value of CA10-90 the values of RI are averaged and displayed by bold lines. There are three bold lines in each plot. The solid lines represent data obtained with only main injections (no stratification) from measurements performed when finding the maximum load. They each represent 4186 individual cycles and are used as a reference. The other bold lines in each figure represent data obtained with EOIs of 30 and 50 CAD bTDC (and hence different levels of stratification), in eight measurements, each with a total of 2392 cycles. The thin lines indicate the standard deviations from the mean. The ringing intensity clearly increases dramatically with reductions in burn duration when the burn duration is shorter than ~5 CAD. In gasoline tests with early second injection the ringing intensities appear to coincide with those observed in the homogenous tests with only a main injection, but with late second injection the ringing intensity seems to be somewhat lower, at least for burn durations longer than 3 CAD. In tests with the primary reference fuel, the ringing intensities in both stratified cases appear to be lower than those observed for the homogenous case, except for early second injection when the burn duration is shorter than 3 CAD. These results indicate that there are differences in this respect between homogenous and stratified operation, but provide no further information to verify or explain the differences.

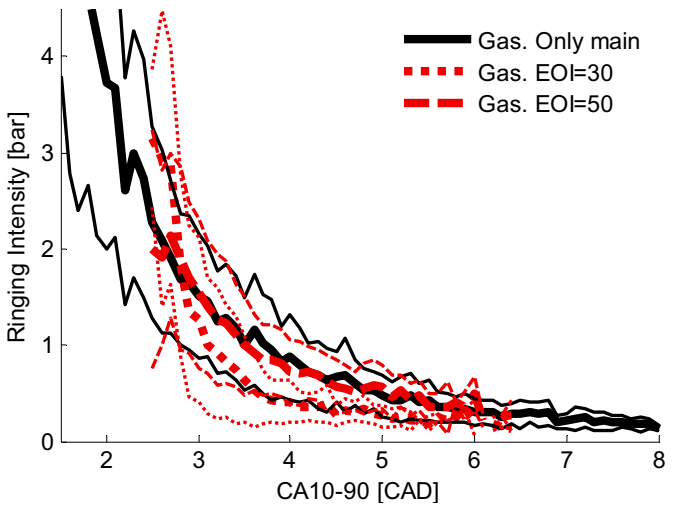

Figure 7. Ringing intensity versus burn duration in individual cycles in gasoline tests. The lines represent all the measurements obtained in the metal engine with gasoline: thick lines correspond to mean values and thin lines to standard deviations from the means.

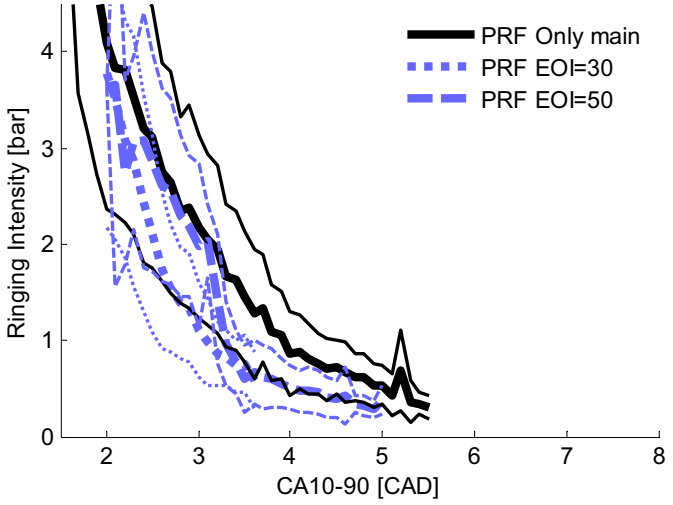

Figure 8. Ringing intensity versus burn duration in individual cycles in PRF tests. The lines represent all the measurements obtained in the metal engine with primary reference fuel: thick lines correspond to mean values and thin lines to standard deviations from the means.

The injection strategy has a major impact on the combustion phasing. If the combustion phasing with given injection parameters is too early, the intake temperature needs to be decreased to counteract this effect and vice versa. Hence, the intake temperature is also an indicator of the impact of the injection settings on combustion phasing. The intake temperature (measured 10 cm upstream from the cylinder head) required to maintain a constant CA50 is shown in Figure 9. For gasoline, the temperature interval required was only about 20°C while for PRF it was about 70°C, indicating that the effect on combustion phasing is much greater with PRF, in accordance with findings reported by Dec *et al.* [16]. Figure 9 also shows the effects on lambda, mainly caused by the change in intake temperatures. The intake temperature needed to be lower in PRF tests with early injection and higher with late injection

compared to the homogeneous case. An explanation for this can be found by investigating the heat release curves.

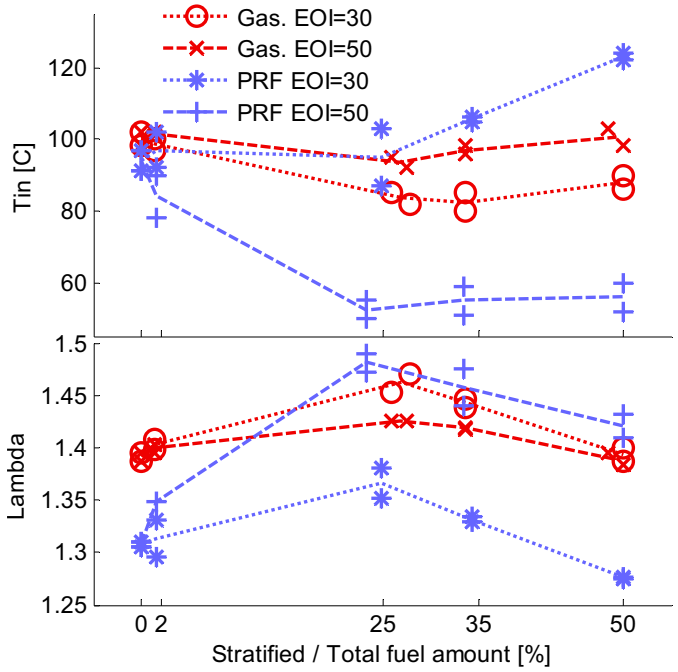

Figure 9. Temperature in the intake manifold 10 cm from the cylinder head and lambda in tests using gasoline (Gas.) and primary reference fuel (PRF) with stratification EOIs at 30 and 50 CAD bTDC. Lines join average data points obtained from repeated measurements

In Figure 10 the cumulative heat release rate and rate of heat release are plotted for each of the settings and fuels. The upper two plots show the average net cumulative heat release rate before the main combustion, while the lower two show the heat release rate for individual cycles selected to represent the average behavior in ringing intensity, combustion phasing, burn duration and maximum pressure rise rate. Heat release calculations are described in the Appendix.

It was, unfortunately, impossible to use the rate of heat release to investigate the low temperature reactions (cool-flame) since the noise was too great. Cumulative heat release results are of greater value, but care must be taken when interpreting these plots. The values for the ratio of specific heats (γ) have been chosen to be representative of the mixture once all the fuel is injected. Before that, γ is underestimated and the curve is shifted upwards. This probably explains at least some of the differences shown in Figure 10 between cumulative heat release curves obtained in tests (using both fuels) with the latest injection and the homogeneous case.

No low temperature heat release can be seen in the gasoline curves that could explain the required reduction in intake temperature. All that is noticeable is the temperature drop caused by the evaporation of the fuel. In contrast, the PRF curves show significant low temperature heat release. For the early injection cases the low temperature heat release is larger than for the homogenous case, explaining the reduction in intake temperature required to keep the combustion phasing constant. There also appears to be more low temperature heat release (or less cooling effect) in the 25% late injection case than in the 50 % case, which may explain why the intake temperature was lowest for the 25% case. The large amount of low temperature heat release may necessitate a lower intake temperature which increases the amount of air, resulting in a globally cooler and more dilute mixture that burns more slowly, accounting for the lower pressure rises and RI values shown in Figure 5. An interesting finding is that for the late injections the energy required for the fuel evaporation seems to oppose or even completely counter the low temperature heat release, especially for the 50% case. This may explain why an increase in intake temperature is required to keep CA50 constant.

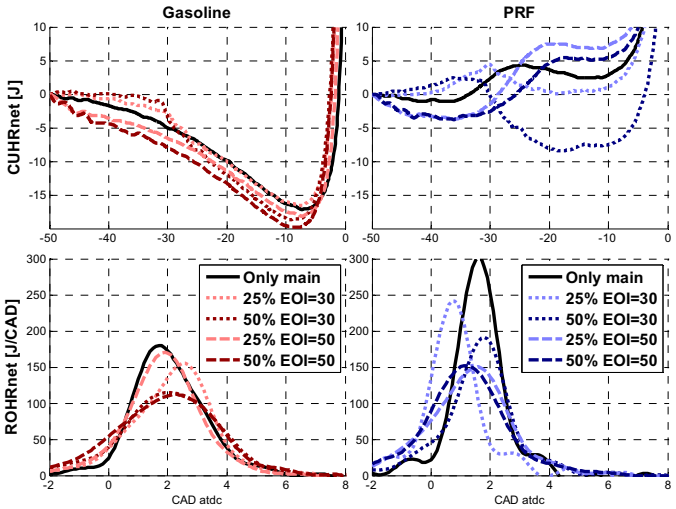

Figure 10. Average net cumulative heat release (CUHRnet, upper two plots) and net heat release rate (lower two plots) taken from individual cycles representative of the average behavior in terms of RI, CA50, CA10-90 & maximum pressure rise rate in tests with both gasoline and PRF.

Introducing a stratified charge also showed potential to increase the combustion stability. This is illustrated in the upper plot of Figure 11, which shows that the standard deviation of IMEPnet is generally minimal with 25-35% stratification. Increasing the stratification amount further seems to decrease combustion stability slightly. The lower plot shows the standard deviations of the combustion phasing, which show no apparent correlation with the IMEPnet standard deviations. Further, while the standard deviation of CA50 decreases with increases in stratification amount in tests with PRF it increases in tests with gasoline.

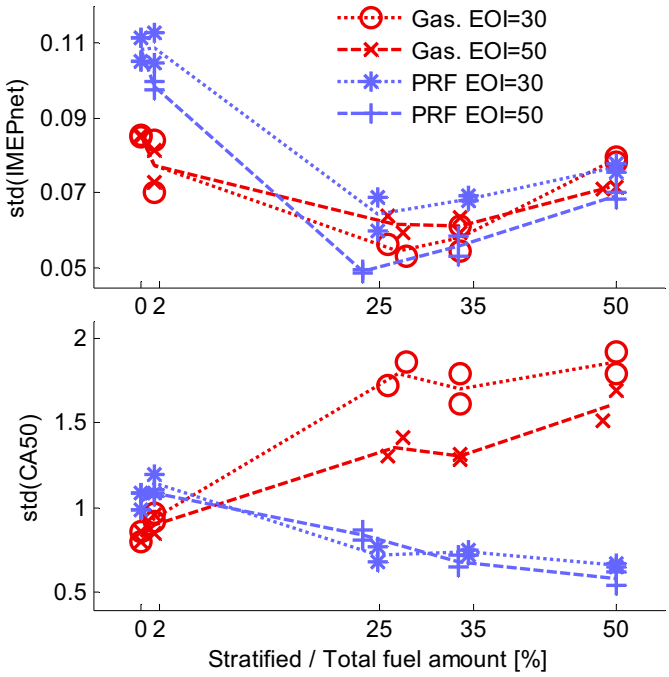

Figure 11. Standard deviation of IMEPnet and CA50 in tests using gasoline (Gas.) and primary reference fuel (PRF) with stratification EOIs at 30 and 50 CAD bTDC. Lines join average data points obtained from repeated measurements.

Obvious drawbacks of dividing the injection into an early main injection and a late stratified charge injection are the accompanying increases in NO_X and CO emissions. Figure 12 shows CO-, NO_X-, & HC-emissions obtained in tests with both fuels and the two late injection timings. NO_X values are high even when using only a main injection, because of early and rapid combustion. When introducing the smallest amount of stratification these values are unaffected, but when the amount of stratification is increased to about 25%, NO_X values increase two to three fold. Further increases in the stratification amount do not have a strong impact on NO_X levels. Since NO_X levels peak at a slightly leaner than stoichiometric AFR [3], this implies that the maximum proportion of the charge with that AFR is reached at 25% stratification.

At these high loads, levels of HC are fairly low and the introduction of charge stratification does not have a strong effect. However, the type of fuel is of greater importance: gasoline yields ca. 50% higher levels of HC than PRF. This is probably an effect of the higher compression ratio for gasoline leading to more fuel in crevices and/or more wall-wetting because of the piston being 2.5 mm closer to the spray.

CO emission levels increase dramatically with a high amount of stratification, especially for the late EOI. Thus, since CO levels increase when there is a lack of oxygen to form CO_2, the high levels obtained when injecting half the fuel late implies that the mixture is burning locally rich. This effect is strongest when the fuel is injected at the latest timing since this gives the least time for mixing. These findings also implicitly verify that increasing and/or retarding the second injection creates more fuel stratification.

The bottom plot in Figure 12 displays the levels of soot measured. Generally the values are low, close to the detection limit of the instrument. Hence soot emission is not a limiting factor when using these moderate stratification levels. The only tests in which higher soot levels were consistently observed were gasoline tests with the smallest amount of second injection (2 %; the smallest amount that could be injected with the equipment used), in which incomplete sprays may have been created with large droplets. This could also explain why HC emission levels were highest with 2% late injection.

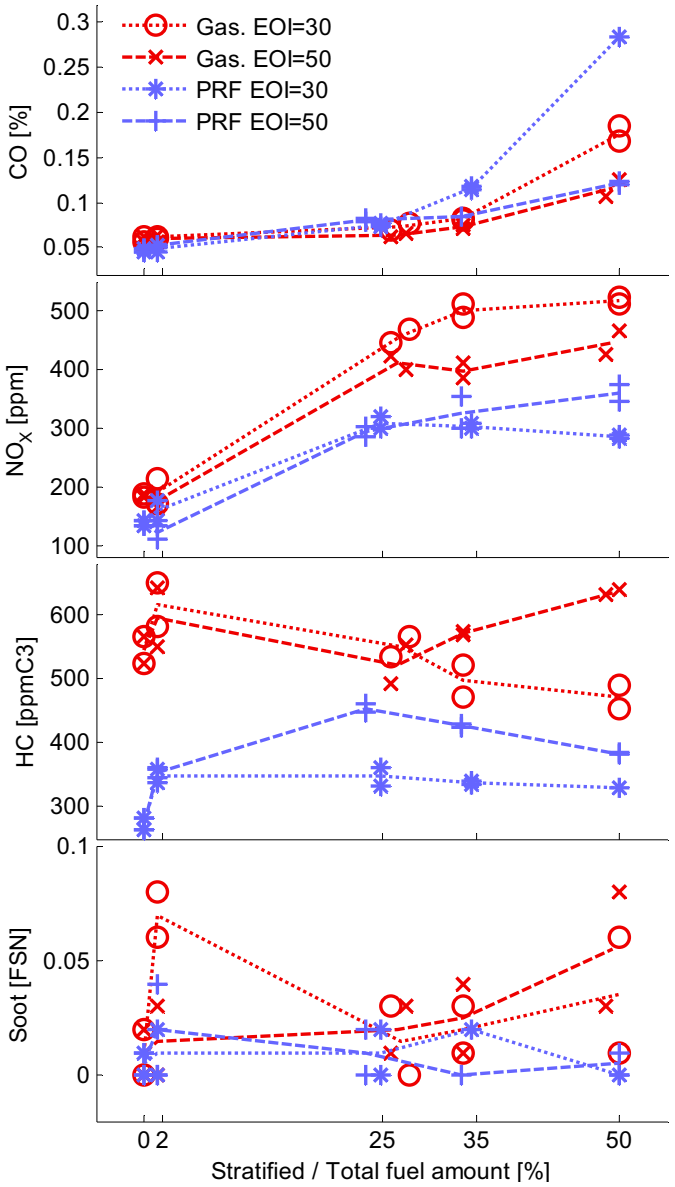

Figure 12. CO, NO_X, HC & soot levels measured in tests using gasoline (Gas.) and primary reference fuel (PRF) with stratification EOIs at 30 and 50 CAD bTDC. Lines join average data points obtained from repeated measurements.

It is difficult to draw any conclusions regarding fuel consumption from the reported experiments since the

spread in the measurements are large, especially in relation to the relative difference between the different settings. As can be seen in Figure 13, fuel consumption seems to be almost unaffected by the stratification amount or timing, especially for gasoline, although it may be slightly lower at 25 and 35 percent stratification than at other stratification levels. These patterns could be correlated with the combustion stability and combustion efficiency patterns shown in Figure 11 and Figure 13 (lower panel), respectively. When the stratification amount is too high both combustion efficiency and combustion stability are reduced. In tests with PRF the combustion efficiency is lowered even with the lowest stratification amount, but this seems to be offset by the large improvement in combustion stability.

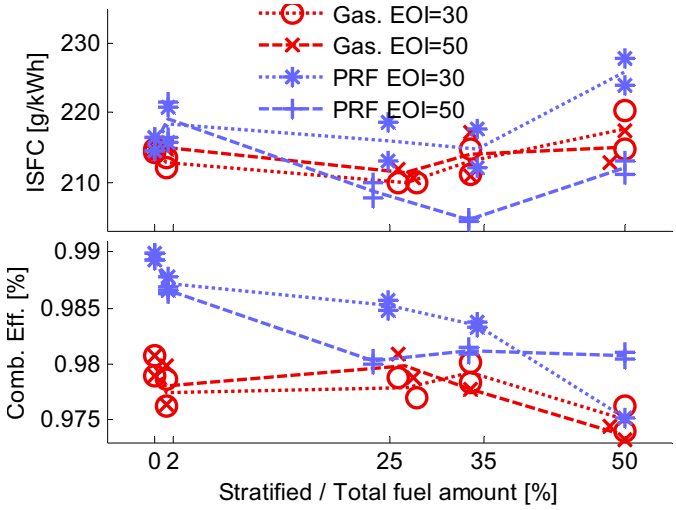

Figure 13. Indicated specific fuel consumption and combustion efficiency in tests using gasoline (Gas.) and primary reference fuel (PRF) with stratification EOIs at 30 and 50 CAD bTDC. Lines join average data points obtained from repeated measurements.

OPTICAL ENGINE – Table 2 summarizes results of the combustion analysis of the pressure traces obtained from the optical engine experiments. These are averaged values of all the measurements: 299x15 for the homogenous case and the late EOI case, and 299x10 for the early EOI case (CH_2O/fuel LIF measurements were not performed for the early EOI case). Since the optical engine was not running under thermally stabilized conditions (the combustion phasing could not be kept constant due to the effects of warming) and the different measurements were taken on different days this table only provides indications of general trends. However, both RI and maximum dP/dθ clearly decrease, while the burn duration increases, when a late injection is introduced, and its effect is strongest at the latest injection timing. In contrast, combustion phasing is advanced when a late injection is introduced, but the effect is strongest with early timing. These results correlate with the trends seen in the metal engine, except that the late injection case should give an even later phasing than in the homogenous case. In addition, the increase in burn duration is not as distinct in the optical engine as in the metal engine when using a late injection. This is probably an effect of the earlier combustion phasing caused by the stratification, and it partially offsets the effects of the charge stratification.

Table 2. Average results of combustion analysis from pressure traces in the optical engine.

Parameter	Homogenous	EOI 50 CAD bTDC	EOI 30 CAD bTDC
RI [bar]	1.95	1.01	0.7
Max dP/dθ [bar/CAD]	8.08	7	6.34
CA10-90 [CAD]	3.03	3.1	3.36
CA50 [CAD atdc]	6.15	0.21	2.54

All images displayed in this section were originally monochromic, but in order to distinguish the different types of measurements readily, different color schemes have been used.

Figure 14 and Figure 15 show images of fuel-tracer-LIF (upper two images) and formaldehyde-LIF (lower two images) distributions obtained during homogenous combustion tests, and for the case with a late second injection containing 50% of the total fuel amount. The images shown are mean images acquired during ten cycles at 25 and 15 CAD bTDC. Disregarding the fact that the intensity of the laser plane was not homogenous for the fuel-tracer-LIF measurements, Figure 14 indicates that both fuel and formaldehyde were evenly distributed throughout the combustion chamber for the homogenous case. In the stratified case (Figure 15) a large concentration of fuel appears at the center of the combustion chamber. Five CAD after the injection, the formation of formaldehyde has not yet been affected by the inhomogeneous fuel distribution, but 15 CAD after the injection an increase in formaldehyde also appears at the center.

Similar images of events closer to TDC do not provide representative indications of either the fuel distribution or formaldehyde distribution, since concentrated zones appear more randomly, and thus averaged images show apparently homogenous distributions, even for the stratified case. Figure 16 therefore shows single images taken 5 CAD bTDC, which verify that concentrations of both fuel and formaldehyde are indeed homogenous in the homogenous case, and that this is not an averaging effect. For the stratified case, shown in the two right images in Figure 16, higher formaldehyde concentrations clearly appear at locations where the concentration of fuel is higher at this late point after the injection.

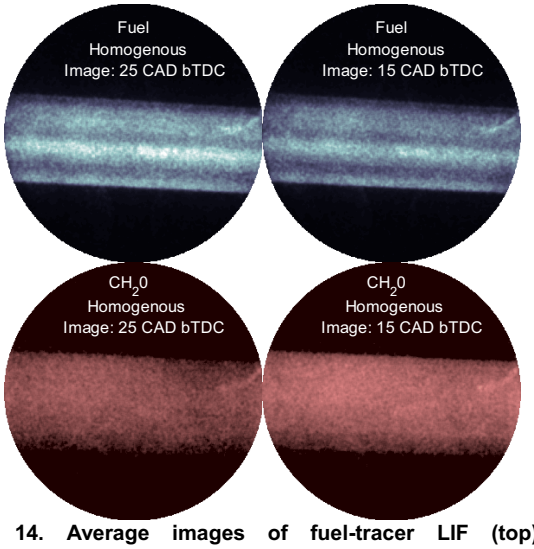

Figure 14. Average images of fuel-tracer LIF (top) and formaldehyde LIF (bottom) at 25 and 15 CAD bTDC obtained in homogenous case tests.

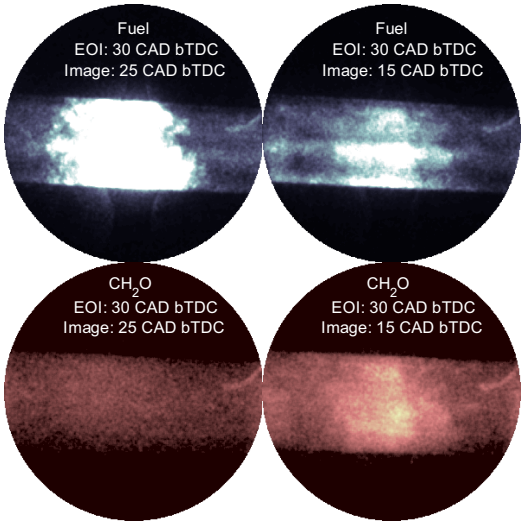

Figure 15. Average images of fuel-tracer LIF (top) and formaldehyde LIF (bottom) obtained at 25 and 15 CAD bTDC in stratified case (50% fuel injected at EOI 30 CAD bTDC) tests.

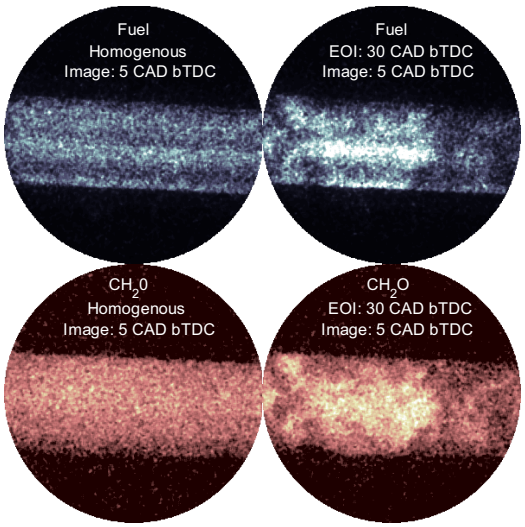

Figure 16. Simultaneous measurements of fuel-tracer LIF (top) and formaldehyde LIF (bottom) at 5 CAD bTDC for the homogenous case (left) and stratified case (right, 50% fuel injected at EOI 30 CAD bTDC).

To provide a better overview of the differences in fuel distributions between the three cases the fuel-tracer LIF images taken simultaneously with the OH LIF images are presented in Figure 17. In the figure, all ten individual images taken at 10 CAD bTDC are shown for the homogenous case (left column), the early second injection case (middle column) and the late second injection case (right column). Again, the fuel distribution is clearly homogenous in the homogenous case, with no significant variations between cycles. The distribution is less homogenous in the early second injection case and highly heterogeneous in the late second injection case. These results indicate that a later second injection gives greater fuel stratification. The authors believe that the amount of fuel injected in the second injection would also have influenced the fuel distribution, as shown in a similar study by Persson *et al.* [30], where a larger amount of fuel in a late DI injection relative a PFI injection caused more heterogeneity of the fuel distribution.

Figure 18 shows images in a similar layout to those in Figure 17, but of OH LIF images taken 10 CAD aTDC. At first glance the OH distribution does not appear to be homogenous in the homogenous case. However, this is partly because the intensity of the laser plane was uneven, being stronger in the upper part and the lowest part, and weaker in the right parts (probably due to variations in light collection efficiency across the cylinder in combination with possible absorption of the laser light). Bearing this in mind it is still obvious that the OH intensity is less homogenous in the two stratified cases, in which islands of high OH concentration and voids with low OH concentrations appear. These effects are most pronounced with the latest second injection.

Figure 19, Figure 20 and Figure 21 present simultaneous measurements (obtained from homogenous case, early second injection and late second injection cases, respectively) of chemiluminescence (from HSV), formaldehyde and OH-radicals. Each row corresponds to a measurement in one cycle. The first four images in each row show chemiluminescence captured with the high speed video camera. The sequence intervals are chosen so that no “light” appeared before the first image. The number in each of these images indicates the crank angle degree after top dead center at which the camera chip was read out, hence the images show the cumulative light emission during two CAD up to the CAD indicated. The fifth image in each row shows LIF of formaldehyde and the sixth image shows LIF of OH-radicals. These are simultaneous images captured at the CAD aTDC shown in the images. Two differences in chemiluminescence separate the homogenous case from the two stratified cases: the intensity is stronger and the distribution more unequal in the stratified cases. A shared feature is that the number of images from first light emission detection until maximum light emission seems to be the same. This is not surprising since difference in burn duration was small relative the HSV inter-frame time.

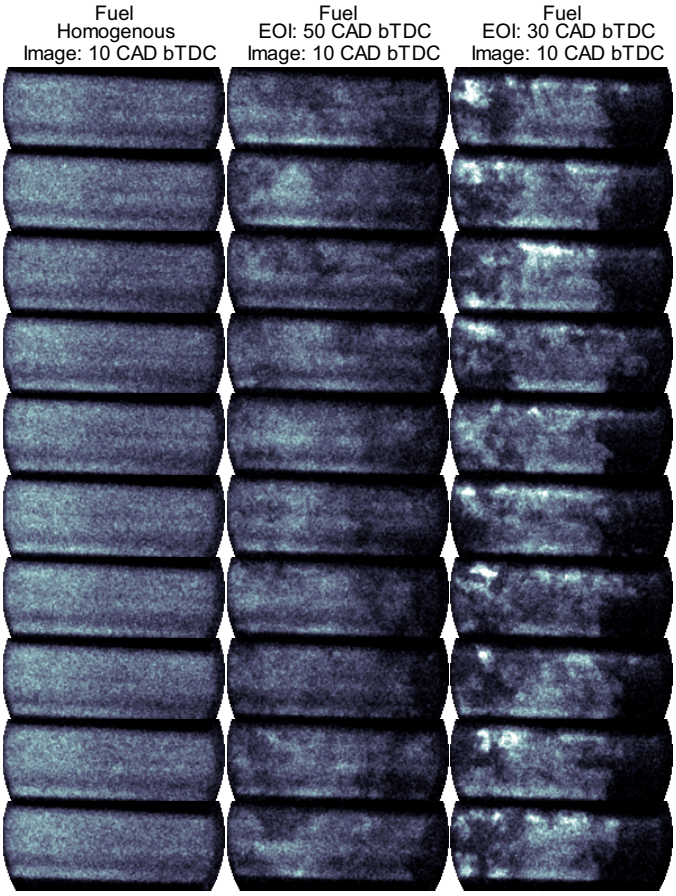

Figure 17. Single fuel-tracer LIF images acquired in homogenous case (left column), early second injection (middle column) and late second injection (right column) tests. All images were taken 10 CAD bTDC.

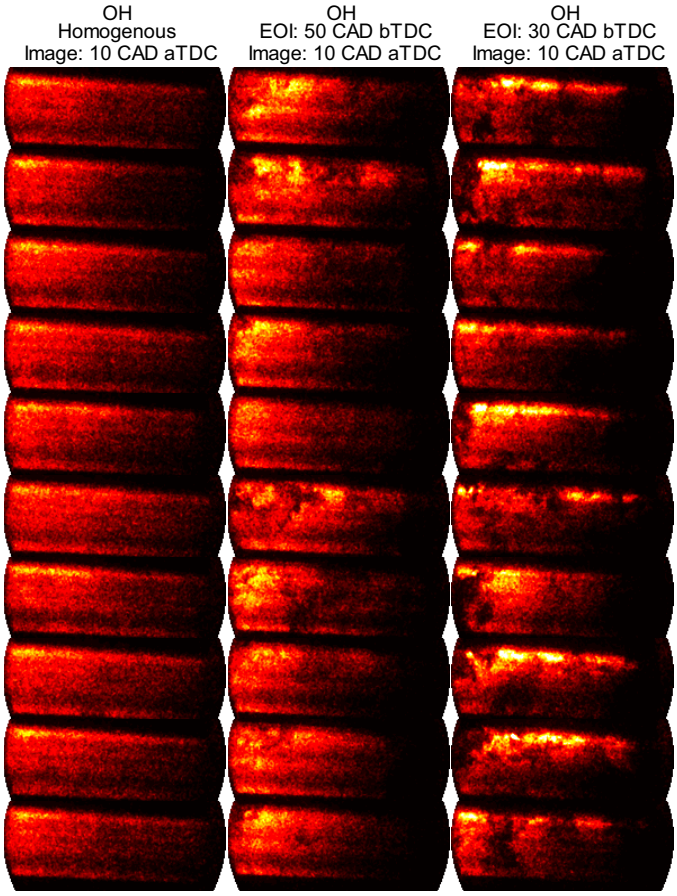

Figure 18. Single OH LIF images acquired in homogenous case (left column), early second injection (middle column) and late second injection (right column) tests. All images were taken 10 CAD bTDC.

As also seen previously in Figure 14 - Figure 16, the concentration of formaldehyde is homogenously distributed in the homogenous case while it is highly inhomogeneous in the two stratified cases, in which the concentrations are highest at the center of the combustion chamber.

Images in row five in Figure 19 and row three in Figure 20 and Figure 21 shows that formaldehyde is consumed where OH-radicals appear and where chemiluminescence is first detected. This co-existence of OH and formaldehyde, albeit in spatially distinct areas, is typically seen soon after initiation of high-temperature chemistry. As shown in Figure 19, it can even be observed for the homogeneous case, although a homogeneous OH distribution is rapidly established, as shown in Figure 18.

Unfortunately, it is difficult to precisely capture the ignition event (the onset of the high-temperature reaction) since LIF-images can only be captured once per cycle, and HSV-images are averages over a relatively long time, here 2 CAD, to obtain sufficient signal intensity. Therefore, too few images are available to be able to draw definitive conclusions about whether the point of ignition is correlated with the fuel/formaldehyde distribution. On one hand it could be argued that the temperature may still be lower in areas with a high fuel concentration due to the heat required for its evaporation. On the other hand the heat released in the low-temperature reactions (associated with the formaldehyde formation) may be sufficient to offset the initially lower temperature, and instead a higher concentration of radicals and higher temperature may promote ignition. There seems to be a high probability that the chemiluminescence and OH radicals will first appear close to the center, where high fuel and formaldehyde concentrations were generally observed (although not in the cycle illustrated in the HSV sequence shown in the upper row of Figure 21, in which the formaldehyde distribution did not show the normal maximum just left of the centre at 10 CAD bTDC). However, in order to determine the point of ignition with certainty, more images with smaller time steps between them need to be taken and analyzed.

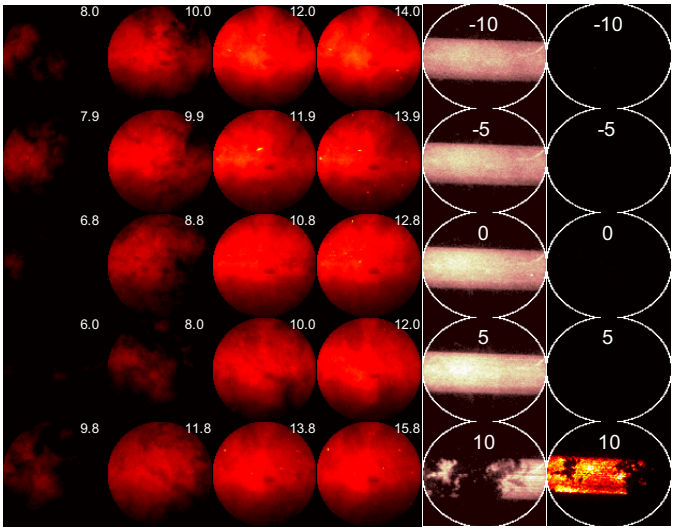

Figure 19. From the left in each row: high-speed video (first four columns), formaldehyde LIF and OH LIF images acquired in a single homogenous case cycle. HSV images were read out and LIF images taken at the CAD aTDC displayed in the images.

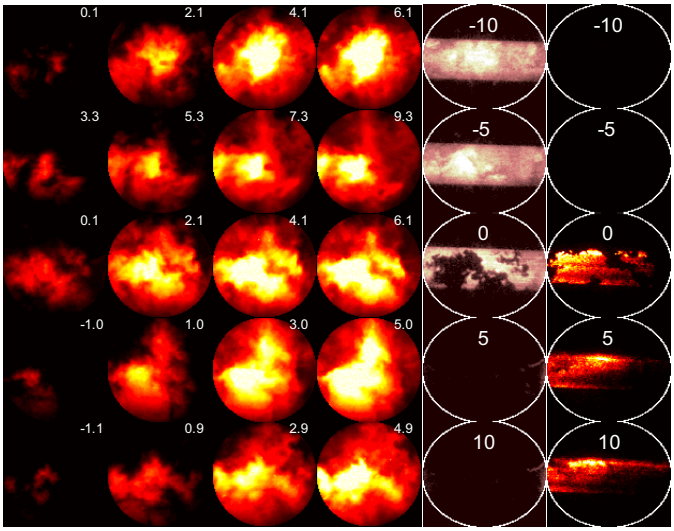

Figure 20. From the left in each row: high-speed video (first four columns), formaldehyde LIF and OH LIF images acquired in a single stratified case (50% at EOI 50 CAD bTDC) cycle. HSV images were read out and LIF images taken at the CAD aTDC displayed in the images.

SUMMARY AND CONCLUSIONS

SCCI was investigated as a means to reduce the maximum rate of pressure rise and ringing intensity, and thus potentially extend the practical load range of an HCCI-engine. The charge stratification was accomplished by using a split injection. Part of the fuel was injected early in the intake stroke and the remainder was injected late in the compression stroke. The results show effects of SCCI on ringing intensity and can be used as guidance for further work in developing a method for increased upper load range of HCCI combustion.

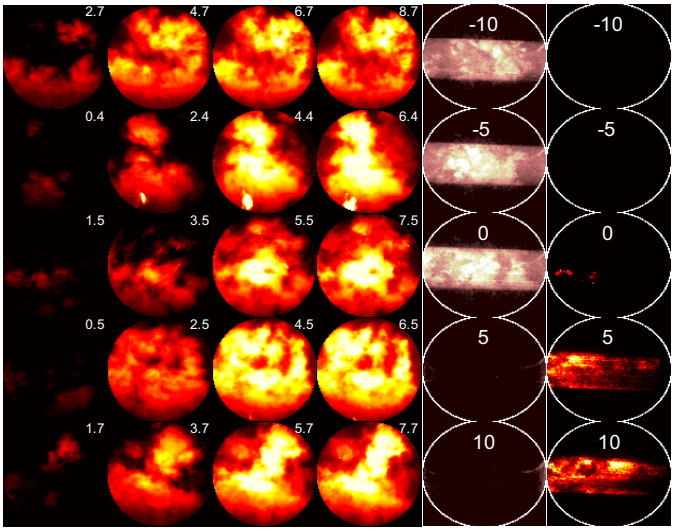

Figure 21. From the left in each row: high-speed video (first four columns), formaldehyde LIF and OH LIF images acquired in a single stratified case (50% at EOI 30 CAD bTDC) cycle. HSV images were read out and LIF images taken at the CAD aTDC displayed in the images.

A metal engine was used to investigate the effects of varying the proportion of fuel injected and the EOI of the late injection. A more stratified charge was found to reduce the maximum rate of pressure rise and ringing intensity when using either gasoline or PRF, and this was mainly an effect of the longer burn duration caused by the stratification. The standard deviation of IMEPnet was also reduced by charge stratification, especially at moderate stratification levels.

CO- and NO_X-emission levels increased with a more stratified charge, but no adverse effects of stratification were detected on either HC- or soot-emissions. Charge stratification was found to have only a small impact on fuel consumption, especially when gasoline was used. The high levels of NO_X obtained with the stratified charge limit the applicability of this technique, since one of the major advantages of HCCI is the low NO_X emission levels.

An optically accessible engine was used to characterize the combustion when using a stratified charge. Fuel tracer LIF was used to verify that the charge was stratified. Slightly after the late injection, a higher concentration of formaldehyde was found at locations where the fuel concentration was higher. Late timing of the late injection gave a higher degree of fuel and formaldehyde stratification.

High speed video images of combustion events showed that the flame luminescence was more intense and more inhomogeneous when using charge stratification than in the homogeneous case. Similarly, the OH distribution was found to be inhomogeneous when using a stratified charge, and the degree of inhomogeneity was higher with a later injection timing.

ACKNOWLEDGMENTS

The authors wish to thank the Program Council for Vehicle Research, the Green Car Project 2 and Volvo Car Corporation for financial support. Volvo Car Corporation is also acknowledged for supplying experimental equipment. Research engineer Rolf Berg is acknowledged for help with the experimental equipment.

REFERENCES

1. The European Automobile Manufacturers Association, http://www.acea.be, 2009
2. European Federation for Transport and Environment, http://www.transportenvironment.org/Article185.html, 2006
3. Heywood, J. B., Internal Combustion engine fundamentals. Singapore: Macgraw-Hill Book Company, 1988
4. Willand, J., Niederding, R-G., Vent, G., Enderle, C., “The Knocking Syndrome – Its cure and Its Potential”, SAE Technical Paper Series, SAE paper 982483, 1998
5. Denbratt, I., ”Method of controlling the process of combustion in an internal combustion engine with means for controlling the engine valves”, Volvo Car Corporation, Patent No. SE521782, 1998
6. Koopmans, L., Denbratt, I., “A Four Stroke Camless Engine, Operated in Homogeneous Charge Compression Ignition Mode with Commercial Gasoline”, SAE Technical Paper Series, SAE paper 2001-01-3610, 2001
7. Koopmans, L., Ogink, R., Denbratt, I., “Direct Gasoline Injection in the Negative Valve Overlap of a Homogeneous Charge Compression Ignition Engine”, JSAE, SAE Technical Paper Series, JSAE paper 20030195, SAE Paper 2003-01-1854, 2003
8. Dahl, D., Denbratt, I., Koopmans, L., ”An Evaluation of Different Combustion Strategies for SI Engines in a Multi-Mode Combustion Engine”, SAE Technical Paper Series, SAE paper 2008-01-0426, 2008
9. Eng, J.A., “Characterization of Pressure Waves in HCCI Combustion”, SAE Technical Paper Series, SAE Paper 2002-01-2859
10. Burgdorf, K., Denbratt, I., “Cylinder Pressure Based Knock Detection Methods”, SAE Technical Paper Series, SAE paper 972932, 1997
11. Amano, T., Morimoto, S., Kawabata, Y., “Modeling of the Effect of Air/Fuel Ratio and Temperature Distribution on HCCI Engines”, SAE Technical Paper Series, SAE Paper 2001-01-1024, 2001
12. Sjöberg, M., Edling, L.-O., Eliassen, T., Magnusson, L., Ångström, H.-E., ”GDI HCCI: Effects of Injection Timing and Air Swirl on Fuel Stratification, Combustion and Emissions Formation”, SAE Technical Paper Series, SAE Paper 2002-01-0106, 2002
13. Marriot, C.D., Reitz, R.D., “Experimental Investigation of Direct Injection-Gasoline for Premixed Compression Ignited Combustion Phasing Control”, SAE Technical Paper Series, SAE Paper 2002-01-0418, 2002
14. Girard, J.W., Dibble, R.W., Flowers, D.L, Aceves, S.A, “An Investigation of the Effect of Fuel-Air Mixedness on the Emissions from an HCCI Engine”, SAE Technical Paper Series, SAE Paper 2002-01-1758
15. Urushihara, T., Hiraya, K., Kakuhou, A., Itoh, T., ”Expansion of HCCI Operating Region by the Combination of Direct Fuel Injection, Negative Valve Overlap and Internal Fuel Reformation”, SAE Paper 2003-01-0749, 2003
16. Dec, J.E., Sjöberg, M., ”Isolating the Effects of Fuel Chemistry on Combustion Phasing in an HCCI Engine and the Potential of Fuel Stratification for Ignition Control”, SAE Technical Paper Series, SAE Paper 2004-01-0557, 2004
17. Aroonsrisopon, T., Werner, P., Waldman, J.O., Sohm, V., Foster, D.E., Morikawa, T., Iida, M., “Expanding the HCCI Operation With the Charge Stratification”, SAE Technical Paper Series, SAE Paper 2004-01-1756, 2004
18. Standing, R., Kalian, N., Ma, T., Zhao, H., Wirth, M., Schamel, A., ”Effects of Injection Timing and Valve Timings on CAI Operation in a Multi-Cylinder DI Gasoline Engine”, SAE Technical Paper Series, SAE Paper 2005-01-0132, 2005
19. Leach, B., Zhao, H., Li, Y., Ma, T., “Control of CAI Combustion Through Injection Timing in a GDI Engine With an Air-Assisted Injector”, SAE Technical Paper Series, SAE Paper 2005-0134, 2005
20. Wang, Z., Wang, J.-X., Shuai, A.-J., Ma, Q.-J., “Effects of Spark Ignition and Stratified Charge on Gasoline HCCI Combustion With Direct Injection”, SAE Technical Paper Series, SAE Paper 2005-01-0137, 2005
21. Thirouard, B., Cherel, J., Knop, V., “Investigation of Mixture Quality Effect on CAI Combustion”, SAE Technical Paper Series, SAE Paper 2005-01-0141, 2005
22. Ozaki, J., Iida, N., “Effect of Degree of Unmixedness on HCCI Combustion Based on Experiment and Numerical Analysis”, SAE Technical Paper Series, SAE Paper 2006-32-0046, 2006
23. Li, Y., Zhao, H., Brouzos, N., Ma, T., Leach, B., “Effect of Injection Timing on Mixture and CAI Combustion in a GDI Engine with an Air-Assisted Injector”, SAE Technical Paper Series, SAE Paper 2006-01-0206, 2006
24. Sjöberg, M., Dec, J.E., “Smoothing HCCI Heat-Release Rates Using Partial Fuel Stratification with Two-Stage Ignition Fuels”, SAE Technical Paper Series, SAE Paper 2006-01-0629, 2006
25. Berntsson, A.W., Denbratt, I., ”HCCI Combustion Using Charge Stratification for Combustion Control”.,

SAE Technical Paper Series, SAE Paper 2007-01-0210, 2007
26. Lee, C., Tomita, E., Lee, K., Characteristics of Combustion Stability and Emission in SCCI and CAI Combustion Based on Direct-Injection Gasoline Engine", SAE Technical Paper Series, SAE Paper 2007-01-1872, 2007
27. Herold, R.E., Foster, D.E., Ghandhi, J.B., Iverson, R.J., Eng, J.A., Najt, P.M., Fuel unmixedness effects in a gasoline homogeneous charge compression ignition engine", Int. J., Engine Res. Vol. 8, p241-257, 2007
28. Brewster, S., Cathcart, G., Zavier, C., "The Potential of Enhanced HCCI/CAI Control Through the Application of Spray Guided Direct Injection". SAE Technical Paper Series, SAE Paper 2008-01-0035, 2008
29. Christensen, M., Homogeneous Charge Compression Ignition (HCCI) Engine, Licentiate Thesis, Lund Institute of Technology, 2000
30. Persson, H., Sjöholm, J., Kristensson, E., Johansson, B., Richter, M., Aldén, M., "Study of Fuel Stratification on Spark Assisted Compression Ignition (SACI) Combustion with Ethanol Using High Speed Fuel PLIF, SAE Technical Paper Series, SAE Paper 2008-01-2401, 2008

CONTACT

Corresponding author:
Daniel Dahl
Chalmers University of Technology
Department of Applied Mechanics
Division of Combustion
Hörsalsvägen 7B
SE-412 96 Göteborg
Sweden
Email: daniel.dahl@chalmers.se

DEFINITIONS, ACRONYMS, ABBREVIATIONS

ATDC: After Top Dead Center

CA10-90: Burn Duration

BTDC: Before Top Dead Center

CA50: Location of 50% heat release

CAD: Crank Angle Degree

CUHR: Cumulative Heat Release

EOI: End Of Injection

EVC: Exhaust Valve Closure

HCCI: Homogeneous Charge Compression Ignition

HPF: High Pass Filtered

HSV: High Speed Video

IMEPnet: Net Indicated Mean Effective Pressure

ISFC: Indicated Specific Fuel Consumption

IVO: Intake Valve Opening

KI: Knock Intensity

LIF: Laser Induced Fluorescence

NVO: Negative Valve Overlap

P: Pressure

PFI: Port Fuel Injection

PRF: Primary Reference Fuel

RI: Ringing Intensity

ROHR: Rate Of Heat Release

SCCI: Stratified Charge Compression Ignition

SI: Spark Ignition

TDC: Top Dead Center

APPENDIX

Pressure trace analysis was carried out using an in-house Matlab code. Values of parameters such as CA50 and CA10-90 were calculated for individual cycles (from low pass-filtered pressure traces at a cutoff frequency of 4000 Hz) then averaged over the 299 cycles monitored for each case. The following equation was used in the net heat-release rate analysis:

$$dQ_n = \frac{\gamma}{\gamma - 1} P \frac{dV}{d\theta} + \frac{1}{\gamma + 1} V \frac{dP}{d\theta}$$

To estimate γ, a function based on the assumption that it decreases linearly with temperature was used, in accordance with Christensen [29]:

$$\gamma = \gamma_0 - \frac{0.08(T - 300)}{1000}$$

where γ_0 is the γ value at the reference temperature 300 K. The temperature was calculated assuming that the gas follows the ideal-gas equation of state:

$$T = \frac{PV}{mR}$$

where the gas constant was taken as the value for air (287 J/kgK). The mass percentage of residuals trapped by the NVO was estimated, using Ricardo Wave simulations, to be ~35%. γ_0 was set to a constant value of 1.37, which was representative for the gas mixture once all the fuel had been injected but before the combustion [3].

Paper VIII

Simultaneous LIF of OH, HCHO, PIV and High Speed Video Imaging combined with Fuel Tracer LIF Measurements in a HCCI engine using Charge Stratification and Spark-assist

Andreas William Berntsson, Mats Andersson and Ingemar Denbratt

Submitted for publication

Title: Characterization of an HCCI Engine Using Charge Stratification and Spark-Assist by Simultaneous PIV, Multi-Species LIF and High Speed Video Analysis

Authors: Andreas W. Berntsson, Mats Andersson, Ingemar Denbratt

Abstract

Future requirements to reduce exhaust emissions and fuel consumption might be met by adopting Homogenous Charge Compression Ignition (HCCI). In this study the feasibility of combining charge stratification and spark-assisted ignition with HCCI to lower the minimum operational HCCI load was studied. Low lift short duration camshafts were used to obtain a negative valve overlap, NVO, and thus trap enough residuals to achieve HCCI in SI engine geometry. To investigate the phenomena occurring near Top Dead Centre (TDC), several optical techniques were used simultaneously in an optical engine, including: laser-induced fluorescence (LIF) of OH and HCHO, particle imaging velocimetry (PIV) and High Speed Video imaging, combined with LIF analysis of the fuel tracer 3-pentanone in addition to conventional cylinder pressure and emission measurements.

The low load limit was extended by using the proposed concept. It was found that the charge stratification, in addition to enriching the region near the sparkplug, induced air motions that contributed to the initial flame propagation and provided a region

with conditions more suitable for HCCI combustion, thus promoting the transition from flame propagation to HCCI.

Introduction

Future requirements to reduce exhaust emissions and fuel consumption are prompting the development of more advanced combustion concepts. Diesel engines have displayed high efficiency, but with the drawback of generating high amounts of NO_X and/or particles, necessitating the use of complex and expensive after-treatment systems. In contrast, traditional gasoline engines have shown the capacity to meet stringent emission standards, but with lower efficiency than diesel engines. Naturally, the aim is to combine high efficiency with the possibility of meeting ultra low emission levels. One promising concept to achieve those goals is Homogeneous Charge Compression Ignition, HCCI [1]. In an HCCI engine the combustion is controlled by chemical kinetics [1, 2], and heat is released more rapidly than with normal flame propagation. Thus, it can approach the ideal air standard SI cycle (the most efficient of the ideal cycles since combustion occurs at constant volume) [3]. The rapid heat release of HCCI combustion and its ability to burn dilute mixtures, thereby requiring less throttled operation, results in greatly improved efficiency compared to SI combustion [4]. HCCI combustion also yields low NO_X and PM emissions [5] as a result of the lean homogenous mixture.

However, several challenges associated with the HCCI concept must be overcome before it can be commercially applied, notably ways must be found to control ignition timing [6], expand its limited operating range [5] and limit the rate of heat release [7].

Combustion phasing – which can be monitored using the CA50, the timing when 50 % of the fuel is combusted – is one of the crucial parameters to control in HCCI combustion [3].

The ability to create charge stratification in DI engines allows various control methods to be adopted to increase the control of HCCI combustion. The authors previously described a hybrid combustion mode in which spark-initiated combustion of a stratified charge is followed by HCCI combustion [8-10]. The charge stratification was shown to affect the maximum rate of heat release as well as combustion phasing for fuels which displayed low temperature reactions [11, 12].

One promising way of initiating HCCI combustion is to retain large quantities of exhaust gases (EGR), thereby retaining sufficient thermal energy to initiate the HCCI combustion. Short duration and low valve lift profiles, and negative valve overlap (NVO), have been used for this purpose [13-15]. This solution offers the possibility to achieve HCCI combustion for part load operation in a traditional SI engine, and when combined with DI-technology a pilot injection can be used to further enhance the combustion control [15]. The concept described in [8-10] appears to be compatible with the NVO concept and its greatest potential will be to achieve HCCI at idle. In the study presented here further information was acquired on the combustion processes, and associated phenomena, that occur when conventional flame propagation and HCCI combustion are combined in the same combustion cycle, thereby extending our understanding of the concept.

Experimental methods

To obtain a greater understanding of the phenomena that occur when flame front propagation and HCCI combustion are combined in the same cycle, various optical measuring techniques were used to evaluate selected properties during combustion. The optical techniques used were: particle imaging velocimetry (PIV), with seeded particles to estimate the in-cylinder flow; laser-induced fluorescence (LIF) analysis of formaldehyde to locate low temperature reactions; LIF of hydroxyl to locate high temperature reactions; LIF of the fuel tracer 3-pentanone to measure fuel concentrations; and high speed video imaging to locate the flame front. These optical techniques were combined with conventional pressure trace and emission measurements. A schematic diagram of the setup can be seen in figure 1. The optical studies were performed in two sequences: one in which the flow field, formaldehyde, hydroxyl and high speed video images were captured simultaneously; and one in which hydroxyl ions and the fuel tracer were measured simultaneously.

The engine used in the study was a single-cylinder optical research engine, equipped with quartz windows as pent roof side walls and a quartz piston top to allow optical access to the combustion chamber. The glass pent roof side walls enabled optical access to the clearance volume, which was especially important since most HCCI combustion occurs near TDC and all laser sheets used in the study passed through the engine 5 mm beneath the sparkplug. The engine specifications can be seen in table 1. In previous studies the optical engine's behaviour when using primary reference fuel has been found to be similar to that of a conventional engine using gasoline, when the intake air temperature is increased for the optical engine to compensate for its lower

compression ratio [19]. An outward-opening, hollow cone, piezo-actuated fuel injector was used in these studies.

OH LIF

Laser-induced fluorescence of OH has been used by various authors to investigate combustion. OH concentrations was quantitatively measured in diffusion flames in both 1-D, using the $S_{21}(8)$ transition, and 2-D, using the $Q_1(8)$ transition [16]. LIF of OH has been used to study: the reaction zones in an SI engine [17]; charge inhomogeneities in an HCCI engine [18]; and, in previous work by the authors of the present study, combustion during negative valve overlaps [19].

In the present study, planar laser-induced fluorescence was applied to detect and image OH molecules, using the $Q_1(6)$ transition in the $A(v=1) - X(v=0)$ band at a wavelength of 283 nm for excitation. This transition was selected since it provides high signal strength with relatively low dependence on rotational population changes due to temperature variations. The $Q_1(6)$ transition overlaps with several weaker transitions in the Q_2, Q_{12} and Q_{21}-branches. This contributes to the signal strength, although these excitations are from low rotational states and their relative strengths decline somewhat at higher temperatures. An absorption spectrum, shown in figure 2, was simulated by LIFBASE [20]. In order to avoid scattered laser light entering the detectors, fluorescence light from the $A(v=0) - X(v=0)$ and $A(v=1) - X(v=1)$ bands in the 300-320 nm-range was used for detection. The tuneable UV-light was generated by a nanosecond dye laser pumped by the 2nd harmonic light of a Nd:YAG laser. The Rhodamine 6G dye provided light in the 560-600 nm wavelength range, the frequency

of which was subsequently doubled to obtain the desired wavelength. The pulse energy of the UV light was about 12 mJ out of the laser. In order to calibrate the wavelength of the laser, the beam could be sent through a propane flame and fluorescence from OH molecules in the flame could be detected by a photomultiplier tube. The images were taken using an image-intensified LaVision Dynamight 2000 camera, providing 1024x1024 pixels resolution, equipped with LaVision DaVis 6.2 software.

HCHO LIF

LIF of formaldehyde has been used by various authors to investigate the low temperature reactions in HCCI engines [21-22], and by the authors of the present study to locate low temperature reactions during both combustion and NVO in previous work [8]. Here, the third harmonic (355 nm) light from a Nd:YAG Spectra Physics laser was used to excite formaldehyde, in order to analyze the location of low temperature reactions during early combustion phases. The laser intensity was adjusted to 90 mJ to provide sufficient signal strength and allow the quartz window's lifetime to be sufficiently long for the measurements to be practically feasible. Excitation and emission spectra of formaldehyde from a cuvette can be seen in figure 2. It can be seen that the third harmonic light of the Nd:YAG excites weak transitions (as noted in [21]), but the high laser intensity makes the signal sufficiently strong.

Fuel tracer LIF

Ketones are suitable as fuel tracers since their sensitivity to oxygen quenching is limited [23], and 3-pentanone was chosen since it has a similar boiling point to iso-octane and n-heptane. The fuel tracer 3-pentanone was excited by laser light with the same wavelength as for the OH measurement, *i.e.* when the OH and the fuel distributions were measured simultaneously only one excitation source was used and the emissions were measured with two LaVision Dynamight cameras. This procedure was adopted due to its simplicity, compared to the setup in previous work, in which the more intense fourth harmonic light of the Nd:YAG was used for excitation [8], and the fuel concentration could be measured only by changing the mirrors and filters to direct emission from OH and the tracer to separate cameras. When fuel-LIF was applied fuel tracer was added at a concentration of 15 % in terms of volume. The excitation and emission spectra for the fuel tracer can be seen in figure 2.

PIV

Particle image velocimetry has been used to investigate in-cylinder flow fields by various authors. Flow fields in motored conditions with NVO valve settings have been studied and quantitatively compared to flow fields obtained with traditional valve settings [24]. However, the flow field measurements carried out in the cited study did not cover the later part of the compression, and the structure of the flow obtained during the induction deteriorated rapidly compared to flow fields with normal valve settings, leaving the flow velocity low during compression with NVO. For this study the focus was on the flow field just prior to, and during, the combustion and connecting acquired information about it with information obtained by the other measurement techniques.

Frequency-doubled light (532 nm) from a Spectra Physics dual cavity Nd:YAG laser was used as the illumination source for the PIV measurements. Images of the illuminated particles were captured by a Kodak MegaPlus ES1.0 camera, with 1018x1008 resolution, and processed in FlowManager (Dantec). The interrogation area over which the flow field was calculated was chosen depending on the seeding density that was achieved; 16x16 pixels was used for the presented flow fields.

In fluid-particle flows the Stokes number is a very important parameter [25] and when related to the particle velocity it can be defined as:

$$St_V = \frac{\tau_V}{\tau_T}$$

where τ_v is the momentum response time for the particle and τ_T is a characteristic time of the flow, which can be approximated (in the clearance volume) for this setup by:

$$\tau_T = \frac{T}{U}$$

where T is the distance between the piston and the cylinder head and U is the velocity of the flow. For $St_V << 1$ the seeded particles will follow the flow since there will be ample time to achieve velocity equilibrium. The momentum response time for spherical particles can be expressed by:

$$\tau_V = \frac{\rho_p D^2}{18\mu_C}$$

where D is the diameter, ρ_p is the density of the particles and μ_C is the dynamic viscosity of the gas. In the experiments the flow was seeded with plastic micro balloons (diameter 18-28 μm, density 60±5 kg/m^3), to allow the flow to be measured during the early stages of the combustion since they were first depleted (to a great extent) after the main HCCI combustion. The Stokes numbers of the balloons of the chosen sizes were far lower than unity under conditions near TDC, hence they could be assumed to follow the flow.

High speed video

A monochromatic Vision Research Phantom v7.1 high-speed CCD camera was used to capture the natural luminosity of the combustion by direct imaging and to obtain several images per combustion cycle (thus capturing the flame propagation prior to and after the complementary, simultaneously recorded LIF and PIV images). The resolution of the camera was set to 256 by 256 pixels, and images were captured every other CAD.

Optics and filters

The pulse energy from the dye laser needed for the OH LIF was assumed to be the limiting factor, and thus great care was taken to minimise losses of its intensity as well as the OH emission signals. The 283 nm beam was introduced as close as

possible to the sheet-forming optics system and dichroic mirrors were used to limit losses, see figure 1. Between the laser and the sheet optics, one-inch dichroic mirrors intended to provide 266 nm light were used, but the angle of attack was changed to suit 283 nm, and to isolate the emission signal efficiently a three inch dichroic mirror intended for use with excimer lasers at 308 nm was used. To further isolate the emission of OH from scattered laser light a WG305 filter was placed in front of the camera. To validate that the setup detected an appropriate wavelength band, the dye laser was tuned to on- and off-resonance of transitions in the OH-molecule. The order of extraction of the emission signals was dictated not only by their respective signal strengths and wavelengths, but also by the need for proper optical coverage of the detectors with their specific lenses. The detectors for the OH and HCHO measurements were identical and set at equal optical distances from the cylinder of the engine. To ensure that the detector for the PIV measurements provided the desired resolution of the combustion chamber, the signal from the seeded particles was extracted next, using a three-inch 532 nm dichroic mirror to reflect the light scattered by the seeded particles to the PIV detector and to allow light of other wavelengths to proceed. An interference filter centred at 532 nm was also used to further isolate the light scattered by the particles. Next, a mirror was used to reflect the emissions from HCHO to the detector and a GG420 filter combined with a wideband BG25 filter was used to isolate the emissions and separate the scattered laser light. Finally, a mirror was used to reflect the rest of the light to the high speed video camera, angled slightly differently from the light directed to the other cameras so it passed just over the mirror reflecting the emissions from the HCHO. The light had been reflected by several mirrors by that point, and large proportions of it had been directed to other detectors,

so the signal strength was limited, hence the sampling rate was limited to 3600 frames per second to ensure there was sufficient exposure time for reasonable signal strength.

When fuel tracer LIF and OH LIF were measured simultaneously the OH setup was kept identical, but the filters for the formaldehyde detection were replaced by a WG360 filter to isolate the emission from 3-pentanone.

Triggering

In order to limit scattered laser light entering the detectors, measurements by each technique were separated in time, in addition to using filters. This temporal separation also limited the demands on the filters' performance, i.e. less steep gradients were needed and stronger signals could be obtained at the detectors. However, the temporal separation was very short, typically 1-2 μs, in comparison to the timescale of the combustion or the flow field, thus the images acquired by the different techniques could be assumed to describe phenomena happening at single points in time. An AVL 4210 instrument controller was used as the main trigger to set the CAD of interest. This signal was sent to the LaVision computer and to a Stanford Research Systems delay generator. The LaVision computer controlled the timing of the Dynamight cameras, while all other equipment was controlled by delay generators. This procedure was adopted due to the high temporal accuracy of the delay generators and the full control of all pulses thus provided. When a measurement was carried out, the Phantom camera was set to wait for the initial Q-switch signal of a 30-pulse burst for the PIV measurement at 2 Hz repetition rate. The 283 nm and 355 nm lasers for the OH and HCHO measurements were run at 10 Hz (to obtain stable pulse energy)

and the cameras were triggered by the DaVis software every 2.2 s (due to the long read-out time of the cameras). To identify the cycle in which each set of measurements by all techniques was simultaneously acquired, the laser pulses for the PIV measurements were measured with a photodiode and logged (since the signal corresponded to a PIV image and the first burst indicated the trigger of the Phantom camera) by an AVL Indimaster data acquisition system and an AVL Indicom indicating system line. The output signal from the intensifiers of the Dynamight cameras was also logged. Logged cycles with signals from the photodiode and output signals from the intensifiers, in which measurements by all techniques were acquired simultaneously, could each be coupled to a specific pressure trace.

Results and discussion

Phenomena at three distinct operational settings were studied, starting from the minimum load achievable (without any misfire) with HCCI combustion using only pilot and main injections (no charge stratification and no spark-assist). This case is designated A and represents the highest load applied in this study (2 bar IMEP). The load was then decreased slightly by injecting a smaller total amount of fuel, but adding a small additional injection in order to create a stratified charge during the compression combined with spark-assist (case B). For this case the initial flame propagation allowed HCCI combustion to occur at a lower load (1.65 bar IMEP) than in case A. For case C the stratification injection was increased, but the total amount of fuel was reduced compared to case B, and the greater stratification injection allowed the initial flame to have a greater impact and thus HCCI was achieved at an even lower load (1.3 bar IMEP). The operational settings applied in the study are listed in

table 2. Great care was taken to ensure that increases in NO_X emissions were modest when flame front combustion and HCCI combustion were combined, since a major advantage of HCCI combustion (which should not be compromised) is that it yields low NO_X emissions. The CO emissions for the three cases were similar, but slight increases in HC emissions were observed for the cases with reduced load.

In figure 3 averaged pressure traces can be seen for each of the studied cases and the derived mass fractions burned (MFB). The pressure trace for the traditional HCCI combustion case (A) shows a retarded combustion phasing (typical for low load HCCI), with a steep rise in pressure, leading (in combination with the relatively high load compared to the other cases) to the in-cylinder pressure being higher than in the other cases. In the cases with initial flame front propagation (B and C) slow initial conversion was followed by a gentler rise than in case A, once the combustion had transitioned to HCCI combustion. Case B also yielded lower NO_X emissions (in molar ratios) than HCCI combustion, while case C yielded slightly higher NO_X emissions (but still low absolute values). The higher NO_X values for case C, compared to case B, were due to the stronger initial flame propagation, through a richer stratified charge, and to the requirement (for the specific load) for more advanced combustion phasing to achieve HCCI combustion.

Results from averaged images

To obtain an overall picture of the phenomena occurring in each case averaged images (each based on information from ten individual images) were calculated to complement the analysis of the simultaneous measurements from individual cycles.

Figure 4 shows images (and corresponding timings) of average LIF signals from the fuel tracer 3- pentanone acquired for cases A - C. In case A the fuel was homogeneously distributed within the combustion chamber until the combustion started to convert the fuel. The images for cases with charge stratification (B and C) clearly show local regions with stronger signals from the fuel tracer during the compression, *i.e.* a stratified charge created in the vicinity of the sparkplug, located just left of the centre in the images. Near TDC spots with reduced intensity indicate regions where fuel was consumed. Images for the late timings displayed lower overall intensity. Besides fuel conversion, several other effects contribute positively or negatively to the signal strength. The compression induces a higher molecular density in the laser plane, which increases the intensity, while increases in pressure and temperature are both expected to reduce fluorescence yields [26].

In figure 5 averaged LIF signals from OH at different timings around TDC can be seen. Significant OH signals were observed during the period of fuel conversion for the conventional HCCI case (A). In this case no significant averaged OH signal was observed at TDC, and the derived mass fraction burned (MFB) values (figure 3) indicate that only very modest reactions had occurred at TDC. At 10 CAD the averaged MFB values indicate that the vast majority of the fuel had been converted, as also indicated by strong LIF signals. The high levels of OH at this timing, in combination with the chosen excitation wavelength (at which absorption is strong absorption, to allow OH to be detected at low concentrations), led to the signal strength being reduced as the laser sheet propagated through the combustion chamber, from left to right in the image. Inhomogeneity in the intensity distribution across the

laser light sheet from the dye laser was also manifested in variations in the intensity at different heights in the image. For cases B and C, the initial flame front propagation can be seen in the averaged images as increasing regions of intensity from the LIF of OH, starting with modest signals close to the spark plug from -10 CAD, strengthening substantially from TDC onwards. The combustion phasing difference between the two cases, as seen in the MFB values, was also seen in the OH images. At TDC the average image for case B shows the OH signals from the propagating flame front, but for case C OH signals from both the propagating flame and HCCI combustion were captured. At 10 CAD the OH signal for case B was still weaker than for case C, since the combustion was almost complete at this point for case C, while full fuel conversion had still not been reached in case B, hence there was a weaker signal in the average image.

Averaged images from formaldehyde LIF can be seen in figure 6. The intensity of the formaldehyde signal is initially weak, at -20 CAD, and increases thereafter. For the traditional HCCI combustion case (A) the HCHO signal reached maximum intensity when only modest amounts of the fuel had been converted at TDC, and was completely depleted at 10 CAD. The total absence of OH and presence of HCHO throughout the cylinder at TDC, and vice versa at +10 CAD, show that the high-temperature combustion had not yet started at TDC, but had reached all parts of the cylinder at +10 CAD. For the cases with charge stratification, strong intensity was seen for an extended period, especially in the rich regions just prior to TDC. Clearly, therefore, the spark-initiated flame induced a temperature increase that contributed to fuel decomposition and HCHO formation. At -10 CAD, and especially at TDC,

evidence of the flame was manifested in a reduced HCHO signal in regions where OH was present, although the complete separation cannot be seen in averaged images.

Averaged in-cylinder flow fields during the late part of the compression can be seen in figure 7. For traditional HCCI the air motion in the studied plane could be considered to be quiescent or in the order of accuracy of the measurements, as shown by the flow field in figure 7 (top). This is consistent with observations by Wilson *et al.* [21], who found that the low lift profiles they applied induced strong air motion early in the cycle that subsequently decayed. However, for the cases with charge stratification, air motion was induced by the stratification injection, as shown in figure 7. At -20 CAD (prior to any significant flame propagation) weak air motion was observed for case B, and for case C (in which greater stratification injections were used) a clear motion induced by the stratification injections was recorded. Later during the compression the air motion was similar, but not identical, to that at the previous timing. For case B differences in intensity and direction of the air motion were observed in regions in which the flame propagated and an expanding, vortex-like structure had developed at TDC. For case C, the air motion induced by the stratification injection was slightly less intense in the measured plane at -10 CAD than at -20 CAD, but it generally retained its direction, while at TDC some similarities in the shape of the motion induced by the injection were still present, but changes in both direction and intensity in regions were observed where the flame propagated. The difference between the flow fields at -20 CAD and at TDC, are represented in figure 7 (bottom), which indicates that the average flow fields prior to any combustion at -20 CAD were influenced by a centrally located expanding source leading to the average flow fields seen at TDC. The flow fields seen at TDC are thus a result of both

the stratification injection and the propagating flame (which cause this central expansion).

Results from simultaneously recorded images

To further investigate the combustion sequence, simultaneous results were studied in addition to the averaged results. This was of particular interest for ignition sequences in which initial flame front propagation transitioned into HCCI combustion, at timings close to the transition, since averaging during this phase of rapidly changing conditions could lead to unrepresentative results.

In figure 8 the flow field, LIF of OH and an iso line for a threshold luminosity value (indicative of the flame front) from one of the high speed video images for case B from the same cycle at TDC can be seen. The exposure time for the high speed video was 2 CAD, but despite this and the fact that only line-of-sight views of the combustion events were acquired, only small discrepancies were found between the images captured by the high speed camera and the OH images for the propagating flame. Accordingly, the high speed video images displayed the reaction zone of the flame, although the wavelength band that was transmitted to the camera was not complete (see figure 1), and the chemiluminescence of CO_2 was the main contributor to the video images. The flow field in figure 8 from this cycle differed from the average field (figure 7) in both intensity and direction; generally the intensity was slightly greater than the average in the measured plane (a natural consequence of averaging a stochastic parameter such as the flow velocity during flame propagation).

Figure 9 shows the flow field and the threshold luminosity iso line (dashed, red) from the high speed video images acquired in the same case B cycle, at TDC, displayed in figure 8. The other iso lines represent the threshold values of the reaction zone in the high speed video images acquired at -4, -2, 2 and 4 CAD (white, green, cyan and magenta lines, respectively), hence the iso lines represent the reaction zone just prior to, during and after the flow field was measured (in addition to measurements by the other techniques). The latest iso line also captured the transition into HCCI combustion, as indicated by the large expansion of the reaction zone. In addition, the average signal from LIF of the fuel tracer is presented (measured at the same timing, but not simultaneously). Correlations between the flame propagation and the flow field were also observed; notably the flame propagated in the direction of the air motion in the region indicated by the numeral 1 in figure 9, and in the opposite direction in region 2. Analysis of the high speed video images from the flame propagation (relative to a fixed geometrical point) showed the flame speed to be quite similar in the two regions, 6 m/s in region 1 and 7.5 m/s in region 2. However, when the flame speed was calculated in relation to the air motion, it was found to be significantly higher in region 2, in which the flame propagated towards richer (or less lean) regions (9.6 m/s), than in region 1, where it propagated towards leaner regions (3.3 m/s). From the high speed video images it was also noted that the transition to HCCI first appeared in the rich regions. This can be seen in the difference between the cyan and magenta lines in the lower left region, since the latter covered a much greater area although there was only a 2 CAD difference in their timings, indicating the transition in combustion. There was also an increase in the rate of the mass fraction burned at the end of recording of the video image, denoted by the magenta line, *i.e.* at 4 CAD. This transition can also be seen in the shift from weak indications

of reactions arising in front of the flame to the left in the video image at 2 CAD to strong signals at 4 CAD from the same region (represented by the iso line).

Figure 10 represents corresponding information to that shown in figure 9, but for the case C at TDC. The average MFB values for the studied cases in figure 3 indicate that combustion was significantly more advanced in case C, on average, and it was also advanced in the specific cycle illustrated in figure 10. At TDC in this cycle slightly less than 50 % of the mass had been combusted and the combustion had just transitioned into HCCI combustion (in contrast to case B, where the transition occurred when 20-30 % of the mass had been combusted). As for case B this can be seen in the abrupt increase in the area covered by the red dashed iso line (corresponding to TDC) compared to the area covered by the green line just before TDC (-2 CAD), and in the video images in which a signal-emitting region can be seen in front of the flame to the left, and there is a sudden increase in area in the lower right region between -2 CAD and TDC. As in case B, the flame appears to follow the flow in region 1 and to propagate in the opposite direction to the flow in region 2 (where the mixture is richer) in case C. The flame propagation speed is 12 m/s in region 1 and 4 m/s in region 2 when related to a fixed geometrical point, but 8.6 m/s and 7 m/s, respectively when related to the flow. Thus, for case C, in which the flame is fully developed at TDC, there is less difference in propagation speeds towards leaner and richer regions. This might be because this corresponds to the later stage of flame propagation, in which the flame is propagating close to the boundaries of the stratified charge with smaller differences between the richer and leaner regions than at TDC in case B, where the flame propagation continues for several CAD after TDC.

In figure 11 the LIF of formaldehyde at TDC and iso lines obtained from the high speed video near TDC can be seen. The transition in combustion from propagating flame to HCCI for case B (cyan to magenta iso line) first occurred in the regions with the highest amounts of formaldehyde. The regions that displayed the highest amounts of formaldehyde could be strongly connected with the regions that displayed high amounts of fuel vapour, *i.e.* the stratified region in the lower left quadrant for case B. For case C the transition had just started when the simultaneous image was taken, however HCCI combustion also developed in regions where formaldehyde signals were strong (between the dashed red and cyan lines).

Conclusions

This study investigated the feasibility of combining initial flame front propagation with subsequent HCCI combustion in order to reduce minimum achievable HCCI loads. Charge stratification was combined with spark-assist to reduce the minimum load of HCCI obtained using NVO with pilot and main injections without any significant increases in NO_X emissions. With a minor stratification injection and modest flame propagation the lower load limit was reduced slightly, and with increased stratification injection and flame propagation the lower load limit was decreased significantly.

PIV measurements showed that conventional HCCI achieved with NVO led to a very weak charge motion near TDC. When charge stratification and flame propagation were used both the stratification injection and the flame contributed to a considerably higher charge motion at TDC.

The charge stratification injection enriched the region near the sparkplug, and thus allowed flame propagation to occur and increased the flame propagation speed during the initial stages of flame propagation.

The delicate transition between initial flame propagation and HCCI was captured by simultaneous LIF measurements and video recordings in single cycles. This transition would be difficult to capture by analysing averaged results alone. The transition to HCCI was initiated in regions with high levels of formaldehyde, which also displayed higher fuel concentrations. Thus, the charge stratification itself played a major role in supplying a region with conditions suitable for HCCI combustion, thereby promoting the transition in addition to enriching the region near the spark plug to such a degree that flame propagation could occur.

Acknowledgement

The authors wish to acknowledge STEM, the Swedish Energy Agency, for funding this work, Volvo Cars for supplying the PIV equipment and engine components, and Mr Göran Josefsson for support with the PIV system.

References

1 **Onishi, S., Hong Jo, S., Shoda, K., Do Jo, P., Kato, S.**, Active Thermo-Atmosphere Combustion (ATAC) – A New Combustion Process for Internal Combustion Engines, SAE World Congress, Detroit, February 26 – March 2 1979, SAE Technical Paper Series, SAE 790501.

2 **Aceves, S., M., Flowers, D., L., Westbrook, C., K., Smith, J., R, Pitz, W., Dibble, R., Christensen, M., Johansson, B.,** A Multi-Zone Model for Prediction of HCCI Combustion and Emissions, SAE World Congress, Detroit, March 6-9 2000, SAE Technical Paper Series, SAE 2000-01-0327.

3 **Heywood, J. B.,** Internal Combustion Engines Fundamentals, Singapore: McGraw-Hill Inc., 1988.

4 **Thring, R. H.,** Homogenous-Charge Compression Ignition (HCCI) Engines, International Fuels and Lubricants Meeting and Exposition, Baltimore, September 25-28 1989, SAE Technical Paper Series, SAE 892068.

5 **Lü, X-C., Chen, W., Huang, Z.,** A fundamental study on the control of the HCCI combustion and emissions by fuel design concept combined with controllable EGR. Part 1. The basic characteristics of HCCI combustion, Fuel, June 2005, Volume 84, Issue 9, Pages 1074-1083.

6 **Wagner, U., Anca, R., Velji, A., Spicher, U.,** An Experimental Study of Homogenous Charge Compression Ignition (HCCI) with Various Compression Ratios, Intake Air Temperatures and Fuels with Port and Direct Fuel Injection, Future Transportation Technology Conference,

Costa Mesa, June 23-25 2003, SAE Technical Paper Series, SAE 2003-01-2293.

7 **Lü, X-C., Chen, W., Huang, Z.,** A fundamental study on the control of the HCCI combustion and emissions by fuel design concept combined with controllable EGR. Part 2. Effect of operating conditions and EGR on HCCI combustion", Fuel, June 2005, Volume 84, Issue 9, Pages 1084-1092.

8 **Berntsson, W. A., Denbratt, I.,** Optical study of HCCI Combustion using NVO and an SI Stratified Charge, 8th International Conference on Engines for Automobile, Capri, September 16-20 2007, SAE Technical Paper Series, SAE 2007-24-0012

9 **Berntsson, A., Denbratt, I.,** HCCI Combustion Using a Spark Ignited Stratified Charge, Annual Congress, Yokohama, May 24-26 2006, Proceedings JSAE Annual Congress, JSAE 20065424.

10 **Berntsson, W. A., Denbratt, I.,** HCCI Combustion Using Charge Stratification for Combustion Control, SAE World Congress, Detroit, April 16-19 2007, SAE Technical Paper Series, SAE 2007-01-0210.

11 **Sjöberg, M., Dec, J. E.,** Smoothing HCCI Heat-Release Rates Using Partial Fuel Stratification with Two-Stage Ignition Fuels, SAE World Congress, Detroit, April 3-6 2006, SAE Technical Paper Series, SAE 2006-01-0629.

12 **Koopmans, L., Denbratt, I.,** A Four Stroke Camless Engine, Operated in Homogenous Charge Compression Ignition Mode with Commercial Gasoline, Fuels and Lubricants Meeting and Exhibition, San Antonio, September 24-27 2001, SAE Technical Paper Series, SAE 2001-01-3610.

13 **Koopmans, L., Backlund, O., Denbratt, I.,** Cycle to Cycle Variations: Their Influence on Cycle Resolved Gas Temperature and Unburned Hydrocarbons from a Camless Gasoline Compression Ignition Engine, SAE World Congress, Detroit, March 4-7 2002, SAE Technical Paper Series, SAE 2002-01-0110.

14 **Koopmans, L., Ström, H., Lundgren, S., Backlund, O., Denbratt, I.,** Demonstrating a SI-HCCI-SI Mode Change on a Volvo 5-Cylinder Electronic Valve Control Engine, SAE World Congress, Detroit, March 3-6 2003, SAE Technical Paper Series, SAE 2003-01-0753.

15 **Koopmans, L., Ogink, R., Denbratt, I.,** Direct Gasoline Injection in the Negative Valve Overlap of a Homogenous Charge Compression Ignition Engine, JSAE International Spring Fuels and Lubricants Meeting, Yokohama, May 19-22 2003, JSAE 20030195.

16 **Puri, R., Moser, M., Santoro, R. J., Smyth, K., C.,** Laser-Induced Fluorescence Measurements of OH Concentration in the Oxidation Region of Laminar, Hydrocarbon Diffusion Flames, The Combustion Institute, Twenty-Fourth Symposium (International) on Combustion, 1992, Pages 1015-1022.

17 **Tamura, M., Sakurai, T., Tai, H.,** Simultaneous Laser Induced Fluorescence Visualisation of Acetone and OH for Study on a Crevice Flow in an SI-Engine, Laser Applications to Chemical and Environmental Analysis (LACEA), Santa Fe, February 11 2000, Vol. 36 of OSA Trends in Optics and Photonics Series, paper SuB2.

18 **Richter, M., Franke, A., Engström, J., Hultqvist, A., Johansson, B., Alden, M.,** The Influence of Charge Inhomogeneity on the HCCI

Combustion Process, International Fuels and Lubricants Meeting and Exposition, Baltimore, October 2000, SAE 2000-01-2868.

19 **Berntsson, W. A., Denbratt, I.,** A LIF-study of OH in the Negative Valve Overlap of a Spark-assisted HCCI Combustion Engine, SAE World Congress, Detroit, April 14-17 2008, SAE Technical Paper Series, SAE 2008-01-0037.

20 **Luque, J., Crosley, D.R.,** LIFBASE: Database and Spectral Simulation Program (Version 1.45), SRI International Report MP 98-021, 1998.

21 **Graf, N., Gronki, J., Schulz, C., Baritaud, T., Cherel, J., Duret, P., Lavy, J.,** In-Cylinder Combustion Visualization in an Auto-Igniting Engine using Fuel Tracer- and Formaldehyde-LIF Imaging, SAE Technical Paper Series, SAE 2001-01-1924.

22 **Zhao, H., Peng, Z., Ma, T.,** Investigation of the HCCI/CAI Combustion Process by 2-D PLIF Imaging of Formaldehyde, SAE Technical Paper Series, SAE 2004-01-1901.

23 **Schulz, C. and Sick, V.,** Tracer LIF diagnostics: quantitative measurement of fuel concentration, temperature and fuel/air ratio in practical combustion systems, Progress in Energy and Combustion Science, Volume 31 (2005), Pages 75-121.

24 **Wilson, T., Haste, M., Xu, H., Richardson, S., Yap, D., Megaritis, T.,** In-cylinder Flow with Negative Valve Overlapping – Characterised by PIV Measurement, SAE Technical Paper Series, SAE 2005-01-2131.

25 **Crowe, C., Sommerfeld, M. and Tsuji, Y.** Multiphase flows with droplets and particles, CRC Press LLC, United States of America, 1998.

26 **Grossman, F., Monkhouse, P.**B., Ridder, M., Sick, V., Wolfrum, J., Temperature and pressure dependence of the laser-induced fluorescence of gas-phase acetone and 3-pentanone, Appl. Phys. B, Volume 62 (1996), Pages 249-253.

Table 1 Engine parameters

Parameter	Value
Bore	83 mm
Stroke	90 mm
Swept volume	487 cm^3
Compression ratio	10:1
Intake valve lift	3 mm
Exhaust valve lift	3 mm
EVO	150 CAD
EVC	270 CAD
IVO	450 CAD
IVC	580 CAD
Fuel	80 % iso-octane 20 % n-heptane
Fuel with fuel tracer	67 % iso-octane 18 % n-heptane 15 % 3-pentanone
Engine speed	1200 rpm
Intake air temperature	100 °C
Fuel pressure	200 bar

Table 2 Operational settings for the test cases.

	Case A	**Case B**	**Case C**
Indicated load	1.3 kW	1 kW	0.8 kW
IMEP	2 bar	1.65 bar	1.3 bar
ISFC	282 g/kWh	270 g/kWh	268 g/kWh
λ	1.21	1.27	1.30
HC (C3)	1725 ± 50 ppm	2525 ± 250 ppm	2275 ± 170 ppm
CO	0.5 - 0.6 $\%_{volume}$	0.5 - 0.6 $\%_{volume}$	0.5 - 0.6 $\%_{volume}$
NO_X	16 ± 2 ppm	10 ± 1 ppm	22 ± 9 ppm
Pilot injection duration	1.6 CAD	1.1 CAD	1.2 CAD
Main injection duration	1.0 CAD	1.1 CAD	0.6 CAD
Stratification injection duration	No stratification	0.8 CAD	1.0 CAD
Spark timing	No spark	-26 CAD	-26 CAD
EOI main	-310 CAD	-310 CAD	-310 CAD
EOI pilot	310 CAD	310 CAD	310 CAD
EOI stratification	No stratification	-30 CAD	-30 CAD

List of Figure captions

Figure 1 Schematic diagram of the setup, showing the signals from emitted species directed to each detector when all measurement techniques were used simultaneously.

Figure 2 Emission spectrum of OH from the optical engine (a), simulated absorption spectrum of OH using LIFBASE [20] (with the chosen excitation wavelength marked) (b), emission spectrum (c) and excitation spectrum (d) of formaldehyde from a cuvette at atmospheric pressure and 90°C, emission spectrum (e) and excitation spectrum (f) of 3-pentanone from a cuvette at atmospheric pressure and 100°C.

Figure 3 Averaged pressure traces (with injection timings) and averaged mass fractions burned for the three studied cases.

Figure 4 Averaged LIF images of the fuel tracer 3-pentanone for the three studied cases (A, upper row; B, middle row; and C, lower row). The columns, from left to right, show images recorded at 30, 20, 10 and 0 CAD before TDC, respectively. The optically accessible combustion chamber (right), X corresponds to the sparkplug position.

Figure 5 Averaged LIF of OH images for the three studied cases (A, upper row; B, middle row; and C, lower row). The columns, from left to right, show images recorded at 20, 10 and 0 CAD before TDC and at 10 CAD after TDC. X corresponds to the sparkplug position.

Figure 6 Averaged LIF of formaldehyde for the three studied cases (A, upper row; B, middle row; and C, lower row). The columns, from left to right, show images recorded at 20, 10 and 0 CAD before TDC and at 10 CAD after TDC. X corresponds to the sparkplug position.

Figure 7 Averaged flow fields (from data acquired during 30 individual cycles) for cases with charge stratification (B and C) between -20 CAD and TDC and at TDC for case A. The differences in flow fields between -20 CAD and TDC for cases B and C are also shown. X corresponds to the sparkplug position. Reference arrows corresponding to 1, 2 and 3 m/s are shown at the top left.

Figure 8 Mass fraction burned and timing of measurements for case B, top, and (below) LIF of OH, flow field and luminosity iso line (indicating the flame front) from one of the high speed video images, all three based on data acquired simultaneously at TDC. X corresponds to the sparkplug position. A vertical reference arrow corresponding to 3 m/s is shown to the right of the flow field, and dimensions of the optical coverage and laser plane width are shown in black.

Figure 9 Mass fraction burned and timing of measurements for case B (top). The timings of the video images correspond to those of the iso lines acquired from video images. Averaged LIF of the fuel tracer, cycle-resolved flow field and iso lines from the high speed video images obtained in the same cycle for case B near TDC (middle). X corresponds to the sparkplug position. A vertical reference arrow corresponding to 3 m/s is shown to the right of the flow field. The iso lines (white, green, dashed red, cyan and magenta) represent threshold values from the video images prior to, during and after TDC (-4 to 4 CAD). Video images from -8 to 10 CAD (bottom).

Figure 10 Mass fraction burned and timing of measurements for case C. The timings of the video images correspond to those of the iso lines acquired from video images

(top). Averaged LIF of the fuel tracer, cycle-resolved flow field and iso lines from the high speed video images obtained in the same cycle for case C near TDC (middle). X corresponds to the sparkplug position. A vertical reference arrow corresponding to 3 m/s is shown to the right of the flow field. The iso lines (white, green, dashed red and cyan) represent threshold values from the video images prior to, during and after TDC (-4 to 2 CAD). Video images from -8 to 10 CAD (bottom).

Figure 11 LIF of formaldehyde images at TDC and iso luminosity lines (from high speed video images acquired prior to, during and after TDC) obtained in the same cycle for cases B and C at TDC. X corresponds to the sparkplug position.

Definitions

CA50: The timing when 50 % of the fuel is combusted

CAD: Crank Angle Degree

CO: Carbon monoxide

CO_2: Carbon dioxide

DI: Direct Injection

EGR: Exhaust Gas Recirculation

HC: Hydrocarbons

HCCI: Homogenous Charge Compression Ignition

HCHO: Formaldehyde

IMEP: Indicated Mean Effective Pressure

LIF: Laser Induced Fluorescence

MFB: Mass Fraction Burned

Nd:YAG: Neodymium:Yttrium Aluminium Garnet

NVO: Negative Valve Overlap

NO_X: Nitrogen Oxides

OH: Hydroxyl

PIV: Particle Image Velocimetry

PM: Particulate Matter

SI: Spark Ignition

TDC: Top Dead Centre

UV: Ultra Violet

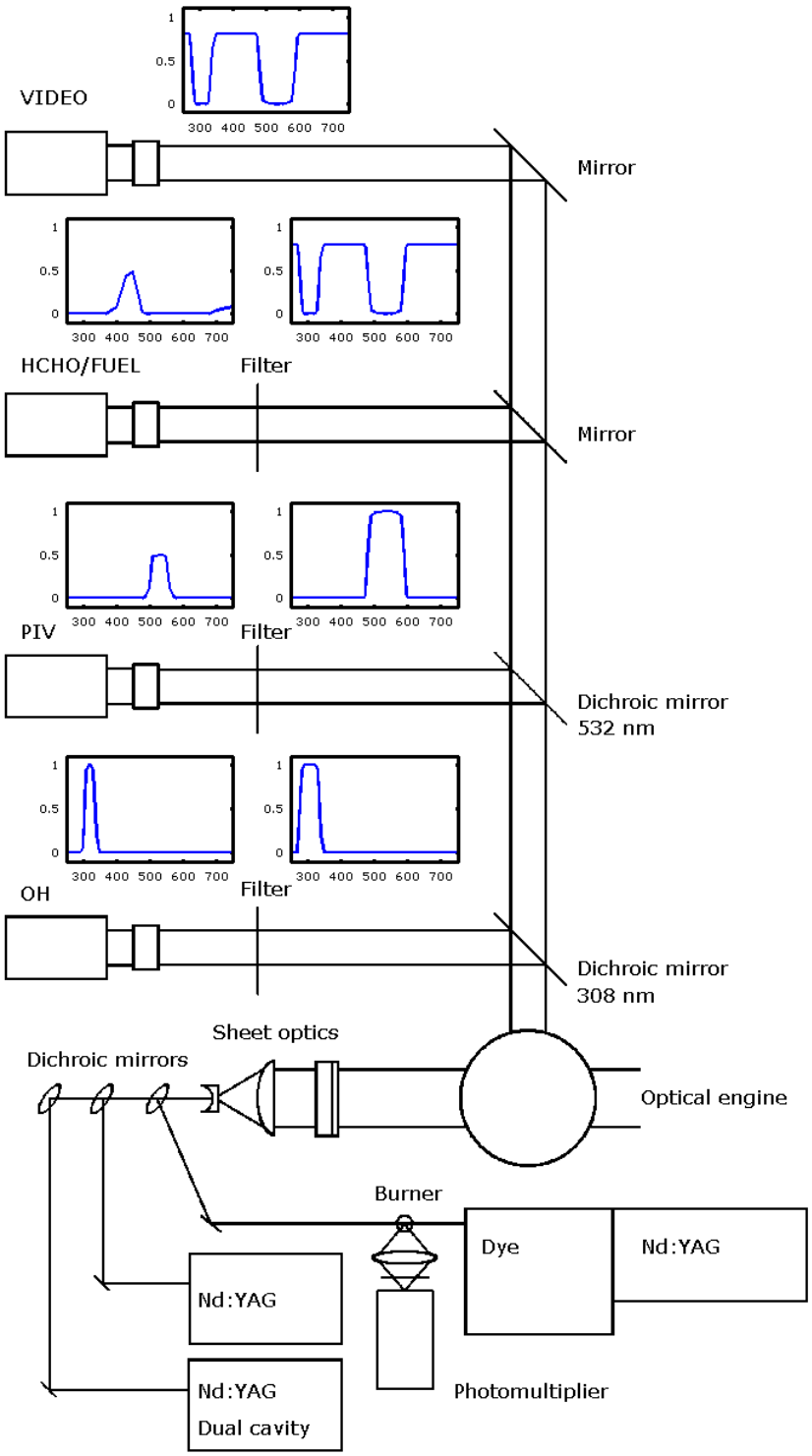

Figure 1 Schematic diagram of the setup, showing the signals from emitted species directed to each detector when all measurement techniques were used simultaneously.

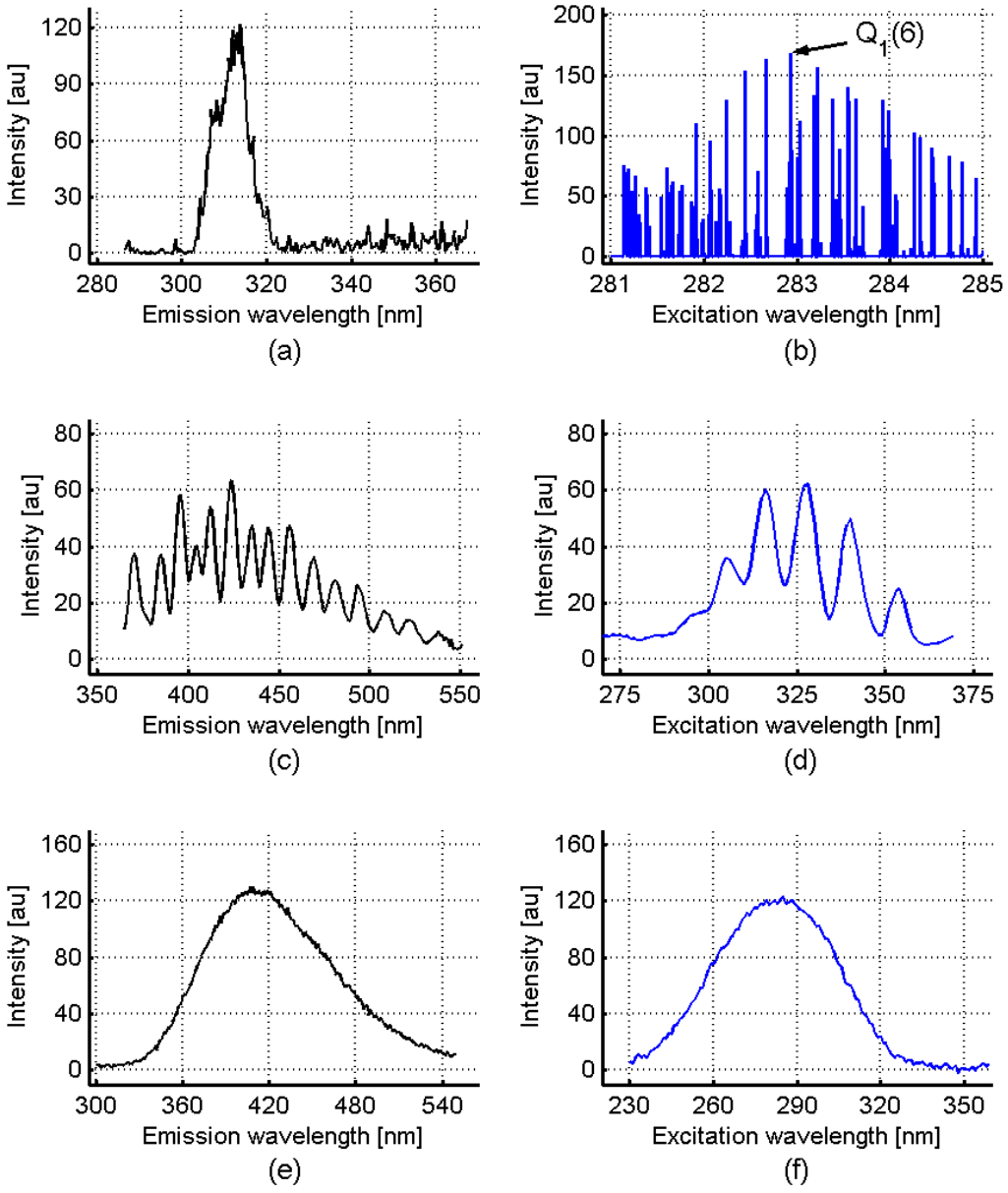

Figure 2 Emission spectrum of OH from the optical engine (a), simulated absorption spectrum of OH using LIFBASE [20] (with the chosen excitation wavelength marked) (b), emission spectrum (c) and excitation spectrum (d) of formaldehyde from a cuvette at atmospheric pressure and 90°C, emission spectrum (e) and excitation spectrum (f) of 3-pentanone from a cuvette at atmospheric pressure and 100°C.

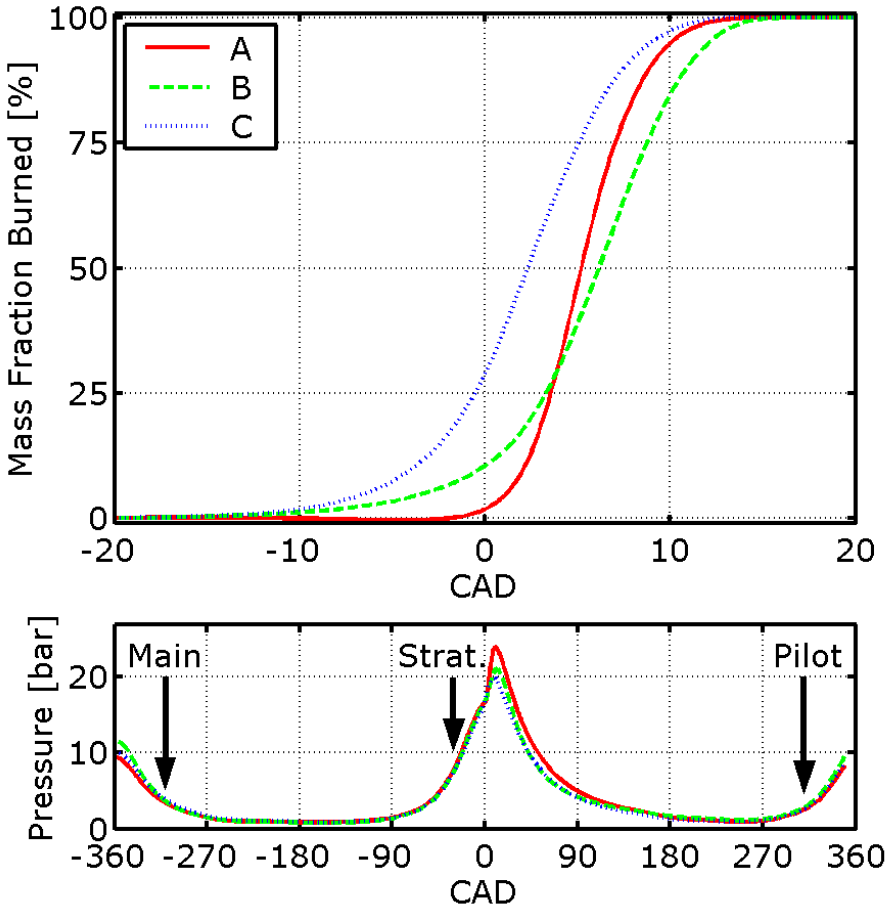

Figure 3 Averaged pressure traces (with injection timings) and averaged mass fractions burned for the three studied cases.

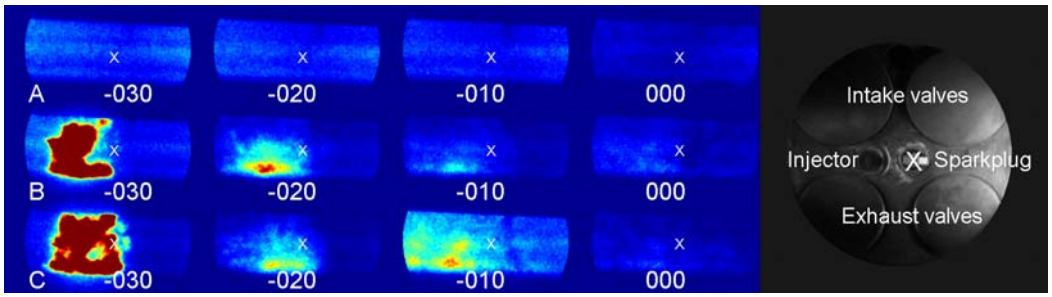

Figure 4 Averaged LIF images of the fuel tracer 3-pentanone for the three studied cases (A, upper row; B, middle row; and C, lower row). The columns, from left to right, show images recorded at 30, 20, 10 and 0 CAD before TDC, respectively. The optically accessible combustion chamber (right), X corresponds to the sparkplug position.

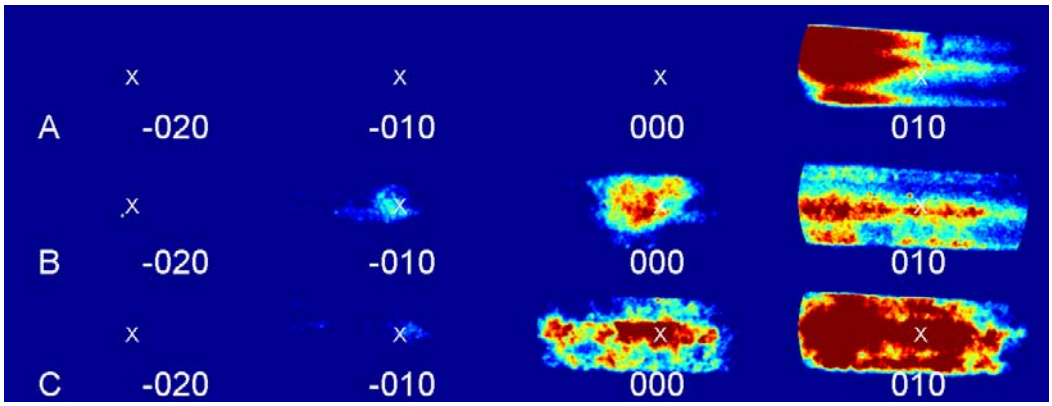

Figure 5 Averaged LIF of OH images for the three studied cases (A, upper row; B, middle row; and C, lower row). The columns, from left to right, show images recorded at 20, 10 and 0 CAD before TDC and at 10 CAD after TDC. X corresponds to the sparkplug position.

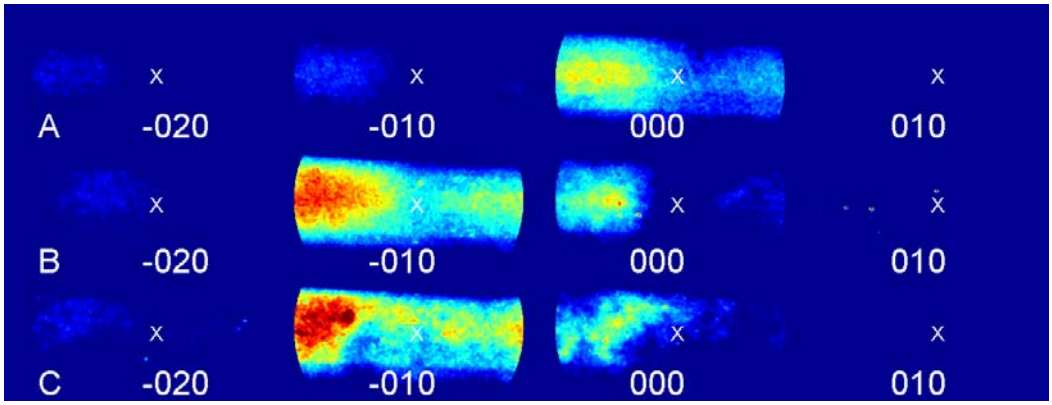

Figure 6 Averaged LIF of formaldehyde for the three studied cases (A, upper row; B, middle row; and C, lower row). The columns, from left to right, show images recorded at 20, 10 and 0 CAD before TDC and at 10 CAD after TDC. X corresponds to the sparkplug position.

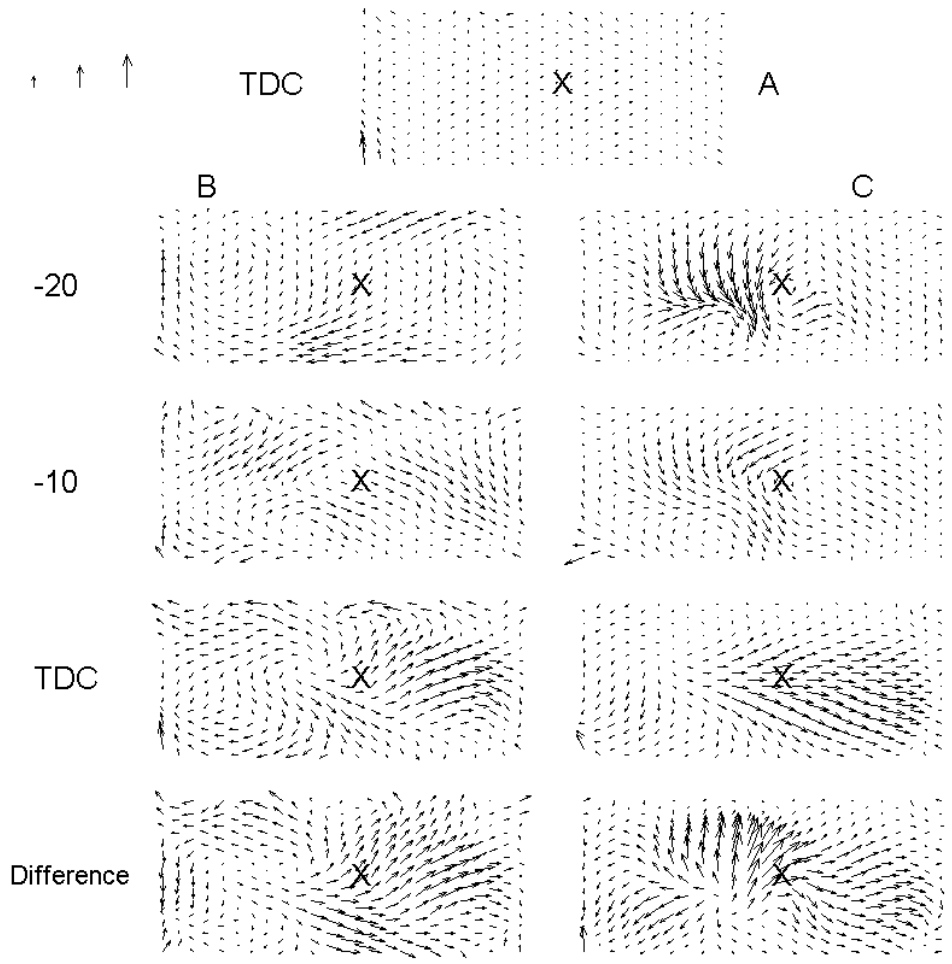

Figure 7 Averaged flow fields (from data acquired during 30 individual cycles) for cases with charge stratification (B and C) between -20 CAD and TDC and at TDC for case A. The differences in flow fields between -20 CAD and TDC for cases B and C are also shown. X corresponds to the sparkplug position. Reference arrows corresponding to 1, 2 and 3 m/s are shown at the top left.

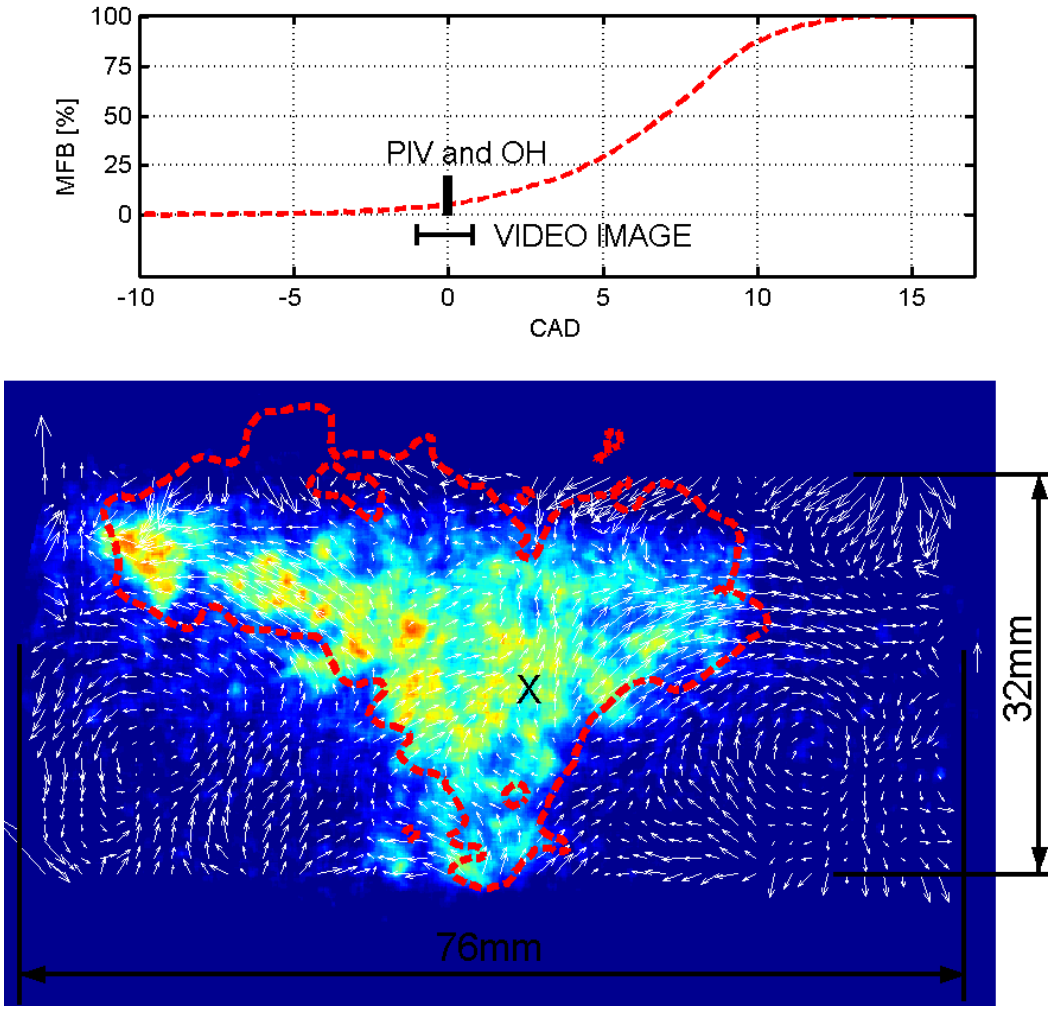

Figure 8 Mass fraction burned and timing of measurements for case B, top, and (below) LIF of OH, flow field and luminosity iso line (indicating the flame front) from one of the high speed video images, all three based on data acquired simultaneously at TDC. X corresponds to the sparkplug position. A vertical reference arrow corresponding to 3 m/s is shown to the right of the flow field, and dimensions of the optical coverage and laser plane width are shown in black.

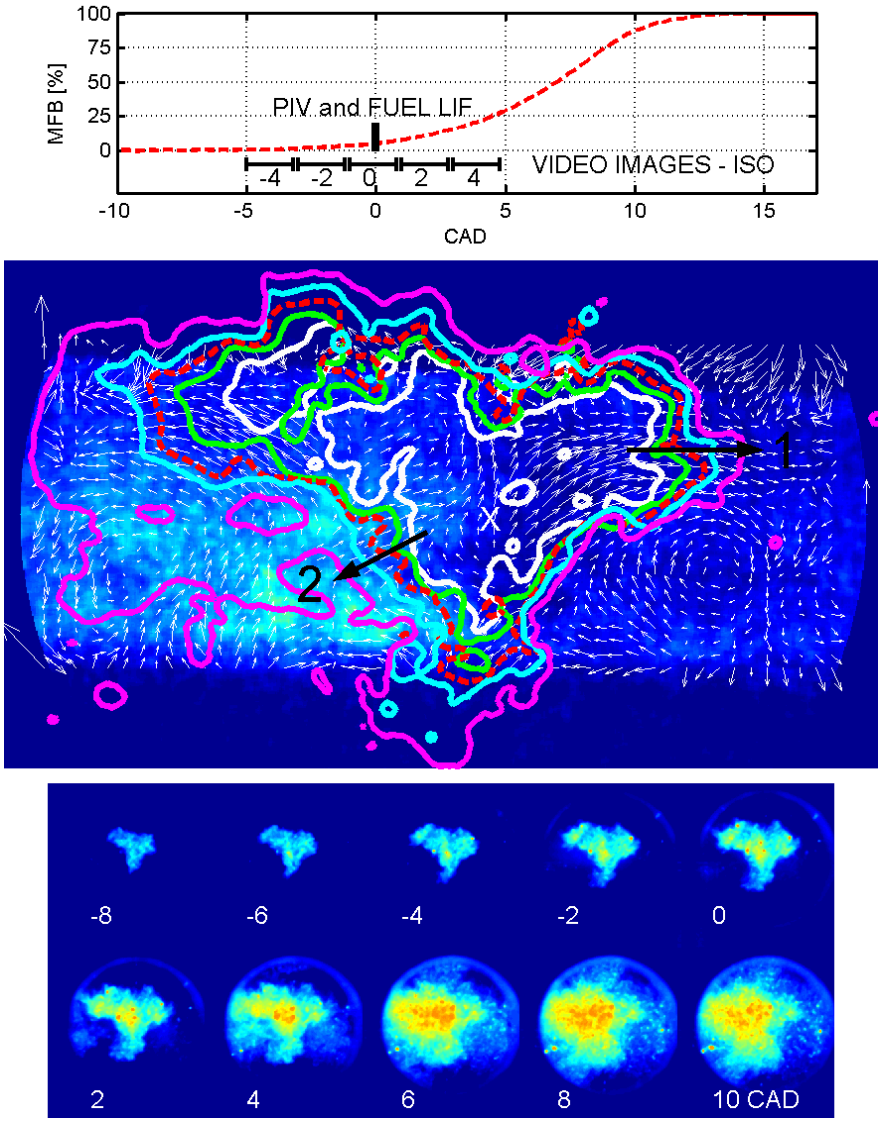

Figure 9 Mass fraction burned and timing of measurements for case B (top). The timings of the video images correspond to those of the iso lines acquired from video images. Averaged LIF of the fuel tracer, cycle-resolved flow field and iso lines from the high speed video images obtained in the same cycle for case B near TDC (middle). X corresponds to the sparkplug position. A vertical reference arrow corresponding to 3 m/s is shown to the right of the flow field. The iso lines (white, green, dashed red, cyan and magenta) represent threshold values from the video images prior to, during and after TDC (-4 to 4 CAD). Video images from -8 to 10 CAD (bottom).

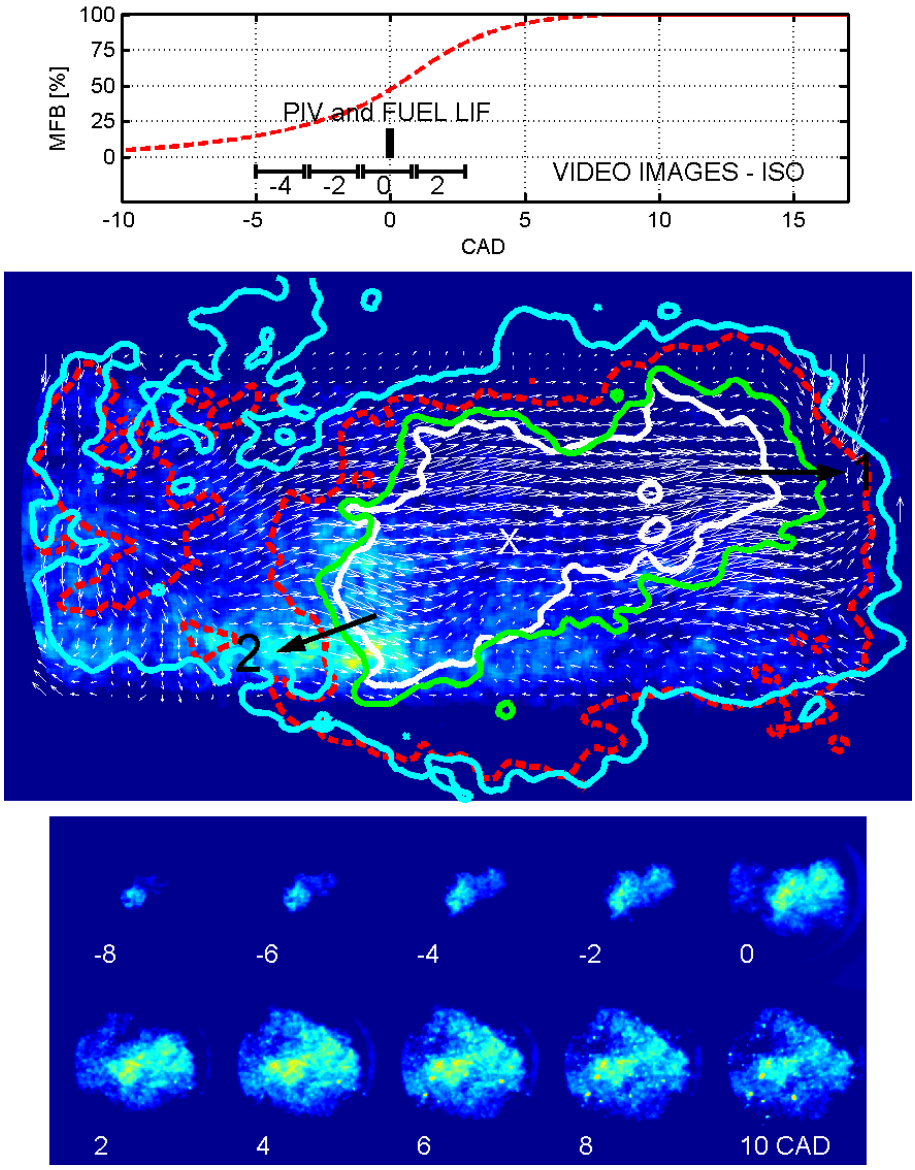

Figure 10 Mass fraction burned and timing of measurements for case C. The timings of the video images correspond to those of the iso lines acquired from video images (top). Averaged LIF of the fuel tracer, cycle-resolved flow field and iso lines from the high speed video images obtained in the same cycle for case C near TDC (middle). X corresponds to the sparkplug position. A vertical reference arrow corresponding to 3 m/s is shown to the right of the flow field. The iso lines (white, green, dashed red and cyan) represent threshold values from the video images prior to, during and after TDC (-4 to 2 CAD). Video images from -8 to 10 CAD (bottom).

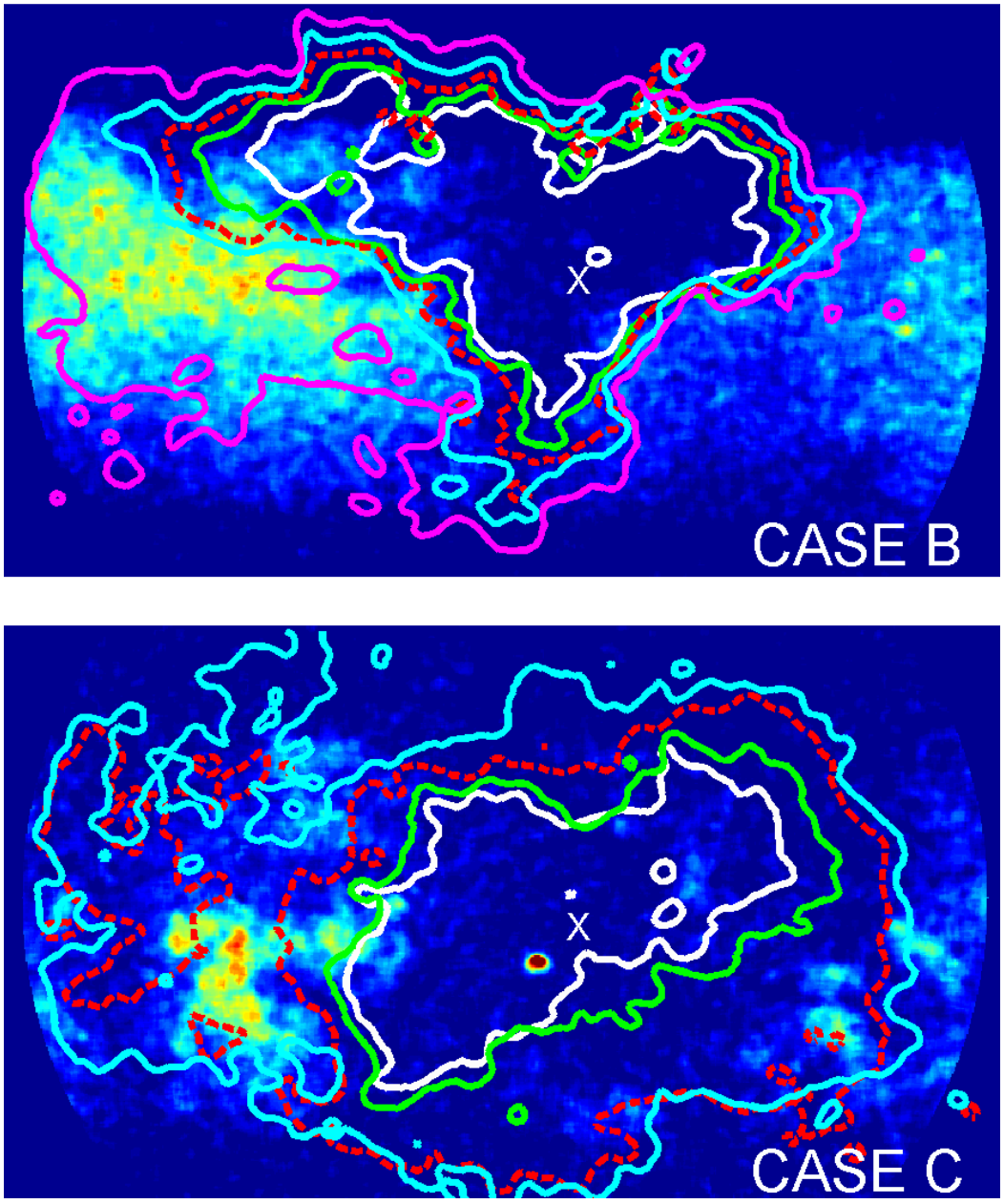

Figure 11 LIF of formaldehyde images at TDC and iso luminosity lines (from high speed video images acquired prior to, during and after TDC) obtained in the same cycle for cases B and C at TDC. X corresponds to the sparkplug position.